Durham E-Theses

Monte Carlo simulations of hard QCD radiation

JONATHAN TULLY

How to cite:

Use policy

Monte Carlo simulations of hard QCD radiation

Jonathan Tully

The Institute for Particle Physics Phenomenology

December 2009

Durham University

A thesis submitted to Durham University
for the degree of Doctor of Philosophy

Abstract

Monte Carlo event generators, such as Herwig++, provide a full simulation of events at collider experiments. They give a fully exclusive description of hadronic final states and are therefore crucial tools for the planning of future experiments and analysing of data from existing experiments.

The key component that allows this description of high-multiplicity final states is the parton shower. There has been much recent progress improving the parton shower description of hard radiation using exact matrix elements. This thesis describes research into implementing and improving such methods within the Herwig++ event generator.

In Chapter 1, the parton-shower formalism is reviewed and the structure of event generators described. Chapter 2 details the specifics of the Herwig++ parton shower.

In Chapters 3 and 4, the POWHEG next-to-leading-order matching procedure is described, and work implementing the scheme within Herwig++ is presented. The method is implemented for the processes $e^+e^- \to$ hadrons and Drell-Yan vector boson production and the results are compared to experimental data from LEP and the Tevatron. This work includes the first full implementation of the truncated shower.

A description of the development and implementation of a modified matrix-element merging scheme is presented in Chapter 5. This scheme is based on CKKW merging but uses an extension of the POWHEG idea to improve the method using truncated showers. The method is implemented first for final-state radiation in $e^+e^- \to$ hadrons and then, in Chapter 6, extended to include initial-state radiation in Drell-Yan vector boson production.

Declaration

This thesis is the result of my own work, except where explicit reference is made to the work of others, and has not been submitted for another qualification to this or any other university.

The work presented in this thesis was done in collaboration with Peter Richardson and Keith Hamilton as part of the Herwig++ collaboration. The work of Chapter 4 was published in Ref. [1]. The work of Chapter 5 was published in Ref. [2].

The copyright of this thesis rests with the author. No quotation from it should be published without the prior written consent and information derived from it should be acknowledged.

The work presented in this thesis was funded by a Science and Technology Facilities Council studentship.

Jonathan Tully

Acknowledgements

Firstly, I would like to thank my supervisor, Peter Richardson, with whom I have greatly enjoyed working. I have learnt a lot from him and am indebted to him for the patience he has shown whilst teaching me and all the guidance and encouragement he has given me over the past four years.

I am grateful to Keith Hamilton with whom I have collaborated throughout my PhD. I have always enjoyed our discussions and he has been a great source of help and support.

I would also like to thank my fellow Herwig++ authors; working within such a thriving collaboration has been a great experience and I am very grateful for the opportunity to be a part of it. In particular, I would like to thank David Grellscheid for helping me with many programming problems and Mike Seymour for his careful reading of various drafts of my papers.

I thank my office mates for making my time in the IPPP an enjoyable one. In particular I would like to thank Sophy, Jules and Jonny.

Finally, I thank those closest to me: my family, Kristin and Beatrix, for all their love and support.

Contents

Contents

Chapter 1

Introduction

Quantum Chromodynamics (QCD) is the component of the Standard Model of particle physics that describes the strong interactions of the constituents of hadronic matter. QCD is constructed as a gauge theory of the SU(3) group of colour, describing the interactions of the fundamental partons: quarks and gluons. The predictions of QCD have been tested at a number of collider experiments, including the Large Electron Positron (LEP) and Tevatron, and it is widely accepted as the correct quantum field theory of strong interactions.

The Large Hadron Collider (LHC) experiment has just begun operation at CERN. Its primary aim is to probe the TeV scale at which it is expected that new physics and corresponding new particles should be found. It is hoped that the experiment will discover the Higgs Boson, the particle responsible for electro-weak symmetry breaking in the Standard Model, as well as particles predicted by theories of physics beyond the Standard Model, such as supersymmetry. In order for these discoveries to be made, it is crucial that the QCD underlying the proton-proton collisions, which give rise to the discovery signals as well as the QCD processes, which comprise the background, are well understood. In particular, discoveries are reliant on accurate Monte Carlo simulations of QCD.

In this chapter we present an overview of the theory of QCD, in Sect. 1.1, leading to a description of how the physics of QCD is simulated in Monte Carlo event generators, in Sect. 1.2. In Sects. 1.1.1 and 1.1.2 we describe the construction of the QCD Lagrangian and the application of the theory to calculations using perturbative QCD and the parton model. In Sect. 1.1.3, we illustrate some of the features of calculations in perturbative QCD using the $e^+e^- \rightarrow$ hadrons cross section. In Sect. 1.1.4, we describe the branching formalism of QCD, providing the treatment of soft and collinear emissions, which forms

Quark	spin	electronic charge / e	Mass
d	1/2	$-1/3$	$(3.5 - 6.0)$ MeV
u	1/2	$+2/3$	$(1.5 - 3.3)$ MeV
s	1/2	$-1/3$	$(70 - 130)$ MeV
c	1/2	$+2/3$	$(1.16 - 1.34)$ GeV
b	1/2	$-1/3$	$(4.13 - 4.37)$ GeV
t	1/2	$+2/3$	$(170.1 - 172.5)$ GeV

Table 1.1: The properties of the six quarks of the Standard Model.

the basis of the parton shower. In Sects. 1.2.1 and 1.2.2, we give an overview of the stages of the simulation of an event and the Monte Carlo principles used to generate it. In Sect. 1.2.3, we give a detailed description of the parton-shower phase of the simulation, where soft and collinear emissions are resummed using a Markovian branching process.

1.1 Quantum Chromodynamics

In this section we briefly review the theory of QCD, following the treatments of Refs. [9–11].

1.1.1 The QCD Lagrangian

In the Standard Model, hadrons are comprised of bound states of six flavours of fermionic partons known as quarks, the properties[1] of which are given in Table 1.1. The Lagrangian density[2] of non-interacting quark fields q_i, of flavour i, is given by the Dirac Lagrangian density[3]

$$\mathcal{L}_{\mathrm{quark}} = \sum_{\mathrm{flavour}} \bar{q}_i \left(i\gamma_\mu \partial^\mu - m_i \right) q_i. \tag{1.1}$$

---

[1]The masses quoted are running masses and are therefore dependent on the renormalisation scheme and scale used to define them. We refer to Ref. [12] for the definitions of these masses.

[2]From this point onwards we use Lagrangian to refer to a Lagrangian density.

[3]We follow the index notation of [11] writing Lorentz indices as lower case Greek letters, colour indices in the fundamental representation (quarks) as lower case letters and colour indices in the adjoint representation (gluons) as upper case letters. Spinor indices are suppressed throughout.

Equation 1.1 exhibits an invariance under the global set of transformations in which the quark fields transform according to

$$q \rightarrow Uq, \tag{1.2}$$

where U is a unitary matrix.

QCD dictates that the quarks possess an additional quantum number, colour charge, and may exist in three colour states. The quark fields may be represented by the vector q_i^a, where $a = [1, 2, 3]$, in the fundamental representation of the SU(3) group of colour. QCD is constructed as a gauge theory, requiring local gauge invariance under the transformations of the SU(3) group of colour.

The SU(N) group

The SU(N) group refers to the group of $N \times N$ unitary matrices with unit determinant. The simplest representation of the group is the fundamental representation, where the group transformations, U^{ab}, are given by the SU(N) matrices themselves. The quark fields in Eq. 1.1 exist in the fundamental representation of the SU(3) group and are therefore represented by a three-component vector, defining the quark's colour state.

The group transformations may be expressed in terms of a set of $N^2 - 1$ hermitian, traceless group generators, t^A, defining the infinitesimal group transformations. The group transformations are expressed in terms of the group generators according to

$$U^{ab} = \exp\left[i\alpha^C t^C\right]^{ab}. \tag{1.3}$$

The conventional representation of these generators is given by the Gell-Mann matrices which are normalised such that

$$\text{tr}\left[t^A t^B\right] = T_F \delta^{AB}, \tag{1.4}$$

where $T_F = 1/2$. The group generators t^A satisfy the Lie algebra,

$$\left[t^A, t^B\right] = if^{ABC}t^C, \tag{1.5}$$

where f^{ABC} are the structure constants of the group which are completely anti-symmetric.

Another important representation of the group is the adjoint representation, where the representation space consists of the group generators.. The Lie algebra of the group generators, T^A,

$$\left[T^A, T^B\right] = if^{ABC}T^C, \tag{1.6}$$

implies that the structure constants themselves provide a representation of the group generators, with a convenient choice being

$$\left(T^A\right)_{BC} = -if^{ABC}. \tag{1.7}$$

The gluon fields, required to construct a Lagrangian that is invariant under local SU(3) transformations, exist in the adjoint representation and may therefore be represented by a vector in the adjoint representation, defining the eight gluon colour states.

An important result, which will feature in calculations involving the generators of the SU(N) group representations, are the Casimir operators, where the operator given by the sum of the generator matrices squared is proportional to the identity matrix,

$$t^A t^A = C_r \mathbf{1}, \tag{1.8}$$

where C_r is the colour factor of the representation r. The colour factors of the fundamental and adjoint representations of the SU(N) group are given by

$$C_F = \frac{N^2 - 1}{2N}, \qquad\qquad C_A = N. \tag{1.9}$$

The SU(3) gauge theory

The theory of QCD is constructed analogously to the gauge theory of Quantum Electrodynamics (QED) where the global gauge invariance exhibited by the free-field Lagrangian is extended to a local gauge invariance by the introduction of a new vector boson field. In QED the gauge symmetry group is U(1) and the introduced gauge boson is the photon; in QCD the gauge symmetry group is SU(3) and the gauge bosons are a set of eight gluon fields.

In order for the Lagrangian in Eq. 1.1 to be invariant under the local gauge transformation

$$q^a \rightarrow U(x)^{ab} q_b, \tag{1.10}$$

the derivative ∂^μ in Eq. 1.1 is replaced by the covariant derivative [10] D^μ defined by

$$(D^\mu)_{ab} = \partial^\mu \delta_{ab} + ig_s \left(t^C G_C^\mu \right)_{ab}. \tag{1.11}$$

This procedure introduces the vector boson fields G_C^μ which correspond to the eight gluon fields and transform under the local gauge transformation according to[4]

$$t^A G_A^\mu \rightarrow U(x) t^A G_A^\mu U^{-1}(x) - \frac{i}{g_s} U(x) \left(\partial^\mu U^{-1}(x) \right), \tag{1.12}$$

guaranteeing that local SU(3) gauge invariance is satisfied. The parameter g_S is the coupling constant of the introduced interaction between the quark and gluon fields. We must include the free-field Lagrangian for the introduced gluon fields which is given by the gauge invariant, renormalisable combination of the field strength tensor,

$$\mathcal{L}_{\text{gluon}} = -\frac{1}{4} G_{\mu\nu}^A G_A^{\mu\nu}, \tag{1.13}$$

where $G_{\mu\nu}^A$ is the field strength tensor defined by

$$G_{\mu\nu}^A = \partial_\mu G_\nu^A - \partial_\nu G_\mu^A - g_s f^{ABC} G_\mu^A G_\nu^B. \tag{1.14}$$

1.1.2 Perturbative QCD

The calculation of S-Matrix elements in the gauge theories of the Standard Model is performed in the paradigm of perturbation theory, where the interaction terms of the Lagrangian are viewed as perturbations to the free Lagrangian. Matrix elements are constructed as series in the couplings of the interaction terms. If these couplings are small then this series may be approximated by truncating the series at finite order in the couplings. These matrix elements, $\mathcal{M}$, are then related to cross sections, σ, according

---

[4]For ease of notation, the indices on the gauge transformation, $U(x)$, and the fundamental representation group generators, t^A, have been suppressed.

to

$$d\sigma\left(p_1, p_2 \to \{p_f\}\right) = \frac{1}{2E_1 2E_2 \left|v_1 - v_2\right|} d\Phi_n \left|\mathcal{M}\right|^2, \qquad (1.15)$$

where $d\Phi_n$ is the Lorentz invariant n-body phase-space element, which is given by

$$d\Phi_n = \left(\prod_f \frac{d^3 p_f}{2E_f(2\pi)^3}\right)(2\pi)^4 \delta^4 \left(p_1 + p_2 - \sum_f p_f\right). \qquad (1.16)$$

The variables $p_{1,2}$ and $v_{1,2}$ are the momenta and velocities of the incoming particles and $\{p_f\}$ are the momenta of the final-state particles. The prescription for calculating the matrix elements is given by the evaluation of all contributing Feynman diagrams by applying a set of Feynman rules.

Feynman rules of QCD

The Feynman rules of QCD may be read off from the QCD Lagrangian. From the quark Lagrangian, we obtain the quark propagator and the $q\bar{q}g$ vertex shown in Fig. 1.1. These rules are analogous to those appearing in QED.

In order to define the propagator of the gluon fields, the operator associated with terms bilinear in the gluon field should be inverted. In order to define an inverse, it is necessary to introduce gauge-fixing terms. This is done according to a prescription due to Faddeev and Popov [16], introducing an additional, gauge-fixing term to the Lagrangian [11],

$$\mathcal{L}_{\text{gauge-fixing}} = -\frac{1}{2\lambda}\left(\partial^\mu G_\mu^A\right)^2. \qquad (1.17)$$

The gluon propagator is given in Fig. 1.2. An important choice of the gauge parameter, λ, is the Feynman gauge, $\lambda = 1$, where the gluon propagator has its simplest form.

The free gluon Lagrangian in Eq. 1.13 contains terms that yield the Feynman rules for three- and four-gluon vertices given in Fig. 1.2. These terms originate from the fact that the QCD field strength tensor in Eq. 1.14 contains an additional term, which is quadratic in the the gluon field, leading to cubic and quartic terms in the free Lagrangian. These extra terms stem from the non-abelian nature of QCD where the group generators do not commute. The gluon self interactions have no analogue in abelian theories and represent the major difference between QCD and QED.
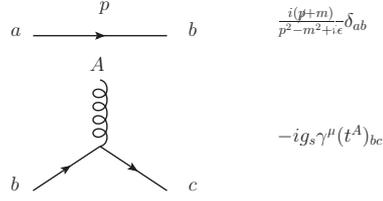
Figure 1.1: Feynman rules obtained from the quark Lagrangian.

In non-abelian gauge theories, an extra ghost term must also be included in order to cancel the propagation of unphysical gluon field polarisations [10]. This is done by adding the ghost Lagrangian

$$\mathcal{L}_{\text{ghost}} = \partial_\mu \phi^{A\dagger} \left\{ D^\mu_{AB} \phi^B \right\}, \tag{1.18}$$

where ϕ^B represents a scalar ghost field of Grassman variables. The ghost Lagrangian results in additional Feynman rules given in Fig. 1.3. These ghost fields are unphysical and should cancel in all calculations.

The full QCD Lagrangian is therefore given by the sum of the quark Lagrangian, the free quark Lagrangian together with the gauge fixing and ghost Lagrangian terms,

$$\mathcal{L}_{QCD} = \mathcal{L}_{\text{quark}} + \mathcal{L}_{\text{gluon}} + \mathcal{L}_{\text{gauge-fixing}} + \mathcal{L}_{\text{ghost}}. \tag{1.19}$$

As an alternate choice of the gauge fixing Lagrangian, we could use

$$\mathcal{L}_{\text{gauge-fixing}} = -\frac{1}{2\lambda} \left(n^\mu G^A_\mu \right)^2, \tag{1.20}$$

introducing the gauge vector n. This defines a class of axial gauges [11], where the gluon propagator has the more complicated form

$$\delta_{AB} \left[-g^{\mu\nu} + \frac{n^\mu p^\mu + p^\mu n^\nu}{n \cdot p} - \frac{\left(n^2 + \lambda p^2 \right) p^\mu p^\nu}{\left(n \cdot p \right)^2} \right] \frac{i}{p^2 + i\epsilon}. \tag{1.21}$$

The advantage of this class of gauges is that the propagator projects out two physical polarisation states, such that unphysical polarisation states do not propagate and thus it is not necessary to introduce ghost fields. For this reason, this gauge is often referred to as the physical gauge.

$$\mu \;\; \text{〜〜〜〜} \;\; \nu \qquad\qquad \delta_{AB}\left[-g^{\mu\nu}+(1-\lambda)\frac{p^\mu p^\nu}{p^2+i\epsilon}\right]\frac{i}{p^2+i\epsilon}$$

$$-g_s f^{ABC}(p_1-p_2)^\rho g^{\mu\nu}$$
$$-g_s f^{ABC}(p_2-p_3)^\mu g^{\nu\rho}$$
$$-g_s f^{ABC}(p_3-p_1)^\nu g^{\rho\mu}$$

$$-ig_s^2 f^{XAC}f^{XBD}\left(g^{\mu\nu}g^{\rho\sigma}-g^{\mu\sigma}g^{\nu\rho}\right)$$
$$-ig_s^2 f^{XAD}f^{XBC}\left(g^{\mu\nu}g^{\rho\sigma}-g^{\mu\sigma}g^{\nu\sigma}\right)$$
$$-ig_s^2 f^{XAB}f^{XCD}\left(g^{\mu\rho}g^{\nu\sigma}-g^{\mu\sigma}g^{\nu\rho}\right)$$
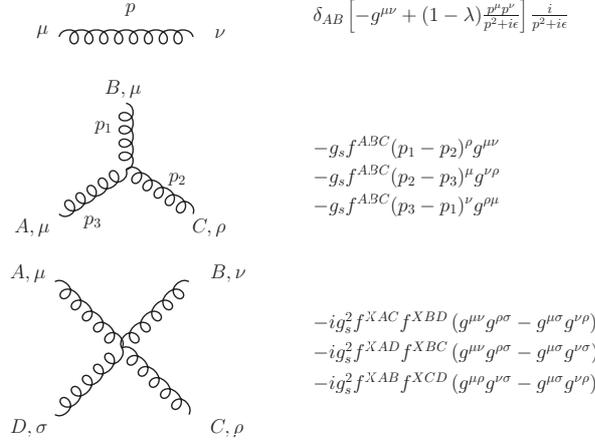
Figure 1.2: Feynman rules obtained from the gluon Lagrangian. All momenta in the three gluon vertex are defined to be incoming.

$$A \;\cdots\!\!\rightarrow\!\!\cdots\; B \qquad\qquad \frac{i\delta_{AB}}{p^2+i\epsilon}$$

$$-g_s f^{ABC}p^\mu$$
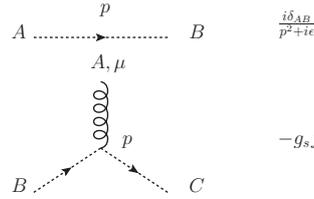
Figure 1.3: Feynman rules obtained from the ghost Lagrangian.

The running coupling of QCD and asymptotic freedom

In Quantum Field Theories, ultra-violet singularities arise from loop diagrams in which virtual particles propagate with unconstrained momentum. These divergent terms are controlled by renormalisation, where the physical set of parameters of the theory are defined in terms of the bare parameters, that appear in the Lagrangian, such that observable quantities are finite. The renormalisation procedure introduces a renormalisation scale (μ^2) and scheme dependence into the physical parameters of the theory. The condition that physical observables should not depend on the unphysical renormalisation scale may be expressed as differential equations known as the renormalisation group equations. The renormalisation group equations describe how these parameters evolve as the renormalisation scale is changed. The most important parameter of the QCD Lagrangian is the coupling g_S, which it is conventional to write in the form

$$\alpha_S = \frac{g_S^2}{4\pi}. \tag{1.22}$$

This strong coupling is referred to as a running coupling, exhibiting a dependence on the scale, Q^2, according to the renormalisation group equation

$$Q^2 \frac{\partial \alpha_S}{\partial Q^2} = \beta(\alpha_S). \tag{1.23}$$

The beta function is given to leading-order by [14, 15]

$$\beta(\alpha_S) = -\alpha_S^2 b + \mathcal{O}(\alpha_S^2), \tag{1.24}$$

with

$$b = \frac{11 C_A - 2 n_f}{12\pi}, \tag{1.25}$$

where n_f is the number of flavours of light quarks. This yields the running coupling as a solution to Eq. 1.23,

$$\alpha_S(Q^2) = \frac{\alpha_S(\mu^2)}{1 + \alpha_S(\mu^2) b \log{(Q^2/\mu^2)}}. \tag{1.26}$$

It is clear that Eq. 1.26 suggests an asymptotically free theory where, in the limit $Q^2 \to \infty$, $\alpha_S(Q^2) \to 0$. This means that, provided we restrict ourselves to hard scattering processes, the strong coupling is small and perturbation theory is valid. This behavior stems from the fact that the β-function of QCD is negative (whereas in QED it is positive), which in turn originates from the presence of the gluon self interaction vertices that have no analogue in QED.

Conversely, Eq. 1.26 suggests that at small scales the strong coupling becomes large, signalling the end of the perturbative regime. We may quantify the region of validity of the perturbative expansion by introducing the scale Λ, defined by [11]

$$\log \frac{Q^2}{\Lambda^2} = -\int_{\alpha_S(Q^2)}^{\infty} \frac{\mathrm{d}x}{\beta(x)}, \tag{1.27}$$

such that Λ characterises the scale at which α_S becomes large and perturbation theory is valid for scales $Q^2 \gg \Lambda^2$. This definition allows the leading-order running coupling Eq. 1.26 to be written as

$$\alpha_S(Q^2) = \frac{1}{b \log{(Q^2/\Lambda^2)}}. \tag{1.28}$$
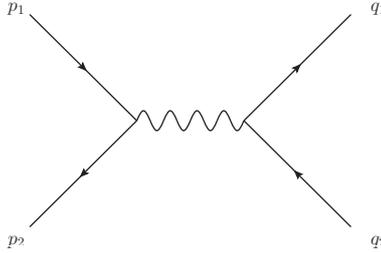
Figure 1.4: The leading-order diagram for the process $e^+e^- \to$ hadrons.

The fact that the running coupling increases as smaller scales are probed also points to the property of confinement. Confinement refers to the phenomenon that partons are found in colour-singlet hadron states and that free partons are never observed. The increased strength of the strong interaction at low scales suggests a potential, between colour-singlet combinations of quarks, from which they cannot escape. A full description of the formation of hadrons is outside the domain of perturbation theory and relies on non-perturbative models of QCD which are not fully developed.

1.1.3 The $e^+e^- \to$ hadrons cross section

One of the simplest QCD processes we can calculate is $e^+e^- \to$ hadrons, describing hadron production at an e^+e^- collider. Since many of the general features of QCD amplitudes are illustrated by this simple process correction, we will spend some time calculating its cross section.

The Born cross section

To leading order there is only a single diagram contributing to the process in which an electron and positron annihilate to an intermediate vector boson which decays to a quark-anti-quark pair, as shown in Fig. 1.4. For simplicity we will, for now, assume that the intermediate boson is a photon and that the emitted quarks and incoming leptons are massless.

Applying the Feynman rules to the diagram in Fig. 1.4 yields the matrix element,

$$\mathcal{M} = iQ_q e^2 \bar{v}(p_2)\gamma_\mu u(p_1)\frac{g^{\mu\nu}}{Q^2}\bar{u}_a(q_1)\gamma_\nu \delta_{ab} v_b(q_2), \tag{1.29}$$

where $Q_q e$ is the charge of the quark, Q is the momentum of the intermediate photon, $q_{1,2}$ are the electron and positron momenta and $q_{1,2}$ are the quark and anti-quark momenta.

In order to calculate the cross section according to Eq. 1.15, we must find the spin-averaged matrix-elements squared by multiplying Eq. 1.29 by its hermitian conjugate, summing over spins and dividing by the number of incoming spin states. In doing this, the result will contain two traces over the fermionic indices: a leptonic trace and a hadronic trace. Furthermore, once integrated over the Lorentz invariant two-body phase space, $d\Phi_2$, the result will have the form [10],

$$\int d\Phi_2 \sum |\mathcal{M}|^2 = Q_q^2 e^4 \frac{1}{Q^2} L_{\mu\nu} \int d\Phi_2 H^{\mu\nu}, \tag{1.30}$$

where, $L_{\mu\nu}$ and $H_{\mu\nu}$ are the tensors resulting from the leptonic and hadronic traces. Since we have integrated over the final-state momenta, the only momenta that $\int d\Phi_2 H^{\mu\nu}$ can depend on is Q and therefore its Lorentz structure must be

$$\int d\Phi_2 H^{\mu\nu} = H_1 g^{\mu\nu} + H_2 Q^\mu Q^\nu. \tag{1.31}$$

Appealing to gauge invariance, both tensors must satisfy Ward identities, implying that

$$Q_\mu H^{\mu\nu} = 0. \tag{1.32}$$

This further limits the Lorentz structure of Eq. 1.31 to

$$\int d\Phi_2 H^{\mu\nu} = H \left(g^{\mu\nu} - \frac{Q^\mu Q^\nu}{Q^2} \right). \tag{1.33}$$

Contracting Eq. 1.33 with the metric tensor we find that

$$H = \frac{1}{3} \int d\Phi_2 g_{\mu\nu} H^{\mu\nu}, \tag{1.34}$$

and, applying the Ward identity (Eq. 1.32) to the leptonic trace, we can write

$$\int d\Phi_2 \sum |\mathcal{M}|^2 = Q_q^2 e^4 \frac{1}{3} \frac{1}{Q^2} g^{\mu\nu} L_{\mu\nu} \int d\Phi_2 g_{\rho\sigma} H^{\rho\sigma}. \tag{1.35}$$

The leptonic production and hadronic decay pieces of the amplitude are now factorised and can be treated independently. This will significantly simplify the calculation of cross sections, especially for higher order radiative corrections. We note, however, that

in performing this decomposition we have essentially integrated out correlations between the initial- and final-state particles.

We now turn our attention to the leptonic tensor $L^{\mu\nu}$. Applying the completeness relations for on-shell fermions,

$$\sum_s u^s(p)\bar{u}^s(p) = \not{p} + m, \quad \sum_s v^s(p)\bar{v}^s(p) = \not{p} - m, \tag{1.36}$$

we can write this as,

$$L_{\mu\nu} = \text{tr}\left[\not{p}_1\gamma_\mu\not{p}_2\gamma_\nu\right]. \tag{1.37}$$

This results in the leptonic factor

$$g^{\mu\nu}L_{\mu\nu} = 8p_1 \cdot p_2 = 4Q^2. \tag{1.38}$$

The hadronic tensor has exactly the same form as the leptonic tensor but also includes a colour factor $\delta^{ab}\delta_{ab} = N_C$, which comes from the colour degrees of freedom of the external quarks, we obtain

$$g^{\mu\nu}H_{\mu\nu} = 8N_C q_1 \cdot q_2 = 4N_C Q^2. \tag{1.39}$$

The two-body phase-space measure, over which the matrix-elements squared should be integrated, is given by

$$d\Phi_2 = \frac{d\Omega}{32\pi^2}, \tag{1.40}$$

where $d\Omega$ represents the integration measure of the solid angle of either particle in the centre-of-mass frame. Finally, integrating over the solid angle and including a flux factor of $1/(2Q^2)$ we obtain the Born cross section

$$\sigma_b = N_C Q_q^2 \frac{4\pi\alpha^2}{3Q^2}, \tag{1.41}$$

where we have introduced $\alpha = e^2/4\pi$.
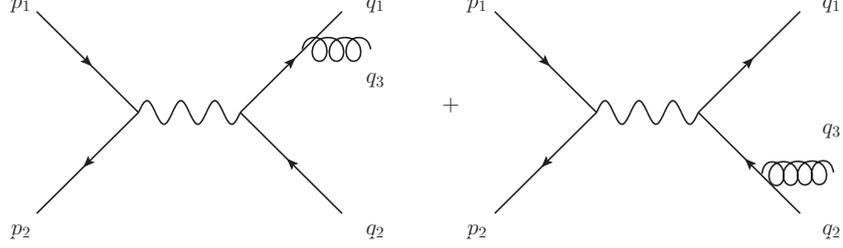
Figure 1.5: The diagrams contributing to the radiative corrections to the process $e^+e^- \rightarrow$ hadrons.

$\mathcal{O}(\alpha_S)$ radiative correction

We now consider the $\mathcal{O}(\alpha_S)$ radiative correction to the process. The correction has two contributing diagrams, as shown in Fig. 1.5, each with a final state containing the quark and anti-quark together with an additional gluon.

The same arguments that we used for the Born cross section apply for the radiative corrections and therefore the radiative diagrams give rise to an amplitude of the same form as Eq. 1.35 but with the replacement $\mathrm{d}\Phi_2 \rightarrow \mathrm{d}\Phi_3$. The leptonic trace $L^{\mu\nu}$ is again given by Eq. 1.38 and the hadronic trace must be calculated from the diagrams in Fig 1.5.

Taking the modulus squared of the radiative diagrams, we find four traces contributing to $H^{\mu\nu}$. Each of these receives an identical colour factor $t^A_{ab} t^A_{ba}$ which we identify as being the trace of the Casimir operator of the fundamental representation of SU(3) (Eq. 1.8), giving the colour factor $N_C C_F$. The hadronic trace is given by

$$H_{\mu\nu} = N_C C_F g_s^2 \quad \left\{ \frac{1}{(q_1 + q_3)^4} \mathrm{tr}\left[(\slashed{q}_1 + \slashed{q}_3)\gamma^\rho \slashed{q}_1 \gamma_\rho (\slashed{q}_1 + \slashed{q}_3)\gamma_\nu \slashed{q}_2 \gamma_\mu\right] \right. \tag{1.42}$$

$$- \frac{1}{(q_1 + q_3)^2 (q_2 + q_3)^2} \mathrm{tr}\left[(\slashed{q}_1 + \slashed{q}_3)\gamma^\rho \slashed{q}_1 \gamma_\nu (\slashed{q}_2 + \slashed{q}_3)\gamma^\rho \slashed{q}_2 \gamma_\mu\right]$$

$$- \frac{1}{(q_1 + q_3)^2 (q_2 + q_3)^2} \mathrm{tr}\left[\slashed{q}_1 \gamma^\rho (\slashed{q}_1 + \slashed{q}_3)\gamma_\nu \slashed{q}_2 \gamma^\rho (\slashed{q}_2 + \slashed{q}_3)\gamma_\mu\right]$$

$$\left. + \frac{1}{(q_2 + q_3)^4} \mathrm{tr}\left[\slashed{q}_1 \gamma_\nu (\slashed{q}_2 + \slashed{q}_3)\gamma^\rho \slashed{q}_2 \gamma_\rho (\slashed{q}_2 + \slashed{q}_3)\gamma_\mu\right] \right\}.$$

This can be evaluated with standard trace identities yielding

$$g^{\mu\nu} H_{\mu\nu} = N_C C_F g_S^2 \frac{4\left[Q^2 (q_1 \cdot q_2) + (q_2 \cdot q_3)^2 + (q_1 \cdot q_3)^2\right]}{(q_1 \cdot q_3)(q_2 \cdot q_3)}. \tag{1.43}$$

The three-body phase space is most conveniently expressed in terms of momentum-fraction variables, $\{x_i\}$. After integrating out angles defining the plane of the final-state particles this is given by

$$\int \mathrm{d}\Phi_3 = \frac{Q^2}{128\pi^3} \int \mathrm{d}x_1 \mathrm{d}x_2, \tag{1.44}$$

where the momentum fraction variables are defined by

$$x_i = \frac{2(q_i \cdot Q)}{Q^2}, \tag{1.45}$$

and the integration region is $\{x_i\} \in [0,1]$ with $x_1 + x_2 > 1$. The invariant mass of all combinations of the external parton momenta can be expressed in terms of the momentum faction variables according to

$$\begin{aligned}
2(q_1 \cdot q_2) &= s(1 - x_3), \\
2(q_1 \cdot q_3) &= s(1 - x_2), \\
2(q_2 \cdot q_3) &= s(1 - x_1), .
\end{aligned} \tag{1.46}$$

where $s = Q^2$ is the centre-of-mass energy squared.

Finally, expressing Eq. 1.43 in terms of the variables $\{x_i\}$ and defining $\alpha_S = g_s^2/(4\pi)$, we obtain the cross section contribution of the $\mathcal{O}(\alpha_S)$ radiative correction

$$\sigma_r = \sigma_b C_F \frac{\alpha_S}{2\pi} \int \mathrm{d}x_1 \mathrm{d}x_2 \frac{x_1^2 + x_2^2}{(1 - x_1)(1 - x_2)}. \tag{1.47}$$

Singularity structure of the radiative corrections

The differential cross section given in Eq. 1.47 is singular in the limits $x_1 \to 1$ and $x_2 \to 1$. The nature of these singularities may be seen by expressing the momentum fractions defined in Eq. 1.45 in terms of the opening angles between the partons θ_{ij},

$$\begin{aligned}
1 - x_1 &= x_2 x_3 (1 - \cos\theta_{23}), \\
1 - x_2 &= x_1 x_3 (1 - \cos\theta_{13}).
\end{aligned} \tag{1.48}$$

The singular regions of the differential cross sections therefore correspond to the limits where the gluon is collinear to the quark ($\theta_{13} \to 0$) or the anti-quark ($\theta_{23} \to 0$) or is soft ($x_3 \to 0$).

Since the cross section is enhanced in the region of phase space where the gluon is collinear to either the quark or anti-quark it is tempting to view the $\mathcal{O}(\alpha_S)$ contribution of Eq. 1.47 as a correction to the Born cross section, describing the emission of a gluon from either the quark or the anti-quark. This picture forms the basis of the parton-shower formalism which we describe in Sect. 1.2.3. For now we will motivate the idea by interpreting Eq. 1.47 as describing a gluon emission which we assign to either the quark or anti-quark.

In order to describe the kinematics of $1 \rightarrow 2$ emissions it is convenient to introduce the Sudakov decomposition of momentum where the parton momenta are parameterised by α_i, β_i and $q_{\perp_i}$, as defined by

$$q_i^\mu = \alpha_i p^\mu + \beta_i n^\mu + q_{\perp_i}^\mu. \tag{1.49}$$

Here, the vectors p and n define the Sudakov basis where, p is the momentum of the emitting parton. The vector n is a general light-like reference vector which we choose to be a light-like vector with three-momenta $-\mathbf{p}$ [3]. The component of momentum transverse to the emitting parton momentum, is given by $q_{\perp_i}$, such that $p \cdot q_{\perp_i} = n \cdot q_{\perp_i} = 0$.

We first consider the *emitter* of the gluon to be the quark and refer to the anti-quark as being a *spectator* to the emission. In the massless limit, the reference vectors p and n are given by the momenta of the quark and anti-quark of the underlying Born parton configuration. In the centre-of-mass frame the basis vectors are

$$p^\mu = \frac{\sqrt{s}}{2} \left(1; 0, 0, 1\right), \qquad n^\mu = \frac{\sqrt{s}}{2} \left(1; 0, 0, -1\right). \tag{1.50}$$

From the definitions of the Sudakov basis in Eqs.1.49-1.50, we find that the momentum fraction variables are given by

$$x_i = \alpha_i + \beta_i. \tag{1.51}$$

If we assume that the direction of the spectator anti-quark is unchanged by the emission, then we have $q_{\perp_2} = 0$ and by momentum conservation we obtain

$$q_{\perp_{1,3}} = \pm p_\perp. \tag{1.52}$$

Momentum conservation also demands that

$$\sum_i \alpha_i = 1, \qquad \sum_i \beta_i = 1. \tag{1.53}$$

The enhanced collinear and soft regions of phase space, correspond to the limit where the gluon's transverse momentum[5], $p_\perp$, goes to zero. It is therefore natural to express the phase space of the emission in terms of the relative transverse momentum and an auxiliary variable. A convenient choice for the auxiliary variable is the momentum fraction of the emission, z, which is defined to be the fraction of the emitter's momentum which is carried by the corresponding parton after the emission. From the definition of the Sudakov basis (Eq. 1.49), we identify $z = \alpha_1$. If we demand that the resultant partons are on-shell, we find the relation,

$$\beta_i = \frac{|q_{\perp_i}|^2}{\alpha_i s}. \tag{1.54}$$

Since we assume the direction of the anti-quark is preserved, we have $\alpha_2 = 0$ and the full set of Sudakov parameters can be expressed in terms of z and $p_\perp$ according to

$$
\begin{aligned}
\alpha_1 &= z, & \beta_1 &= \frac{p_\perp^2}{zs}, \\
\alpha_2 &= 0, & \beta_2 &= 1 - \frac{p_\perp^2}{z(1-z)s}, \\
\alpha_3 &= 1-z, & \beta_3 &= \frac{p_\perp^2}{(1-z)s}.
\end{aligned} \tag{1.55}
$$

Equation 1.51 may then be solved, yielding

$$
\begin{aligned}
p_\perp^2 &= \frac{s(1-x_1)(1-x_2)(x_1+x_2-1)}{x_2^2}, \\
z &= \frac{x_1+x_2-1}{x_2}.
\end{aligned} \tag{1.56}
$$

The phase-space measure defined in Eq. 1.44 may be written in terms of these variables according to the relation,

$$\mathrm{d}x_1 \mathrm{d}x_2 = z(1-z)(2-x_1-x_2)\mathrm{d}z\frac{\mathrm{d}p_\perp^2}{p_\perp^2}. \tag{1.57}$$

---

[5]In the following, it is assumed that $p_\perp$ refers to the modulus of the magnitude of the space-like transverse momenta $q_{\perp_{1,2}}$.

The corresponding kinematics for the limit where we consider the gluon to be emitted from the anti-quark is given by the same expressions under the replacement $x_1 \leftrightarrow x_2$.

The integral in Eq. 1.47 is dominated by the enhanced regions of phase space, approached in the limit $p_\perp \to 0$. We can therefore approximate the integral by expanding the integrand in $p_\perp$ and neglecting terms which do not receive an enhancement. For emissions where the quark is the emitter, this approach yields,

$$\sigma_r = \sigma_b C_F \frac{\alpha_S}{2\pi} \int \mathrm{d}z \frac{\mathrm{d}p_\perp^2}{p_\perp^2} \left[\frac{1+z^2}{1-z} + \mathcal{O}\left(p_\perp^2\right) \right]. \tag{1.58}$$

The divergent regions of this integral can be regulated by introducing the cut-offs, Q_0 and ϵ, parameterising the singular regions of the emission phase space, according to

$$Q_0^2 < p_\perp^2, \qquad \epsilon < z < 1 - \epsilon. \tag{1.59}$$

The integral in Eq. 1.58 then yields single and double logarithmic terms of the form

$$\propto \frac{\alpha_S}{2\pi} \log\left(\frac{Q^2}{Q_0^2}\right), \qquad \propto \frac{\alpha_S}{2\pi} \log\left(\frac{Q^2}{Q_0^2}\right) \log\left(\frac{1}{\epsilon}\right). \tag{1.60}$$

Here, the single logarithm terms may be attributed to collinear regions of phase space and the double logarithm to soft and collinear regions of phase space.

The presence of these divergent terms appears to spoil the interpretation of σ_r as the leading-order contribution to the observable three-jet cross section. However, in order to define this observable we must define what is meant by a three-jet configuration and therefore define jet resolution criteria. In our example, this corresponds to introduction cuts to the phase space of the gluon emission, avoiding the regions of soft and collinear emission where the third jet is not resolved, exactly as was done in Eq. 1.59. The parameters, Q_0 and ϵ, that we introduced as regulators can therefore be thought of a physical parameters defining what is meant by a resolvable emission.

Furthermore, according to a general theorem due to Kinoshita, Lee and Nauenberge [18–20], singularities of this type will cancel, at all orders in α_S, in any infra-red safe observable, defined as an observable that is insensitive to the emission of soft or collinear partons. For the inclusive cross section for $e^+e^- \to$ hadrons, the singularities that we have seen are introduced from the $\mathcal{O}(\alpha_S)$ radiative corrections are cancelled by identical singularities of opposite sign that arise from the $\mathcal{O}(\alpha_S)$ virtual corrections.
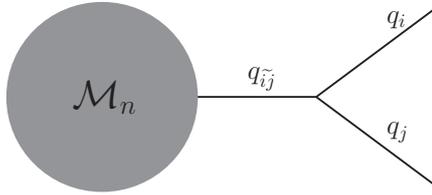
Figure 1.6: A correction to a general process with matrix element, $\mathcal{M}_n$, due to the branching of an external parton $\widetilde{ij}(q_{\widetilde{ij}}) \to i(q_i)j(q_j)$.

1.1.4 The parton-branching formalism

The presence of enhanced terms corresponding to soft and collinear emissions is a general feature of perturbation theory. In order to illustrate their origin we consider the correction to a general process, characterised by the matrix element $\mathcal{M}_n$, resulting from the branching of an external parton $\widetilde{ij}$ into partons i and j, as shown in Fig. 1.6. The matrix element of this correction will contain a factor, arising from the denominator of the *emitter* (parton $\widetilde{ij}$),

$$\frac{1}{q_{\widetilde{ij}}^2 - m_{\widetilde{ij}}^2}. \tag{1.61}$$

This denominator is singular in the limit that the emitter is on-shell ($q_{\widetilde{ij}}^2 \to m_{\widetilde{ij}}^2$). In the limit where the partons are massless, this becomes

$$\frac{1}{E_i E_j \left(1 - \cos\theta_{ij}\right)}, \tag{1.62}$$

where $E_{i,j}$ and θ_{ij} are the energies of the emitted partons and the angle between them respectively. We therefore find the general result that a matrix element is divergent in the limit that either, an external parton is soft ($E_{i,j} \to 0$) or a pair of external partons are collinear ($\theta_{i,j} \to 0$), as was seen in Sect. 1.1.3. These divergent regions are the same as those found in Sect. 1.1.3.

An important result of QCD is that, in the enhanced soft and collinear limits, these corrections factorise into a universal set of Altarelli-Parisi splitting function [21], $P_{\widetilde{ij} \to ij}(z)$, according to

$$d\sigma_{n+1} = d\sigma_n \frac{\alpha_S\left(p_\perp^2, z\right)}{2\pi} \frac{dp_\perp^2}{p_\perp^2} dz P_{\widetilde{ij} \to ij}(z). \tag{1.63}$$
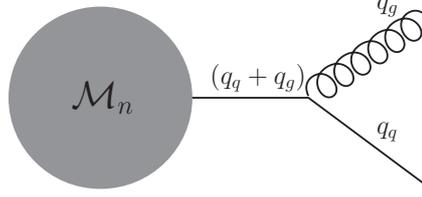
Figure 1.7: A correction, $\mathcal{M}_{n+1}$, to a general process with matrix element, $\mathcal{M}_n$, due to the emission of a gluon from a final-state quark.

These splitting functions are independent of the underlying process, depending only on the parton species involved in the branching.

In order to illustrate this factorisation, we consider the case of a gluon emission from a final-state quark. The branching is shown in Fig. 1.7. Applying the Feynman rules to this diagram yields the matrix element

$$\mathcal{M}_{n+1} = g_s t_{ab}^C \epsilon_\mu^{\star C}(q_g) \bar{u}_b(q_q) \gamma^\mu \frac{(\slashed{q}_q + \slashed{q}_g)}{2(q_q \cdot q_g)} \mathcal{M}'_{na}, \tag{1.64}$$

where $\mathcal{M}'_{na}$, refers to the underlying n-body matrix element with the spinor of the emitting parton removed and has an implicit spinor index.

Taking the modulus squared of this and summing over colours and spins, yields the matrix-element squared

$$\sum |\mathcal{M}_{n+1}|^2 = g_s^2 C_F \sum \epsilon_\mu \epsilon_\nu^\star \frac{1}{(2q_q \cdot q_g)^2} \text{tr}\left[\mathcal{M}'^\dagger_{na} \gamma^0 (\slashed{q}_q + \slashed{q}_g) \gamma^\mu \slashed{q}_q \gamma^\nu (\slashed{q}_q + \slashed{q}_g) \mathcal{M}'_{na} \right]. \tag{1.65}$$

It is convenient to work in the physical gauge [9] with a light-like gauge vector n where the sum over polarisation vectors gives

$$\sum_{\text{polarisations}} \epsilon_\mu(q) \epsilon_\nu^\star(q) = -g_{\mu\nu} + \frac{q_\mu n_\nu + q_\nu n_\mu}{n \cdot q}. \tag{1.66}$$

Applying the usual Dirac algebra to Eq. 1.65, yields[6]

$$\sum_{\text{spin,colour}} |\mathcal{M}_{n+1}|^2 = g_s^2 C_F \frac{1}{(q_q \cdot q_g)(q_g \cdot n)} \tag{1.67}$$
$$\times \text{tr}\left[\mathcal{M}'^\dagger_{na} \gamma^0 \left(n \cdot (q_q + q_g)(\slashed{q}_q + \slashed{q}_g) + n \cdot q_q \slashed{q}_q - q_q \cdot q_g \slashed{n} \right) \mathcal{M}'_{na} \right].$$

---

[6]The $\sum$ here denotes summation over external spin, colour and polarisation states.

We now appeal to the Sudakov decomposition, as defined in Eq. 1.49, writing Eq. 1.67 in terms of the relative transverse momentum of the branching, $p_\perp$. This can then be evaluated, retaining only terms at $\mathcal{O}(1/p_\perp^2)$ that are associated with enhanced emissions. The reference vectors of the Sudakov basis may be conveniently chosen by setting p to the on-shell ($p^2 = 0$) momenta of the parton correspond to the emitter in the underlying process. The gauge vector is set equal to the Sudakov reference vector n which is taken to be a light-like vector with three-momentum opposite that of p. Applying momentum conservation and on-shell relations to this basis, together with the definition $\alpha_q = z$, we write the external parton momenta as,

$$
\begin{aligned}
q_q^\mu &= z p^\mu + \frac{p_\perp^2}{2zp \cdot n} n^\mu + p_\perp^\mu, \\
q_g^\mu &= (1-z)p^\mu + \frac{p_\perp^2}{2(1-z)p \cdot n} n^\mu - p_\perp^\mu.
\end{aligned}
\tag{1.68}
$$

Inserting these momenta into Eq. 1.67, we find

$$
\sum |\mathcal{M}_{n+1}|^2 = g_s^2 C_F \frac{1}{(q_q \cdot q_g)} \left(\frac{1+z^2}{1-z} \mathrm{tr}\left[\mathcal{M}_{na}'^\dagger \gamma^0 \not{p} \mathcal{M}_{na}' \right] + \mathcal{O}(p_\perp) \right).
\tag{1.69}
$$

We now note that the remaining momentum, p, featuring in the trace, is the on-shell momentum of the external momentum corresponding to the underlying n-body process. We can therefore apply the spin sum relation

$$
\sum_{\mathrm{spin}} u(p)\bar{u}(p) = \not{p},
\tag{1.70}
$$

where $\bar{u}(p)$ is precisely the spinor that was removed from $\mathcal{M}_n$ in our definition of $\mathcal{M}_{na}'$. We can therefore write Eq. 1.69 in the factorised form

$$
\left|\bar{\mathcal{M}}_{n+1}\right|^2 = 8\pi\alpha_S \frac{1}{(q_q \cdot q_g)} \frac{1+z^2}{1-z} \left|\bar{\mathcal{M}}_n\right|^2.
\tag{1.71}
$$

The $n+1$-body phase space of these corrections can also be written in terms of the n-body phase space of the underlying process. Singling out the the momentum of the emitter, p, we can write the n-body phase-space measure as,

$$
\int \mathrm{d}\Phi_n = \int \cdots \frac{\mathrm{d}^3\mathbf{p}}{(2\pi)^3 2E_p},
\tag{1.72}
$$

where we have omitted the integrals over other momenta and the δ-function ensuring momentum conservation. The $n + 1$-body phase space of the correction may similarly be written, highlighting the integrals over the momentum of the partons involved in the branching, as

$$\int d\Phi_{n+1} = \int \cdots \frac{d^3\mathbf{q}_q}{(2\pi)^3 2E_q} \frac{d^3\mathbf{q}_g}{(2\pi)^3 2E_g}. \tag{1.73}$$

In the Sudakov decomposition, the three-momentum of the off-shell momentum emitter in the correction, $\mathbf{q}_q + \mathbf{q}_g$, is related to the three momentum of the on-shell emitter in the n-body process, $\mathbf{p}$, according to

$$\mathbf{q}_q + \mathbf{q}_g = \mathbf{p}\left(1 - \frac{p_\perp^2}{4E_p z(1-z)}\right), \tag{1.74}$$

and therefore we can write Eq. 1.73 as

$$\int d\Phi_{n+1} = \int \cdots \frac{d^3\mathbf{p}}{(2\pi)^3 2E_q} \frac{d^3\mathbf{q}_g}{(2\pi)^3 2E_g}. \tag{1.75}$$

The integral over the gluon momentum can be written in terms of z and $p_\perp$ according to

$$\int \frac{d^3\mathbf{q}_g}{(2\pi)^3 2E_g} = \frac{dz\, dp_\perp^2}{16\pi^2(1-z)}, \tag{1.76}$$

where we have integrated over the azimuthal angle[7]. Finally we note that we can write $E_q = zE + \mathcal{O}(p_\perp)$, yielding the factorised phase-space measure,

$$\int d\Phi_{n+1} = \int d\Phi_n \frac{dz\, dp_\perp^2}{16\pi^2 z(1-z)}. \tag{1.77}$$

Combining the factorised phase-space measure with the the factorised matrix-element result (Eq. 1.71) we find the factorised cross section correction

$$d\sigma_{n+1} = d\sigma_n \frac{dp_\perp^2}{p_\perp^2} dz \frac{\alpha_S}{2\pi} P_{q \to qg}, \tag{1.78}$$

---

[7]This corresponds to ignoring spin correlations which we do throughout.
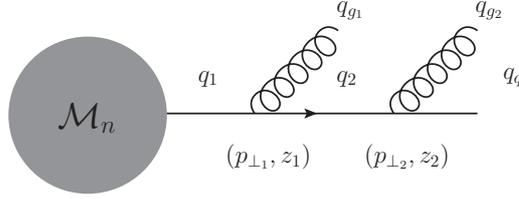
Figure 1.8: A time-like shower line with two successive gluon emissions. The diagram gives a LL contribution only in the region where the emissions are strongly ordered, $q_1^2 \gg q_2^2$.

where,

$$P_{q \to qg} = C_F \left[\frac{1 + z^2}{1 - z} \right], \tag{1.79}$$

is the Altarelli-Parisi splitting function for the branching, $q \to qg$. We note that this general result matches Eq. 1.58.

The collinear splitting functions of branchings involving other partons may be derived by a similar treatment with the result

$$P_{g \to gg} = C_A \left[\frac{z}{1 - z} + \frac{1 - z}{z} + z(1 - z) \right], \tag{1.80}$$

$$P_{g \to q\bar{q}} = T_F \left[1 - 2z(1 - z) \right]. \tag{1.81}$$

Space-like emissions

So far we have considered collinear emissions from final-state partons. This results in the intermediate parton, along the emission line, gaining a virtuality, $q_a^2 > 0$ and is therefore referred to as a *time-like branching*. Exactly the same factorisation result (Eq. 1.63) applies for emissions from initial-state partons. In this case the corresponding intermediate parton gains a virtuality, $q_a^2 < 0$ and is referred to as a *space-like branching*.

Multiple collinear emissions

We now consider the corrections due to multiple collinear emissions from a parton. Figure 1.8 shows the correction due to the successive emission of two collinear gluons from a quark line.

The approximations leading to the factorised form in Eq. 1.78 relied on the fact that the quark, from which the gluon was emitted, was on-shell prior to the emission.

Working backwards along the emitting line in Fig. 1.8, we see that in emitting the gluon at $(p_{\perp_2}, z_2)$, the corresponding emitter becomes off-shell by a virtuality

$$q_2^2 = (q_q + q_{g_2})^2 = \frac{p_{\perp_2}^2}{z_2(1 - z_2)}. \tag{1.82}$$

In treating the emissions at $(p_{\perp_1}, z_1)$, this finite virtuality can only be neglected in the limit that it is small in comparison to the virtuality of the emitter momentum, q_1, i.e. $q_1^2 \gg q_2^2$.

This condition is known as *strong ordering*. The relationship between the virtuality of the emitter and relative transverse of the emission dictates that, for non-soft emissions, the strong-ordering condition can be equivalently expressed as

$$p_{\perp_1}^2 \gg p_{\perp_2}^2. \tag{1.83}$$

Taking the non-soft, collinear limit of Eq. 1.78 we find that in this case, the emissions shown in Fig. 1.8 result in a correction proportional to,

$$\left(\frac{\alpha_S}{2\pi}\right)^2 \int_{Q_0^2}^{Q^2} \frac{\mathrm{d}p_{\perp_1}^2}{p_{\perp_1}^2} \int_{Q_0^2}^{p_{\perp_1}^2} \frac{\mathrm{d}p_{\perp_2}^2}{p_{\perp_2}^2} = \frac{1}{2} \left(\frac{\alpha_S}{2\pi}\right)^2 \log^2\left(\frac{Q^2}{Q_0^2}\right). \tag{1.84}$$

The double logarithms here are seen to only feature for emissions in which the strong-ordering condition holds. In particular, reversing the ordering condition to the region where $p_{\perp_1}^2 \ll p_{\perp_2}^2$, will yield only a single large logarithm while still containing two powers of α_S, such a configuration is therefore subleading.

While the divergent regions of Eq. 1.58 are avoided by introducing resolution criteria, a description of exclusive jet observables will contain the logarithmic terms of Eq. 1.60. If the resolution parameters are small then these logarithms will dominate the observable. Furthermore, each extra power of α_s will also introduce a large logarithm, invalidating the truncation of the perturbative series and necessitating an all-orders-in-α_S resummation of these enhanced contributions. The DGLAP equation, which we will go on to discuss, provides the means of performing this *leading-logarithmic* (LL) resummation.

We note that for the non-soft, collinear emissions the strong ordering in virtuality not only implies ordering in the transverse momentum of the emission but also the opening angle of the emissions or any variable that parameterises the collinear limit of the emission. The variable with which the strong-ordering condition is applied is referred

to as the *ordering variable* and is a key characteristic of parton showers. Different choices of ordering variable do not change the treatment of the leading logarithms but will affect subleading terms.

The DGLAP equation

The branching formalism, introduced in Sect. 1.1.4, leads to a picture of partons evolving in an ordering variable, t, (which may be virtuality or otherwise) undergoing an emission in evolving from $t \to t + \delta t$ with probability $\mathcal{P}_{\widetilde{ij} \to ij}(t) \delta t$, where from Eq. 1.63,

$$\mathcal{P}_{\widetilde{ij} \to ij}(t) \delta t = \frac{\delta t}{t} \int dz \frac{\alpha_S(t, z)}{2\pi} P_{\widetilde{ij} \to ij}(z). \tag{1.85}$$

Parton density functions (for initial-state partons) and fragmentation functions (for final-state fractions), $f_i(x, t)$, describe the probability of finding a parton species i with light-cone momentum fraction x at a scale defined by the ordering variable t. The DGLAP equation [21,22] describes how parton distribution functions and fragmentation functions develop as we evolve in t.

The DGLAP equation may be derived by considering the change in $f_i(x, t)$ in moving from a scale t to $t + \delta t$. For simplicity, we consider only a single flavour of parton.

The increase in $f(x, t)$ is the integral of all possible terms describing branchings from a higher momentum fraction x' leaving a parton with momentum fraction x, given by

$$\delta f_{\text{in}}(x, t) = \frac{\delta t}{t} \int_0^1 dz \int_0^1 dx' \frac{\alpha_S(t, z)}{2\pi} P(z) f(x', t) \delta(x - zx'). \tag{1.86}$$

Performing the integration over x' yields

$$\delta f_{\text{in}}(x, t) = \frac{\delta t}{t} \int_0^1 \frac{dz}{z} \frac{\alpha_S(t, z)}{2\pi} P(z) f(x/z, t). \tag{1.87}$$

The corresponding decrease in $f(x, t)$ is given by the integral of all branchings occurring from a fraction x to a lower fraction, given by,

$$\delta f_{\text{out}}(x, t) = \frac{dt}{t} \int_0^1 dz \int_0^x dx' \frac{\alpha_S(t, z)}{2\pi} P(z) f(x, t) \delta(zx - x'). \tag{1.88}$$

Again, we integrate over x' giving

$$\delta f_{\text{out}}(x,t) = \frac{\delta t}{t} \int_0^1 \mathrm{d}z \frac{\alpha_S(t,z)}{2\pi} P(z) f(x,t). \tag{1.89}$$

The overall infinitesimal change in $f(x,t)$ in moving to a scale $t+\delta t$ is then given by

$$\delta f(x,t) = \delta f(x,t)_{\text{in}} - \delta f(x,t)_{\text{out}}, \tag{1.90}$$

implying the differential equation

$$t\frac{\partial f(x,t)}{\partial t} = \int_0^1 \mathrm{d}z \frac{\alpha_S(t,z)}{2\pi} P(z) \left[\frac{1}{z} f(x/z,t) - f(x,t) \right]. \tag{1.91}$$

This is the DGLAP equation which forms the basis of the parton-shower resummation. In order to formulate the parton shower we must rewrite Eq. 1.91, in terms of the no-emission probability, introducing the concept of the Sudakov form factor.

The Sudakov form factor

The Sudakov form factor $\Delta(t)$, is defined as being the probability for evolving from the scale t down to the scale t_0 with no resolvable emissions. The Sudakov form factor at the scale $t+\delta t$ is given by the product of $\Delta(t)$ with the probability of having no emissions in the infinitesimal evolution step $t \to t+\delta t$

$$\Delta(t+\delta t) = \Delta(t)\mathcal{P}_{\text{no-emission}}(t)\delta t. \tag{1.92}$$

Unitarity implies that the infinitesimal no-emission probability is given by

$$\mathcal{P}_{\text{no-emission}}(t)\delta t = 1 - \mathcal{P}(t)\delta t, \tag{1.93}$$

where $\mathcal{P}(t)\delta t$ is given by the single-branching-type analogue of Eq. 1.85. This implies the differential equation,

$$\frac{\partial \Delta(t)}{\partial t} = -\mathcal{P}(t)\Delta(t). \tag{1.94}$$

The solution to this equation is

$$\Delta(t) = \exp\left[-\int_{t_0}^t \frac{\mathrm{d}t'}{t'} \int \mathrm{d}z \frac{\alpha_S(t',z)}{2\pi} P(z) \right], \tag{1.95}$$

where we have used the definition of $\mathcal{P}$ from Eq. 1.85. We define the combination of Sudakov form factors,

$$\Delta(t_1, t_2) = \frac{\Delta(t_1)}{\Delta(t_2)}, \tag{1.96}$$

which we identify as the probability of evolving from t_1 to t_2 with no resolvable emissions.

The introduction of the Sudakov form factor allows the DGLAP equation (Eq. 1.91) to be written in the form

$$t\frac{\partial}{\partial t}\left(\frac{f(x,t)}{\Delta(t)}\right) = \frac{1}{\Delta(t)}\int\frac{\mathrm{d}z}{z}\frac{\alpha_S(t,z)}{2\pi}P(z)f(x/z,t). \tag{1.97}$$

Taking into account multiple types of emission, $\widetilde{ij} \to ij$, this equation generalises to

$$t\frac{\partial}{\partial t}\left(\frac{f_i(x,t)}{\Delta_i(t)}\right) = \frac{1}{\Delta_i(t)}\sum_{i,j}\int\frac{\mathrm{d}z}{z}\frac{\alpha_S(t,z)}{2\pi}P_{\widetilde{ij}\to ij}(z)f_{\widetilde{ij}}(x/z,t). \tag{1.98}$$

Soft emissions and colour coherence

So far we have considered only collinear emissions, where we found that the resulting leading logarithms may be taken into account by a strongly-ordered DGLAP resummation. We now consider the case of soft gluon emission.

Returning to the branching in Fig. 1.7, we consider the case of soft gluon emission. The momentum of the gluon may be expressed as

$$q_g^\mu = E_g(1; \mathbf{n}_g), \tag{1.99}$$

where $\mathbf{n}_g$ is a unit vector giving the direction of the gluon. In the limit that the emitted gluon is soft, $E_g \to 0$, the matrix elements for the emission factorises into a product of a spin independent *eikonal factor*, a colour factor and the coupling constant

$$\mathcal{M}_{n+1} = g_s t_{ab}^C \frac{q_q \cdot \epsilon(q_g)^{\star C}}{(q_q \cdot q_g)}\mathcal{M}_{n\,ab}. \tag{1.100}$$

The form of this factorisation is a general result for the emission of a soft gluon from any on-shell external parton, with only the colour factor depending on the emitting parton species.

This amplitude-level factorisation appears to spoil the classical interpretation of the emissions, in that it results in the cross section containing interference between emissions from different external partons. In calculating the cross section correction due to soft gluon emissions, we must sum Eq. 1.100 over all external partons and square, where combining with Eq. 1.77, we find [11]

$$\mathrm{d}\sigma_{n+1} = \mathrm{d}\sigma_n \frac{\mathrm{d}E_g}{E_g} \frac{\mathrm{d}\Omega}{2\pi} \frac{\alpha_S}{2\pi} \sum_{i,j} C_{ij} W_{ij}, \tag{1.101}$$

where the sum over i, j refers to a sum over pairs of external partons. The factor C_{ij} is the relevant colour factor and W_{ij} is the *radiation function*. The radiation function results from the product of eikonal factors from the external partons and is given, for massless partons, by

$$W_{ij} = E_g^2 \frac{p_i \cdot p_j}{p_i \cdot q_g p_j \cdot q_g}. \tag{1.102}$$

The radiation function can be written in terms of the opening angles between the partons i, j and g, where for massless partons, we obtain

$$W_{ij} = \frac{1 - \cos\theta_{ij}}{(1 - \cos\theta_{ig})(1 - \cos\theta_{jg})}. \tag{1.103}$$

We note that the soft singularity factor is accompanied by a collinear singularity as expected. We define

$$W_{ij}^{(i,j)} = \frac{1}{2}\left(W_{ij} + \frac{1}{1 - \cos\theta_{(i,j)g}} - \frac{1}{1 - \cos\theta_{(j,i)g}}\right), \tag{1.104}$$

allowing us to write the radiation function as

$$W_{ij} = W_{ij}^{(i)} + W_{ij}^{(j)}, \tag{1.105}$$

where the terms singular as $\theta_{ig} \to 0$ and $\theta_{jg} \to 0$ have been separated. The function $W_{ij}^{(i,j)}$ gives the soft-radiation pattern for soft emissions from the pair ij which is collinear to the parton (i, j). It is convenient to perform the integral over the solid angle of the gluon, Ω_g, relative to the parton to which the gluon is collinear, as illustrated in Fig. 1.9.
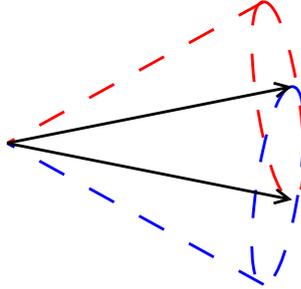
Figure 1.9: The regions into which soft gluons may be radiated from a pair of external partons. Destructive interference between soft emissions from the two lines results in no radiation being produced outside of the cones.

The functions $W_{ij}^{(i,j)}$ exhibit a property of *angular ordering* [23–30] whereby, after integrating over the azimuthal integration measure $\mathrm{d}\phi_{(i,j)g}$ [11], we find

$$\int_0^{2\pi} \frac{\mathrm{d}\phi_{(i,j)g}}{2\pi} W_{ij}^{(i,j)} = \frac{1}{1 - \cos\theta_{(i,j)g}} \Theta\left(\theta_{ij} - \theta_{(i,j)g}\right) \tag{1.106}$$

This result shows that the interference is completely destructive outside of a cone centered on the line (i, j) extending as far as the partner line (j, i). The regions into which soft gluons may be radiated from a pair of external parton lines is illustrated in Fig 1.9.

When parton masses are taken into account, it is seen that [37] the same angular ordering applies but with an inaccessible region collinear to massive quarks. This phenomenon is known as the *dead cone.*

Finally, we note that, in the collinear limit, the correction in Eq. 1.101 approximates the general soft-collinear form of Eq. 1.63 and we can therefore treat soft and collinear emissions on an equal footing so long as we ensure that the interference effects are taken into account. This idea forms the basis of the angular-ordered parton shower that we describe in Sect. 1.2.3.

1.2 Monte Carlo event generators

Monte Carlo event generators aim to give an event-by-event description of collisions at particle accelerator experiments, providing as full as possible a simulation of the physics involved. The flexibility provided by the event-by-event simulation allows predictions to

be found for any number of observable quantities and the straightforward application of experimental cuts to these predictions. It also allows for the combination of a range of physics models to be applied and as such they are able to describe a wide variety of phenomena. In particular in QCD, they provide a means, via the parton shower, of evolving from hard scales, where partons are produced in fixed-order perturbation theory, to soft scales, where non-perturbative models must be applied. This allows an exclusive description of the observed QCD jet structure. As such, event generators have proven to be invaluable tools in both planning future experiments and analysing data from current experiments.

Historically, the main general purpose Monte Carlo event generators were Pythia [39] and HERWIG [7]. These programs were based on the FORTRAN language and, though they were extremely successful and incorporated a wide range of physics models covering many processes, maintaining them became impractical as they grew. As the era of the LHC approached, a decision was made that these generators should be superceded by a new generation of event generators, with an object-orientated structure in the C++ language. The HERWIG and Pythia programs were rewritten as such, with simultaneous physics improvements, as the Herwig++ [6] and Pythia 8 [40] event generators. A further event generator, SHERPA [41], was also developed. The different event generators have notable differences in the details of the simulation they provide, with associated strengths and weaknesses. However, all have a common event structure around which the simulation is based.

1.2.1 The structure of event generators

The physics included in event generators can be divided into two distinct regimes: the perturbative and non-perturbative domains. Asymptotic freedom tells us that the validity of perturbation theory is restricted to the region of hard scattering, where the strong coupling is small. The perturbative domain is characterised by momentum transfers $Q^2 \gg \Lambda^2$. Perturbative QCD describes only the interactions of partons, however confinement dictates that only colour singlet, hadronic states are observed and not free partons. In order to provide a simulation of the hadronic final-state, non-perturbative models, describing physics at the low scales characteristic of the production of hadrons, must also be applied. The domains of perturbative and non-perturbative domains are separated by a *hadronisation scale*, Q_0 which is typically of the order $1\,\mathrm{GeV}$.

At present the only way of carrying out complete calculations in QCD relies on the perturbative expansion. Non-perturbative models may be based on well motivated physical assumptions, however they are essentially phenomenological models which contain a number of free parameters which must be *tuned* to data. In order for such models to retain their predictive power, they must be applied to parton configurations at a low scale: the hadronisation scale. The parton model motivates a factorised form of QCD physics, where low scale physics is unaffected by high scale physics. If the physics of the perturbative domain is taken into account down to the hadronisation scale, then universal hadronisation models may be applied describing the production of hadrons. These hadronisation models should be independent of the hard subprocess, depending only on the partonic configuration at the hadronisation scale. The parton shower provides the means of evolving partonic states from the hard scales, associated with the hard subprocess, down to the hadronisation scale where hadronisation models are applied.

The perturbative physics described in Monte Carlo event generators consists of the hard subprocess, perturbative decays, and parton showers. In general, the hard subprocess is calculated using leading-order tree-level matrix elements. Each external parton then initiates a parton shower which evolves from the scale of the hard subprocess down to the hadronisation scale, undergoing soft and collinear emissions. This corresponds to a DGLAP resummation of the LL terms. Additionally, unstable particles produced in the hard subprocess are decayed, possibly having emitted radiation via the parton shower, according to decay rates calculated in perturbation theory.

A schematic illustration of the structure of the event simulation provided by the generators is given in Fig. 1.10. The event shown is an example $t\bar{t}$ event at a hadron-hadron collider with semi-leptonic decays of the top quarks. The phases of the simulation, in the order in which they are applied, are:

1. a configuration describing the hard subprocess is generated according to the leading-order cross section, including the PDFs of the incoming partons;

2. perturbative decays are applied to any unstable particles;

3. external partons undergo initial- and final-state parton showers, evolving the configurations down to the hadronisation scale;

4. a hadronisation model is applied to the final-state partonic configuration;

5. unstable hadrons are decayed, according to their observed decay rates, leaving a hadronic final-state made up of stable hadrons.
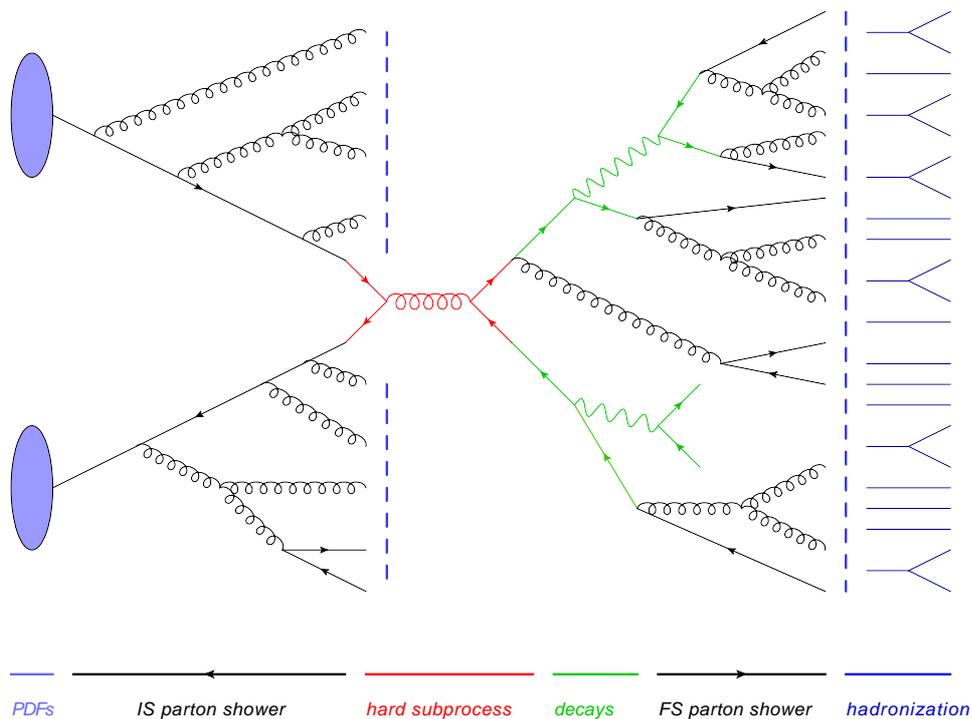
Figure 1.10: Schematic diagram showing the stages of evolution in a Monte Carlo event generator. The event shown is an example $t\bar{t}$ event at a hadron-hadron collider with semi-leptonic decays. Working from the initial-state on the left to the final-state on the right, the various stages are: extraction of the incoming partons from PDFs describing the content of the colliding hadrons; initial-state parton showers; the hard subprocess; perturbative decays (in this case of the t and Ws); final-state parton showers; the application of hadronisation models; hadronic decays leaving stable final-state hadrons. The dashed blue lines represent the application of hadronisation models.

Another important part of the simulation, not shown in Fig. 1.10, is the treatment of the remnant of the beam particles after the incoming partons have been removed. This further non-perturbative simulation describes the soft underlying event.

The focus of this thesis is the parton-shower phase of the event generator. We explore the treatment of QCD radiation provided by the parton shower and improvements that can be made to the description, as well as the interplay that exists between the hard subprocess and the parton shower.

1.2.2 Monte Carlo methods

The calculation of an observable quantity in an event generator, by Monte Carlo techniques, or otherwise, amounts to performing an integral over the phase space of all final-state particles. The particle multiplicity of an event may be high; typical events at the LHC have $\mathcal{O}(100)$ final-state hadrons. Event generators are therefore required to perform integrals over many dimensions. This necessitates the use of Monte Carlo techniques based on random numbers. A review of Monte Carlo algorithms can be found in Ref. [42].

We now illustrate the principle of Monte Carlo algorithms with the simplest example of d-dimensional Monte Carlo integration. The integral of a function $f(\mathbf{x})$ over a d-dimensional region, R, of volume V, can be related to its expectation value according to

$$I = \int_R \mathrm{d}^d\mathbf{x} f(\mathbf{x}) = V\langle f(\mathbf{x})\rangle. \tag{1.107}$$

If we have a random number generator that allows us to generate uniformly distributed points in the integration region R, we can also estimate the expectation value of the function by taking the mean value of a sample of N points. In the limit $N \to \infty$ this estimate approaches the result

$$I = \lim_{N\to\infty} \frac{V}{N} \sum_{i=1}^{N} f(\mathbf{x}_i), \tag{1.108}$$

where $\mathbf{x}_i$ refers to a randomly chosen point in the region R. This may be found from d random numbers $\mathcal{R}$ in the interval $[0, 1]$, by calculating

$$\mathbf{x}_i = (\mathcal{R}_1 \left[x_{1\max} - x_{1\min}\right], ..., \mathcal{R}_d \left[x_{d\max} - x_{d\min}\right]) \tag{1.109}$$

and rejecting the generated point if it is not within the integration region R.

A measure of the error of approximating Eq. 1.108 with a finite sample of N points is given by the standard deviation of $f(\mathbf{x})$, which in turn may be estimated according to

$$\sigma\left[f(\mathbf{x})\right] = \left[\frac{1}{N}\sum_{i=1}^{N}\left(f(\mathbf{x}_i) - \langle f(\mathbf{x})\rangle\right)^2\right]^{\frac{1}{2}}. \tag{1.110}$$

The key point is that the error in the result is proportional to $N^{-1/2}$ regardless of the dimension of the integration. This compares to other numerical integration techniques such as the trapezium and Simpson's methods where the error develops according to $N^{-2/d}$ and $N^{-4/d}$ respectively. Thus for high dimensional integrals Monte Carlo algorithms become the only feasible choice.

There are a number of advantages to providing an event-by-event description using Monte Carlo techniques. The main virtues of the approach are:

- a good convergence of integrals in any dimension;
- any number of observable quantities may be histogrammed from the generated event sample;
- an estimate of the error of an observable is always available in the form of the standard deviation of the sample.

The Monte Carlo algorithms that were used in this thesis are presented in more detail in the appendix.

1.2.3 The parton shower

The parton shower is based on the fact that the branching formalism of the DGLAP equation (Eq. 1.98) can be interpreted in a probabilistic form as a Markov process [31,32,32–34], describing a series of independent branchings. This interpretation is most easily seen via the introduction of the Sudakov form factor [34], where, upon integrating Eq. 1.98 with respect to the ordering variable, the DGLAP equation can be written in integral equation form as

$$f_i(x,t) = \Delta_i(t)f(x,t_0) + \int_{t_0}^{t}\frac{\mathrm{d}t'}{t'}\frac{\Delta_i(t)}{\Delta_i(t')}\sum_i\int\frac{\mathrm{d}z}{z}\frac{\alpha_S(t',z)}{2\pi}P_{\widetilde{ij}\to ij}(z)f_{\widetilde{ij}}(x/z,t'). \tag{1.111}$$

$$1 = \quad \overbrace{\hspace{2cm}}^{} \quad + \quad \overbrace{\hspace{2cm}}^{} \Big|_{\text{unresolved}} + \quad \overbrace{\hspace{2cm}}^{} \Big|_{\text{resolved}}$$

Figure 1.11: Unitarity relation between resolved and unresolved emissions for the branching $q \to qg$ in the LL approximation where the sum of virtual, resolved-radiative and unresolved-radiative corrections must give one.

This equation can be solved by iterative substitution and has a straightforward probabilistic interpretation. The first term on the right of Eq. 1.111 corresponds to the probability of having no emissions in evolving from the scale t down to the hadronisation scale t_0, undergoing no resolvable emissions. The second term corresponds to the probability of having a branching $\widetilde{ij} \to ij$, at a scale t' with momentum fraction z. This is given by the product of the probability of evolving between t and t', undergoing no resolvable emissions, $\frac{\Delta_{\widetilde{ij}}(t)}{\Delta_{\widetilde{ij}}(t')}$, and the probability of then undergoing an emission at (t', z). Iterating Eq. 1.111, we see that the resultant fragmentation function $f_i(x/z, t')$, in the second term then undergoes an evolution from the scale t' with equivalent no-emission and emission probabilities. The other daughter partons, produced at each branching, should undergo the same evolution.

This recursive parton-shower procedure is most conveniently expressed by introducing the generating functional [11], $\mathcal{S}_i(t)$, to represent the parton shower evolving from a scale t. For our purposes it is sufficient to understand that, $\mathcal{S}_i(t)$, encodes the configurations and corresponding probabilities of the the states accessible to the parton shower. The parton shower may be represented by,

$$\mathcal{S}_{\widetilde{ij}}(t) = \Delta_{\widetilde{ij}}(t, t_0)\mathcal{S}_{\widetilde{ij}}(t_0) + \int_{t_0}^{t} \frac{\mathrm{d}t'}{t'} \Delta_{\widetilde{ij}}(t, t') \sum_i \int \mathrm{d}z \frac{\alpha_S(t', z)}{2\pi} P_{\widetilde{ij} \to ij}(z) \mathcal{S}_i(t')\mathcal{S}_j(t').$$

$$(1.112)$$

This parton shower resums the effect of enhanced collinear emissions to all orders in α_S in the LL approximation. We note that, although formulated solely from the consideration of radiative corrections, this resummation also includes the effects of virtual correction. These corrections are taken account via unitarity and the Sudakov form factor. In deriving the Sudakov form factor we introduced the infinitesimal probability for having no resolvable emissions, which, by unitarity, is given by Eq. 1.92. For the branching $q \to qg$, this unitarity condition corresponds to the Feynman diagrams in Fig. 1.11, thus including the virtual correction.

Implicit in the integral over z in Eq. 1.112 are the limits defined in Eq. 1.59 which avoid the divergent regions of the splitting function, correspond to soft parton emission. The choice of these cut-offs define what is considered to be a resolvable emission. In general the resolution parameters, ϵ, are dependent on the scale and parton species of the parent parton.

The argument of the running coupling, α_S, should be a scale of the order of that of the branching it is involved in, however there is a certain amount of freedom in its precise form. Different choices of this scale result in differences at $\mathcal{O}(\alpha_S^2)$, corresponding to subleading terms in the LL approximation. A natural choice is the scale of the branching defined by the ordering variable, t, however it is shown in Ref. [38], that by using the relative transverse of momentum of the branching, an important set of the next-to-leading-log (NLL) terms may be included in the resummation.

The parton shower amounts to generating a series of branchings defined by the variables (t_i, z_i). Given that the probability for no emissions between t and t' is $\Delta_i(t)/\Delta_i(t')$, the scale of the emission in Eq. 1.112 can be found by generating a random number, $\mathcal{R}$, in the interval $[0, 1]$ and solving

$$\mathcal{R} = \frac{\Delta_i(t)}{\Delta_i(t')}, \tag{1.113}$$

for t'. The momentum faction of the branching, z, can then be generated by solving[8]

$$\int_\epsilon^z \mathrm{d}z \frac{\alpha_S(t', z)}{2\pi} P(z) = \mathcal{R} \int_\epsilon^{1-\epsilon} \mathrm{d}z' \frac{\alpha_S(t', z')}{2\pi} P(z'). \tag{1.114}$$

The parton-shower algorithms in Eqs. 1.113 and 1.114 require the Sudakov form factors to be tabulated such that Eq. 1.113 can be solved. An alternative algorithm is provided by the *veto algorithm*, which is described in Appendix A.2.

Initial-state parton showers

In the initial-state shower, of a hadron-hadron process, we have two parton lines connecting the incoming partons of the hard subprocess, at a scale Q^2, to the partons that are extracted from the incoming hadrons at a scale Q_0^2. These incoming lines are illustrated in Fig. 1.12. The incoming partons have space-like virtualities $t_i = -q_i^2$ increasing

---

[8]$\mathcal{R}$ represents a new random number in the interval $[0, 1]$.
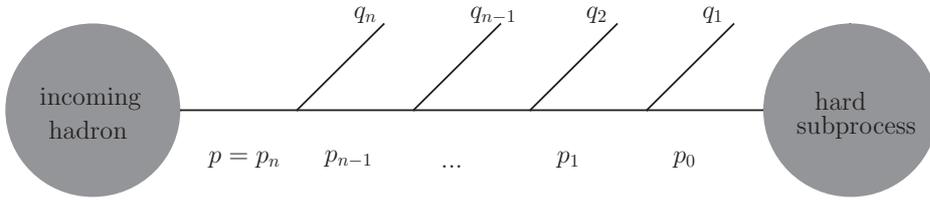
Figure 1.12: A space-like parton shower line joining the parton that is extracted from the incoming hadron to the parton entering the hard subprocess. The intermediate partons along this line have space-like virtualities, ordered such that $\left|p^2\right| < \left|p_{n-1}^2\right| < .. < \left|p_1^2\right| < \left|p_0^2\right|$.

towards the subprocess. The fraction of beam momenta carried by the incoming partons is given by x_i and decreases as we move towards the hard subprocess.

The initial-state shower describes parton emissions in the LL approximation via the DGLAP equation. The DGLAP equation for initial-state branchings is identical to that describing final-state branchings and therefore naively, the initial-state shower could be generated by extracting partons from the incoming hadrons at the hadronisation scale and showering according to Eq. 1.112. There are however, several problems with this. First, there is no clear way of deciding which partons correspond to the incoming partons of the hard subprocess and the scale at which the shower should be stopped and the hard subprocess applied. Second, the hard subprocess generally corresponds to a highly peaked distribution and therefore importance sampling must be adopted in order to achieve efficient generation. If we are to generate the hard subprocess with pre-determined incoming parton momentum, importance sampling cannot be applied, and therefore a high proportion of events must be rejected. Forward evolution implementations of the initial-state showers therefore result in ambiguities in the showering scheme and inefficiencies in the event generation.

Forward evolution implementations of the initial-state parton shower are therefore considered unworkable and instead backwards shower schemes are employed [13, 35]. In the backward evolution shower formalism, the hard subprocess is generated first and the initial-state parton shower is generated by evolving from the incoming partons of the hard subprocess down to the hadronisation scale where partons are assigned to the incoming hadrons.

If we are to generate the hard subprocess first, then we have included a PDF $f_i(Q^2, x)$, describing the parton entering the hard subprocess. This PDF describes the inclusive DGLAP evolution from Q_0^2 up to Q^2. In order to provide an exclusive distribution of

the radiation, we must deconstruct $f_i(Q^2, x)$, in terms of the parton shower in such a way that it can be generated as a backward shower.

The integral form of the DGLAP equation in Eq. 1.111, provides an iterative solution for $f_i(Q^2, x)$ which we expand along the initial-state line. This can be manipulated into the form[9] [9]

$$
\begin{aligned}
1 = \quad & \Pi_i\left(t, t_0; x\right) \qquad\qquad\qquad\qquad\qquad\qquad\qquad\qquad\qquad\qquad\qquad (1.115)\\
+ \quad & \int_{t_0}^t \frac{\mathrm{d}t_1}{t_1} \int \mathrm{d}z_1 \Pi_i\left(t, t_1; x\right) \frac{\alpha_S(t_1, z_1)}{2\pi} P_{\widetilde{ij}\to ij}(z_1) \frac{f_{\widetilde{ij}}(x/z_1, t')}{z_1 f_i(x, t_1)} \Pi_{\widetilde{ij}}\left(t_1, t_0; x/z_1\right)\\
+ \quad & \int_{t_0}^t \frac{\mathrm{d}t_1}{t_1} \int \mathrm{d}z_1 \int_{t_0}^{t_1} \frac{\mathrm{d}t_2}{t_2} \int \mathrm{d}z_2\\
\times \quad & \Pi_i\left(t, t_1; x\right) \frac{\alpha_S(t_1, z_1)}{2\pi} P_{\widetilde{ij}\to ij}(z_1) \frac{f_{\widetilde{ij}}(x/z_1, t_1)}{z_1 f_i(x, t_1)}\\
\times \quad & \Pi_{\widetilde{ij}}\left(t_1, t_2; \frac{x}{z_1}\right) \frac{\alpha_S(t_2, z_2)}{2\pi} P_{\widetilde{ijk}\to\widetilde{ij}}(z_2) \frac{f_{\widetilde{ijk}}(x/z_1/z_2, t_2)}{z_2 f_{\widetilde{ij}}(x/z_1, t_2)} \Pi_{\widetilde{ijk}}\left(t_2, t_0; \frac{x}{z_1 z_2}\right)\\
+ \quad & ...,
\end{aligned}
$$

where we have introduced the function,

$$
\Pi_i(t_1, t_2; x) = \Delta_i(t_1, t_2) \frac{f_i(x, t_2)}{f_i(x, t_1)}. \tag{1.116}
$$

This function represents a modified Sudakov form factor, which we interpret as the probability of backward evolving a parton of flavour i and momentum fraction x from a scale t down to t_0, with no resolvable emissions. In order to justify this interpretation, we take the derivative of $\Pi_i(t, t_0, x)$ with respect to the ordering variable t,

$$
t\frac{\partial \Pi_i(t, t_0; x)}{\partial t} = -\Pi_i(t, t_0; x)\left[\frac{1}{f_i(x, t)} t\frac{\partial f_i(x, t)}{\partial t} + \int \mathrm{d}z \frac{\alpha_s(t, z)}{2\pi} P_{\widetilde{ij}\to ij}(z)\right]. \tag{1.117}
$$

The DGLAP equation (1.91) can then be applied to the first term in square brackets yielding

$$
t\frac{\partial \Pi_i(t, t_0; x)}{\partial t} = -\Pi_i(t, t_0; x) \int \frac{\mathrm{d}z}{z} \frac{\alpha_s(t, z)}{2\pi} P_{\widetilde{ij}\to ij}(z). \tag{1.118}
$$

We now observe that, in the backwards evolution from a scale t, the probability of undergoing an emission in the evolution measure δt, from a parton of flavour i with

---

[9]The summation over all possible branchings is implicit in the splitting functions.

momentum fraction x is given by[10]

$$\mathcal{P}_{\text{back}\,i}(t)\delta t = \frac{\delta f_i(x,t)}{f_i(x,t)} = \frac{\delta t}{t} \int \frac{\mathrm{d}z}{z} \frac{\alpha_s(t,z)}{2\pi} P_{\widetilde{ij}\to ij}(z) \frac{f_{\widetilde{ij}}\left(\frac{x}{z},t\right)}{f_i(x,t)}. \tag{1.119}$$

Using this result, Eq. 1.118 can be written analogously to Eq. 1.94 as

$$\frac{\partial \Pi_i(t,t_0;x)}{\partial t} = -\mathcal{P}_{\text{back}\,i}(t)\Pi_i(t,t_0;x), \tag{1.120}$$

thus confirming the interpretation of $\Pi_i(t,t_0;x)$ as the no-emission probability for backwards evolution. Furthermore, Eq. 1.120 implies that $\Pi_i(t,t_0;x)$ can equivalently be written in the alternate form,

$$\Pi_i(t,t_0;x) = \exp\left[-\int_{t_0}^t \frac{\mathrm{d}t'}{t'} \int \mathrm{d}z \frac{\alpha_S(t',z)}{2\pi} P_{\widetilde{ij}\to ij}(z) \frac{f_{\widetilde{ij}}(x/z,t')}{z f_i(x,t')}\right]. \tag{1.121}$$

Equation 1.115 represents the correctly normalised sum of all emissions in the initial-state parton shower, where branchings are generated according to the probability given by the product of the probabilities of having no emissions in evolving down to t, and the branching probability for the branching (t,z), which is given by

$$\frac{\alpha_S(t,z)}{2\pi} P_{\widetilde{ij}\to ij}(z) \frac{f_{\widetilde{ij}}(x/z,t)}{z f_i(x,t)}. \tag{1.122}$$

This may be achieved by employing Monte Carlo algorithms analogous to those used in the time-like case. Starting from an incoming parton i, from the hard subprocess, with momentum fraction x and scale t, the scale of the first branching, t', may be found by solving

$$\mathcal{R} = \Pi_i(t,t';x). \tag{1.123}$$

The momentum fraction, z, of the branching may then be generated by solving

$$\int_\epsilon^z \mathrm{d}z' \frac{\alpha_S(t',z')}{2\pi} P(z') \frac{f_{\widetilde{ij}}(x/z',t)}{z f_i(x,t)} = \mathcal{R} \int_\epsilon^{1-\epsilon} \mathrm{d}z' \frac{\alpha_S(t',z')}{2\pi} P(z') \frac{f_{\widetilde{ij}}(x/z',t)}{z f_i(x,t)}. \tag{1.124}$$

---

[10]The term $\delta f_i(x,t)$ is given by Eq. 1.89 with no $\delta f_{\text{in}\,i}(x,t)$ term since, in the backwards formalism, we have isolated the incoming line.

We note that, for the form of the modified Sudakov form factor given in Eq. 1.121, the exponent of the Sudakov form factor matches this branching probability and is therefore suitable for the application of the veto algorithm.

Each branching from an initial-state parton produces a space-like parent parton and a time-like daughter parton which continue to evolve according to the backward initial-state and forward final-state parton-shower algorithms. The full initial-state shower may be expressed, analogously to Eq. 1.112, as a generating functional, $\bar{\mathcal{S}}_i(t, x)$ evolving according to

$$
\begin{aligned}
\bar{\mathcal{S}}_i(t, x) &= \Pi_i(t, t_0; x)\bar{\mathcal{S}}_i(t_0, x) \qquad\qquad\qquad\qquad\qquad\qquad\qquad (1.125) \\
&+ \int_{t_0}^t \frac{\mathrm{d}t'}{t'}\Pi_i(t, t', x)\sum_{\widetilde{ij}} \int \mathrm{d}z \frac{\alpha_S(t', z)}{2\pi}P_{\widetilde{ij}\to ij}(z)\bar{\mathcal{S}}_{\widetilde{ij}}(t', x/z)\frac{f_{\widetilde{ij}}(x/z, t')}{z f_i(x, t')}\mathcal{S}_j(t').
\end{aligned}
$$

The angular-ordered parton shower

In the previous treatment of parton showers only collinear emissions were treated. In Sect. 1.1.4, we described how soft gluons may be taken into account to LL approximation by treating the emission of soft gluons from external partons. Interference effects between emissions from pairs of external partons result in the property of angular ordering, where soft emissions are confined to a cone around the emitting parton with half-angle given by the angle between the two external quarks.

In the parton-shower formalism, it has been shown that coherent soft gluon effects may be taken into account by choosing the ordering variable of the parton shower to be the opening angle of emissions [36]. This is known as the angular-ordered parton shower. It is clear from our discussion of the strong ordering of parton-shower emissions, that such a change in ordering variable should not change the description of non-soft emissions in the LL approximation. In this section, we outline the arguments that lead to this prescription giving the correct treatment of coherent soft gluon radiation.

For a given parton configuration, the soft-gluon radiation pattern is given by Eq. 1.101. Considering the simplest case of a $q\bar{q}$ configuration, we have radiation from a single pair of partons. The full soft-radiation pattern is therefore simply that shown in Fig. 1.9 and the corresponding colour factor is $C_{ij} = C_F$.

In order to proceed to a more complicated example, we note that the colour factors C_{ij} may be found by representing the colour charge of each parton by a vector, Q_i, such

that $Q_i^2 = C_F$ for a quark and $Q_i^2 = C_A$ for a gluon. The colour factor in Eq. 1.101 then corresponds to $C_{ij} = -Q_i \cdot Q_j$.

We now consider the radiation pattern from inserting a soft gluon emission from an external parton in a general configuration. In order to infer the general structure of such corrections to the parton shower, we write the radiation pattern highlighting two partons, i and j, which we may consider to be a collinear pair resulting from the parton shower [13]. The radiation function is given by

$$W = \sum_{n,m} C_{nm} W_{nm} = -Q_i \cdot Q_j W_{ij} - \sum_l Q_i \cdot Q_l W_{il} \qquad (1.126)$$
$$- \sum_l Q_j \cdot Q_l W_{jl} - \sum_{l \neq l'} Q_l \cdot Q_{l'} W_{ll'},$$

where the summation of l and l' denotes summation over the other external partons. The external partons form a colour singlet and so we have the relation of the colour charges,

$$Q_i + Q_j + \sum_l Q_l = 0. \qquad (1.127)$$

Since we assume i and j are the result of a collinear emission from a parent, $\widetilde{ij}$, we make the approximation $i, j \to \widetilde{ij}$ in any term that is non-singular in θ_{ig} and θ_{jg}. Utilising this approximation, the colour singlet relation and the decomposition of Eq. 1.105, we may write the radiation pattern as,

$$W = Q_i^2 \left[W_{ij}^i + \frac{1}{2} \sum_l \left(\tilde{W}_{il}^j - \tilde{W}_{jl}^i \right) \right] + Q_j^2 \left[W_{ij}^j + \frac{1}{2} \sum_l \left(\tilde{W}_{jl}^i - \tilde{W}_{il}^j \right) \right]$$
$$+ \left(\sum_l Q_l \right)^2 \frac{1}{2} \sum_l \left[W_{il}^l + W_{jl}^l + \tilde{W}_{lj}^i + \tilde{W}_{li}^j \right] - \sum_{l \neq l'} Q_l \cdot Q_{l'} W_{ll'}, \qquad (1.128)$$

where the function $\tilde{W}_{ij}^k$ is defined as

$$\tilde{W}_{ij}^k = W_{ik}^k - W_{jk}^k. \qquad (1.129)$$

We note that the function $\tilde{W}_{ij}^k$ is non-singular and under azimuthal averaging, applying the angular-ordering approximation, Eq. 1.106, yields

$$\tilde{W}_{ij}^k = \frac{1}{(1 - \cos\theta_{kg})} \left[\Theta\left(\theta_{ik} - \theta_{kg}\right) - \Theta\left(\theta_{jk} - \theta_{kg}\right) \right]. \tag{1.130}$$

The directions i and j may also be approximated by the parent direction $\widetilde{ij}$ in the non-singular $\tilde{W}$ terms. The charge of the parent is given by $Q_{\widetilde{ij}} = Q_i + Q_j$. If we have only a single additional parton l then under this approximation Eq. 1.128 becomes,

$$W = Q_i^2 W_{ij}^i + Q_j^2 W_{ij}^j + Q_{\widetilde{ij}} \cdot Q_{\widetilde{ij}} \tilde{W}_{l\widetilde{ij}}^{\widetilde{ij}} + Q_l \cdot Q_l W_{\widetilde{ij}l}^l. \tag{1.131}$$

There is a clear parton-shower interpretation for generating this radiation pattern.

This soft gluon radiation pattern may be assigned to the partons as follows. The first two terms in this equation, correspond to radiation in cones of half angle θ_{ij} around the partons i and j being generated with a probability proportional to their respective colour charges. The third term corresponds to radiation emitted around the intermediate parton $\widetilde{ij}$ according to its colour charge in a cone of half angle between $\theta_{\widetilde{ij}l}$ and θ_{ij}. The third term corresponds to emissions from the parton l according to its colour charge in a cone of half angle $\theta_{\widetilde{ij}l}$.

This picture can be extended to emitting a soft gluon from any number of external partons [37] and iterated to any number of soft gluon emissions. The result is that the correct soft radiation pattern is obtained by emitting soft gluons from parton lines i with the probability

$$\mathrm{d}\mathcal{P}_{\text{soft}}(\theta_{iq}, E_g) = \frac{\mathrm{d}E_g}{E_g} \mathrm{d}\cos\theta_{ig} \frac{\alpha_S}{2\pi} Q_i^2 \frac{1}{1 - \cos\theta_{ig}}, \tag{1.132}$$

with soft emissions along the parton line ordered in opening angle. Since this emission probability coincides with Eq. 1.101 in the enhanced region, and strong ordering allows a change in the ordering variable without modification of the collinear LL resummation, a simple modification can be made to the parton-shower formalism to take into account coherent soft gluon radiation: the ordering variable of the parton shower should be taken to be the opening angle of emissions.

This angular-ordered shower forms the basis of the HERWIG and Herwig++ parton showers. Other parton-shower formulations, as employed in the Pythia and SHERPA

generators, that use virtuality and transverse momentum as the ordering variable must employ vetoes to enforce angular ordering and account for color coherence effects. While this procedure is not exactly equivalent to the correct prescription of having an angular-ordered parton shower, comparisons between the generators have shown it to give acceptable results.

1.3 Summary

QCD is widely accepted as the correct theory of strong interactions and a good understanding of QCD phenomenology is crucial for the success of collider experiments. Monte Carlo event generators, based around parton showers, allow a full simulation of the physics at collider experiments and provide a flexible event-by-event description. As such, Monte Carlo event generators have become indispensable experimental tools.

The parton shower is based on the parton-branching formalism where corrections due to soft and collinear parton emissions have a universal factorised form. Such emissions correspond to enhanced emissions which result in LL corrections. The parton shower provides an all-orders-in-α_S resummation of these LL terms.

Parton showers were first formulated in terms of an evolution in virtuality which formally only provides a correct treatment of collinear emissions. Coherent soft-gluon emissions may be taken into account by instead ordering emissions in the opening angle of branchings. Angular-ordered parton showers are used in the HERWIG and Herwig++ event generators.

Chapter 2

Herwig++ Shower

2.1 Introduction

The Herwig++ parton shower is an angular-ordered shower based on the HERWIG parton shower but with modifications in order to provide an improved degree of Lorentz invariance and description of mass effects. In this chapter we describe the main features of the parton shower. In Sect. 2.2 the details of the kinematics, dynamics and implementation of the initial- and final-state showers are discussed and in Sect. 2.3 a technique for improving the parton-shower description, using exact matrix elements, is introduced.

2.2 The Herwig++ parton shower

In the HERWIG parton shower the evolution variable, describing the scale of an emission $\widetilde{ij} \to ij$, is given by [36]

$$\tilde{t} = 2E_{\widetilde{ij}}^2 \frac{q_i \cdot q_j}{E_i E_j} = \frac{q_{\widetilde{ij}}^2}{z(1-z)},\tag{2.1}$$

where z is the fraction of the parent partons energy carried by the emitted parton i which reduces to $E^2 \theta_{ij}^2$ in the limit that $\theta_{ij} \to 0$ and therefore can be used to define an angular ordered shower[1]. In Herwig++ the ordering variable is generalised to a mass dependent variable $\tilde{q}$, characterising how close to being on-shell the emitting parton is,

---

[1]The evolution variable in Eq. 2.1 is used since it simplifies the parton-shower kinematics.

defined as

$$\tilde{q}^2 = \frac{q_{\widetilde{ij}}^2 - m_{\widetilde{ij}}^2}{z(1-z)}, \tag{2.2}$$

where z is defined as the light-cone momentum fraction in the Sudakov decomposition and q_{ij}^2 and m are the virtuality and mass of the emitting parton. This evolution variable has the limiting behavior,

$$\tilde{q} = E_{\widetilde{ij}}\theta_{ij} + \mathcal{O}\left(\theta_{ij}^2\right), \tag{2.3}$$

and thus takes into account coherent soft gluon emission via angular ordering. It also allows for the correct description of evolution within the *dead cone* by taking into account the mass of the emitted parton. In the HERWIG shower the dead cone is given an approximate treatment by applying a hard cut, preventing the radiation into this region, while in the Herwig++ shower an exact treatment may be applied using the mass dependent evolution variable in Eq. 2.2 and a set of mass dependent splitting functions.

2.2.1 Shower kinematics

In the Herwig++ parton shower each external parton is interpreted as a *progenitor*, with momentum p_J, for a parton shower. Final-state progenitors initiate forward time-like showers and initial-state progenitors initiate backward space-like showers. These parton showers correspond to generating a series of emission variables $(\tilde{q}, z, \phi)$. This set of splitting variables defines the momentum of the partons in the shower according to the Sudakov decomposition, where the momentum of the ith parton in the parton shower initiated by the progenitor J, is given by

$$q_i = \alpha_i p_J + \beta_i n_J + q_{\perp i}, \tag{2.4}$$

where p_J is the on-shell progenitor momentum, n_J is chosen to be a light-like reference vector with three-momenta equal to that of the colour connected progenitor, defining an appropriate frame in which p and n are back-to-back. The vector $q_{\perp i}$ is defined as the component of momentum transverse to both p_J and n_J, such that the reference vectors satisfy the relations

$$
\begin{aligned}
p_J^2 &= m_J^2, & p_J \cdot q_{\perp i} &= 0, \\
n_J^2 &= 0, & n_J \cdot q_{\perp i} &= 0.
\end{aligned}
\tag{2.5}
$$

The momentum fraction z of each branching is

$$z = \frac{\alpha_i}{\alpha_{\widetilde{ij}}}, \tag{2.6}$$

the scale of the emission $\tilde{q}$ is defined in Eq. 2.2. The relative transverse momentum of the branching is defined by

$$p_{\perp i} = q_{\perp i} - z q_{\perp \widetilde{ij}}. \tag{2.7}$$

The $p_{\perp i}$ vector is written in terms of the azimuthal angle ϕ

$$p_{\perp} = \left(0; |p_{\perp}| \cos\phi, |p_{\perp}| \sin\phi, 0\right). \tag{2.8}$$

The Sudakov decomposition in Eq. 2.4 implies the relation between the Sudakov parameters and virtuality of a parton[2],

$$\beta_i = \frac{\mathbf{q}_{\perp i}^2 + q_i^2 - \alpha_i^2 m^2}{2\alpha_i \left(p \cdot n\right)}, \tag{2.9}$$

where $\mathbf{q}_{\perp i}^2 = -q_{\perp i}^2$ is the positive definite transverse momentum squared.

Momentum conservation implies that the virtuality of the emitting parton in Eq. 2.2 is given by

$$\begin{aligned} q_{\widetilde{ij}}^2 &= q_i^2 + q_j^2 + 2q_i \cdot q_j \tag{2.10} \\ &= q_i^2 + q_j^2 + 2\alpha_i\alpha_j m^2 - 2\mathbf{q}_{\perp i} \cdot \mathbf{q}_{\perp j} + 2p \cdot n \left(\alpha_i\beta_j + \alpha_j\beta_i\right). \end{aligned}$$

Applying Eq. 2.9 to this and utilising the definition of z in Eq. 2.6, the virtuality of the emitter can be written as

$$q_{\widetilde{ij}}^2 = \frac{q_i^2}{z} + \frac{q_j^2}{1-z} - 2\mathbf{q}_{\perp i} \cdot \mathbf{q}_{\perp j} + \frac{z}{1-z}\mathbf{q}_{\perp i}^2 + \frac{1-z}{z}\mathbf{q}_{\perp j}^2. \tag{2.11}$$

We now note that the definition of the transverse momentum in Eq. 2.7 implies the relation

$$\mathbf{p}_{\perp}^2 = (1-z)^2\mathbf{q}_{\perp i}^2 + z^2\mathbf{q}_{\perp j}^2 - z(1-z)\mathbf{q}_{\perp i}^2 \cdot \mathbf{q}_{\perp j}^2, \tag{2.12}$$

---

[2]In this equation we suppress the jet index but it is understood that a different set of reference vectors is used for the shower originating from each progenitor.

so the virtuality of the emitting parton can be expressed in terms of the relative transverse momentum and momentum fraction of the branching together with the virtuality of the resultant partons as

$$q_{\tilde{ij}}^2 = \frac{q_i^2}{z} + \frac{q_j^2}{1-z} + \frac{\mathbf{p}_\perp^2}{z(1-z)}. \tag{2.13}$$

In the parton-shower approximation the resultant partons are deemed on-shell and therefore the Eqs. 2.2 and 2.13 yield the following result for the evolution variable,

$$z(1-z)\tilde{q}^2 = \frac{\mathbf{p}_\perp^2}{z(1-z)} - m_{\tilde{ij}}^2 + \frac{m_i^2}{z} + \frac{m_j^2}{1-z}. \tag{2.14}$$

2.2.2 Shower dynamics

The branching probability is approximated in the *quasi-collinear limit* [8], where the transverse momentum squared, $\mathbf{p}_\perp^2$, and mass squared, m^2, of the branching partons are considered to be small, but $\mathbf{p}_\perp^2/m^2$ is not assumed to be small. In this approximation, the probability of a branching, $\tilde{ij} \to ij$, occurring in the interval $[\tilde{q}^2, \tilde{q}^2 + \mathrm{d}\tilde{q}^2]$, with light-cone momentum fraction in the interval $[z, z + \mathrm{d}z]$, is given by

$$\mathrm{d}\mathcal{P}_{\tilde{ij}\to ij} = \frac{\alpha_S(\tilde{q}, z)}{2\pi} \frac{\mathrm{d}\tilde{q}^2}{\tilde{q}^2} \mathrm{d}z P_{\tilde{ij}\to ij}(z, \tilde{q}), \tag{2.15}$$

where the function $P_{\tilde{ij}\to ij}(z, \tilde{q})$ is the corresponding quasi-collinear splitting function, as derived in Ref. [8]. The strong coupling is evaluated at the scale given by the relative transverse momentum of the branching, $p_\perp(\tilde{q}, z)$, so that the parton shower resumms some important NLL terms in the perturbative series. The splitting functions may be expressed in terms of the branching variables $(\tilde{q}, z)$ with the relevant set of functions for QCD branchings being given by,

$$P_{q\to qg} = \frac{C_F}{1-z}\left[1 + z^2 - \frac{2m_q^2}{z\tilde{q}^2}\right], \tag{2.16}$$

$$P_{g\to gg} = C_A\left[\frac{z}{1-z} + \frac{1-z}{z} + z(1-z)\right], \tag{2.17}$$

$$P_{g\to q\bar{q}} = T_R\left[1 - 2z(1-z) + \frac{2m_q^2}{2(1-z)\tilde{q}^2}\right]. \tag{2.18}$$

The infinitesimal branching probability in Eq. 2.15, gives rise to the Sudakov form factor, as derived in Sect.1.1.4,. This defines the no-emission probability from a parton of flavour

$\widetilde{ij}$, in evolving between the scales $\tilde{q}_1$ and $\tilde{q}_2$,

$$\Delta_{\widetilde{ij}}\left(\tilde{q}_1, \tilde{q}_2\right) = \prod_{i,j} \Delta_{\widetilde{ij}\to ij}\left(\tilde{q}_1, \tilde{q}_2\right), \tag{2.19}$$

where $\Delta_{\widetilde{ij}\to ij}\left(\tilde{q}_1, \tilde{q}_2\right)$ is the no-emission probability for the specific branching $\widetilde{ij} \to ij$ and is given by

$$\Delta_{\widetilde{ij}\to ij}\left(\tilde{q}_1, \tilde{q}_2\right) = \exp\left[-\int_{\tilde{q}_2}^{\tilde{q}_1} \frac{\mathrm{d}\tilde{q}^2}{\tilde{q}^2} \int_{z_-(\tilde{q})}^{z_+(\tilde{q})} \mathrm{d}z \frac{\alpha_S}{2\pi} P_{\widetilde{ij}\to ij}\left(z, \tilde{q}\right)\right]. \tag{2.20}$$

The Herwig++ time-like parton shower can be described, analogously to Eq. 1.112, as a generating functional evolving from a shower progenitor of flavour $\widetilde{ij}$ and initial scale $\tilde{q}_I$, according to

$$\begin{aligned}
\mathcal{S}_{\widetilde{ij}}(\tilde{q}_I) &= \Delta_{\widetilde{ij}}(\tilde{q}_I, \tilde{q}_0)\mathcal{S}_{\widetilde{ij}}(\tilde{q}_0) \\
&+ \int_{\tilde{q}_0}^{\tilde{q}_I} \Delta_{\widetilde{ij}}(\tilde{q}_I, \tilde{q})\mathrm{d}\mathcal{P}_{\widetilde{ij}\to ij}(\tilde{q}, z)\mathcal{S}_i\left(z\tilde{q}\right)\mathcal{S}_j\left((1-z)\tilde{q}\right).
\end{aligned} \tag{2.21}$$

The scales from which the daughter partons i and j evolve are set to $z\tilde{q}$ and $(1-z)\tilde{q}$ respectively, rather than just $\tilde{q}$. This is a consequence of the fact that the evolution variable is approximated by $\tilde{q} \approx E_{\widetilde{ij}}\theta_{ij}$, while $E_i \approx zE_{\widetilde{ij}}$ and $E_j \approx (1-z)E_{\widetilde{ij}}$. Therefore, in order to satisfy the angular ordering condition, that subsequent branchings from the daughter partons must have an opening angle less than θ_{ij}, the factors of z and $1-z$ must be introduced in the maximum evolution scales of the daughter partons, as in Eq. 2.21. Along each shower line this angular ordering condition corresponds to the requirement,

$$\tilde{q}_{i+1} < z_i\tilde{q}_i. \tag{2.22}$$

The region of resolvable emissions is defined by the limits on the integral over z in Eq. 2.20, which are given by $z_\pm$. These limits also ensure that the divergent regions of the splitting functions are avoided. In Herwig++ these limits are imposed by introducing a minimum mass, Q_g, such that all partons are assigned a mass[3]

$$\mu = \max(m, Q_g), \tag{2.23}$$

---

[3]This is used only to define the phase space for resolvable emissions. The physical parton masses are used in the splitting functions.

where m is the physical mass of the parton. A set of natural limits for the integration over z can be found from the requirement that the transverse momentum is real, $\mathbf{p}_\perp^2 > 0$. Equation 2.14 then implies that the limits $z_\pm(\tilde{q})$ can then be found by solving

$$z(1-z)\tilde{q}^2 + \mu_{\tilde{ij}}^2 - \frac{\mu_i^2}{z} - \frac{\mu_j^2}{1-z} > 0. \tag{2.24}$$

This results in a complicated phase-space boundary for resolvable emissions in the $(\tilde{q}, z)$ plane, however it can be shown [6] that an overestimate of the allowed phase-space region is provided by

$$\frac{\mu}{\tilde{q}} < z < 1 - \frac{\mu}{\tilde{q}}. \tag{2.25}$$

The threshold scale at which there is no phase space for resolvable emissions is therefore found somewhere above the scale Q_g. The scale Q_g can thus be taken to be the hadronisation scale at which the parton-shower evolution is terminated. It should be set large enough ($\mathcal{O}(1\,\mathrm{GeV})$) that regions of phase space in which the perturbative expansion is not valid, are avoided.

2.2.3 The initial-state parton shower

The initial-state parton shower is generated as a backward shower, as introduced in Sect. 1.2.3, evolving from the hard sub-process to the incoming hadrons, with soft emissions taken into account by angular ordering. For space-like branchings along the incoming parton line the correct angular ordering prescription is given by [13]

$$E_{i+1}\theta_{i+1} < E_i\theta_i, \tag{2.26}$$

where E_i is the energy of the incoming partons[4] and θ_i is the angle between the incoming parton and the incoming hadron. In HERWIG this is implemented by using the evolution variable

$$\tilde{t} = \frac{-q_i^2}{1-z}, \tag{2.27}$$

which is approximated by $E_i^2\theta_i^2$ so that ordering emissions in this variable satisfies the angular ordering condition. As for the time-like case, in Herwig++ this evolution variable

---

[4]The index of the incoming parton is defined such that is increases in moving along the incoming shower line, away from the hard sub-process, as in Fig. **??**.

is generalised to include the mass of the emitter by defining the evolution variable

$$\tilde{q}^2 = \frac{m_i^2 - q_i^2}{1 - z}. \tag{2.28}$$

The virtuality of the space-like daughter, q_i^2, is related to the transverse momentum squared of the branching according to Eq. 2.13, yielding the expression for the initial-state evolution scale,

$$\tilde{q}^2 = \frac{\mathbf{p}_\perp^2}{(1-z)^2} - \frac{zm_j^2}{(1-z)^2} - \frac{zm_{\widetilde{ij}}^2}{1-z} + \frac{m_i^2}{1-z}. \tag{2.29}$$

The modified Sudakov form factor, as derived in Sect. 1.2.3, giving the no-emission probability for backwards evolution from a parton of flavour i and momentum fraction x, between scales $\tilde{q}_1$ and $\tilde{q}_2$, is

$$\Pi_i\left(\tilde{q}_1, \tilde{q}_2; x\right) = \exp\left[-\sum_{\widetilde{ij}} \int_{\tilde{q}_2}^{\tilde{q}_1} \frac{\mathrm{d}\tilde{q}^2}{\tilde{q}^2} \int_x^{z_+(\tilde{q})} \mathrm{d}z \frac{\alpha_S}{2\pi} P_{\widetilde{ij} \to ij}\left(z, \tilde{q}\right) \frac{f_{\widetilde{ij}}(x/z, \tilde{q})}{z f_i(x, \tilde{q})}\right]. \tag{2.30}$$

The space-like shower can then be described by a generating functional, analogously to Eq. 1.125, which evolves from an initial-state shower progenitor of flavour i, momentum fraction x and initial scale $\tilde{q}_I$, according to

$$\begin{aligned}
\bar{\mathcal{S}}_i(\tilde{q}_I, x) &= \Pi_i(\tilde{q}_I, \tilde{q}_0; x)\bar{\mathcal{S}}_i(\tilde{q}_0, x) \tag{2.31}\\
&+ \int_{\tilde{q}_0}^{\tilde{q}_I} \Pi_i(\tilde{q}_I, \tilde{q}, x) \sum_{\widetilde{ij}} \mathrm{d}\mathcal{P}_{\widetilde{ij} \to ij}(\tilde{q}, z)\bar{\mathcal{S}}_{\widetilde{ij}}(\tilde{q}, x/z) \frac{f_{\widetilde{ij}}(x/z, \tilde{q})}{z f_i(x, \tilde{q})}\mathcal{S}_j((1-z)\tilde{q}).
\end{aligned}$$

We note that in the backward evolution along the incoming line, ordering in $\tilde{q}$ corresponds to angular ordering and so the initial scale of the space-like parent parton, $\widetilde{ij}$, is simply $\tilde{q}$ whereas, for the time-like daughter it must include a factor of the momentum fraction and be set to $(1 - z)\tilde{q}$ to satisfy angular ordering.

In order to define the region of resolvable emissions and in turn the limits on the z integral we introduce a minimum mass for the time-like daughter, assigning a mass according to Eq. 2.23. The lower limit on the z-integration measure is given by the light-cone momentum fraction x in order to prevent the backwards evolution to a parton with $x > 1$ and so we are free to set the masses along the incoming line, m_i and $m_{\widetilde{ij}}$ to zero.

This simplifies the evolution variable to

$$\tilde{q}^2 = \frac{zm_j^2 + \mathbf{p}_\perp^2}{1-z}. \tag{2.32}$$

Assigning a mass, μ (Eq. 2.23), to the time-like daughter parton, together with the requirement that the transverse momentum is real then yields the exact limits on the phase space for a resolvable emission

$$x < z < 1 + \frac{\mu^2}{2\tilde{q}^2} - \sqrt{\left(1 + \frac{\mu^2}{2\tilde{q}^2}\right)^2 - 1}. \tag{2.33}$$

The space-like parton shower is terminated as soon as it evolves below the threshold scale, where there is no phase space available for a resolvable emission.

2.2.4 Initial parton-shower scale

The scale, $\tilde{q}_I$, from which the parton shower is initiated, determines the phase-space region that is accessible to parton-shower emissions. This initial scale is set for each shower progenitor according to the colour flow of the hard sub-process. The initial scales are chosen such that the emission phase space available to each progenitor does not overlap while providing as full as possible a coverage of phase space.

In this section we review the discussion of Ref. [3], considering the two cases that are used in this thesis: the case of two colour connected partons in the final state and the case of two colour connected partons in the initial state.

Final-final colour connection

We consider the case of two colour-connected final-state progenitors b and c, coming from the process $a \rightarrow b + c$, where a is a colour singlet with virtuality Q^2. An example of a hard process of this sort is $e^+e^- \rightarrow q\bar{q}$. In the rest frame of the colour singlet system, we can write the on-shell momentum of the jet progenitors as,

$$p_b = \frac{Q}{2}\left(1 + b - c; 0, 0, \lambda\right) \qquad p_c = \frac{Q}{2}\left(1 - b + c; 0, 0, -\lambda\right), \tag{2.34}$$

where $b = m_b^2/Q^2$, $c = m_c^2/Q^2$ and

$$\lambda = \sqrt{1 + b^2 + c^2 - 2b - 2c - 2bc}. \tag{2.35}$$

In order to explore the phase-space coverage of parton-shower emissions from the two progenitors it is useful to express the phase space for a single emission in terms of the Dalitz variables

$$x_i = \frac{2p_a \cdot q_i}{Q^2}. \tag{2.36}$$

We first consider the case of an emission from parton b where the Sudakov reference vectors are given by the progenitor momentum, p_b, and a light-like vector with three momentum equal to that of c,

$$n_b = \frac{Q}{2}\left(\lambda; 0, 0, -\lambda\right). \tag{2.37}$$

The momentum fractions are therefore given, in terms of the Sudakov parameters, by

$$x_i = (1 + b - c)\,\alpha_i + \lambda\beta_i. \tag{2.38}$$

The momenta of the three parton system, q_b, q_c and q_g, are constructed from the shower emission variables $(\tilde{q}, z)$, such that the momentum of the colour singlet, $p_a = q_b + q_c + q_g$, is preserved. Applying momentum conservation and on-shell conditions to the parton momenta q_i, together with the definitions of the shower variables in Eqs. 2.6 and 2.14, it can be shown that the momentum fractions are given by [3]

$$\begin{aligned}
x_c &= 1 - b + c - z(1 - z)\tilde{k}, \\
x_b &= (2 - x_c)\,r + (z - r)\,\sqrt{x_c^2 - 4c}, \\
x_g &= (2 - x_c)\,(1 - r) - (z - r)\,\sqrt{x_c^2 - 4c}.
\end{aligned} \tag{2.39}$$

where

$$r = \frac{1}{2}\left(1 + \frac{b}{1 + c - x_c}\right), \tag{2.40}$$
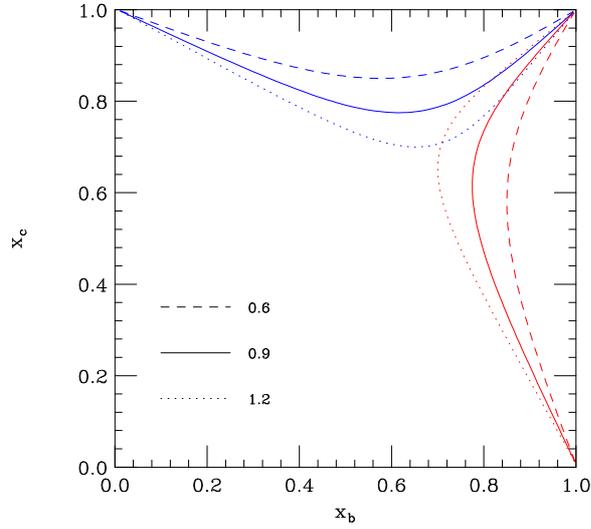
Figure 2.1: Contours of constant $\tilde{k} = 0.6$, 0.9, 1.2 in Dalitz space for an emission from parton b (red) and c (blue).

and we have introduced the dimensionless variant of the evolution variable,

$$\tilde{k} = \frac{\tilde{q}^2}{Q^2}. \tag{2.41}$$

The equivalent expressions for emission from parton c are given by the Eqs. 2.39 with the replacements $b \to c$ and $x_b \to x_c$.

Equations 2.39 can be used to eliminate z, defining a contour of constant $\tilde{k}$. This is shown for a selection of values of $\tilde{k}$ in Fig. 2.2.4. The limit to the phase-space region accessible to emissions from each progenitor is given by the initial scale, $\tilde{k}_I = \tilde{q}^2/Q^2$, which we define as $\tilde{k}_b$ and $\tilde{k}_c$ respectively for the progenitors b and c.

These regions are chosen such that they do not overlap while providing a smooth coverage of the phase space of enhanced emissions. This is obtained by requiring that in the limit of a soft emission, $z \to 1$, the phase-space limits of the two regions coincide. In the limit $z \to 1$, Eq. 2.39 yields the contour,

$$\lim_{\substack{b \text{ emits}}} x_c(\tilde{k}) = 1 - b + c + \frac{(x_b - 1 - b + c)\,2b\tilde{k}}{2b\lambda + \tilde{k}\,(1 - b - c - \lambda)}. \tag{2.42}$$

The equivalent contour for emission from parton c is given by

$$\lim_{c\text{ emits}} x_c(\tilde{k}) = 1 - b + c + \frac{(x_b - 1 - b + c)\left(\lambda + \tilde{k}(1 - b - c - \lambda)\right)}{\tilde{k}}. \tag{2.43}$$

The requirement that the phase-space limits for the two emitters coincide in the soft limit can be expressed as

$$\lim_{b\text{ emits}} x_c(\tilde{k}_b) = \lim_{c\text{ emits}} x_c(\tilde{k}_c) \tag{2.44}$$

which, from Eqs 2.42 and 2.43, gives the condition that the initial scale must satisfy,

$$\left(\tilde{k}_b - b\right)\left(\tilde{k}_c - c\right) = \frac{1}{4}(1 - b - c + \lambda)^2. \tag{2.45}$$

The default choice for the initial scales is taken to be the most symmetric choice of scales q_b and q_c, satisfying Eq. 2.45

$$\tilde{q}_b = \frac{Q^2}{2}(1 + b - c + \lambda), \tag{2.46}$$

$$\tilde{q}_c = \frac{Q^2}{2}(1 + c - b + \lambda), \tag{2.47}$$

such that in the case where the masses of the progenitors b and c are equal, the initial scales are the same and the emission phase space is split evenly between the two progenitors.

The phase-space regions for emission from the two progenitors are illustrated in Fig. 2.2.4, for the case in which the masses of the two progenitors are equal. We see that the allowed regions provide a smooth coverage of the enhanced soft and collinear regions of phase space. However, there is also a central region that is inaccessible to parton-shower emissions from either progenitor. This is referred to as the *dead zone* and corresponds to emissions with large transverse momentum.

Initial-initial colour connection

We now consider the case of a hard process consisting of two colour connected partons b and c in the initial state taking part in a process $b + c \rightarrow a$ where a is a colour singlet system with virtuality Q^2. An example of a process of this type is Drell-Yan vector boson production. In this case the two incoming partons in the hard process are taken
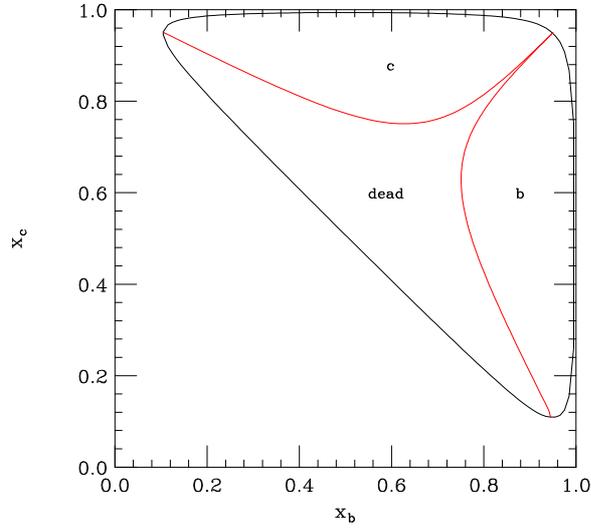
Figure 2.2: The allowed phase-space region for an emission from a pair of colour connected final-state partons b and c with masses $m_b = m_c = 5\,\text{GeV}$, at a centre-of-mass energy $Q = 91.2\,\text{GeV}$. The regions shown are the phase space for emissions from partons b and c and the dead zone which is not accessible to emissions from either parton.

to be progenitors of initial-state showers. The momentum of these progenitors is given by

$$p_b = \frac{Q}{2}\,(1; 0, 0, 1) \qquad\qquad p_c = \frac{Q}{2}\,(1; 0, 0, -1)\,, \tag{2.48}$$

where the mass of the incoming momentum is taken to be zero, as is done throughout for initial-state partons. The reference vectors, defining the Sudakov basis, are therefore given by $p = p_b$, $n = p_c$ for emission from parton b and $p = p_c$, $n = p_b$ for emission from parton c.

The phase space covered by the emission of a gluon of momentum, q_g, from partons b and c is conveniently expressed in terms of a set of dimensionless Mandelstam variables, which are defined by

$$\bar{s} = \frac{(q_b + q_c)^2}{Q^2}, \qquad \bar{t} = \frac{(q_b - q_g)^2}{Q^2}, \qquad \bar{u} = \frac{(q_c - q_g)^2}{Q^2}, \tag{2.49}$$

where q_b and q_c are the momenta of the incoming partons, as reconstructed from the shower variables $(\tilde{q}, z)$. The full allowed phase-space region is given by the limits

$$1 < \bar{s} < s/Q^2, \qquad 1 - \bar{s} < t < 0, \tag{2.50}$$

where s is the beam centre-of-mass energy squared.

In constructing the parton momentum from the shower variables describing the emission, the colour singlet system, a, obtains a recoil transverse momentum so we cannot preserve the momentum of the colour singlet system, as was done in the final-state case. Instead we choose to preserve its mass and rapidity. Following this procedure, the Mandelstam variables can be written in terms of the shower variables as [3]

$$\bar{s} = \frac{1}{z}\left[1 + (1 - z)\tilde{k}\right], \qquad \bar{t} = -(1 - z)\tilde{k}, \qquad \bar{u} = -(1 - z)\bar{s}. \qquad (2.51)$$

The corresponding Mandelstam variables for an emission from parton c are given by the same equations with the replacement $\bar{t} \leftrightarrow \bar{u}$.

Eliminating z from Eqs. 2.51, we find contours of constant $\tilde{k}$, which are given by

$$\bar{t} = \frac{(1 - \bar{s})\tilde{k}}{(\bar{s} + \tilde{k})}, \qquad (2.52)$$

for emission from parton b and

$$\bar{t} = \frac{(1 - \bar{s})\bar{s}}{(\bar{s} + \tilde{k})}, \qquad (2.53)$$

for emission from parton c.

We require a smooth coverage of the region of phase space associated with enhanced emissions. The phase space regions accessible to emissions from the two progenitors should also not overlap. This dictates that in the soft limit, which is characterised by $\bar{s} \to 1$, the limits of the available phase space for the two progenitors should coincide. As in the final-state case, the important phase-space limit is given by the contours in Eqs. 2.52 and 2.53 evaluated at the maximum scales for $\tilde{k}_b$ and $\tilde{k}_c$, respectively. This gives

$$\tilde{k}_b\tilde{k}_c = 1. \qquad (2.54)$$

As in the final-state case, by default the most symmetric choice is taken where $\tilde{k}_b = \tilde{k}_c = 1$.

The allowed regions of emission with this choice of initial scale are illustrated in Fig. 2.2.4. Again, we see that requiring that the two-emission regions do not overlap leads to a dead-zone region that is not accessible to emissions from either parton.
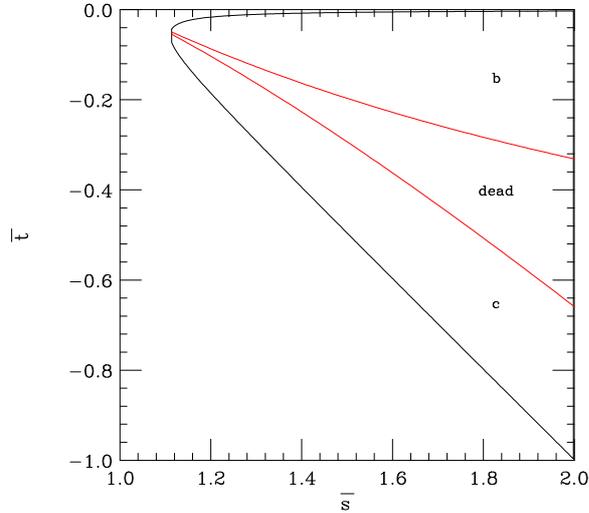
Figure 2.3: The allowed phase-space region for an emission from a pair of colour connected
initial-state partons b and c with the mass of the emitted parton $m_g = 5\,\text{GeV}$, at
a centre-of-mass energy $Q = 91.2\,\text{GeV}$. The regions shown are the phase space
for emissions from partons b and c and the dead zone which is not accessible to
emissions from either parton.

2.2.5 The shower algorithm

The generation of the variables $(\tilde{q}_i, z_i, \phi_i)$, describing the emissions of the parton shower,
is performed in Herwig++ using the *veto algorithm*. This algorithm is discussed in
Appendix A.2. In this section we present the specifics of the algorithm used in Herwig++.

In Herwig++ the azimuthal angle of each branching, ϕ, is generated flat in the region
$[0, 2\pi]$. This amounts to neglecting the effects of spin correlations whereby the parton-
shower algorithm reduces to the generation of the variables $(\tilde{q}_i, z_i)$.

The final-state shower algorithm

The bivariant veto algorithm, described in Appendix A.3, dictates how we may gen-
erate an evolution variable, t, and an auxiliary splitting variable, z, according to the
distribution

$$f(t, z) \exp - \left[\int_t^{t_I} \mathrm{d}t \int \mathrm{d}z' f\left(z', t'\right) \right]. \tag{2.55}$$

The veto algorithm is then constructed by defining a bounding function for $f(t,z)$, defined such that

$$g_t(t)g_z(z) > f(t,z) \qquad \forall (t,z). \tag{2.56}$$

This function must be simple enough that its primitive integral and associated inverse can be found.

From the final-state shower equation (Eq. 2.21), we see that the expression corresponding to $f(t,z)$ for the final-state parton shower is given by

$$\frac{\alpha_S(\tilde{q},z)}{2\pi} \frac{1}{\tilde{q}^2} P_{\widetilde{ij}\to ij}\left(z,\tilde{q}\right), \tag{2.57}$$

where the evolution variable, t, corresponds to $\tilde{q}^2$ in Herwig++. A bounding function can be found by introducing the constant α_S^{over} which provides a bound for the running coupling and a set of functions of z, $P_{\widetilde{ij}\to ij}^{\text{over}}(z)$, which provide a bound to the splitting functions. The overestimates for the relevant splitting functions are given by,

$$P_{q\to qg}^{\text{over}} = \frac{2C_F}{1-z}, \tag{2.58}$$

$$P_{g\to gg}^{\text{over}} = C_A\left[\frac{1}{1-z} + \frac{1}{z}\right], \tag{2.59}$$

$$P_{g\to q\bar{q}}^{\text{over}} = T_R. \tag{2.60}$$

We define the primitive integral of these functions as $I_{\widetilde{ij}\to ij}(z)$.

The limits on z for an emission to be considered resolvable are found by requiring that the transverse momentum, constructed from the shower variables, is real. For the case of time-like emissions this corresponds to a complicated boundary in $(\tilde{q},z)$ space, however the limits for a general branching can be approximated in terms of the minimum parton virtuality, Q_g,

$$z_{\max} = \frac{Q_g}{\tilde{q}}, \qquad z_{\min} = 1 - \frac{Q_g}{\tilde{q}}. \tag{2.61}$$

In practice, tighter, branching specific limits are employed, as detailed in Ref. [6], to allow a more efficient algorithm.

The veto algorithm generation of the next time-like emission, $(\tilde{q},z)$, from a parton of flavour $\widetilde{ij}$ and scale $\tilde{q}_I$, proceeds according to:

1. start at $i = 0$ with $\tilde{q}_0 = \tilde{q}_I$;

2. the next scale is generated according to

$$\tilde{q}_i^2 = \tilde{q}_{i-1}^2 \mathcal{R}^{C(\tilde{q}_{i-1})}, \tag{2.62}$$

where $C(\tilde{q}_{i-1})$ is defined as

$$C(\tilde{q}) = \frac{2\pi}{\alpha_S^{\text{over}}} \left[I_{\widetilde{ij}\to ij} \left(z_{\max} \right) - I_{\widetilde{ij}\to ij} \left(z_{\min} \right) \right], \tag{2.63}$$

3. a light-cone momentum fraction z is simultaneously generated according to

$$z = \left[\mathcal{R} \left(I_{\widetilde{ij}\to ij} \left(z_{\max} \right) - I_{\widetilde{ij}\to ij} \left(z_{\min} \right) \right) + I_{\widetilde{ij}\to ij} \left(z_{\min} \right) \right]; \tag{2.64}$$

4. the emission $(\tilde{q}, z)$ is accepted if

$$\mathcal{R} < w_1(\tilde{q}, z) w_2(\tilde{q}, z) w_3(\tilde{q}, z) \tag{2.65}$$

where the weights $w_{1,2,3}$ are the veto probabilities that are required to compensate for the approximations used in the phase-space limits, splitting function and strong coupling respectively;

5. if the emission is rejected then return to step 2.

The weights $w_{1,2,3}$, used as the acceptance probabilities in step 4 of the algorithm, are given by

$$
\begin{aligned}
w_1(\tilde{q}, z) &= \theta \left(\mathbf{p}_\perp^2 \right), \\
w_2(\tilde{q}, z) &= \frac{P_{\widetilde{ij}\to ij} \left(z, \tilde{q} \right)}{P_{\widetilde{ij}\to ij}^{\text{over}} \left(z \right)}, \\
w_3(\tilde{q}, z) &= \frac{\alpha_S \left(\tilde{q}, z \right)}{\alpha_S^{\text{over}} \left(\tilde{q}, z \right)}.
\end{aligned}
\tag{2.66}
$$

In order to take into account that several branching types, $\widetilde{ij} \to ij$, may be generated from a shower line of flavour $\widetilde{ij}$, this algorithm is augmented to *generate by competition*, as discussed in Appendix A.4. This means that an emission, $(\tilde{q}, z)$, of each possible type is generated and the one with the highest evolution scale, $\tilde{q}$, selected.

The initial-state shower algorithm

The Herwig++ backward initial-state parton shower is defined by Eq. 3.35 and can by generated using a veto algorithm in a similar manner to the final-state parton shower. As in the final-state case, each initial-state emission, $(\tilde{q}, z)$ is selected from a probability distribution of the form given in Eq. 2.55. The branching probability is in this case given by

$$\frac{\alpha_S}{2\pi} \frac{1}{\tilde{q}^2} P_{\widetilde{ij} \to ij}(z, \tilde{q}) \frac{f_{\widetilde{ij}}(x/z, \tilde{q})}{z f_i(x, \tilde{q})}, \tag{2.67}$$

which differs from the final-state case by the inclusion of a function of PDFs and momentum fractions,

$$\frac{f_{\widetilde{ij}}(x/z, \tilde{q})}{z f_i(x, \tilde{q})}, \tag{2.68}$$

for which we can define a constant upper bound K_{PDF}.

The initial-state branchings can therefore be generated with the algorithm of Sect. 2.2.5 with the following modifications,

- the function $C(\tilde{q})$ used in step 2 gains an extra factor of K_{PDF} becoming

$$C(\tilde{q}) = \frac{2\pi}{\alpha_S^{\text{over}} K_{PDF}} \left[I_{\tilde{ij} \to ij}(z_{\max}) - I_{\tilde{ij} \to ij}(z_{\min}) \right]; \tag{2.69}$$

- an extra veto is applied in step 4 with a probability given by the weight

$$w_4(\tilde{q}, z) = \frac{f_{\widetilde{ij}}(x/z, \tilde{q})}{z f_i(x, \tilde{q}) K_{PDF}}. \tag{2.70}$$

2.2.6 Momentum reconstruction

Once all of the partons have evolved down to the hadronisation scale, the shower evolution is stopped and the momentum of all external and intermediate partons are reconstructed from the shower variables. This is done in the centre-of-mass frame via the Sudakov decomposition as defined in Eq. 2.4. This procedure is referred to as the *momentum reconstruction*. We will go on to describe how this is performed for final- and initial-state parton showers.

Final-state momentum reconstruction

The Sudakov variables α_i, β_i and $q_{\perp i}$, defining the reconstructed shower momentum q_i are calculated from the shower variables recursively for all partons in the shower jet[5]. This is done starting from the shower progenitor, where we set the parameters $\alpha_0 = 0$ and $q_{\perp 0} = \mathbf{0}$. The α_i parameters can then all be found by working recursively down all shower lines and applying the definition of z in Eq. 2.6. The definition of the evolution variable in Eq. 2.14, together with the definition of the azimuthal angle in Eq. 2.8, allow the relative transverse momentum, $\mathbf{p}_\perp$, to be determined. The definition of the relative transverse momentum in Eq. 2.7 then allows the parameters q_i to be found by following all shower lines recursively from the shower progenitor. The remaining parameters, β_i, are related to the partons virtuality according to Eq. 2.9. The virtuality is fixed only for the end points of the shower which are given their on-shell mass. The β-parameters of the other partons can then be found by following the shower lines backwards from the shower end points to the shower progenitors and applying the momentum conservation condition,

$$\beta_{\widetilde{ij}} = \beta_i + \beta_j. \tag{2.71}$$

Having calculated the Sudakov parameters for all partons in the shower, their momenta are constructed according to Eq. 2.4.

Final-state reshuffling

After the momentum reconstruction procedure, the momenta of the reconstructed shower progenitors, q_J, are pushed off their mass-shell. In the hard sub-process these partons were assumed to be on-shell and this therefore leads to the loss of global momentum conservation. The parton-shower momenta must therefore be *shuffled* in order to enforce global momentum conservation while disturbing the jet structure as little as possible. This is done by the application of a set of longitudinal boosts to each shower jet such that momentum conservation is restored. These reshuffling boosts are defined for each jet by the transformation

$$\left(\mathbf{q}_J; \sqrt{\mathbf{q}_J^2 + q_J^2} \right) \to \left(k\mathbf{p}_J; \sqrt{k^2\mathbf{p}_J^2 + q_J^2} \right) \equiv q_J'. \tag{2.72}$$

---

[5]The term *shower jet* is used here to refer to the set of partons produced by showering a progenitor.

Momentum conservation is ensured by requiring that the rescaling parameter k satisfies

$$\sum_J \sqrt{k^2 \mathbf{p}_J^2 + q_J^2} = \sqrt{s}. \tag{2.73}$$

This equation can be solved to find k, defining a boost for each shower jet according to Eq. 2.72. These boosts should be applied to the momenta of all partons in the shower jet, determining the full set of shuffled parton momenta.

Initial-state momentum reconstruction

In the case of an initial-state parton shower, the reference vectors defining the Sudakov basis are given by the on-shell (massless) beam momenta, $p_\oplus$. It is now the end point of the backwards evolving shower, parton k, that has transverse momentum,

$$q_{\perp k} = \mathbf{0}, \tag{2.74}$$

and therefore it is here that the momentum reconstruction begins. Since the reference vector p_J is given by the corresponding beam momentum, the α-parameter of this parton is given by its light-cone momentum fraction, which is

$$\alpha_k = \prod_{i=0}^{k} \frac{x}{z_i}, \tag{2.75}$$

where x is the light-cone momentum fraction of the parton involved in the hard sub-process. Since this is an external parton and parton masses along the initial state line are set to zero, Eq. 2.9 tells us also that

$$\beta_k = 0. \tag{2.76}$$

The momentum of the end point of the initial-state shower, q_k is then fully determined.

In order to determine the Sudakov parameters for the other partons along the initial-state shower we trace along this line from the end point to the hard sub-process. At each emission along this line the momenta of the partons in the shower initiated by the time-like daughter can be constructed. The momentum of the space-like daughter parton, q_i, can then be constructed from the momentum of the space-like parent, $q_{\widetilde{ij}}$,

and the momentum of the time-like daughter from momentum conservation,

$$q_i = q_{\widetilde{ij}} - q_j. \tag{2.77}$$

This procedure can be iterated all the way along the initial-state line, constructing the momentum of all the partons in the initial-state shower.

Initial-state reshuffling

After reconstructing the momentum of the partons in the shower, the two initial-state partons entering the hard sub-process have both a transverse momentum and space-like virtuality. This results in a mismatch between the incoming shower partons and the incoming partons of the hard sub-process which were assumed to be on-shell and have zero transverse momentum.

As in the final-state case, we are therefore required to apply reshuffling boosts to the shower momenta and the momenta of the particles produced in the hard sub-process in order to enforce global momentum conservation.

In order to make our notation clear at this point, we review the different momentum definitions that we make use of, for the incoming partons entering the hard sub-process:

- the (on-shell) momenta of the incoming partons from the hard sub-process, $p_{\oplus}$, are given by

$$p_{\oplus} = x_{\oplus} P_{\oplus}, \tag{2.78}$$

  where $P_{\oplus}$ are the beam momenta;
- the momenta of the incoming partons entering the hard sub-process after the shower momentum reconstruction, $q_{\oplus}$;
- the corresponding reshuffled momenta, $q'_{\oplus}$.

In order to discuss the reshuffling procedure, we limit ourselves to the case of hard sub-processes describing the production of a colour singlet system, such as Drell-Yan vector boson production. For hard sub-processes with coloured partons in both final- and initial-states, a more complicated procedure must be employed, as detailed in Ref. [3]. However, for the processes considered in this thesis the simpler procedure we describe is sufficient.

The reshuffling boosts, that are to be applied to all partons produced in the showers generated from the two initial-state progenitors, are defined by

$$q_{\oplus} \rightarrow q'_{\oplus} = \alpha_{\oplus} k_{\oplus} p_{\oplus} + \frac{\beta_{\oplus}}{k_{\oplus}} p_{\oplus} + q_{T\oplus}, \tag{2.79}$$

where the two boosts are determined by the parameters, $k_{\oplus}$

As discussed in Sect. 2.2.4, the momentum of the colour-singlet system produced in the hard sub-process must receive a recoil transverse momentum and therefore we cannot require these boosts to preserve the momentum of the hard sub-process. Instead we choose a set of boosts that preserve the invariant mass and rapidity of the centre-of-mass system. The requirement that the rapidity is preserved yields the equation,

$$\frac{x_{\oplus}}{x_{\ominus}} = \frac{\alpha_{\oplus} k_{\oplus} + \frac{\beta_{\ominus}}{k_{\ominus}}}{\alpha_{\ominus} k_{\ominus} + \frac{\beta_{\oplus}}{k_{\oplus}}}. \tag{2.80}$$

Requiring that the invariant mass is preserved results in the equation

$$s x_{\oplus} x_{\ominus} = \left(\alpha_{\oplus} k_{\oplus} + \frac{\beta_{\ominus}}{k_{\ominus}} \right) \left(\alpha_{\ominus} k_{\ominus} + \frac{\beta_{\oplus}}{k_{\oplus}} \right) s + \left(q_{\perp\oplus} + q_{\perp\ominus} \right)^2, \tag{2.81}$$

where s is the hadronic centre-of-mass energy squared. Equations 2.81 and 2.80 may be solved to obtain $k_{\oplus}$ and $k_{\ominus}$, allowing the two boosts to be obtained from their definition in Eq. 2.79. These boosts are applied recursively to all partons resulting from the shower initiated by the incoming progenitors. Finally, since the reshuffling boosts were required to preserve the invariant mass of the system, the momentum of the colour singlet produced in the hard sub-process, $p_a = p_{\oplus} + p_{\ominus}$, and the momentum of the colour singlet after the shower momentum construction and reshuffling, $q'_a = q'_{\oplus} + q'_{\ominus}$, are related by a boost. Thus, by applying the boost defined by,

$$p_{\oplus} + p_{\ominus} \xrightarrow{\text{boost}} q'_{\oplus} + q'_{\ominus}, \tag{2.82}$$

to the colour-singlet system and all its decay products, it receives the recoil transverse momentum and global momentum conservation is restored.

2.3 Improving the parton shower

While the parton shower accurately simulates soft and collinear radiation, it does not provide a reliable description of hard (high transverse momentum) emissions. In particular the presence of the dead zone represents a deficiency in the description of hard radiation. Even within the accessible shower regions of phase space, the distribution of radiation involves some degree of approximation, since at any given fixed order in perturbation theory, the parton shower effectively approximates the real emission corrections to the hard scattering process by a product of splitting functions and Sudakov form factors, summed over all combinations of branchings which give rise to the same final state. The approximations account for the NLL corrections associated with soft and collinear radiation in the perturbative series.

Fixed-order matrix elements have a number of advantages over the parton-shower description, in particular they provide:

- a reliable treatment in the high-transverse-momentum region;
- an exact treatment of interference effects;
- an exact treatment of finite $N_C = 3$ effects.

It is therefore appealing to combine the virtues of the parton shower and fixed-order matrix elements such that the best features of both are included. Schemes that do this are referred to as matrix-element merging and matching schemes. The development of these schemes has been one of the major advances in Monte Carlo QCD in recent years and has received much attention. In this thesis we focus on improving the description of the Herwig++ parton shower, in the large-transverse-momentum region, with two such schemes. In chapters 3 and 4, we describe an implemention of the POWHEG matching scheme which combines NLO matrix elements with the parton shower. In chapter 5, an implementation of a modified CKKW matrix-element merging scheme is described, which combines higher-order tree-level matrix elements with the parton shower.

In the following section we describe the *matrix-element correction* method, which is the default scheme implemented in Herwig++.

2.3.1 Matrix-element corrections

The earliest and simplest means of forming this combination is known as the matrix-element correction method [43, 44]. This corrects the hardest emission generated by the parton shower such that it is distributed according to the real single emission matrix-element squared. This technique has been successfully applied to important processes in a number of generators [45, 46], including Herwig++ [6].

The method consists of two distinct corrections: *hard* and *soft* matrix-element corrections. We proceed to describe these methods and their implementation in Herwig++.

Soft matrix-element corrections

The soft matrix-element correction aims to correct the hardest parton-shower emission such that it is generated according to the exact $\mathcal{O}(\alpha_S)$ radiative correction. In the parton-shower approximation, the infinitesimal branching probability is given by $\mathrm{d}\mathcal{P}_{\widetilde{ij} \to ij}$ as defined in Eq. 2.15. In order for the hardest emission to be generated according to the exact radiative cross section, σ_r, we require the replacement

$$\mathrm{d}\mathcal{P}_{\widetilde{ij} \to ij}(\tilde{q}, z) \to \mathrm{d}\mathcal{P}^{ME}_{\widetilde{ij} \to ij}(\tilde{q}, z) = \mathrm{d}\tilde{q}^2 \mathrm{d}z \frac{1}{\sigma_b} \frac{\mathrm{d}^2\sigma_r}{\mathrm{d}\tilde{q}^2 \mathrm{d}z}. \tag{2.83}$$

If the strong coupling in σ_r is evaluated at the transverse momentum, as in the parton shower, then this will preserve the NLL resummation of the shower.

For processes where the parton-shower branching probability provides an overestimate of the matrix-element corrected branching probability, [6] in Eq. 2.83, it is straightforward to achieve the required replacement. This is done by augmenting the parton-shower veto algorithm, described in Sect. 2.2.5 to include an extra weight,

$$w_{\mathrm{ME}} = \frac{\mathrm{d}\mathcal{P}^{ME}_{\widetilde{ij} \to ij}(\tilde{q}, z)}{\mathrm{d}\mathcal{P}_{\widetilde{ij} \to ij}(\tilde{q}, z)}, \tag{2.84}$$

in the acception probability of step 4 of the veto algorithm. This results in the hardest emission being generated according to

$$\mathrm{d}\mathcal{P}^{ME}_{\widetilde{ij} \to ij}(\tilde{q}, z) \exp\left(-\int_{\tilde{q}}^{\tilde{q}_I} \mathrm{d}\mathcal{P}^{ME}_{\widetilde{ij} \to ij}(\tilde{q}, z) \right), \tag{2.85}$$

---

[6]This is the case for $e^+e^- \to$ hadrons and Drell-Yan vector boson production.

as required. For processes in which the parton-shower branching probability does not overestimate the matrix-element branching probability it is possible to introduce an enhancement factor to the parton-shower emissions, which is then taken into account in the acceptance probability, such that the same procedure can be used.

The hardest emission in the Herwig++ parton shower is not necessarily the first emission and may be preceded by wide-angle soft emissions. However, since the corrected branching probability in Eq. 2.83 matches that of the parton shower in the NLL approximation, the matrix-element veto can also be applied to these emissions with only subleading differences. The procedure used is to apply the correction to any emission that is the hardest so far.

Hard matrix-element corrections

Hard matrix-element corrections fill the dead zone with emissions generated according to the $\mathcal{O}(\alpha_S)$ radiative correction. This is done by generating at most one emission according to

$$\frac{1}{\sigma_b} \int_{R_{\mathrm{dead}}} \mathrm{d}x_1 \mathrm{d}x_2 \frac{\mathrm{d}^2 \sigma_r}{\mathrm{d}x_1 \mathrm{d}x_2}, \tag{2.86}$$

where R_{dead} refers to the dead-zone region of phase space, corresponding to the condition $\tilde{q}(x_1, x_2) > \tilde{q}_I$. The radiative variables, x_1 and x_2, parameterise the phase space for the radiative correction (as suggested by the notation, they are the Dalitz variables for the case of $e^+e^- \to$ hadrons).

In order to fill the dead zone, a hard emission is generated before the parton shower begins according to the distribution in Eq. 2.86. This is done by first, generating a set of radiative variables, (x_1, x_2), in the dead region and then accepting the emission if

$$w_{\mathrm{ME-hard}} > \mathcal{R}, \tag{2.87}$$

where

$$w_{\mathrm{ME-hard}} = \frac{1}{\sigma_b} \frac{\mathrm{d}^2 \sigma_r}{\mathrm{d}x_1 \mathrm{d}x_2}. \tag{2.88}$$

If the emission is rejected, no hard emission is generated in the dead zone. The parton shower is then initiated from the resulting partons.

This correction does not include a Sudakov form factor in the distribution of the hardest emission generator and therefore corresponds to approximating the exclusive hardest emission probability with the inclusive distribution given by the radiative cross section. This approximation is valid since the contribution of the cross section in the dead-zone region is generally small and therefore the corresponding Sudakov form factor is close to one.

2.4 Summary

The Herwig++ parton shower is an angular-ordered shower based on a new ordering variable which represents an improvement over that of the HERWIG parton shower in terms of Lorentz invariance and the treatment of mass effects. In this chapter we have described the details of the Herwig++ initial- and final-state parton showers which form the foundation of the work of this thesis.

The technique of matrix-element corrections, where the parton-shower description is improved using exact matrix elements, was also introduced. In Chapters 3-6, we focus on the implementation of more sophisticated matrix-element merging methods.

Chapter 3

NLO matching with the POWHEG method

3.1 Introduction

The parton shower represents an indispensable tool for describing high-multiplicity final states, however this approach is traditionally based around a leading-order cross section. For sufficiently inclusive observables, the best available description comes instead from fixed-order calculations, which may be performed beyond leading order, for which next-to-leading-order has become standard. In this chapter we discuss NLO matching techniques which aim to combine parton showers with fixed-order NLO calculations such that the virtues of each approach are retained.

The chapter is organised as follows. In Sect. 3.2, the general features of NLO calculations are reviewed and existing NLO matching techniques are reviewed. In Sect 3.3, a novel approach to NLO matching, known as the POWHEG method, is reviewed. In Sect 3.4, an implementation of the POWHEG method, in Herwig++, for the process $e^+e^- \to$ hadrons, is described.

3.2 Matching NLO calculations with parton showers

3.2.1 NLO calculations

For a general $2 \to n$ process, where the incoming parton momenta are given by $p_\oplus$ and the final-state momenta are given by p_i, the NLO cross section can be written in the

form

$$d\sigma_{NLO} = B(\mathbf{\Phi_n})d\Phi_n + V_0(\mathbf{\Phi_n})d\mathbf{\Phi_n} + R_0(\mathbf{\Phi_{n+1}})d\mathbf{\Phi_{n+1}}, \tag{3.1}$$

where $\mathbf{\Phi_n}$ and $\mathbf{\Phi_{n+1}}$ represent the phase space of n and $n+1$ final-state particles and the functions $B(\mathbf{\Phi_n})$, $V_0(\mathbf{\Phi_n})$ and $R_0(\mathbf{\Phi_{n+1}})$ represent the Born, virtual and radiative contributions respectively. The subscript on the virtual and radiative terms denotes that these are divergent quantities.

To be more specific, we define $\mathbf{\Phi_n}$ as the set of variables describing the phase space of the final-state particle momenta, p_i, and light-cone momentum fractions of the incoming partons, $x_{\oplus}$,

$$\mathbf{\Phi_n} = \{x_{\oplus}, x_{\ominus}, p_1, ..., p_n\}. \tag{3.2}$$

The corresponding phase-space element is

$$d\mathbf{\Phi_n} = dx_{\oplus}dx_{\ominus}d\Phi_n\left(p_{\oplus} + p_{\ominus}; p_1, ..., p_n\right), \tag{3.3}$$

where $d\Phi_n$ is the usual Lorentz invariant phase-space element, as given in Eq. 1.16. The equivalent phase-space variables and integration element for configurations with $n+1$ final-state particles are given by the same equations with $n \to n+1$.

The functions $B(\mathbf{\Phi_n})$, $V_0(\mathbf{\Phi_n})$ and $R_0(\mathbf{\Phi_{n+1}})$ are given products of the appropriate matrix elements squared with corresponding flux factor and luminosity functions, $\mathcal{L}(x_{\oplus}, x_{\ominus})$. The luminosity functions contain the PDFs of the incoming partons and are defined by,

$$\mathcal{L} = f_{\oplus}\left(x_{\oplus}\right)f_{\ominus}\left(x_{\ominus}\right). \tag{3.4}$$

For the case of lepton-lepton scattering, the PDFs are replaced by $\delta\left(x_{\oplus} - 1\right)$.

The matrix elements squared in the virtual contribution, $\mathcal{V}(\mathbf{\Phi_n})$, come from the interference between the Born diagram and the one-loop corrections to it. The contribution contains both ultra-violet and infra-red divergences. The ultra-violet divergences are removed by renormalisation, where the divergences are absorbed into the physical parameters of the QCD Lagrangian. In the following we assume that all ultra-violet have been renormalised and that Eq. 3.1 contains only infra-red divergences.

As well as in the virtual contribution, infra-red divergences occur in the radiative contributions. As discussed in Sect. 1.1.4, these divergences arise whenever an external final-state parton is soft or in a configuration where it is collinear to another final-state parton or one of the initial-state partons. We refer to these three cases as soft (S), final-state-collinear (FSC) and initial-state-collinear (ISC) divergences, respectively. These divergences can be parameterised using dimensional regularisation, where the divergent contributions are calculated in $d = 4 - 2\epsilon$ dimensions where they are integrable. The singularities then appear as terms with poles in ϵ. The KLN theorem [19] dictates that, for any infrared-safe observable, the soft and final-state-collinear divergences must cancel. The initial-state-collinear divergences from the radiative contribution are not cancelled by the virtual contribution but should instead be factorised into the definition of the physical PDFs.

The expectation value of a general infra-red safe observable, O, may be written, at NLO in α_S, as

$$\langle O \rangle = \int d\boldsymbol{\Phi}_n O_n\left(\boldsymbol{\Phi}_n\right) \left[B\left(\boldsymbol{\Phi}_n\right) + V_0\left(\boldsymbol{\Phi}_n\right)\right] + \int d\boldsymbol{\Phi}_{n+1} O_{n+1}\left(\boldsymbol{\Phi}_{n+1}\right) R_0\left(\boldsymbol{\Phi}_{n+1}\right), \quad (3.5)$$

where the functions O_n and O_{n+1} give the observable quantity as a function of the n and $n + 1$ final-state momenta, respectively. By explicitly cancelling the regulated S and FSC divergences between virtual and radiative corrections and absorbing the ISC divergences into the PDFs, this integral can be evaluated to calculate finite values for infra-red safe observables.

3.2.2 Subtraction

It is desirable to provide an exclusive treatment of Eq. 3.1, using Monte Carlo methods to generate final-state configurations, $\boldsymbol{\Phi}_n$ and $\boldsymbol{\Phi}_{n+1}$, from which any observable quantities may be calculated. This requires a numerical evaluation of Eq. 3.5. Furthermore, as more complicated processes are considered, the procedure of cancelling the divergences in the radiative terms becomes more difficult and numerical methods become a necessity.

The complication in doing this comes from the fact that the terms generating $\boldsymbol{\Phi}_n$ and $\boldsymbol{\Phi}_{n+1}$ in Eq. 3.5 are separately divergent and it is only their combination which yields a finite result. In order to address this, the NLO cross section is reorganised according to a subtraction procedure.

To define the subtraction procedure, it is useful to parameterise the $n+1$-body phase space in terms of the n-body phase space. We therefore embed the n-body phase-space variables in the $n+1$-body variables and introduce a set of additional radiative variables $\mathbf{\Phi}_r$. The phase-space element can then written

$$\mathrm{d}\mathbf{\Phi_{n+1}} = \mathrm{d}\mathbf{\Phi_n}\mathrm{d}\Phi_r \tag{3.6}$$

In the subtraction formalism, a set of counterterms, $C^\alpha\left(\mathbf{\Phi}_{n+1}\right)$, are introduced. The counterterms are defined such that in each divergent region, α, the singular part of the radiative correction matches that of the counterterm, C^α. This guarantees that the combination

$$R\left(\mathbf{\Phi}_{n+1}\right) = R_0\left(\mathbf{\Phi}_{n+1}\right)\mathrm{d} - \sum_\alpha C^\alpha\left(\mathbf{\Phi}_{n+1}\right), \tag{3.7}$$

is finite[1].

Since the counterterms are chosen to match the radiative contributions in the divergent regions, the KLN theorem dictates that the singularities resulting from the integration of the counterterms over the radiative phase space, must match (with the opposite sign) those present in that in the virtual contribution. The sum of the virtual contribution with the counterterms therefore yields a finite contribution which we define as

$$V\left(\mathbf{\Phi}_n\right) = V_0\left(\mathbf{\Phi}_n\right) + \sum_\alpha \int \mathrm{d}\Phi_r C^\alpha\left(\mathbf{\Phi}_{n+1}\right). \tag{3.8}$$

The counterterms can be chosen to be functions that are simple enough that they can be be integrated in d-dimensions giving the singularities as poles in ϵ.

By adding and subtracting the integrated counterterms from Eq. 3.1, the differential cross section can be written as

$$\mathrm{d}\sigma_{NLO} = \left[B(\mathbf{\Phi}_n) + V(\mathbf{\Phi}_n)\right]\mathrm{d}\mathbf{\Phi}_n + R(\mathbf{\Phi_{n+1}})\mathrm{d}\Phi_r\mathrm{d}\mathbf{\Phi}_n. \tag{3.9}$$

The first term in the square brackets on right of Eq. 3.9 corresponds to n-body configurations while the second term corresponds to $n+1$-body configurations. The subtraction

---

[1]This statement assumes that the Born contribution is free of divergences, as is the case whenever the cross section corresponds to an infra-red safe observable.

procedure results in both of these terms now being separately finite. In particular, the term relating to $n+1$-body configurations can now be evaluated in four dimensions. This equation is suitable for a numerical treatment using Monte Carlo techniques or otherwise. A general NLO subtraction prescription, defining a universal set of counterterms and their associated integrals in d-dimensions, is given in Ref. [47].

3.2.3 Matching NLO calculations with parton showers

Fixed-order NLO calculations provide the best available results for sufficiently inclusive observables. However, in many cases we would like a more exclusive description and to calculate observables that are sensitive to higher multiplicity configurations, as simulated by parton showers. In particular, the parton shower is required in order to evolve from the low multiplicity, high energy configurations, described by fixed-order matrix elements, to high multiplicity, low energy configurations to which universal hadronisation models are applied. It is therefore desirable to be able to combine NLO calculations with parton showers in order to get the best of both worlds.

Prescriptions for combining NLO calculations with parton showers are known as NLO matching schemes. The aims of a NLO matching scheme are to provide the parton shower resummation of soft and collinear emissions while giving NLO results for all infrared-safe observables upon expansion in α_S. These matching prescriptions are complicated because the regions of phase space filled by the higher-order matrix elements and the parton shower must be smoothly separated in order to avoid problems such as *double-counting* where the shower and matrix elements radiate in the same region.

The first successful NLO matching scheme was the MC@NLO approach, [50–55] which has been implemented with the HERWIG event generator for many processes. The MC@NLO method generates sets of n- and $n + 1$-body configurations according to the subtracted NLO differential cross section. A naive implementation of this approach would be to simply shower these configurations and assign weights according to the appropriate terms in the differential cross section. However, this would result in a double-counting of parton shower emissions. This results from the fact that the phase space accessible to emissions from the n-body configuration is also included in the phase space that is accessible to the radiative corrections described in the $n + 1$-body configurations. In order to remedy this problem, the MC@NLO procedure dictates that the weight assigned to $n + 1$-body configurations should be given by the associated NLO weight minus the parton shower approximation to the radiative correction.

A feature that makes the MC@NLO particularly simple to implement is the fact that it does not require any modification of the parton shower itself and can be constructed as a separate generator that provides configurations which are interfaced to the standard parton shower. The method has two drawbacks:

- since the implementation of the method relies on subtracting an approximation of the parton shower result, it is heavily dependent on the details of the parton shower algorithm used by the event generator;

- the subtraction of the shower approximation means that the weight assigned to radiative events is not positive definite and results in a fraction of events with a negative weight[2].

3.3 The POWHEG method

In Ref. [48] a novel method, referred to as POWHEG (POsitive Weight Hardest Emission Generator), was introduced to achieve the same aims as MC@NLO while creating only positive weight events and being independent of the event generator with which it is implemented. The POWHEG method has been applied to Z pair hadroproduction [49], heavy flavour hadroproduction [58], e^+e^- annihilation to hadrons [59], Drell-Yan vector boson production [1,60], Higgs production [61,62] and single top production [63]. A general outline of the ingredients required for POWHEG with two popular NLO subtraction schemes is given in Ref. [57].

The POWHEG method is constructed on the basis that if the hardest emission (the emission with the greatest transverse momentum) is generated according to the exact NLO cross section then all infrared-safe observables will also be given according to their NLO distributions. This is true since subsequent emissions are softer and therefore affect the observables only at next-to-next-to-leading-order (NNLO). In a transverse-momentum-ordered shower this corresponds to correcting the first emission, however for showers ordered in other variables the procedure is more complicated. In the following we describe the method, as it appeared in the original publication [48], for the case of an angular-ordered shower such as Herwig++.

---

[2]It should be noted that while the presence of negative weight events is unappealling, it does not necessarily constitute a problem. In principle, these events may be included in any histograms as contributing a negative weight to a bin and the result should still be positive provided the observable is infrared-safe and we have sufficient statistics.

3.3.1 Shower reorganisation

In this section we present the POWHEG reorganisation of the Herwig++ parton shower which allows the hardest emission to be generated separately before generating the rest of the shower around it. This procedure is described separately for final- and initial-state showers.

Final-state reorganisation

The Herwig++ time-like shower can be represented by the generating functional of Eq. 2.21, which we repeat here for clarity

$$
\begin{aligned}
\mathcal{S}_{\widetilde{ij}}(\tilde{q}_I) &= \Delta_{\widetilde{ij}}(\tilde{q}_I, \tilde{q}_0)\mathcal{S}_{\widetilde{ij}}(\tilde{q}_0) \\
&+ \int_{\tilde{q}_0}^{\tilde{q}_I} \Delta_{\widetilde{ij}}(\tilde{q}_I, \tilde{q}) \sum_{\widetilde{ij}\to ij} \left(\mathrm{d}\mathcal{P}_{\widetilde{ij}\to ij}(\tilde{q}, z)\right) \mathcal{S}_i\left(z\tilde{q}\right) \mathcal{S}_j\left((1-z)\tilde{q}\right).
\end{aligned}
\tag{3.10}
$$

The hardest emission in this parton shower is described by the shower variables $(\tilde{q}_h, z_h, \phi_h)$ and has an associated transverse momentum $p_{\perp_h}$. Since the ordering of this parton shower corresponds to ordering in the opening-angle rather than transverse momentum, the hardest emission is not guaranteed to be the first emission. These prior emissions consist of wide-angle soft gluon radiation, corresponding to the limit $z \to 1$ in the shower variables. For reasons that will become apparent, we refer to these emissions as *truncated emissions*.

In order to motivate the identification of the truncated emissions, we follow the arguments of Ref. [48]. In this publication, the hardest emission and truncated emissions are shown to have three important properties:

1. the hardest emission is always found along the shower line defined by following the line with $z > 1/2$ at each emission;

2. the truncated emissions consist purely of soft gluon emissions;

3. from the first non-soft emission down to the last, the evolution variable of emissions must satisfy $\tilde{q} \lesssim p_{\perp_h}$.

These statements are most easily seen using the massless limit of the evolution variable,

$$
\tilde{q} = \frac{p_\perp}{z(1-z)},
\tag{3.11}
$$

but should hold for arbitrary masses.

To see that statement 1 is true, we consider a general truncated emission with emission variables $(\tilde{q}_t, z_t)$. Combining the condition that the emission has a lower transverse momentum than the hardest emission,

$$\tilde{q}_t z_t (1 - z_t) < \tilde{q}_h z_h (1 - z_h), \tag{3.12}$$

with the angular ordering condition,

$$z_t \tilde{q}_t > \tilde{q}_h, \tag{3.13}$$

yields the inequality for z_t

$$z_t > \frac{3}{4}. \tag{3.14}$$

Statement 2 is proved by defining that a non-soft emission is any emission away from the soft region, $z \to 1$. This implies that for non-soft truncated emissions the emission scale is of the order of the transverse momentum, $\tilde{q}_t \sim p_{\perp_t}$. The requirement that the emission is softer than the hardest emission then yields the inequality

$$\tilde{q}_t \lesssim p_{\perp_h}, \tag{3.15}$$

which, via Eq. 3.11, can be written in terms of the scale of the hardest emission as

$$\tilde{q}_t \lesssim \tilde{q}_h. \tag{3.16}$$

This tells us that the scale of a non-soft truncated emission is of the order of or greater than that of the hardest emission. Such an emission therefore does not correspond to a strongly ordered variable in the angular evolution variable and thus results in a subleading contribution that can be neglected. Since only gluon emissions are enhanced in the $z \to 1$ limit, we conclude that the truncated emissions correspond to soft gluon emissions, which do not change the flavour of the shower line.

Finally, for the first non-soft emission $(\tilde{q}, z)$, whether it is the hardest emission itself or occurs afterwards, we have

$$\tilde{q} \lesssim p_{\perp_h}, \tag{3.17}$$

which by angular ordering must also hold for all subsequent emissions, proving statement 3.

It is possible to expand Eq. 3.10 along the line of the hardest emission. The shower may produce any number of truncated emissions before the hardest emission and any number of emissions after it but all of these must have $p_\perp < p_{\perp_h}$. The shower can therefore be written as

$$
\begin{aligned}
\mathcal{S}_{\widetilde{ij}}(\tilde{q}_I) &= \Delta_{\widetilde{ij}}(\tilde{q}_I, \tilde{q}_0)\mathcal{S}_{\widetilde{ij}}(\tilde{q}_0) \\
&+ \int_{\tilde{q}_0}^{\tilde{q}_I} \tilde{\mathcal{S}}_{\widetilde{ij}}^T (\tilde{q}_I, \tilde{q}_h; p_{\perp_h}) \sum_{\widetilde{ij}\to ij} \mathrm{d}\mathcal{P}_{\widetilde{ij}\to ij}(\tilde{q}_h, z_h)\tilde{\mathcal{S}}_i^V (z_h\tilde{q}_h; p_{\perp_h}) \tilde{\mathcal{S}}_j^V ((1-z_h)\tilde{q}_h; p_{\perp_h}),
\end{aligned}
\tag{3.18}
$$

where $\tilde{\mathcal{S}}^T$ refers to a *truncated shower* and $\tilde{\mathcal{S}}^V$ refers to a *vetoed shower*. The truncated shower is responsible for evolving from the initial scale down to the scale of the hardest emission producing any number of truncated emissions and the vetoed shower evolves from the scale of the hardest emission down to the hadronisation scale. The evolution of the vetoed shower is defined by

$$
\begin{aligned}
\tilde{\mathcal{S}}_{\widetilde{ij}}^V (\tilde{q}_h; p_{\perp_h}) &= \Delta_{\widetilde{ij}}(\tilde{q}_h, \tilde{q}_0)\tilde{\mathcal{S}}_{\widetilde{ij}}(\tilde{q}_0) \\
&+ \int_{\tilde{q}_0}^{\tilde{q}_h} \Delta_{\widetilde{ij}}(\tilde{q}_h, \tilde{q}) \sum_{\widetilde{ij}\to ij} \mathrm{d}\mathcal{P}_{\widetilde{ij}\to ij}(\tilde{q}, z)\Theta(p_{\perp_h} - p_\perp(\tilde{q}, z)) \\
&\times \tilde{\mathcal{S}}_i^V (z\tilde{q}; p_{\perp_h}) \tilde{\mathcal{S}}_j^V ((1-z)\tilde{q}; p_{\perp_h}).
\end{aligned}
\tag{3.19}
$$

The recursive equation describing the evolution of the truncated shower is given by

$$
\begin{aligned}
\tilde{\mathcal{S}}_{\widetilde{ij}}^T (\tilde{q}_I, \tilde{q}_h; p_{\perp_h}) &= \Delta_{\widetilde{ij}}(\tilde{q}_I, \tilde{q}_h) \\
&+ \int_{\tilde{q}_h}^{\tilde{q}_I} \Delta_{\widetilde{ij}}(\tilde{q}_I, \tilde{q})\mathrm{d}\mathcal{P}_{\widetilde{ij}\to \widetilde{ij}g}(\tilde{q}, z)\Theta(p_{\perp_h} - p_\perp(\tilde{q}, z)) \\
&\times \tilde{\mathcal{S}}_{\widetilde{ij}}^T (z\tilde{q}, \tilde{q}_h; p_{\perp_h}) \tilde{\mathcal{S}}_g^V ((1-z)\tilde{q}; p_{\perp_h}).
\end{aligned}
\tag{3.20}
$$

The Sudakov form factors and splitting functions appearing in Eqs. 3.19 and 3.20 are identical to those in the standard shower equation of Eq. 3.10 with the exception that the splitting functions in both new showers have an additional Θ-function. This Θ-function guarantees that no emissions with transverse momentum greater than that of the hardest emission are generated. Standard Monte Carlo techniques require that the splitting functions of a parton shower match those appearing in the Sudakov form

factors. The introduction of the Θ-functions mean that this is not the case for the vetoed and truncated showers in Eq. 3.18; we highlight this in our notation with a tilde.

In order to make the truncated and vetoed showers suitable for a Monte Carlo treatment, the original the Sudakov form factor appearing in Eqs. 3.19 and 3.20 is split into two parts according to

$$\Delta_f(z_i \tilde{q}_i, \tilde{q}_{i+1}) = \Delta_f^V(z_i \tilde{q}_i, \tilde{q}_{i+1}; p_{\perp_h}) \bar{\Delta}_f^R(z_i \tilde{q}_i, \tilde{q}_{i+1}; p_{\perp_h}). \tag{3.21}$$

Here, Δ_f^V refers to a *vetoed Sudakov* in which the exponent contains a Θ-function, which matches that in the splitting function of Eqs. 3.20 and 3.19 which was introduced to ensure that the transverse of these emissions is less than that of the hardest emission. In full the vetoed Sudakov form factor is given by

$$\Delta_{\widetilde{ij}}^V(z_i \tilde{q}_i, \tilde{q}_{i+1}; p_{\perp_h}) = \exp\left[-\sum_{\widetilde{ij} \to ij} \int_{\tilde{q}_{i+1}}^{z_i \tilde{q}_i} \mathrm{d}\mathcal{P}_{\widetilde{ij} \to ij}(\tilde{q}, z) \Theta\left(p_{\perp_h} - p_\perp(\tilde{q}, z)\right) \right]. \tag{3.22}$$

The other factor, $\bar{\Delta}_f^R$, contains the opposite Θ-function and is referred to as a *remnant Sudakov* given by

$$\bar{\Delta}_{\widetilde{ij}}^R(z_i \tilde{q}_i, \tilde{q}_{i+1}; p_{\perp_h}) = \exp\left[-\int_{\tilde{q}_{i+1}}^{z_i \tilde{q}_i} \sum_{\widetilde{ij} \to ij} \mathrm{d}\mathcal{P}_{\widetilde{ij} \to ij}(\tilde{q}, z) \Theta\left(p_\perp(\tilde{q}, z) - p_{\perp_h}\right) \right]. \tag{3.23}$$

The combination of the splitting functions in Eqs. 3.20 and 3.19 and the vetoed Sudakov form factors results in a parton shower that may be generated with standard vetoes allowing only emissions with $p_\perp < p_{\perp_h}$, however, the presence of the remnant Sudakov form factors appears to spoil this picture. On the contrary, it turns out that the seemingly awkward remnant factors have a key role to play in formalising how to generate the hardest emission first.

In Ref. [48] it is shown that statements 1-3 result in the remnant Sudakov form factors, $\bar{\Delta}_f^R$, combining to form a single remnant Sudakov form factor, Δ_f^R. Statements 1 and 2 show that all radiation, other than soft radiation in the limit $z \to 1$, is subleading and therefore in this region the approximation $z \to 1$ can be applied in the remnant Sudakov form factors (Eq. 3.23) resulting from the truncated shower. Furthermore, statement 3 implies that for all emissions occurring after the first non-soft emission, the Θ-function in Eq. 3.23 sets the integral to zero. This means that the approximation $z \to 1$ also hold in the remnant Sudakov form factors resulting from the vetoed showers.

The net result of these replacements is that the product of all remnant Sudakov form factors combine to give the remnant Sudakov factor:

$$\Delta_{\widetilde{ij}}^{R}(\tilde{q}_I, \tilde{q}_0; p_{\perp_h}) = \exp\left[-\sum_{\widetilde{ij}\to ij}\int_{\tilde{q}_0}^{\tilde{q}_I}\mathrm{d}\mathcal{P}_{\widetilde{ij}\to ij}(\tilde{q}, z)\Theta\left(p_\perp(\tilde{q}, z) - p_{\perp_h}\right)\right]. \qquad (3.24)$$

The full POWHEG reorganisation of the shower may be written as [3]

$$\begin{aligned}
\mathcal{S}_{\widetilde{ij}}(\tilde{q}_I) &= \Delta_{\widetilde{ij}}^{R}(\tilde{q}_I, \tilde{q}_0; 0)\mathcal{S}_{\widetilde{ij}}(\tilde{q}_0) &(3.25)\\
&+ \int_{\tilde{q}_0}^{\tilde{q}_I}\mathcal{S}_{\widetilde{ij}}^{T}(\tilde{q}_I, \tilde{q}_h; p_{\perp_h})\,\Delta_{\widetilde{ij}}^{R}(\tilde{q}_I, \tilde{q}_0; p_{\perp_h})\sum_{\widetilde{ij}\to ij}\mathrm{d}\mathcal{P}_{\widetilde{ij}\to ij}(\tilde{q}_h, z_h)\\
&\times\ \mathcal{S}_i^{V}\left(z_h\tilde{q}_h; p_{\perp_h}\right)\mathcal{S}_j^{V}\left((1-z_h)\tilde{q}_h; p_{\perp_h}\right).
\end{aligned}$$

The vetoed shower is defined by

$$\begin{aligned}
\mathcal{S}_{\widetilde{ij}}^{V}\left(\tilde{q}_h; p_{\perp_h}\right) &= \Delta_{\widetilde{ij}}^{V}(\tilde{q}_h, \tilde{q}_0)\mathcal{S}_{\widetilde{ij}}^{V}(\tilde{q}_0) &(3.26)\\
&+ \int_{\tilde{q}_0}^{\tilde{q}_h}\Delta_{\widetilde{ij}}^{V}(\tilde{q}_h, \tilde{q})\sum_{\widetilde{ij}\to ij}\mathrm{d}\mathcal{P}_{\widetilde{ij}\to ij}(\tilde{q}, z)\Theta(p_{\perp_h} - p_\perp(\tilde{q}, z))\\
&\times\ \mathcal{S}_i^{V}\left(z\tilde{q}; p_{\perp_h}\right)\mathcal{S}_j^{V}\left((1-z)\tilde{q}; p_{\perp_h}\right),
\end{aligned}$$

and corresponds to a standard shower with vetoes applied such that only emissions with $p_\perp < p_{\perp_h}$ are generated. The truncated shower is defined by

$$\begin{aligned}
\mathcal{S}_i^{T}\left(\tilde{q}_I, \tilde{q}_h; p_{\perp_h}\right) &= \Delta_i^{V}(\tilde{q}_I, \tilde{q}_h) &(3.27)\\
&+ \int_{\tilde{q}_h}^{\tilde{q}_I}\Delta_i^{V}(\tilde{q}_I, \tilde{q})\mathrm{d}\mathcal{P}_{i\to ig}(\tilde{q}, z)\Theta(p_{\perp_h} - p_\perp(\tilde{q}, z))\\
&\times\ \mathcal{S}_i^{T}\left(z\tilde{q}, \tilde{q}_h; p_{\perp_h}\right)\mathcal{S}_g^{V}\left((1-z)\tilde{q}; p_{\perp_h}\right),
\end{aligned}$$

and corresponds to a standard vetoed parton shower line, constrained not to produce any flavour changing emissions, that is stopped once the truncated line has evolved down to the scale $\tilde{q}_h$.

---

[3]Here we have written the no-emission term also in terms of the remnant Sudakov form factor which we are free to do since by definition $\Delta_{\widetilde{ij}}^{R}(\tilde{q}_I, \tilde{q}_0; 0) = \Delta_{\widetilde{ij}}(\tilde{q}_I, \tilde{q}_0)$.

The POWHEG treatment results in a reorganisation of the shower such that the hardest emission may be generated first. The Monte Carlo interpretation of this reorganisation (Eq. 3.25) is:

1. the hardest emission (q_h, z_h, ϕ_h) is generated[4] from the appropriate splitting function reweighted with the remnant Sudakov form factor, according to

$$\sum_{\widetilde{ij} \to ij} \mathrm{d}\mathcal{P}_{\widetilde{ij} \to ij}(\tilde{q}_h, z_h) \Delta_{\widetilde{ij}}^{R}(\tilde{q}_I, \tilde{q}_0; p_{\perp_h}); \qquad (3.28)$$

2. a truncated shower, allowing only non-flavour-changing emissions with $p_\perp < p_{\perp_h}$ is initiated, evolving the shower from $\tilde{q}_I$ down to $\tilde{q}_h$;

3. the hardest emission is forced with shower variables (q_h, z_h, ϕ_h);

4. showers with a veto, allowing only emissions with $p_\perp < p_{\perp_h}$, evolve all external lines down to the hadronisation scale.

A shower generated in this way should differ from the standard shower by only sub-leading terms.

Initial-state POWHEG reordering

In the initial-state case, the parton shower evolution is described by Eq. 3.35. The hardest emission, defining the NLO correction, must occur along the initial-state line. The hardest emission can therefore be singled out by expanding Eq. 3.35 along the initial-state line, analogously to Eq. 3.18, absorbing emissions before the hardest emission into a truncated shower and emissions after the hardest emission into vetoed showers.

The truncated emissions can be shown to correspond to soft gluon emissions by following analogous arguments to those presented for the time-like case. The transverse momentum of an emission is related to the initial-state evolution scale, neglecting masses, according to

$$p_\perp = \tilde{q}(1 - z). \qquad (3.29)$$

The evolution scale of a non-soft truncated emission therefore has an evolution scale of the order of its transverse momentum. Since this transverse momentum is required to be less than that of the hardest emission, this, as in the final-state case, implies Eq. 3.16. This does not correspond to a strongly ordered emission and does not produce

---

[4]As usual in the parton shower the azimuthal angle, ϕ_h, is generated flat in the region $[0, 2\pi]$.

a LL contribution. Truncated emissions are therefore identified as soft emissions which, provided the momentum fraction of the process x is not too low, correspond solely to gluon emissions in the $z \to 1$ limit which do not change the flavour of the initial-state parton.

Since the angular-ordering condition applied along the initial-state line is $\tilde{q}_{i+1} < \tilde{q}_i$, the definition of the remnant Sudakov form is simpler in this case. The initial-state Sudakov form factor is separated into two pieces, a vetoed and remnant Sudakov form factor, according to

$$\Pi_i \left(\tilde{q}_1, \tilde{q}_2; x \right) = \Pi_i^V \left(\tilde{q}_1, \tilde{q}_2; x; p_\perp \right) \Pi_i^R \left(\tilde{q}_1, \tilde{q}_2; x; p_\perp \right). \tag{3.30}$$

The vetoed Sudakov form factor is defined by

$$\Pi_i^V \left(\tilde{q}_1, \tilde{q}_2; x; p_\perp \right) = \exp \left[-\sum_{\widetilde{ij}} \int_{\tilde{q}_2}^{\tilde{q}_1} \frac{\mathrm{d}\tilde{q}^2}{\tilde{q}^2} \int_x^{z_+(\tilde{q})} \mathrm{d}z \frac{\alpha_S}{2\pi} P_{\widetilde{ij} \to ij} \left(z, \tilde{q} \right) \right. \tag{3.31}$$
$$\left. \times \frac{f_{\widetilde{ij}}(x/z, \tilde{q})}{z f_i(x, \tilde{q})} \Theta \left(p_{\perp_h} - p_\perp(\tilde{q}, z) \right) \right],$$

such that it contains a Θ-function to match that appearing in the splitting function of the truncated and vetoed emissions. The remnant Sudakov form factors contain a Θ-function with opposite argument and is given by

$$\Pi_i^R \left(\tilde{q}_1, \tilde{q}_2; x, p_\perp \right) = \exp \left[-\sum_{\widetilde{ij}} \int_{\tilde{q}_2}^{\tilde{q}_1} \frac{\mathrm{d}\tilde{q}^2}{\tilde{q}^2} \int_x^{z_+(\tilde{q})} \mathrm{d}z \frac{\alpha_S}{2\pi} P_{\widetilde{ij} \to ij} \left(z, \tilde{q} \right) \right. \tag{3.32}$$
$$\left. \times \frac{f_{\widetilde{ij}}(x/z, \tilde{q})}{z f_i(x, \tilde{q})} \Theta \left(p_\perp(\tilde{q}, z) - p_{\perp_h} \right) \right].$$

The remnant Sudakov form factors are removed from the truncated and vetoed shower, such that these correspond to standard vetoed showers. The same arguments that led to the approximation $z \to 1$ in the final-state Sudakov remnants can also be utilised in the initial-state case allowing the remnant Sudakov form factors from the m emissions along the initial-state line are combined into a single remnant Sudakov form factor

$$\prod_{i=1}^{m} \Pi_i^R \left(\tilde{q}_i, \tilde{q}_{i+1}; x_i, p_\perp \right) \approx \Pi_i^R \left(\tilde{q}_I, \tilde{q}_0; x, p_\perp \right), \tag{3.33}$$

where

$$x_i = \frac{x}{\prod_{j=1}^{i} z_j}.$$

(3.34)

In this approximation, the POWHEG reorganised initial-state shower is described by

$$
\begin{aligned}
\bar{\mathcal{S}}_i(\tilde{q}_I; x) &= \Pi_i(\tilde{q}_I, \tilde{q}_0; x)\bar{\mathcal{S}}_i(\tilde{q}_0; x) \\
&+ \int_{\tilde{q}_0}^{\tilde{q}_I} \bar{\mathcal{S}}_i^T(\tilde{q}_I, \tilde{q}_h; x, p_{\perp_h})\Pi_i^R(\tilde{q}_I, \tilde{q}_h; x, p_{\perp_h}) \sum_{\widetilde{ij}} \mathrm{d}\mathcal{P}_{\widetilde{ij} \to ij}(\tilde{q}_h, z_h) \frac{f_{\widetilde{ij}}(x/z, \tilde{q}_h)}{z f_i(x, \tilde{q}_h)} \\
&\times \bar{\mathcal{S}}_{\widetilde{ij}}^V(\tilde{q}_h; x/z_h, p_{\perp_h})\mathcal{S}_j^V((1 - z_h)\tilde{q}_h; p_{\perp_h}).
\end{aligned}
$$

(3.35)

The initial-state truncated shower is defined by

$$
\begin{aligned}
\bar{\mathcal{S}}_i^T(\tilde{q}_1, \tilde{q}_2; x, p_\perp) &= \Pi_i^V(\tilde{q}_I, \tilde{q}_0; x, p_\perp) \\
&+ \int_{\tilde{q}_0}^{\tilde{q}_I} \Pi_i^V(\tilde{q}_I, \tilde{q}_h; x, p_{\perp_h})\mathrm{d}\mathcal{P}_{i \to ig}(\tilde{q}, z) \frac{f_i(x/z, \tilde{q})}{z f_i(x, \tilde{q})} \\
&\times \bar{\mathcal{S}}_i^T(\tilde{q}, \tilde{q}_2; x/z, p_\perp)\mathcal{S}_g^V((1 - z)\tilde{q}; p_\perp),
\end{aligned}
$$

(3.36)

and the vetoed shower by

$$
\begin{aligned}
\bar{\mathcal{S}}_i^V(\tilde{q}_1; x, p_\perp) &= \Pi_i^V(\tilde{q}_1, \tilde{q}_0; x, p_\perp)\bar{\mathcal{S}}_i^V(\tilde{q}_0; x, p_\perp) \\
&+ \int_{\tilde{q}_0}^{\tilde{q}_1} \Pi_i^V(\tilde{q}_1, \tilde{q}_h; x, p_\perp)\mathrm{d}\mathcal{P}_{\tilde{ij} \to ij}(\tilde{q}, z) \sum_{\tilde{ij}} \frac{f_{\tilde{ij}}(x/z, \tilde{q})}{z f_i(x, \tilde{q})} \\
&\times \bar{\mathcal{S}}_{\tilde{ij}}^V(\tilde{q}; x/z, p_\perp)\mathcal{S}_j^V((1 - z)\tilde{q}; p_\perp),
\end{aligned}
$$

(3.37)

The Monte Carlo interpretation of Eq. 3.35 is completely analogous to the final-state case.

3.3.2 Generating the hardest emission according to the NLO cross section

Having singled out the hardest emission such that it may be generated separately, the remaining task is to generate this emission according to exact NLO formulae. In the original POWHEG publication [48] this is done by performing an expansion of the parton shower at NLO in α_S and comparing this to the exact NLO cross section. NLO corrected

splitting functions and associated Sudakov forms may then be defined in terms of the contributions of the NLO cross section.

In the standard Monte Carlo approach, each event is assigned the leading-order weight $B(\mathbf{\Phi_n})$ and all partonic external legs, l, initiate a parton shower. The parton-shower approximation to Eq. 3.9 is determined by the distribution of the hardest emission. The hardest emission can occur along any of the parton shower lines and, from Eq. 3.25, it is distributed according to

$$\mathrm{d}\sigma^{(\mathrm{PS})} = B(\mathbf{\Phi_n})\mathrm{d}\mathbf{\Phi_n}\left\{\Delta^R(\tilde{q}_I, \tilde{q}_0; 0) + \Delta^R\left(\tilde{q}_I, \tilde{q}_0; p_\perp\right)F\left(\tilde{q}, z\right)\mathrm{d}\tilde{q}\mathrm{d}z\right\}, \tag{3.38}$$

where we have defined the combination of remnant Sudakov form factors for all parton-shower legs,

$$\Delta^R(\tilde{q}_I, \tilde{q}_0; p_\perp) = \prod_l \Delta_l^R(\tilde{q}_I, \tilde{q}_0; p_\perp), \tag{3.39}$$

and the infinitesimal splitting probability summed over all parton-shower legs,

$$F(\tilde{q}, z)\mathrm{d}\tilde{q}\mathrm{d}z = \sum_{\widetilde{ij}}\sum_{\widetilde{ij}\to ij}\mathrm{d}\mathcal{P}_{\widetilde{ij}\to ij}(\tilde{q}_h, z_h), \tag{3.40}$$

where the summation over $\widetilde{ij}$ denotes summation over the external legs which initiate the parton shower. The NLO cross-section approximation is therefore provided by the α_S-expansion of Eq. 3.38 giving

$$\mathrm{d}\sigma^{(\mathrm{PS})} = B(\mathbf{\Phi_n})\mathrm{d}\mathbf{\Phi_n}\left\{1 + F(\tilde{q}, z)\mathrm{d}\tilde{q}\mathrm{d}z - \int_{\tilde{q}_0}^{\tilde{q}_I}F(\tilde{q}, z)\mathrm{d}\tilde{q}\mathrm{d}z + \mathcal{O}(\alpha_S^2)\right\}. \tag{3.41}$$

The exact NLO cross section in Eq. 3.9 can be manipulated to match the form of Eq. 3.41 by writing it as

$$\begin{aligned}\mathrm{d}\sigma_{NLO} &= \left[V(\mathbf{\Phi_n}) + \int\mathrm{d}\Phi_r R(\mathbf{\Phi_{n+1}})\right]\mathrm{d}\mathbf{\Phi_n} \\ &+ B(\mathbf{\Phi_n})\mathrm{d}\mathbf{\Phi_n}\left[1 + \frac{R_0(\mathbf{\Phi_{n+1}})\mathrm{d}\Phi_r}{B(\mathbf{\Phi_n})} - \frac{\int R_0(\mathbf{\Phi_{n+1}})\mathrm{d}\Phi_r}{B(\mathbf{\Phi_n})}\right].\end{aligned} \tag{3.42}$$

The second term in square brackets now has exactly the form of the parton shower cross section in Eq. 3.41 with the following substitutions

$$F(\tilde{q}, z) \to \frac{R_0(\mathbf{\Phi_{n+1}})}{B(\mathbf{\Phi_n})}, \qquad \mathrm{d}\tilde{q}\mathrm{d}z \to \mathrm{d}\Phi_r. \tag{3.43}$$

Taking this correspondence a stage further, a remnant Sudakov form can be defined according to

$$\Delta^R(p_\perp) = \exp\left[-\int \mathrm{d}\Phi_r \frac{R_0(\mathbf{\Phi_{n+1}})}{B(\mathbf{\Phi_n})} \Theta\left(p_\perp(\mathbf{\Phi_{n+1}}) - p_\perp\right)\right], \tag{3.44}$$

and the cross section can be written analogously to Eq. 3.38 as

$$
\begin{aligned}
\mathrm{d}\sigma_{NLO} &= \left[V(\mathbf{\Phi_n}) + \int \mathrm{d}\Phi_r R(\mathbf{\Phi_{n+1}})\right] \mathrm{d}\mathbf{\Phi_n} \\
&+ B(\mathbf{\Phi_n})\mathrm{d}\mathbf{\Phi_n}\left[\Delta^R(p_{\perp_\mathrm{min}}) + \Delta^R(p_\perp)\frac{R_0(\mathbf{\Phi_{n+1}})\mathrm{d}\Phi_r}{B(\mathbf{\Phi_n})}\right].
\end{aligned}
\tag{3.45}
$$

This equation has the same expansion at NLO in α_S as Eq. 3.9 but also generates the same distribution of the hardest emission as Eq. 3.38 in the LL approximation. Therefore, together with the shower reorganisation it satisfies the requirements of a NLO matching prescription.

Equation 3.45 has a simple Monte Carlo interpretation. The second term corresponds to the distribution of events containing the hardest emission which should be generated accordingly and attached to truncated and vetoed showers as dictated by the POWHEG shower reorganisation. The terms in the first square brackets are formally of higher order in α_S and can therefore be implemented by generating n-body events with the corresponding weight and applying the standard shower. While this implementation is workable, like the MC@NLO scheme, it suffers from negative weights, since the first term is not positive definite.

The POWHEG scheme circumvents the issue of negative weights by introducing the function

$$\bar{B}(\mathbf{\Phi_n}) = B(\mathbf{\Phi_n}) + V(\mathbf{\Phi_n}) + \int \mathrm{d}\Phi_r R(\mathbf{\Phi_{n+1}}), \tag{3.46}$$

whereupon Eq. 3.45 can be rewritten, with only NNLO differences, as

$$\mathrm{d}\sigma_{NLO} = \bar{B}(\mathbf{\Phi_n})\mathrm{d}\mathbf{\Phi_n} \left[\Delta^R(p_{\perp_{\min}}) + \Delta^R(p_\perp)\frac{R_0(\mathbf{\Phi_{n+1}})\mathrm{d}\Phi_r}{B(\mathbf{\Phi_n})} \right]. \tag{3.47}$$

The $\bar{B}$ function is positive definite as long as perturbation theory is valid and therefore Eq. 3.47 can be used to provide a NLO correction of the hardest emission without producing any negative weights.

The transverse momentum cut off, $p_{\perp_{\min}}$, is introduced in order to define what is considered a resolvable emission, avoiding the singular regions of the radiative corrections.

Equation 3.47 can be considered to be the central POWHEG formula and the main task of an implementation is the manipulation of the NLO cross section into this form.

3.4 POWHEG implementation: $e^+e^- \to$ hadrons

The simplest useful process for which the POWHEG scheme can be implemented is $e^+e^- \to$ hadrons. This process provides an important test bed for the implementation since it is a clean process, not complicated by the presence of initial-state hadrons, described by a large amount of data from the LEP experiments and is already well described by Monte Carlo event generators. An implementation for the process in Herwig++, for light quarks, was presented in Ref. [59]. In this section we present a separate implementation employing different methods and including some massive quark effects. The implementation also features an exact treatment of the truncated shower which was not included in Ref. [59].

3.4.1 Hardest emission

In this section we present the ingredients required for the generation of the hardest emission according to Eq. 3.47. A finite quark mass defined by,

$$\rho = \frac{m^2}{s}, \tag{3.48}$$

is taken into account in the generation of the hardest emission.

Kinematics

In separating the production and decay processes in Sect. 1.1.3, we integrated over correlations between the two, resulting in the Born cross section being given by a constant. In this implementation we will also follow this simplifying procedure but will employ a trick which will allow us to regain the correct correlations. This simplification means that we do not have any Born variables and the integration measure over the n-body configuration can simply be set to one,

$$\mathrm{d}\mathbf{\Phi_n} = 1. \tag{3.49}$$

The phase space of the NLO radiative correction to the cross section is conveniently expressed in terms of the Dalitz variables, x_i, as defined in Eq. 1.45. However, since the remnant Sudakov form factor (Eq. 3.44) contains the Θ-function,

$$\Theta\left(p_\perp(\mathbf{\Phi_{n+1}}) - p_\perp\right), \tag{3.50}$$

the generation of the hardest emission may be simplified by choosing the transverse momentum, $p_\perp$, as one of the radiative variables. In this case, the Θ-function results in the lower limit of the integral over $p_\perp$ being set to $p_{\perp_h}$ which makes it suitable for a straightforward implementation with the veto algorithm.

The exact parton shower transverse momentum may be calculated from the Dalitz variables by solving Eq. 2.39[5] for the parton shower emissions. This gives

$$p_\perp^2 = \frac{s}{4(1 - x_2 + \rho)(x_2^2 - 4\rho)} \quad \left[(x_2 - 1)(\sqrt{x_2 - 4\rho} + x_g - x_1) + 2\rho x_g\right] \tag{3.51}$$

$$\times \; \left[(x_2 - 1)(\sqrt{x_2 - 4\rho} - x_g + x_1) - 2\rho x_g\right],$$

for emissions from the quark (parton 1) and the same expression with $x_1 \leftrightarrow x_2$ for emission from the anti-quark. This is just the generalisation of Eq. 1.56 for quarks of finite mass.

Instead of using the exact transverse momentum, $p_\perp$, it is convenient to use a simpler transverse momentum variable, $\bar{p}_\perp$, that provides a single mapping for the whole phase-space region. This leads to a significantly more straightforward implementation due to simpler kinematics and the fact that an emitter does not need to be assigned until after

---

[5]The notation here relates to that of Eq. 2.39 with the substitution $x_{b,c} \leftrightarrow x_{1,2}$.

the radiative variables have been generated. The chosen variable must approximate the parton-shower variable such that it approaches it in the soft and collinear limits.

Once a hardest emission has been generated, its transverse momentum in the parton shower variable can be calculated with the exact mapping in Eq. 3.51. This exact transverse momentum can then be used in the subsequent POWHEG truncated and vetoed showers.

The transverse momentum variable used in this implementation is chosen as

$$\bar{p}_\perp^2 = s(1 - x_1)(1 - x_2). \tag{3.52}$$

An auxiliary variable is also required to parameterise the phase-space region. This is chosen to be a rapidity variable in which the radiative cross section is expected to be relatively stable, so that the hardest emission may be generated using sampling a flat sampling of the phase space in this variable. The rapidity variable used is defined as

$$y = \frac{1}{2} \log \left(\frac{1 - x_1}{1 - x_2} \right). \tag{3.53}$$

These variables were used in the Ariadne dipole shower, described in Ref. [64]. The corresponding solutions for the Dalitz variables in terms of these radiative variables are

$$x_{1,2} = 1 - \frac{\bar{p}_\perp}{\sqrt{s}} \exp(\mp y). \tag{3.54}$$

The radiative phase-space element in the Dalitz variables may be related to the phase-space element in $(\bar{p}_\perp, y)$ by a simple Jacobean factor

$$\mathrm{d}\Phi_r = \mathrm{d}x_1 \mathrm{d}x_2 = \frac{2\bar{p}_\perp}{s} \mathrm{d}\bar{p}_\perp \, dy. \tag{3.55}$$

The allowed region of phase space for radiative emission from a quark of finite mass is given by the inequality

$$\Delta \left(x_1^2 - 4\rho, x_2^2 - 4\rho, x_3^2 \right) < 0, \tag{3.56}$$

where the function $\Delta(a, b, c)$ is defined by

$$\Delta(a, b, c) = a^2 + b^2 + c^2 - 2ab - 2bc - 2ca. \tag{3.57}$$

Matrix elements

In this section we present a calculation of the Born and radiative matrix elements that are required for the generation of the hardest emission according to the POWHEG formula, Eq. 3.47.

In order to separate the implementation of production and decay processes, we employ a trick that is valid only in the massless limit. However, while this is strictly only a massless correction, we include mass terms in the radiative matrix elements of the radiative corrections, where they may improve the description of, for example, low-transverse-momentum emissions from bottom quarks.

The matrix elements for the Born and radiative contributions to this process, for the case of massless quarks with an intermediate photon, were calculated in Sect. 1.1.3. In order to extend these calculations to include an intermediate Z boson, we use the narrow width approximation. As in Sect. 1.1.3, we treat the production and decay processes separately, neglecting interferences between the two. The Z boson propagator then introduces an additional Breit-Wigner factor describing the Z boson resonance,

$$\frac{1}{\left(p^2 - M_Z^2\right)^2 + M_Z^2 \Gamma^2}, \tag{3.58}$$

where p, M_Z and Γ are the momentum, mass and decay width of the Z boson. In generating the hardest emission, this factor will always cancel between the Born and radiative contributions and we omit it from this point onwards.

The Z boson also introduces separate axial- and vector-couplings. We may write the general vector-boson-fermion-fermion vertex as

$$ig_A \gamma^\mu \gamma^5 + ig_V \gamma^\mu, \tag{3.59}$$

where g_A and g_V are the axial and vector coupling constants. In terms of the electronic charge e and weak mixing angle θ_w, the coupling constants are given by

$$g_A = 0, \qquad g_V = eQ_i, \tag{3.60}$$

for a photon and

$$g_A = \frac{e}{2 \sin \theta_w \cos \theta_w} t_{3L\,i}, \qquad g_V = \frac{e}{2 \sin \theta_w \cos \theta_w} \left(t_{3L\,i} - Q_i \sin^2 \theta_w\right), \tag{3.61}$$

for a Z boson. The constants Q_i and t_{3Li} are the fractional electronic charge and weak isospin of the interacting fermion, i. The weak isospin is $+1/2$ for up-type quarks and $-1/2$ for down type quarks.

For the process considered, the interference terms between the vector and axial currents vanish and the matrix elements squared for the production process can be written in the form

$$|\mathcal{M}|^2 = g_A^2 \mathrm{Tr}_A + g_V^2 \mathrm{Tr}_V, \tag{3.62}$$

where Tr_A and Tr_V refer to the terms coming from the evaluation of the traces of the vector and axial currents respectively. In the case of massless quarks, the vector and axial contributions are identical and we find a straightforward generalisation of the results of Sect. 1.1.3. The Born cross section is given by

$$\sigma_b = \sigma_0 N_C \left(g_A^2 + g_V^2 \right), \tag{3.63}$$

where we define

$$\sigma_0 = \frac{(g_A^2 + g_V^2)}{12\pi s}. \tag{3.64}$$

The radiative contribution to the cross section is

$$\sigma_r = \sigma_0 N_C C_F \frac{(g_A^2 + g_V^2)}{8\pi^2} \int \mathrm{d}x_1 \mathrm{d}x_2 \frac{x_1^2 + x_2^2}{(1 - x_1)(1 - x_2)}. \tag{3.65}$$

We note that Eqs. 3.63 and 3.65 reduce to the expressions of Eqs. 1.41 and 1.47 in the case that the vector boson is a photon.

If we introduce a finite quark mass the contributions from the axial and vector currents are no longer equal. In this case it is found [65] that the Born contribution is given by

$$\sigma_b = \sigma_0 N_C \left[g_A^2 v^3 + g_V^2 (1 + 2\rho)v \right], \tag{3.66}$$

where v is the quark velocity, $v = \sqrt{1 - 4\rho}$. The radiative corrections are given by

$$\sigma_r = \sigma_0 N_C C_F \frac{\alpha_S}{2\pi} \int \mathrm{d}x_1 \mathrm{d}x_2 \left[g_A^2 F_A(x_1, x_2, \rho) + g_V^2 F_V(x_1, x_2, \rho) \right], \tag{3.67}$$

where F_A is the contribution from the trace over the axial current and is given by

$$
\begin{aligned}
F_A &= \frac{(x_1 + 2\rho)^2 + (x_2 + 2\rho)^2 - 2\rho\left[(3 + x_g)^2 - 19 + 4\rho\right]}{(1 - x_1)(1 - x_2)} \\
&\quad - \frac{2\rho v^2}{(1 - x_1)^2} - \frac{2\rho v^2}{(1 - x_2)^2},
\end{aligned}
\tag{3.68}
$$

and F_V is the contribution from the vector current trace,

$$
F_V = \frac{(x_1 + 2\rho)^2 + (x_2 + 2\rho)^2 - 8\rho(1 + 2\rho)}{(1 - x_1)(1 - x_2)} - \frac{2\rho(1 + 2\rho)}{(1 - x_1)^2} - \frac{2\rho(1 + 2\rho)}{(1 - x_2)^2}.
\tag{3.69}
$$

Hardest emission generation

The matrix elements and kinematics that have been described lead to the identification of the POWHEG NLO splitting function, from Eq. 3.47, as

$$
\frac{R_0(\mathbf{\Phi_{n+1}})}{B(\mathbf{\Phi_n})} \mathrm{d}\Phi_r = F^{(\mathrm{NLO})}(\bar{p}_\perp, y)\mathrm{d}\bar{p}_\perp \mathrm{d}y.
\tag{3.70}
$$

where

$$
F^{(\mathrm{NLO})}(\bar{p}_\perp, y) = C_F \frac{\alpha_S}{2\pi} \frac{\left[g_A^2 F_A(x_1, x_2, \rho) + g_V^2 F_V(x_1, x_2, \rho)\right]}{\left[g_A^2 v^3 + g_V^2 (1 + 2\rho)v\right]} \frac{2\bar{p}_\perp}{s}.
\tag{3.71}
$$

The radiative variables $(\bar{p}_\perp, y)$ that describe the hardest emission are generated according to Eq. 3.47 using the bivariant veto algorithm. This requires us to define a simple function that provides an upper bound to $F^{(\mathrm{NLO})}(\bar{p}_\perp, y)$. A suitable choice for this function is

$$
g(\bar{p}_\perp) = \frac{K}{\bar{p}_\perp},
\tag{3.72}
$$

where

$$
K = \frac{2C_F \alpha_{S_{\max}}}{\pi}.
\tag{3.73}
$$

The allowed phase-space limits can be approximated by the rectangular region

$$
\bar{p}_{\perp_{\min}} < \bar{p}_\perp < \bar{p}_{\perp_{\max}}, /; /; /; /; /; /; /; /; y_{\min} < y < y_{\max}.
$$

The limit $\bar{p}_{\perp\mathrm{max}}$ is set to the highest kinematically accessible value

$$\bar{p}_{\perp\mathrm{min}} = \frac{\sqrt{s}}{2}. \tag{3.74}$$

The limit $\bar{p}_{\perp\mathrm{min}}$ is a cut parameter that must be set in order to avoid the singular region of $F^{(\mathrm{NLO})}(\bar{p}_\perp, y)$ and define what is considered a resolvable emission. The kinematically accessible limits to y are then given by

$$y_{\mathrm{max,min}} = \pm \cosh^{-1}\left(\frac{\sqrt{s}}{2p_{\perp\mathrm{min}}}\right). \tag{3.75}$$

The generation of the hardest emission variables $(\bar{p}_\perp, y)$ then proceeds according to:

1. $\bar{p}_{\perp 0}$ is set to $p_{\perp_{max}}$;
2. a new $(p_\perp, y)$ configuration is generated from $\bar{p}_{\perp i} = \bar{p}_{\perp i-1}\mathcal{R}^{\frac{1}{K(y_{max} - y_{min})}}$ and $y = y_{min} + \mathcal{R}(y_{max} - y_{min})$;
3. if $\bar{p}_{\perp i} < \bar{p}_{\perp_{min}}$ then a no-emission event is generated;
4. if the generated configuration is outside the exact phase-space boundaries in Eq. 3.56, then return to step 2;
5. if $W(\bar{p}_{\perp i}, y)/g(\bar{p}_{\perp i}) > \mathcal{R}$ then accept the configuration, otherwise return to step 2.

3.4.2 The $\bar{B}$ function

Since all Born variables have been integrated over, the $\bar{B}$ function is also a constant and corresponds simply to the integrated NLO cross section, which, for massless partons, is given by the well known function

$$\bar{B}\mathrm{d}\boldsymbol{\Phi_n} = B\mathrm{d}\boldsymbol{\Phi_n}\left(1 + \frac{\alpha_S}{\pi}\right). \tag{3.76}$$

This corresponds to a trivial reweighting of the leading-order configuration that is generated according to Born matrix elements in the standard Monte Carlo treatment.

3.4.3 Momentum reconstruction

The momenta of the three-parton state defined by the hardest emission variables and Born configuration, are constructed in the Sudakov basis, using a process analogous to that of the parton shower momentum reconstruction detailed in Sect. 2.2.6.

The gluon must be assigned as an emission from either the quark or anti-quark; the other parton is then referred to as the spectator. This choice is made based on which parton the gluon is closer to in angle. This corresponds to choosing the emitter to be the quark if

$$x_1 < x_2, \tag{3.77}$$

and assigning the anti-quark as the emitter otherwise. In the following we refer to variables relating to the emitter with a subscript e and variables relating to the spectator with a subscript s.

The momenta are constructed in the centre-of-mass frame with the Sudakov reference vectors $p_{q\bar{q}}^{\mu}$ and $n_{q\bar{q}}^{\mu}$ for emissions from the quark and anti-quarks, defined by

$$p_{q\bar{q}}^{\mu} = \frac{\sqrt{s}}{2}\left(1; 0, 0, \pm v\right), \qquad n_{q\bar{q}}^{\mu} = \frac{\sqrt{s}}{2}\left(v; 0, 0, \mp v\right). \tag{3.78}$$

The Dalitz variables, representing the hardest emission, are related to the parton-shower variables by

$$\begin{aligned}
z &= r + \frac{x_e - (2 - x_s)r}{\sqrt{x_s^2 - 4\rho}}, \\
\tilde{k} &= \frac{1 - x_s}{z(1 - z)},
\end{aligned} \tag{3.79}$$

where r is defined by

$$r = \frac{1}{2}\left(1 + \frac{\rho}{1 + \rho - x_s}\right), \tag{3.80}$$

and $\tilde{k}$ is the dimensionless evolution variable defined in Eq. 2.41. The α-parameters in the Sudakov basis are then given by

$$\begin{aligned}
\alpha_e &= \frac{z}{(1 + v)}\left[1 + z(1 - z)\tilde{k} + \sqrt{(1 - z(1 - z)\tilde{k})^2 - 4\rho}\right], \\
\alpha_s &= \frac{2}{(1 + v)} - \frac{\alpha_e}{z}, \\
\alpha_g &= \frac{1 - z}{z}\alpha_e.
\end{aligned} \tag{3.81}$$

The β-parameters are related to the α-parameters by requiring the momenta to be on-shell, giving

$$\beta_i = \frac{2}{v(1+v)} \left[\frac{(m_i^2 + p_{\perp i}^2)}{\alpha_i s} - \alpha_i \rho \right] \tag{3.82}$$

Finally, the transverse component of the momentum $q_{\perp_i}^\mu$ of each parton is given by

$$q_{\perp_{e,g}}^\mu = (0; \pm p_\perp \sin\phi, \pm p_\perp \cos\phi, 0), \qquad q_{\perp_s}^\mu = \mathbf{0}, \tag{3.83}$$

where the azimuthal angle ϕ is generated uniformly in the region $[0, 2\pi]$.

The parton momenta are constructed in the frame defined by the basis choice in Eq. 3.78, according to Eq. 1.49. The correlations between the production and decay processes are correctly generated by employing a simple prescription, introduced in Ref. [66]. This dictates that the parton momenta should be rotated by uniformly generated angle, in the region $[0, 2\pi]$, around a direction chosen to be that of the quark (anti-quark) with relative probability x_1^2 (x_2^2).

3.4.4 Shower implementation

In order to produce the full parton shower around the hardest emission, the POWHEG scheme requires a set of modifications to the standard parton shower. We are required to implement truncated and vetoed showers which, for final-state showers, evolve according to Eqs. 3.27 and 3.26 respectively.

As discussed in Sect. 3.3.1, the vetoed shower corresponds to a standard vetoed shower which is already implemented in modern event generators. This corresponds to simply augmenting the veto algorithm described in Sect. 2.2.5 so that configurations with $p_\perp(\tilde{q}, z) > p_{\perp_h}$ are rejected.

The implementation of a truncated emission requires a non-trivial modification of the parton shower. An approximate implementation of the truncated shower was given in Ref. [59], describing at most a single truncated emission. The implementations described in this thesis represent the first exact implementation of the POWHEG truncated shower.

The implementation of the truncated shower is achieved by interpreting the $n+1$-momenta configuration, describing the hardest emission, as a standard Herwig++ emission from an underlying n-momenta configuration. The parton-shower variables

$(\tilde{q}_h, z_h, \phi_h)$ can then be calculated by inverting the momentum reconstruction procedure described in Sect. 2.2.6. This then allows a straightforward implementation of the truncated and vetoed showers, as a single shower evolution, via simple modifications of the standard parton shower, as described below.

1. The hardest emission is interpreted as a parton-shower emission $(\tilde{q}_h, z_h, \phi_h)$ which is assigned to a parton-shower line.

2. The truncated shower is initiated along that line from the standard starting scale q_I.

3. The shower evolves down in $\tilde{q}$. Vetoes are applied such that only emissions satisfying the following conditions are allowed:
   - $p_\perp < p_{\perp_h}$;
   - $z\tilde{q} > \tilde{q}_h$;
   - non-flavour-changing (gluon emissions only);

4. Once the truncated shower has evolved to the scale of the hard emission $\tilde{q}_h$, the truncated shower is stopped and the hardest emission is forced with emission variables $(\tilde{q}_h, z_h, \phi_h)$.

5. All partons undergo vetoed parton-shower evolution down to the hadronisation scale as a standard parton shower with the requirement that all emissions satisfy

$$p_\perp < p_{\perp_h}.$$

Inverse momentum reconstruction

The ability to interpret the $n + 1$-body momenta configuration, describing the hardest emission, as a shower emission from an underlying n-body configuration is the key component of the POWHEG implementation. In this section we outline a scheme for doing this, providing a mapping between the $n + 1$-momenta and the shower variables $(\tilde{q}_h, z_h, \phi_h)$. This mapping should work such that on initiating the parton shower from the n-body configuration and forcing a single emission at the hardest emission variables, the momenta of the $n + 1$-body configuration are reproduced exactly.

This procedure is also useful for schemes in which more than one emission is corrected, as described in Chapters 5 and 6. We therefore present a general description for finding the shower variables of m emissions from an $n + m$-body momentum configuration. In order to do this, the $n + m$ momenta must be assigned a *pseudo-shower history*, describing formation of the $n + m$ configuration as a series of $1 \rightarrow 2$ emissions from an underlying n-body configuration. For the POWHEG case of a single emission this

corresponds simply to defining an emitter. The momenta of all intermediate partons in the pseudo-shower history can be calculated by requiring momentum conservation in the $1 \rightarrow 2$ emissions.

The mapping to the shower variables corresponds to inverting the momentum reconstruction procedure described in Sect. 2.2.6; this requires two steps. First, the reshuffling boost applied to each shower jet in order to conserve global momentum must be found and its inverse applied to the momenta of the shower jet. Second, the resulting momenta are decomposed into the shower variables according to Eq. 2.4.

The momentum of the n-body configuration in the pseudo-shower history can be thought of as a set of shuffled shower progenitors, q_J', which correspond to the momenta on the right hand side of Eq. 2.72. The original on-shell progenitors p_J are related to q_J' by

$$p_J = \left(\sqrt{\frac{\mathbf{q}_J'^2}{k^2} + m_J^2} ; \frac{\mathbf{q}_J'}{k} \right) , \qquad (3.84)$$

where m_J is the on-shell mass of the jet progenitor. The set of on-shell progenitors respect global momentum conservation therefore we can find the boost parameter k by solving

$$\sum_J \sqrt{\frac{\mathbf{q}_J'^2}{k^2} + m_J^2} = \sqrt{s}. \qquad (3.85)$$

Once k is found, the reference vector p_J is given by Eq. 3.84; similarly n_J is given by

$$n_J = \left(\sqrt{\frac{\mathbf{q}_{\bar{J}}'^2}{k^2}} ; \frac{\mathbf{q}_{\bar{J}}'}{k} \right) , \qquad (3.86)$$

where $\bar{J}$ refers to the colour partner jet of the shower jet J. In the reconstruction procedure, the Sudakov parameters of the progenitor partons are set to $\alpha_0 = 1$ and $q_{\perp 0} = 0$. Furthermore, Eq. 2.4 implies that

$$\beta_0 = \frac{q_J^2 - m_J^2}{2p \cdot n}. \qquad (3.87)$$

Since q_J' and q_J are related by a boost, we also have $q_J^2 = q_J'^2$. The momentum of the reconstructed progenitors q_J can then be constructed according to Eq. 2.4. This

defines the reshuffling boost as in Eq. 2.72. The boosts for all shower jets can then be calculated, inverted and applied to all momenta in each jet. The momentum can then be decomposed into Sudakov parameters and the shower variables $(\tilde{q}, z, \phi)$ for each branching calculated from Eqs. 2.6–2.8 and 2.14.

3.4.5 Results

In this section we present the results of the implementation at a centre-of-mass energy of 91.2 GeV. Since the POWHEG method provides a parton-shower correction that should be equivalent to the matrix-element corrections, with only sub-leading differences between the two, we provide a comparison of the two approaches. This is done first at parton level where differences should be easily visible and not hidden by hadronisation corrections. We then present results at hadron-level with a comparison to LEP data.

Parton-level results

An important feature that POWHEG implementation should achieve is the filling of the dead zone region of phase space, corresponding to emissions with $\tilde{q}_h > \tilde{q}_I$. This is verified by looking at a Dalitz scatter plot of the distribution of hardest emissions. This is shown in Fig. 3.1 and demonstrates a smooth coverage of the full allowed phase space, including the dead zone.

A simple observable that is sensitive to the three-parton configurations generated in the POWHEG scheme is the variable y_{23}, which is defined as the scale at which three-jets are resolved in a jet resolution variable. Figure 3.4.5 shows a comparison of the distributions of y_{23} in the Durham jet algorithm for the bare parton shower, POWHEG parton shower and the parton shower with matrix-element corrections. The distributions all match fairly closely. In particular, the POWHEG and matrix-element-corrected distributions coincide in the hard tail. This is to be expected since this region corresponds to the high-transverse-momentum region in which emissions are generated according to the radiative correction in both methods. The parton shower is also very close to the two corrected distributions demonstrating that the parton shower provides a close approximation to the exact matrix elements for this process. The parton shower distribution is lower than the corrected distributions in the very high region, which can be attributed to the fact that it does not fill the dead zone.
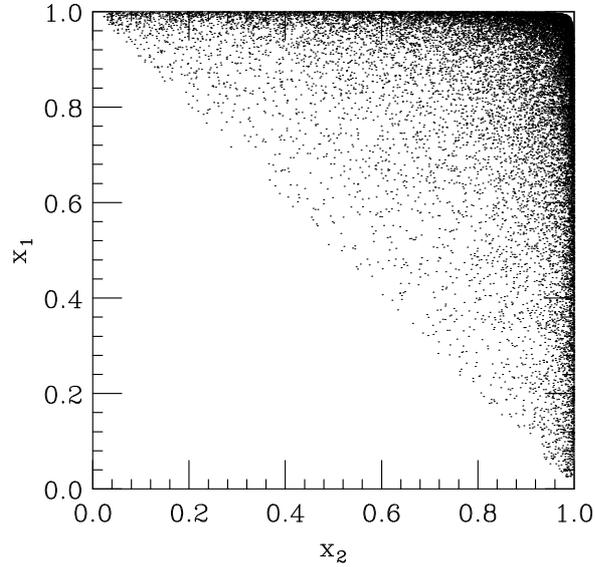
Figure 3.1: A scatter plot of the Dalitz variables produced in the POWHEG hardest emission for $e^+e^- \to$ hadrons at $\sqrt{s} = 91.2$ GeV.
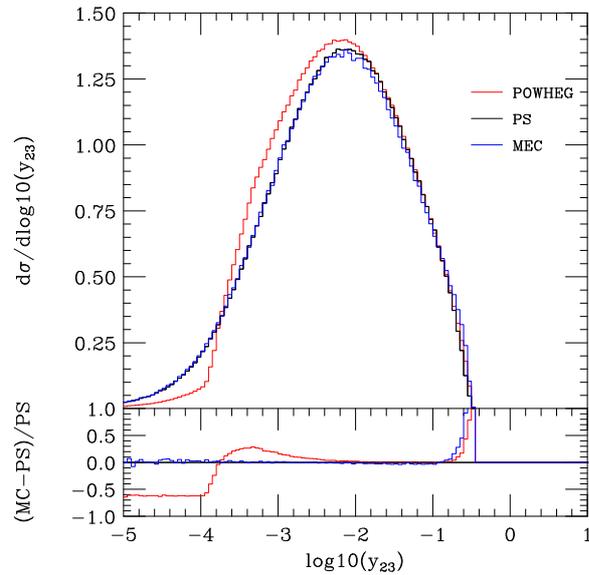
Figure 3.2: The parton-level distributions of y_{23} in the Durham jet measure for $e^+e^- \to$ hadrons at $\sqrt{s} = 91.2$ GeV. Distributions are shown for the standard partons shower (PS), POWHEG implementation, and parton shower with matrix-element corrections (MEC) in Herwig++.

The POWHEG distribution shows significant differences from the other two distributions in the low-y_{23} region. This may be attributed to the different cut-off and emission resolution criteria that have been applied. In both the bare parton shower and matrix-element-corrected cases the cut-off scheme described in Sect. 2.2.2 is applied, whereas in the POWHEG scheme the cut-off is in the $\bar{p}_\perp$ variable, which in this implementation was set to $\bar{p}_{\perp_{\min}} = 1$ GeV. Since these differences occur only in the low-transverse-momentum region they can be affected by hadronisation corrections. The differences observed therefore indicate that a separate tune of the hadronisation parameters is required for the POWHEG implementation but do not constitute a problem with the description.

Hadron-level results

In order to compare the descriptions of the hadronic final state it is necessary to study the distributions of a set of *event shape variables*. In this section we present comparisons of hadron-level observables for the POWHEG implementation and the default (matrix-element corrected) Herwig++ parton shower to LEP data. We concentrate on a set of observables that are particularly sensitive to the three-jet configuration. A tune of the hadronisation parameters, for the POWHEG implementations, was performed using a full set of LEP observables, as detailed in Ref. [6]. The distributions of the thrust, oblateness, sphericity and planarity event shape variables are shown in Fig. 3.3. The distribution of the three-jet resolution variable in the Durham jet measure is given in Fig. 3.4. The χ^2 values for the two approaches are given in Table 3.1. It is seen that the POWHEG implementation provides a reasonable description of LEP data, on a similar level to the that provided by the default Herwig++, with a slight improvement demonstrated by the χ^2 values of Table 3.1.

3.5 Conclusions

Parton showers and NLO fixed-order calculations represent complimentary approaches whose virtues may be combined with a NLO matching method. The most well-developed of these methods is the MC@NLO scheme, however the POWHEG method is a novel scheme which has the advantage of producing only positive-weight events and having a decreased dependence on the parton shower in which it is implemented.

In this chapter the POWHEG method has been reviewed and an implementation of the method in Herwig++, for the process $e^+e^- \rightarrow$ hadrons was presented. This is the
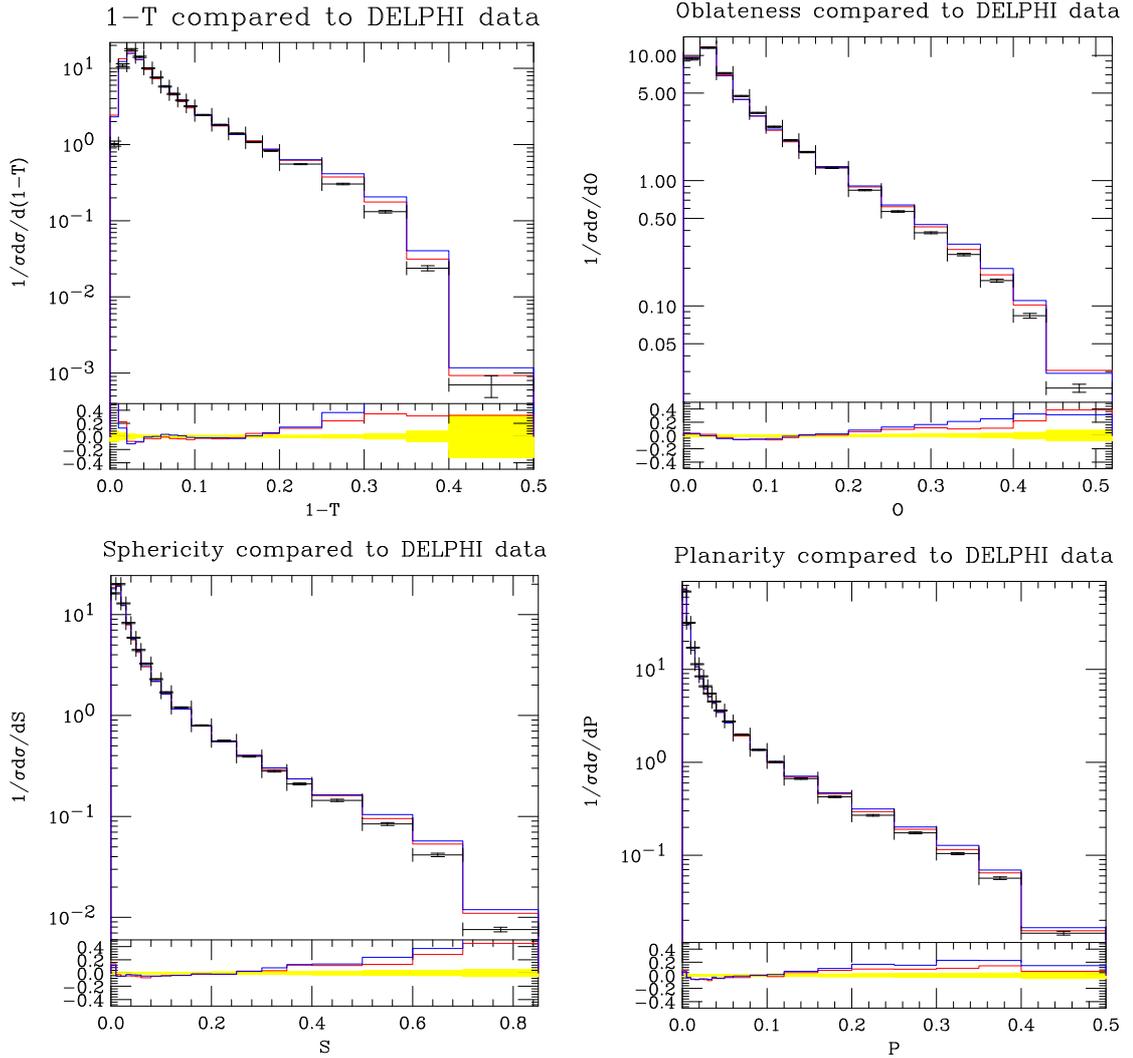
Figure 3.3: Distributions of the event shape variables thrust, oblateness, sphericity and planarity for $e^+e^- \to$ hadrons at a centre-of-mass energy of $\sqrt{s} = 91.2\,\mathrm{GeV}$ in comparison to LEP data (black) [98]. The red line gives the POWHEG distribution and the blue line gives the default (matrix-element corrected) Herwig++ distribution.
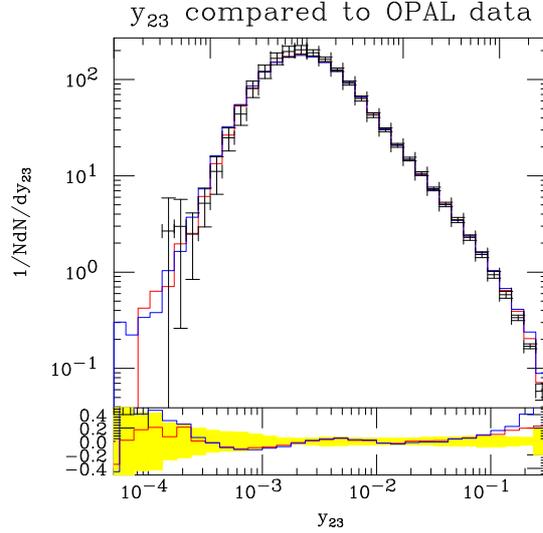
Figure 3.4: Distributions of the scale at which three jets are resolved in the Durham jet measure for $e^+e^- \to$ hadrons at a centre-of-mass energy of $\sqrt{s} = 91.2\,\text{GeV}$ in comparison to LEP data [99]. The colours of the lines are the same as those in Fig. 3.3.

Observable	Hw+ME χ^2/d.o.f	POWHEG χ^2/d.o.f
Thrust	23.48	20.01
Sphericity	5.638	4.782
Oblateness	2.450	3.546
Planarity	1.249	1.663
y_{23}	2.400	0.944

Table 3.1: A comparison of the χ^2 per degree of freedom for event shape observables in $e^+e^- \to$ hadrons with default Herwig++, with matrix-element corrections, and the POWHEG implementation.

simplest possible process and represents an important test bed for the implementation of the method. The implementation presented is the first to provide a full treatment of the truncated shower.

The POWHEG implementation was found to give a reasonable description of LEP data. No significant differences between the matrix-element correction and POWHEG methods are observed for this process. This is to be expected since both methods correspond to a correction of the hardest emission that is equivalent in the NLL approximation.

Chapter 4

Implementing the POWHEG method for Drell-Yan vector boson production

4.1 Introduction

In this chapter the work of Ref. [1] is presented, in which the POWHEG approach is applied to Drell-Yan vector boson production with the Herwig++ event generator.

The implementation follows closely that described in Chapter 3 but involves a more complicated NLO cross section and an initial-state POWHEG emission. In particular, the implementation for this process is complicated by a non-trivial $\bar{B}$-function which requires a careful manipulation of the NLO cross section.

The chapter is organised as follows. In Sect. 4.2 we collect the essential formulae relating to the NLO cross section, for implementation in the simulation. In Sect. 4.3 we give details of the event generation process for the hard configurations and subsequent POWHEG shower. In Sect. 4.4 we present the results of the implementation, comparing it to Tevatron data.

4.2 Next-to-leading order cross section

Although the NLO cross section for the Drell-Yan process was calculated 30 years ago [68, 69], we have implemented an independent calculation of it more suited to our present goal, including the decay of the vector boson and γ/Z interference effects. In this section we collect the ingredients that arise in the NLO calculation for $q + \bar{q} \rightarrow l + \bar{l}$,

102

necessary to describe the implementation of the POWHEG method.

4.2.1 Kinematics and phase space

The leading-order process under study is of the type, $\bar{p}_\oplus + \bar{p}_\ominus \rightarrow \bar{p}_1 + ... + \bar{p}_n$, in which all particles in the n-body final state are colourless. We denote the incoming hadron momenta $P_\oplus$, for hadrons incident in the $\pm z$ directions, respectively. The corresponding massless parton momenta, with momentum fractions $\bar{x}_\oplus$ and $\bar{x}_\ominus$, are given by $\bar{p}_\oplus = \bar{x}_\oplus P_\oplus$. The momenta of the particles produced in the leading-order n-body process are $\bar{p}_i$, where i ranges from 1 to n. The leading-order phase-space element $\mathbf{\Phi_n}$ is defined in Eq. 3.3.

It will also be convenient to define $\bar{p}$ as the total momentum of the colour neutral particles, $\bar{p} \equiv \bar{x}_\oplus P_\oplus + \bar{x}_\ominus P_\ominus$, and $\bar{y}$ as the rapidity of $\bar{p}$ in the hadronic centre-of-mass frame. The partons' momentum fractions are then given by

$$\bar{x}_\oplus = \sqrt{\frac{\bar{p}^2}{s}} \exp\left(\pm\bar{y}\right). \tag{4.1}$$

The phase-space element for the leading-order process can therefore be written as

$$\mathrm{d}\mathbf{\Phi_n} = \frac{1}{s}\,\mathrm{d}\bar{p}^2\,\mathrm{d}\bar{y}\,\mathrm{d}\Phi_n, \tag{4.2}$$

where s is the hadronic centre-of-mass energy and $\mathrm{d}\Phi_n$ is the Lorentz invariant phase space for the partonic process, in $d = 4 - 2\epsilon$ dimensions.

The real emission corrections to the leading-order process consist of $2 \rightarrow n + 1$ processes, $p_\oplus + p_\ominus \rightarrow p_1 + ... + p_n + k$, where we denote the momenta of the n final-state colourless particles p_i and that of the extra colour charged parton by k. The momentum fractions of the incoming partons are distinguished from those in the $2 \rightarrow n$ process as $x_\oplus$ and $x_\ominus$ ($p_\oplus = x_\oplus P_\oplus$). For these processes we introduce the Mandelstam variables $\hat{s}$, $\hat{t}$, $\hat{u}$ and the related *radiative variables* $\Phi_r = \{x, v, \phi\}$, which parameterise the extra emission:

$$\hat{s} = (p_\oplus + p_\ominus)^2 = \frac{p^2}{x}, \tag{4.3a}$$

$$\hat{t} = (p_\oplus - k)^2 = \frac{p^2}{x}(x-1)(1-v), \tag{4.3b}$$

$$\hat{u} = (p_\ominus - k)^2 = \frac{p^2}{x}(x-1)v, \tag{4.3c}$$

where ϕ is the azimuthal angle of k with respect to the beam direction and p is the total momentum of the colourless particles, $p \equiv x_\oplus P_\oplus + x_\ominus P_\ominus - k$. In the hadronic centre-of-mass frame, the momentum of the incoming partons, radiated parton and colourless particles are given by,

$$
p_\oplus = \frac{1}{2}\sqrt{s}\left(x_\oplus; 0, 0, +x_\oplus\right), \; p = \left(\sqrt{p^2 + p_\perp^2}\cosh y; p_\perp \sin\phi, p_\perp \cos\phi, \sqrt{p^2 + p_\perp^2}\sinh y\right),
$$

$$
p_\ominus = \frac{1}{2}\sqrt{s}\left(x_\ominus; 0, 0, -x_\ominus\right), \; k = \left(p_\perp \cosh y_k; -p_\perp \sin\phi, -p_\perp \cos\phi, p_\perp \sinh y_k\right), \tag{4.4}
$$

where $p_\perp$ is the transverse momentum of the radiated parton, relative to the beam direction, which is given by

$$
p_\perp^2 = \frac{\hat{t}\hat{u}}{\hat{s}} = \frac{p^2}{x}v(1-v)(1-x)^2, \tag{4.5}
$$

and y_k is the rapidity of the radiated parton, given by

$$
y_k = y + \frac{1}{2}\log\left[\frac{v(x + v(1-x))}{(1-v)(1-v(1-x))}\right]. \tag{4.6}
$$

The momentum fractions of the partons for $2 \to n+1$ processes are therefore related to those of the $2 \to n$ process by

$$
x_\oplus = \frac{\bar{x}_\oplus}{\sqrt{x}}\sqrt{\frac{1-(1-x)(1-v)}{1-(1-x)v}}, \quad x_\ominus = \frac{\bar{x}_\ominus}{\sqrt{x}}\sqrt{\frac{1-(1-x)v}{1-(1-x)(1-v)}}. \tag{4.7}
$$

The Lorentz invariant $n+1$-body phase-space element may be written in a form factorised in the n-body phase-space element according to

$$
\mathrm{d}\Phi_{n+1} = \frac{\mathrm{d}p^2}{2\pi}\mathrm{d}\Phi_{2(P)}\mathrm{d}\Phi_n. \tag{4.8}
$$

The measure $\mathrm{d}\Phi_{2(P)}$ is the two-body phase space of the radiated parton and total system of colourless particles. After integrating over transverse momentum components this is given, in terms of the radiative variables, by[1]

$$
\mathrm{d}\Phi_{2(P)} = \frac{1}{8\pi}\frac{(4\pi)^\epsilon}{\Gamma(1-\epsilon)}\left(\frac{\mu^2}{p^2}\right)^\epsilon x^\epsilon(1-x)^{1-2\epsilon}v^{-\epsilon}(1-v)^{-\epsilon}\mathrm{d}v. \tag{4.9}
$$

---

[1] For convenience we also include a factor of $\mu^{2\epsilon}$, where μ^2 is regularisation scale. This factor will be present in the radiative matrix elements squared when evaluated in d dimensions.

The integration over incoming momentum fractions may be parameterised in terms of the radiative variable x and the rapidity of the colourless system, y, according to

$$\mathrm{d}x_\oplus \mathrm{d}x_\ominus = \frac{\hat{s}}{xs}\mathrm{d}x\mathrm{d}y. \tag{4.10}$$

We may provide a simultaneous Monte Carlo sampling of the n- and $n+1$-body phase spaces by choosing $\bar{p}^2 \equiv p^2$ and $\bar{y} \equiv y$. The full $n+1$-body phase space, can then be written, in a form factorised from that of the n-body system, as

$$\mathrm{d}\boldsymbol{\Phi_{n+1}} = \mathrm{d}\boldsymbol{\Phi_n}\mathrm{d}\Phi_r \frac{K(\epsilon)}{(4\pi)^2}\frac{\hat{t}\hat{u}}{p^2}\mathcal{J}(x,v), \tag{4.11}$$

where

$$\mathcal{J}(x,v) = x^\epsilon(1-x)^{-1-2\epsilon}v^{-1-\epsilon}(1-v)^{-1-\epsilon}, \tag{4.12}$$

$$K(\epsilon) = \left(\frac{4\pi\mu^2}{p^2}\right)^\epsilon \frac{1}{\Gamma(1-\epsilon)}, \tag{4.13}$$

and the radiative integration measure is

$$\mathrm{d}\Phi_r = \mathrm{d}v\mathrm{d}x. \tag{4.14}$$

The matrix elements squared for the radiative corrections contain S and ISC divergences corresponding to the limits $\hat{t} \to 0$ and $\hat{u} \to 0$ for emissions collinear to the directions $p_\oplus$ and $p_\ominus$ and $\hat{t}\hat{u} \to 0$ for soft emissions. The factor of $\hat{t}\hat{u}$ in Eq. 4.11 therefore means that all singularities appearing in the resulting cross sections have been absorbed into the function $\mathcal{J}(x,v)$.

In order to extract the singularities from the radiative contributions, a subtraction scheme must be employed, as detailed in Sect. 3.2.2. We choose to do this using the *plus-prescription*. The plus prescription can be used to extract the singularities from integrals of the type,

$$I = \int_0^1 \mathrm{d}F(x)G(x), \tag{4.15}$$

where $G(x)$ is a finite function and $F(x)$ is divergent in the limit $x \to 1$. Adding and subtracting $F(x)G(1)$ from the integrand, the integral may be written by

$$I = \int_0^1 \mathrm{d}x F_+(x)G(x) - G(1) \int_0^1 \mathrm{d}x F(x), \qquad (4.16)$$

where the first term defines the plus distribution as

$$\int_0^1 \mathrm{d}x F_+(x)G(x) = \int_0^1 \mathrm{d}x \left(F(x)G(x) - F(x)G(1) \right), \qquad (4.17)$$

which is finite. The second term in Eq. 4.16 contains the singularity and, which provided $F(x)$ is sufficiently simple, can be evaluated in d dimensions yielding the singularities as poles in ϵ.

Applying this procedure to the function $\mathcal{J}(x,v)$ in Eq. 4.11, as detailed in Appendix B.1, yields

$$\mathcal{J}(x,v) = \left[\mathcal{S}\delta(1-x) + \mathcal{C}(x)(\delta(v) + \delta(1-v)) + \mathcal{H}(x,v) \right], \qquad (4.18)$$

where

$$\mathcal{S} = \frac{1}{\epsilon^2} - \frac{\pi^2}{6}, \qquad (4.19a)$$

$$\mathcal{C}(x) = -\frac{1}{\epsilon} \frac{1}{(1-x)_+} - \frac{\log x}{(1-x)} + 2\left(\frac{\log(1-x)}{1-x}\right)_+, \qquad (4.19b)$$

$$\mathcal{H}(x,v) = \frac{1}{(1-x)_+}\left(\frac{1}{v_+} + \frac{1}{(1-v)_+}\right). \qquad (4.19c)$$

The labeling $\mathcal{S}$, $\mathcal{C}$, $\mathcal{H}$ reflects the fact that the $\mathcal{S}$ and $\mathcal{C}$ terms are multiplied by δ-functions which limit their contributions to configurations with S $(x \to 1)$ and ISC $(v \to 0,1)$ emissions, while $\mathcal{H}$ is not associated with soft or collinear configurations but instead contributes to hard emissions of the extra parton k.

4.2.2 Matrix elements

Radiative corrections:

The matrix elements contributing to the radiative corrections for this process are given in Fig. 4.1 There are three contributing partonic processes in which the processes are initiated by quark-antiquark, quark-gluon and gluon-antiquark incoming parton configurations.
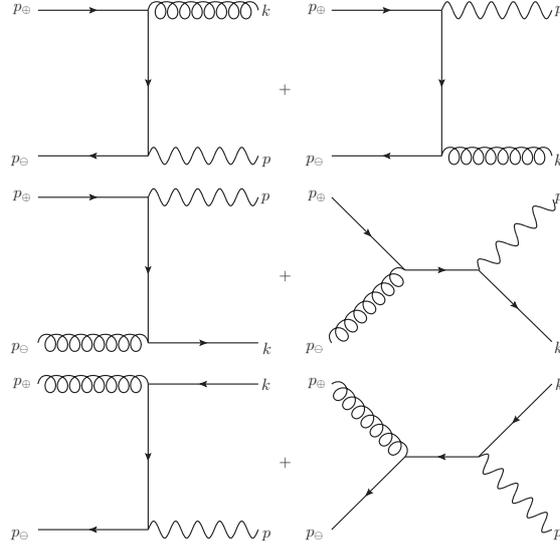
Figure 4.1: The $\mathcal{O}(\alpha_S)$ radiative corrections to Drell-Yan vector boson production.

The matrix elements for the radiative corrections should be calculated in d dimensions resulting in terms of $\mathcal{O}(\epsilon)$ in addition to those appearing in the 4-dimensional result. These matrix elements must be integrated over the phase space in Eq. 4.11, from which it is clear that all terms of $\mathcal{O}(\epsilon)$ will only contribute in the physical $\epsilon \to 0$ limit if they multiply a term containing a δ-function. These δ-functions correspond to the soft and collinear limits where the matrix elements have a universal factorised form. We therefore consider the radiative matrix elements in the three regions separately: non-soft, non-collinear emissions; soft emissions; and collinear emissions. In the first region we may evaluate the matrix elements in 4-dimensions allowing us to apply a technique referred to as the *Kleiss trick* [66, 70] to write the matrix elements in a factorised form. Such a factorisation of the matrix element is not necessary for the implementation of the POWHEG method but it improves the flexibility and generality of our implementation of the Drell-Yan process.

In four dimensions, the matrix elements may be calculated helicity-wise and the Kleiss trick dictates that we should work in the CALKUL [67] gauge where the $\not{\epsilon}$-tensor is given by

$$\not{\epsilon}(k,\rho) = N\left(\frac{1}{2}(1+\rho\gamma^5)\not{k}\not{p}_\ominus\not{p}_\oplus - \not{p}_\ominus\not{p}_\oplus\not{k}\frac{1}{2}(1+\rho\gamma^5)\right), \tag{4.20}$$

where ρ is the helicity of the emitted parton and

$$N = (4(p_\oplus \cdot p_\ominus)(p_\oplus \cdot k)(p_\ominus \cdot k))^{-\frac{1}{2}} . \tag{4.21}$$

In this gauge the two diagrams in each partonic subprocess correspond to different helicity configurations and therefore the interference between the two diagrams is absorbed into the $\not\!\epsilon$-tensor, allowing the n-body matrix element to be factorised out. This calculation is described in Ref. [70] and gives

$$\left|\bar{\mathcal{M}}_{q\bar{q}}^{n+1}\right|^2 = \frac{8\pi\alpha_S C_F}{p^2 \hat{t} \hat{u}} \left[\left(\hat{s}+\hat{t}\right)^2 \left|\bar{\mathcal{M}}_{q\bar{q}}^B(\tilde{p}_q, \tilde{p}_{\bar{q}g})\right|^2 \right. \tag{4.22}$$
$$\left. + (\hat{s}+\hat{u})^2 \left|\bar{\mathcal{M}}_{q\bar{q}}^B(\tilde{p}_{qg}, \tilde{p}_{\bar{q}})\right|^2 \right],$$

$$\left|\bar{\mathcal{M}}_{qg}^{n+1}\right|^2 = -\frac{8\pi\alpha_S T_F}{p^2 \hat{u} \hat{s}} \left[\left(\hat{t}+\hat{u}\right)^2 \left|\bar{\mathcal{M}}_{q\bar{q}}^B(\tilde{p}_{qg}, \tilde{p}_{\bar{q}})\right|^2 \right. \tag{4.23}$$
$$\left. + \left(\hat{t}+\hat{s}\right)^2 \left|\bar{\mathcal{M}}_{q\bar{q}}^B(\tilde{p}_q, \tilde{p}_{\bar{q}g})\right|^2 \right],$$

$$\left|\bar{\mathcal{M}}_{g\bar{q}}^{n+1}\right|^2 = -\frac{8\pi\alpha_S T_F}{p^2 \hat{s} \hat{t}} \left[(\hat{u}+\hat{s})^2 \left|\bar{\mathcal{M}}_{q\bar{q}}^B(\tilde{p}_{qg}, \tilde{p}_{\bar{q}})\right|^2 \right. \tag{4.24}$$
$$\left. + \left(\hat{u}+\hat{t}\right)^2 \left|\bar{\mathcal{M}}_{q\bar{q}}^B(\tilde{p}_q, \tilde{p}_{\bar{q}g})\right|^2 \right],$$

where, for a more uniform notation we have denoted the final-state quark momentum in the qg initiated process by $p_{\bar{q}}$ and the final-state antiquark momentum in the $g\bar{q}$ process by p_q. The shifted momenta $\tilde{p}_i$, $\tilde{p}_{jg}$ are given by

$$\tilde{p}_i = \frac{1}{x_i} p_i ,$$
$$x_i = \frac{2p.p_i}{p^2} , \tag{4.25}$$
$$\tilde{p}_{jg} = p - \tilde{p}_i ,$$

The shifted momenta satisfy

$$\tilde{p}_i^2 = \tilde{p}_{jg}^2 = 0, \qquad\qquad\qquad \tilde{p}_i + \tilde{p}_{jg} = p, \tag{4.26}$$

and therefore satisfy requirements for them to be considered as describing a kinematic configuration for the leading-order process, hence they are valid arguments for $\bar{\mathcal{M}}_{q\bar{q}}^B$.

We now consider the regions of soft and collinear emission where the matrix elements have a universal factorised form which we give in d-dimensions. In the soft limit, $x \to 1$,

only the radiative processes describing a gluon emission contribute. In the limit that a soft gluon is emitted, the matrix elements factorise according to

$$\lim_{x \to 1} \left| \bar{\mathcal{M}}_{ab}^{n+1} \right|^2 = 8\pi \alpha_S 2 C_{ab} \frac{\hat{s}}{\hat{t}\,\hat{u}} \left| \bar{\mathcal{M}}_{ab}^n \left(\bar{p}_\oplus, \bar{p}_\ominus \right) \right|^2. \tag{4.27}$$

where $ab = (q\bar{q}, qg, q\bar{q})$ and the colour factor, C_{ab}, is equal to C_A for the qg and $g\bar{q}$ channels and C_F for the $q\bar{q}$ channel[2]. In the collinear limits, $v \to 0, 1$, the matrix elements factorise according to

$$\lim_{v \to 1} \left| \bar{\mathcal{M}}_{ab}^{n+1} \right|^2 = \frac{\hat{s}}{x\hat{t}\hat{u}} 8\pi \alpha_S \left(1 - x \right) P_{cd} \left(x; \epsilon \right) \left| \bar{\mathcal{M}}_{ab}^n \left(x\bar{p}_\oplus, \bar{p}_\ominus \right) \right|^2, \tag{4.28}$$

$$\lim_{v \to 0} \left| \bar{\mathcal{M}}_{ab}^{n+1} \right|^2 = \frac{\hat{s}}{x\hat{t}\hat{u}} 8\pi \alpha_S \left(1 - x \right) P_{cd} \left(x; \epsilon \right) \left| \bar{\mathcal{M}}_{ab}^n \left(\bar{p}_\oplus, x\bar{p}_\ominus \right) \right|^2, \tag{4.29}$$

where the flavour indices $cd(ab)$ are $cd = qq$ for the $q\bar{q}$ channel and $cd = gq$ for the qg and $g\bar{q}$ channels[3].

The functions $P_{cd}\left(x; \epsilon \right)$ are the unregularised splitting functions in d dimensions and are given by the standard splitting functions introduced in Sect. 1.1.4 with additional $\mathcal{O}(\epsilon)$ terms according to

$$P_{cd}\left(x; \epsilon \right) = P_{cd}\left(x \right) + \epsilon P_{cd}^\epsilon \left(x \right) + \mathcal{O}(\epsilon^2), \tag{4.30}$$

where

$$\begin{aligned} P_{qq}^\epsilon \left(x \right) &= -(1 - x), \\ P_{gg}^\epsilon \left(x \right) &= 0, \\ P_{gq}^\epsilon \left(x \right) &= -2x(1 - x). \end{aligned} \tag{4.31}$$

Virtual corrections:

The $\mathcal{O}(\alpha_S)$ contribution to the virtual correction comes from the interference of the one-loop vertex correction diagram, shown in Fig. 4.2, with the leading-order diagram. In d dimensions the matrix element squared from this contribution is given by

$$\left| \bar{\mathcal{M}}_{q\bar{q}}^V \right|^2 = \frac{\alpha_S C_F}{2\pi} K(\epsilon) \left[-\frac{2}{\epsilon^2} - \frac{3}{\epsilon} - 8 + \pi^2 \right] \left| \bar{\mathcal{M}}_{q\bar{q}}^B \left(p_q, p_{\bar{q}} \right) \right|^2. \tag{4.32}$$

---

[2]For the process considered, it is only the $q\bar{q}$ which contributes in the soft limit.

[3]For ease of notation we have used an alternate labeling of the splitting functions to that used in previous chapters, where the labeling $\widetilde{iji}$ is equivalent to $\widetilde{ij \to ij}$.
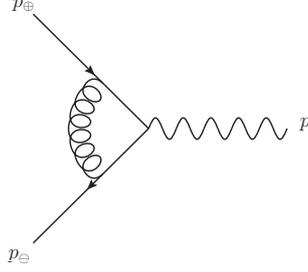
Figure 4.2: The $\mathcal{O}(\alpha_S)$ one-loop correction to Drell-Yan vector boson production.

4.2.3 Differential cross section

Having calculated the matrix elements and phase space, we may define the terms $B(\mathbf{\Phi}_n)$, $R(\mathbf{\Phi}_{n+1})$ and $V(\mathbf{\Phi}_n)$ in the NLO cross section in Eq. 3.9. Each of these terms consists of the matrix elements, a phase-space factor and a parton-flux factor.

The partonic flux due to parton a in hadron A and parton b in hadron B, at scale μ^2, with momentum fractions $x_\oplus$ and $x_\ominus$ respectively, is defined as

$$\mathcal{L}_{ab}\left(x_\oplus, x_\ominus\right) = f_a^A\left(x_\oplus, \mu^2\right) f_b^B\left(x_\ominus, \mu^2\right). \tag{4.33}$$

The functions $f_i^I\left(x_i, \mu^2\right)$ are the parton distribution functions (PDFs) for finding a parton i in hadron I with momentum fraction x_i at scale μ^2. The contribution to the differential cross section from the leading-order process is therefore

$$\mathrm{d}\sigma_{q\bar{q}}^B = B\left(\mathbf{\Phi_n}\right) \mathrm{d}\mathbf{\Phi_n}, \tag{4.34}$$

where

$$B\left(\mathbf{\Phi_n}\right) = \frac{1}{2p^2}\left|\bar{\mathcal{M}}_{q\bar{q}}^B\left(\bar{p}_\oplus, \bar{p}_\ominus\right)\right|^2 \mathcal{L}_{q\bar{q}}\left(\bar{x}_\oplus, \bar{x}_\ominus\right). \tag{4.35}$$

The divergent radiative contributions in Eq. 3.1 are given by

$$R_0\left(\mathbf{\Phi_{n+1}}\right) = \frac{K(\epsilon)}{(4\pi)^2}\frac{\hat{t}\hat{u}}{p^2}\mathcal{J}\left(x, v\right)\frac{1}{2\hat{s}}\sum_{ab}\left|\bar{\mathcal{M}}_{ab}^{n+1}\right|^2 \mathcal{L}_{ab}\left(x_\oplus, x_\ominus\right). \tag{4.36}$$

Since we have defined, $p^2 = \bar{p}^2$ and $y = \bar{y}$, the shifted incoming momenta, appearing as the arguments of the leading-order matrix elements in Eqs. 4.22 and 4.28, are related

to those of the Born process by a boost. Lorentz invariance of the matrix elements implies that we can equate

$$\left| \bar{\mathcal{M}}^B_{q\bar{q}} (\tilde{p}_i, \tilde{p}_j) \right|^2 \mathrm{d}\mathbf{\Phi_n} = \left| \bar{\mathcal{M}}^B_{q\bar{q}} (\bar{p}_\oplus, \bar{p}_\ominus) \right|^2 \mathrm{d}\mathbf{\Phi_n}, \tag{4.37}$$

leading to a complete factorisation of the Born contribution[4]. Therefore the radiative contribution can be written in the factorised form

$$R_0 \left(\mathbf{\Phi_{n+1}} \right) = \sum_{ab} \frac{\alpha_S C_{ab}}{2\pi} \frac{\mathcal{R}_{0\,ab}}{x} \hat{\mathcal{L}}_{ab} \left(x_\oplus, x_\ominus \right) B \left(\mathbf{\Phi_n} \right), \tag{4.38}$$

where we have defined the radiative weights

$$\mathcal{R}_{0\,ab} = K(\epsilon) \mathcal{J} \left(x, v \right) \frac{x^2 \hat{t} \hat{u}}{p^2} \frac{\left| \bar{\mathcal{M}}^{n+1}_{ab} \right|^2}{8\pi \alpha_s C_{ab} \left| \bar{\mathcal{M}}^n_{q\bar{q}} (\bar{p}_\oplus, \bar{p}_\ominus) \right|^2}, \tag{4.39}$$

and the ratio of flux factors

$$\hat{\mathcal{L}}_{ab} \left(x_\oplus, x_\ominus \right) = \frac{\mathcal{L}_{ab} \left(x_\oplus, x_\oplus \right)}{\mathcal{L}_{q\bar{q}} \left(\bar{x}_\oplus, \bar{x}_\ominus \right)}. \tag{4.40}$$

Each of the radiative weight functions (Eq. 4.39) can be written as

$$\mathcal{R}_{0\,ab} = \mathcal{S}_{0\,ab} \delta(1-x) + \mathcal{C}_{0\,ab} \left(\delta(v) + \delta(1-v) \right) + \mathcal{H}_{ab}, \tag{4.41}$$

where $\mathcal{S}_{0\,ab}$ and $\mathcal{C}_{0\,ab}$ are the divergent soft and collinear contributions respectively and $\mathcal{H}_{ab}$ are the finite non-soft, non-collinear contributions.

The divergent virtual contribution is given by

$$V_0 \left(\mathbf{\Phi_n} \right) = \frac{\alpha_S C_F}{2\pi} K(\epsilon) \left[-\frac{2}{\epsilon^2} - \frac{3}{\epsilon} - 8 + \pi^2 \right] B \left(\mathbf{\Phi_n} \right). \tag{4.42}$$

The KLN theorem dictates that the singularities in this contribution should cancel with those coming from the soft contribution in the radiative corrections. This soft contribution comes exclusively from the $q\bar{q}$ channel and corresponds to $\mathcal{S}_{0\,q\bar{q}}$ which consists of two terms,

$$\mathcal{S}_{0\,q\bar{q}} = \mathcal{S}^S_{0\,q\bar{q}} + \mathcal{S}^{SC}_{0\,q\bar{q}}. \tag{4.43}$$

---

[4]In order to obtain the correct correlations between the production and decay processes, the different shifted momenta must still be taken into account when constructing the momenta.

The first soft term comes from the phase-space term in Eq. 4.19a and the matrix element squared in Eq. 4.27, giving

$$
\mathcal{S}^S_{0\,q\bar{q}} = K(\epsilon) \left[\frac{2}{\epsilon^2} - \frac{\pi^2}{3} \right]. \tag{4.44}
$$

A further soft-collinear contribution comes from the product of the collinear factorised matrix elements squared in Eq. 4.28 with the first term of the phase-space contribution in Eq. 4.19b. This gives

$$
\mathcal{S}^{SC}_{0\,q\bar{q}} = K(\epsilon)\frac{3}{\epsilon} - 3\log\left(\frac{\mu^2}{p^2}\right). \tag{4.45}
$$

Putting together the contributions in Eqs. 4.42-4.45 and expanding to $\mathcal{O}(\epsilon)$, yields the finite, subtracted virtual contribution

$$
V\left(\mathbf{\Phi_n}\right) = \frac{\alpha_S C_F}{2\pi} \mathcal{V} B\left(\mathbf{\Phi_n}\right), \tag{4.46}
$$

where

$$
\mathcal{V} = \frac{2\pi^2}{3} - 8 - 3\log\left(\frac{\mu^2}{p^2}\right), \tag{4.47}
$$

and we have used the expansion of $K(\epsilon)$

$$
K(\epsilon) = 1 + \epsilon\left(\log(4\pi) + \log\left(\frac{\mu^2}{p^2}\right) - \gamma_E\right) + \mathcal{O}(\epsilon^2). \tag{4.48}
$$

Having subtracted the soft contributions with the virtual singularities, the radiative contributions become

$$
\mathcal{R}_{0\,ab} = \left[-\frac{K(\epsilon)}{\epsilon}\hat{P}_{cd} + \mathcal{C}_{ab}\right](\delta(v) + \delta(1-v)) + \mathcal{H}_{ab}, \tag{4.49}
$$

where $\hat{P}_{ab}$ are the regularised splitting functions and $\mathcal{C}_{ab}$ are the finite collinear contributions.

For the $q\bar{q}$ contribution, the relevant functions are given by

$$\hat{P}_{qq} = \left(\frac{1 + x^2}{1 - x}\right)_+, \tag{4.50a}$$

$$\mathcal{C}_{q\bar{q}} = \left(1 + x^2\right)\left(\frac{1}{(1-x)_+}\log\left(\frac{p^2}{x\mu^2}\right) + 2\left(\frac{\log(1-x)}{1-x}\right)_+\right) + 1 - x, \tag{4.50b}$$

$$\mathcal{H}_{q\bar{q}} = \frac{1}{(1-x)_+}\left(\frac{1}{v_+} + \frac{1}{(1-v)_+}\right)\left((1-x)^2(1 - 2v(1-v)) + 2x\right). \tag{4.50c}$$

For the qg contribution we have

$$\hat{P}_{gq} = x^2 + (1-x)^2, \tag{4.51a}$$

$$\mathcal{C}_{qg} = \left(x^2 + (1-x)^2\right)\left(\log\left(\frac{p^2}{\mu^2 x}\right) + 2\log(1-x)\right) + 2x(1-x), \tag{4.51b}$$

$$\mathcal{H}_{qg} = \frac{1}{v_+}\left(2x(1-x)v + (1-x)^2 v^2 + x^2 + (1-x)^2\right). \tag{4.51c}$$

The function $\mathcal{R}_{0\,g\bar{q}}$ is equal to $\mathcal{R}_{0\,qg}$ under the replacement $v \leftrightarrow 1 - v$.

The remaining divergences are ISC divergences proportional to P_{ab}. Working in the $\overline{\text{MS}}$ scheme these are absorbed into the definition of the PDFs. In full, the finite radiative contribution is

$$R\left(\mathbf{\Phi_{n+1}}\right) = \frac{\alpha_S}{2\pi}\sum_{ab}C_{ab}\frac{\mathcal{R}_{ab}}{x}\hat{\mathcal{L}}_{ab}\left(x_\oplus, x_\ominus\right)B\left(\mathbf{\Phi_n}\right), \tag{4.52}$$

where the functions $\mathcal{R}_{ab}$ are given by

$$\mathcal{R}_{q\bar{q}} = \mathcal{C}_{q\bar{q}}\left(\delta(1-v) + \delta(v)\right) + \mathcal{H}_{q\bar{q}},$$

$$\mathcal{R}_{qg} = \mathcal{C}_{qg}\delta(v) + \mathcal{H}_{qg}, \tag{4.53}$$

$$\mathcal{R}_{g\bar{q}} = \mathcal{C}_{g\bar{q}}\delta(1-v) + \mathcal{H}_{g\bar{q}}. \tag{4.54}$$

4.3 Implementation in Herwig++

In the following section we describe the generation of the hardest emission. In Sect. 4.3.3 we describe the simulation of further, lower $p_\perp$, emissions, from the radiative events, using the truncated and vetoed shower algorithms.

4.3.1 Generation of the n-body configurations

The n-body configurations should be generated according to the $\bar{B}-$function, defined in Eq. 3.46, which corresponds to the differential NLO cross section integrated over the radiative variables. The way in which the leading-order process is factorised inside the real emission terms, R_{ab}, results in the $\bar{B}$ function

$$\bar{B}\left(\boldsymbol{\Phi_n}\right) = B\left(\boldsymbol{\Phi_n}\right) \left[1 + \frac{\alpha_S C_F}{2\pi}\mathcal{V} + \sum_{ab}\int \mathrm{d}\Phi_r \frac{\alpha_S C_{ab}}{2\pi}\frac{\mathcal{R}_{ab}}{x}\hat{\mathcal{L}}_{ab}(x_\oplus, x_\ominus)\right], \qquad (4.55)$$

which can be implemented as a straightforward reweighting of the leading-order cross section.

For convenience the radiative phase space $\mathrm{d}\Phi_R$ is reparameterised by variables on the interval $[0,1]$ such that the radiative-phase-space volume is unity, a three-dimensional unit cube. This is achieved by a trivial change of variables $\phi \to \bar{\phi} = \phi/2\pi$ and $x \to \tilde{x}$, where $\tilde{x}$ is defined by

$$x\left(\tilde{x}, v\right) = \bar{x}\left(v\right) + \left(1 - \bar{x}\left(v\right)\right)\tilde{x}, \qquad (4.56)$$

where $\bar{x}(v)$ is the lower limit on the x integration. Numerical implementation of the $\bar{B}\left(\boldsymbol{\Phi_n}\right)$ distribution requires that all plus distributions should be replaced by regular functions, according to the identities given in Appendix B.2.

The generation of the n-body configuration proceeds as follows:

1. a leading-order configuration is generated using the standard Herwig++ leading-order matrix element generator, providing the Born variables $\boldsymbol{\Phi_n}$ with an associated weight $B\left(\boldsymbol{\Phi_n}\right)$;

2. radiative variables Φ_R are then generated by sampling $\bar{B}\left(\boldsymbol{\Phi_n}\right)$, parameterised in terms of the 'unit-cube' variables $\tilde{x}$, v, $\bar{\phi}$, using the Auto-Compensating Divide-and-Conquer (ACDC) phase space generator [71], which implements a variant of the VEGAS algorithm [72];

3. the leading-order configuration is accepted with a probability proportional to the integrand of Eq. 4.55 evaluated at $\{p^2,\ y,\ \Phi_R\}$.

4.3.2 Generation of the hardest emission

The hardest emission is generated from the n-body configuration according Eq. 3.47 with the modified Sudakov form factor of Eq. 3.44. The integrand in the exponent of the Sudakov form factor is given by

$$\frac{R_0\left(\boldsymbol{\Phi_{n+1}}\right)}{B\left(\boldsymbol{\Phi_n}\right)} = \sum_{ab} \frac{\alpha_S C_{ab}}{2\pi} \frac{\hat{\mathcal{H}}_{ab}}{x} \hat{\mathcal{L}}_{ab}\left(x_\oplus, x_\ominus\right), \tag{4.57}$$

where $\hat{\mathcal{H}}_{ab}$ is equal to $\mathcal{H}_{ab}$ without the plus prescription.

In generating the hardest emission we choose to parameterise the radiative phase space in terms of the transverse momentum and rapidity of the emitted parton in order to simplify the implementation of the Θ-function in the modified Sudakov form factor. These variables are defined in Eqs. 4.5 and 4.6 and introduce a further Jacobean factor according to

$$d\Phi_r = dxdv = \frac{2p_\perp}{\hat{s}} \frac{x}{(1-x)} dp_\perp dy_k. \tag{4.58}$$

The integrand in the exponent of the Sudakov form factor for each channel $ab=q\bar{q}$ is therefore given by

$$W_{ab} = \frac{R_{0\,ab}\left(\boldsymbol{\Phi_{n+1}}\right)}{B\left(\boldsymbol{\Phi_n}\right)} = \frac{\alpha_S C_{ab}}{\pi} \hat{\mathcal{H}}_{ab} \, \hat{\mathcal{L}}_{ab}\left(x_\oplus, x_\ominus\right) \frac{p_\perp}{\hat{s}(1-x)}. \tag{4.59}$$

The modified Sudakov form factor for each channel therefore has the form

$$\Delta_{ab}^R\left(p_\perp\right) = \exp\left(-\int_{p_\perp}^{p_{\perp max}} dp_\perp dy_k W_{ab}\right). \tag{4.60}$$

In order to generate the radiative variables $(p_\perp, y_k)$ with the veto algorithm we define bounding functions for each channel. Functions of the form,

$$g_{ab}\left(p_\perp\right) = \frac{K_{ab}}{p_\perp^2}, \tag{4.61}$$

are used, with suitable values of K_{ab} for each channel together with an overestimate of the limits for the rapidity integral, $y_{k_{\min}}$ and $y_{k_{\max}}$. The generation procedure then proceeds as follows:

1. $p_\perp$ is set to $p_{\perp_{\max}}$;

2. a new $(p_\perp, y_k)$ configuration is generated using two random numbers according to

$$p_\perp = \left(\frac{1}{p_\perp} - \frac{1}{K_{ab} \left(y_{k_{\max}} - y_{k_{\min}} \right)} \log \mathcal{R} \right)^{-1}, \qquad (4.62\text{a})$$

$$y_k = y_{k_{\min}} + \mathcal{R} \left(y_{k_{\max}} - y_{k_{\min}} \right); \qquad (4.62\text{b})$$

3. if $p_\perp < p_{\perp_{\min}}$ then no radiation is generated;

4. if the generated configuration is outside of the exact phase space boundaries then return to step 2;

5. if $W_{ab}/g_{ab}(p_\perp) > \mathcal{R}$ then accept the configuration, otherwise return to step 2.

For this process there are three partonic channels contributing to the radiative corrections, this is dealt with by using *competition*, where a $(p_\perp, y_k)$ configuration is generated, as outlined above, for each channel individually and the configuration with the highest $p_\perp$ accepted. This algorithm is discussed in Appendix A.4.

In generating the Born and radiative variables, the shifted momenta appearing in the factorised Born matrix elements in Eq. 4.22 could be ignored. In reconstructing the momenta of the $n + 1$-configuration however they must be taken into account. This is achieved by employing a simple prescription [70] to generate the azimuthal angle that ensures the leptonic correlations are correctly generated. For the $q\bar{q}$ channel, the prescription proceeds as follows:

1. momenta are first constructed in the vector boson rest frame;

2. the $p_\oplus$ direction is chosen with probability

$$\left(\hat{s} + \hat{t} \right)^2 / \left(\left(\hat{s} + \hat{t} \right)^2 + \left(\hat{s} + \hat{u} \right)^2 \right), \qquad (4.63)$$

otherwise the $p_\ominus$ direction is chosen. The momenta are then rotated around the chosen direction by a random angle generated uniformly on the interval $[0, 2\pi]$;

3. momenta are boosted back to the lab frame such that the rapidity of the vector boson is the same as for the n-body configuration.

The same procedure is used for the qg and $g\bar{q}$ initiated channels with the replacements $\hat{s} \to \hat{t}, \hat{t} \to \hat{u}, \hat{u} \to \hat{s}$ and $\hat{s} \to \hat{u}, \hat{t} \to \hat{s}, \hat{u} \to \hat{t}$, respectively.

4.3.3 Truncated and vetoed parton showers

The full parton shower is produced around the hardest emission with initial-state trun-
cated and vetoed showers which evolve according to Eqs. 3.36 and 3.37 respectively. The
implementation of these showers follows closely that of the final-state case, as described
in Eq. 3.4.4. This implementation requires an inverse momentum reconstruction for the
initial-state shower in order to provide a mapping to the hardest emission shower vari-
ables $(\tilde{q}_h, z_h, \phi_h)$.

4.3.4 Inverse momentum reconstruction

We now describe the process of inverting the momentum reconstruction procedure, pro-
viding a mapping between the reshuffled parton momenta, q', and the shower variables,
$(\tilde{q}, z, \phi)$. The shuffled progenitor momenta may be written in the Sudakov basis as

$$q'_\oplus = \alpha'_\oplus P_\oplus + \beta'_\oplus P_\ominus + q'_{\perp\oplus}. \tag{4.64}$$

The unshuffled progenitor momenta in the same basis are given by

$$q_\oplus = \alpha_\oplus P_\oplus + \beta_\oplus P_\ominus + q_{\perp\oplus}. \tag{4.65}$$

From the definition of the reshuffling boosts in Eq. 2.79, we see that boost parameters
$k_\oplus$, are given by

$$k_\oplus = \frac{\alpha'_\oplus}{\alpha_\oplus}, \tag{4.66}$$

where the α-parameter of the shuffled progenitor is obtained from the momenta according
to

$$\alpha'_\oplus = \frac{q'_\oplus \cdot P_\ominus}{P_\oplus \cdot P_\ominus}. \tag{4.67}$$

By construction the α-parameters of the unshuffled progenitors are given by their light-
cone momentum fraction, $x_\oplus$, which in turn, in the beam centre-of-mass frame, are
related to the preserved rapidity and invariant mass of the system by Eq. 4.1. This
allows the boost parameters to be determined.

Having calculated the boost parameters, the unshuffled progenitor momenta $q_\oplus$, are
given by Eq. 2.79, defining the reshuffling boosts. These boosts are then calculated,
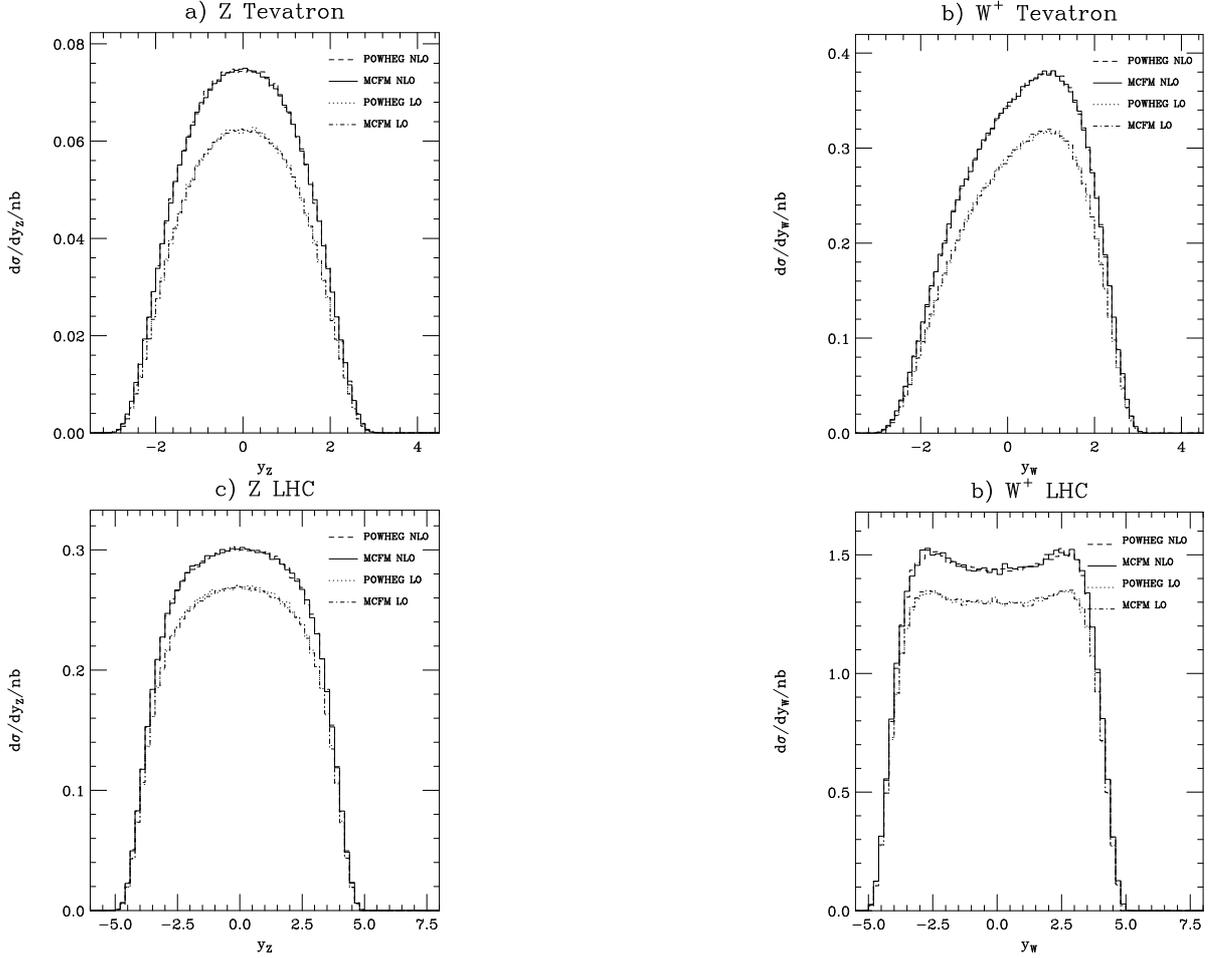
Figure 4.3: Comparisons of $d\sigma/dy$ for the POWHEG implementation and MCFM [73] for Z and W^+ production at the Tevatron ($\sqrt{s} = 2\,\text{TeV}$) and the LHC ($\sqrt{s} = 14\,\text{TeV}$).

inverted and applied to all parton shower momenta, yielding the full set of unshuffled parton momenta. The shower variables can then be obtained recursively from their definitions in Eqs. 2.32, 2.6, 2.7 and 2.8.

4.4 Results

As a check of the calculation of the $\bar{B}\left(\boldsymbol{\Phi_n}\right)$ function, distributions of the vector boson rapidity produced by the POWHEG implementation and the NLO program MCFM [73] were compared. Figure 4.3 shows distributions for γ/Z and W^+ production at the Tevatron (proton-antiproton at $\sqrt{s} = 2\,\text{TeV}$) and the LHC (proton-proton at $\sqrt{s} = 14\,\text{TeV}$). In all cases the total cross sections from MCFM and the POWHEG implementation
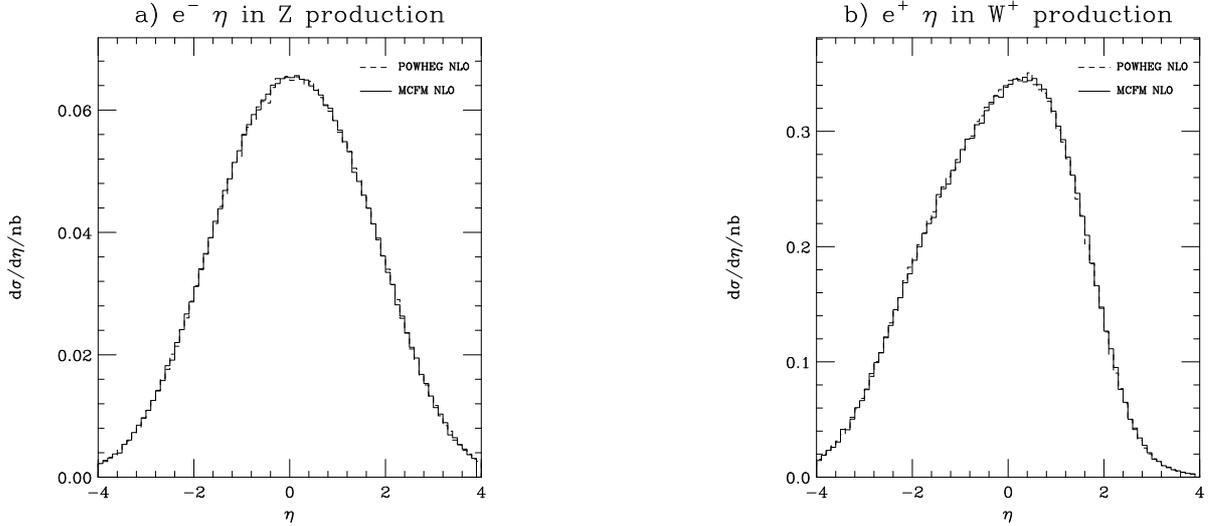
Figure 4.4: The rapidity of a) the electron in Z and b) the positron in W^+ production at
the Tevatron including the leptonic decay of the gauge boson for the POWHEG
implementation and MCFM [73] at the Tevatron ($\sqrt{s} = 2$ TeV).

agreed to within 0.5 %. The distribution of the rapidity of the lepton produced in the
γ/Z and W decay is shown in Fig. 4.4 and is also in good agreement. For both Herwig++
and MCFM in this comparison, the parton density functions used were the MRST2001
NLO [74] set with the LHAPDF interface [75].

In Figs. 4.5-4.8, distributions from the Drell-Yan POWHEG implementations for the
rapidity and transverse momentum of the vector bosons are compared to Tevatron data.
The bottom panel in each of these plots shows the $(\mathrm{Theory} - \mathrm{Data})/\mathrm{Data}$ value for each
bin. In Fig. 4.5 the rapidity distribution of γ/Z bosons of mass 71-111 GeV is compared
to D0 Run II data [76]. Figure 4.6 shows the transverse momentum distribution of γ/Z
bosons of mass 66-116 GeV compared to CDF Run I data [77]. Figure 4.7 shows the
transverse momentum distribution of γ/Z bosons of mass 40-200 GeV compared to D0
Run II data [78]. Figure 4.8 shows the transverse momentum distribution of W bosons
compared to Run I D0 data [79]. In addition to the results from the implementation of
the POWHEG method the results from Herwig++ including a matrix-element correction
and MC@NLO [50–55] are shown.

The Herwig++ results were generated using an intrinsic $p_\perp$ of 2.2 GeV which was
obtained by fitting to the Run I W and Z $p_\perp$ distributions [6]. The POWHEG results
used the same intrinsic $p_\perp$ as for Herwig++ and a minimum $p_\perp$ of 2 GeV for the hardest
emission. The MC@NLO and HERWIG results were generated using an intrinsic p_T of
1.6 GeV from a fit to D0 data [80].
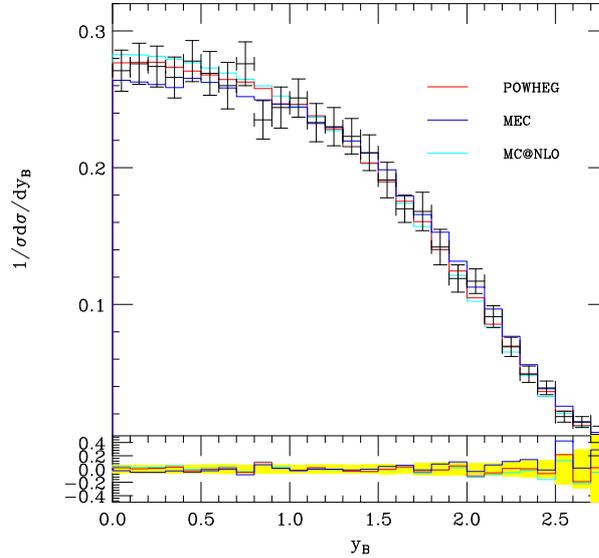
Figure 4.5: Rapidity distribution for Z production compared to D0 Run II Tevatron data [76]. The solid line shows the prediction of the POWHEG implementation, the dotted line is the prediction of MC@NLO and the dashed line is the default Herwig++ result.

The leading-order parton distribution functions of [74] were used for the Herwig++ result and the central value of the NLO parton distributions of [81] for the POWHEG and MC@NLO results.

All the approaches give good agreement for the rapidity of the Z boson however they differ in the description of the $p_\perp$ spectrum of the gauge boson. The chi squared per degree of freedom for the various $p_\perp$ spectra and approaches are given in Table 4.1. All the approaches are in good agreement with the Run I data from CDF and D0 for the $p_\perp$ of the Z and W. However, with the exception of the results of the HERWIG program including a matrix-element correction, which gave the worst agreement with the Run I Z data, all the results are below the new D0 Z $p_\perp$ data at high transverse momentum.

There is a common trend that the matrix-element correction gives the largest result at large $p_\perp$, followed by the POWHEG approach with MC@NLO giving the lowest value. This is due to the treatment of the hardest emission in the different approaches. In MC@NLO method the result at large $p_\perp$ is the leading-order matrix element for the production of a vector boson and a hard QCD jet. However in this region, as we are normalising to the total cross section, the matrix-element correction result is essentially the matrix element for vector boson plus jet production multiplied by the K-factor[5]

---

[5]The K-factor here is the ratio of the NLO cross section for inclusive vector boson production divided by the leading-order cross section.
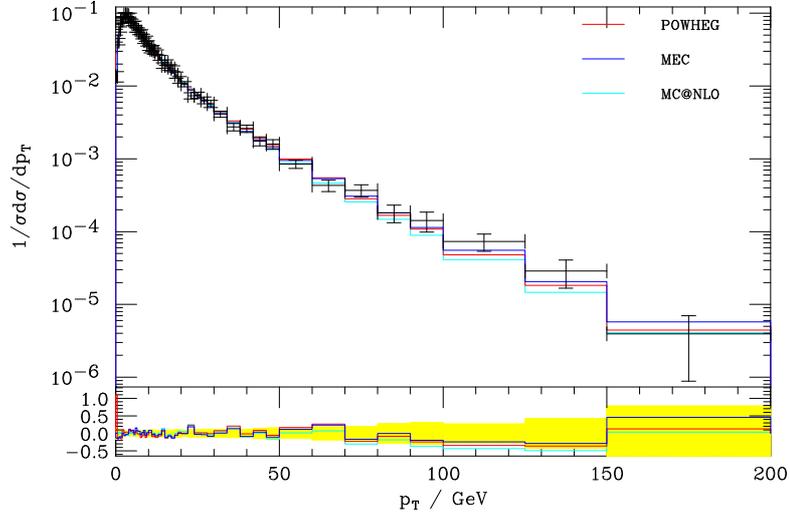
Figure 4.6: Transverse momentum distribution for Z production compared to CDF Run I
Tevatron data [77]. The solid line shows the prediction of the POWHEG imple-
mentation, the dotted line is the prediction of MC@NLO and the dashed line is
the default Herwig++ result.

giving a larger result. In the large $p_\perp$ region the POWHEG result, because the real-
emission matrix element is exponentiated, is the real-emission matrix element multiplied
by the $\bar{B}$ function, which results in a K-factor-like correction, and the Sudakov form
factor which causes the result to be slightly smaller than the default Herwig++ result.
The POWHEG result has the significant advantage that rather than using a global
rescaling of the cross section to get the NLO normalisation, which can lead to a poor
description of observables, such as the boson rapidity, which are non-zero at leading
order the NLO correction is calculated for each momentum configuration.

In general all the results lie below the D0 Run II $Z\,p_\perp$ data between 50 and 100 GeV
which results in the relatively poor chi squared, however in general the POWHEG ap-
proach gives comparable results to the other state-of-the-art techniques. The effect of
varying the scale used for the parton distributions and α_S between $0.5\hat{s}$ and $2\hat{s}$ for the
$\bar{B}$ term and between $0.5(M_B^2 + p_T^2)$ and $2(M_B^2 + p_T^2)$ for the hardest emission is shown
in Fig. 4.9. While this variation moves the POWHEG result closer to the data, it is still
below the experimental result in the intermediate p_T region.

The effect of the truncated shower is illustrated in Fig. 4.10 which shows the low $p_\perp$
region of the transverse momentum distribution for W and Z production compared to
D0 and CDF data. In this region where the highest $p_\perp$ emission is at a low scale and there
is often a large region for the evolution of the truncated shower it has the largest effect.
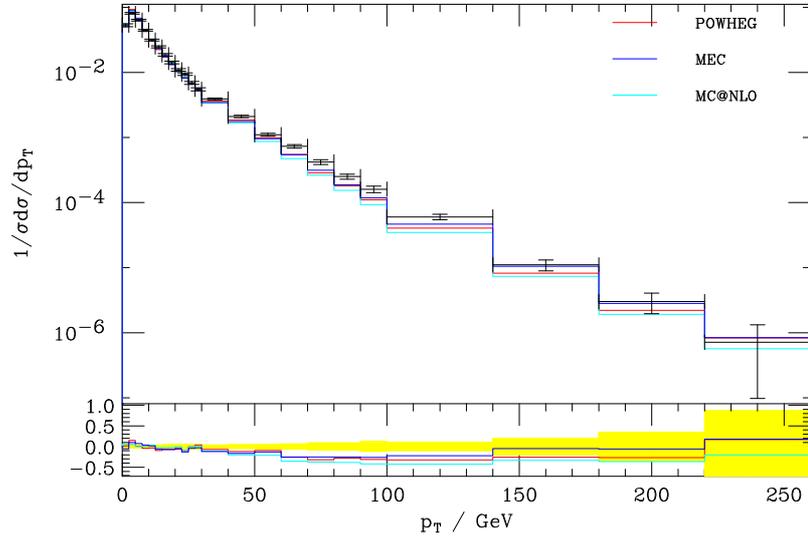
Figure 4.7: Transverse momentum distribution for Z production compared to D0 Run II Tevatron data [78]. The solid line shows the prediction of the POWHEG implementation, the dotted line is the prediction of MC@NLO and the dashed line is the default Herwig++ result. The inset shows an expanded view of the low-$p_\perp$ region.
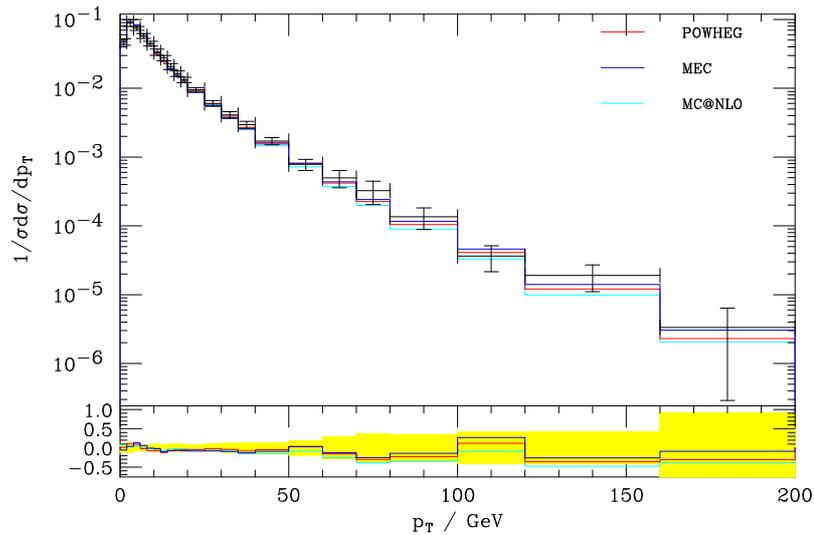
Figure 4.8: Transverse momentum distribution for W production compared to D0 Run I data [79]. The solid line shows the prediction of the POWHEG implementation, the dotted line is the prediction of MC@NLO and the dashed line is the default Herwig++ result. The inset shows an expanded view of the low-$p_\perp$ region.

Approach	Data Set					
	D0 W $p_\perp$		CDF Z $p_\perp$		D0 Z $p_\perp$	
	All	$p_\perp > 30\,\text{GeV}$	All	$p_\perp > 30\,\text{GeV}$	All	$p_\perp > 30\,\text{GeV}$
MC@NLO	0.51	0.82	0.70	0.96	7.2	13.9
Herwig++	0.67	0.42	0.89	0.61	5.1	7.0
POWHEG	0.54	0.33	1.99	1.00	5.3	6.9
HERWIG	0.69	1.08	2.45	4.47	2.0	1.9

Table 4.1: Chi squared per degree of freedom for MC@NLO, Herwig++, the implementation of the POWHEG method in Herwig++ and HERWIG compared to Tevatron vector boson $p_\perp$ data. The chi-squared values are calculated for the shapes of the distributions, *i.e.* normalising them to unity. In order to compare the high $p_\perp$ region and minimise the effect of tuning the intrinsic transverse momentum the chi squared per degree of freedom is given for both the full $p_\perp$ region and only for the data points with $p_\perp > 30\,\text{GeV}$.
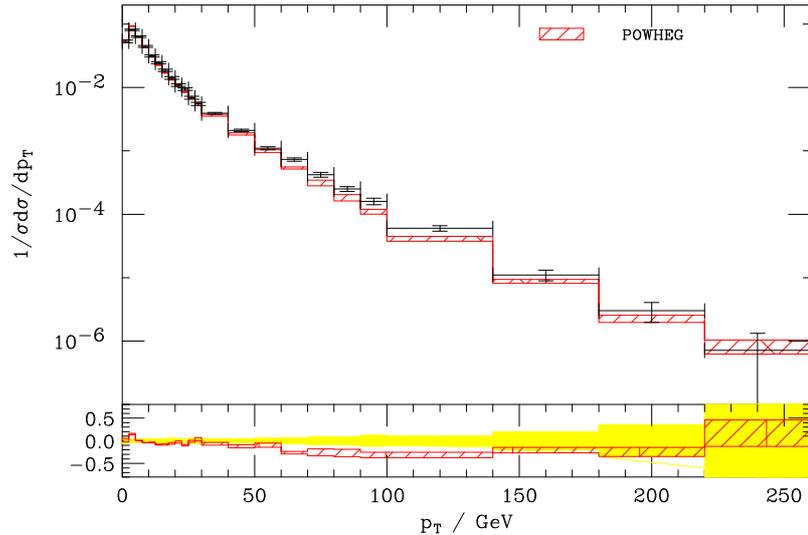
Figure 4.9: Transverse momentum distribution for Z production compared to D0 Run II data [78]. The band shows the effect of varying the scale used for the parton distributions and α_S between $0.5\hat{s}$ and $2\hat{s}$ for the $\bar{B}$ term and between $0.5(M_B^2 + p_T^2)$ and $2(M_B^2 + p_T^2)$ for the hardest emission.
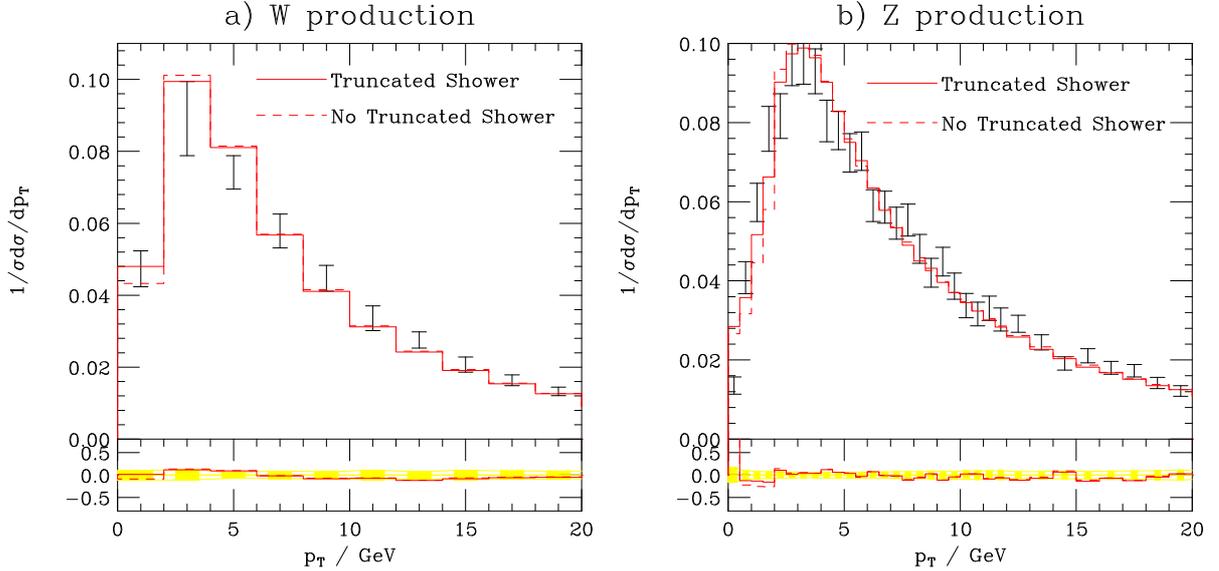
Figure 4.10: Transverse Momentum distribution for a) W production compared to D0 Run I data [79] and b) Z production compared to CDF Run I Tevatron data [77]. The solid line includes the truncated shower whereas the dashed line does not.

However the effect is relatively small at least for the transverse momentum distribution, equivalent to a small change in the intrinsic transverse momentum.

4.5 Conclusions

In this chapter we have described an implementation of the POWHEG NLO matching scheme within Herwig++ for vector boson production. The implementation of the NLO cross section has been compared to the MCFM NLO generator, showing an acceptable level of agreement. The implementation demonstrates a good description of Tevatron data for a range of observables exhibiting a slight improvement on the description provided by MC@NLO.

Chapter 5

A modified CKKW matrix-element merging algorithm in Herwig++

5.1 Introduction

Matrix-element corrections represent the simplest of merging algorithms where a single emission is corrected with tree-level matrix elements. In recent years, more general matrix-element merging algorithms have been introduced. These combine tree-level matrix elements with parton showers, for a given process, for all parton multiplicities below some maximum N. Hence these algorithms correct all distributions involving up to N external partons, instead of just that of the hardest emission. Several schemes of this type have been developed and successfully implemented in event generators. The most well known of these are the CKKW [82–84], CKKW-L [85], MLM [86] and pseudo-shower [87] methods. All these methods have the same general approach [88,89] whereby the phase space for parton emissions is divided into two regions by a merging scale y_{MS}, defined in some jet measure. Above the merging scale, emissions are described by exact matrix elements while below it emissions are produced by the parton shower.

In this chapter we present a matrix-element merging scheme based on the CKKW algorithm. A fundamental ingredient in the CKKW method is the association of a *pseudo-shower history* to the configurations generated according to the fixed-order matrix elements. Each shower history is constructed by clustering the two most closely separated partons, according to the transverse momentum measure defining the merging scale, until a leading-order parton configuration is obtained. The resulting branchings in the shower history are therefore ordered according to the jet measure, which may

not equate to the ordering variable of the parton shower, as is the case for the angular-ordered parton shower of Herwig++. This discrepancy is understood to give rise to serious problems, in particular it spoils the colour coherence properties of these shower algorithms. Although this was already noted, and an attempt made to address it, in the original CKKW paper, realisations of the method highlight the fact that the colour structure in the events is nevertheless in conflict with that expected on the grounds of colour coherence, moreover, they show that this is not simply an esoteric consideration but a cause of significant practical problems, including a dependence on the unphysical merging scale [87, 88].

We shall present and validate a modified version of the CKKW method, intended to optimise the implementation of these colour coherence effects, by a fully consistent merging of an angular-ordered parton shower with fixed-order matrix elements. The idea behind this method was originally proposed by Nason in Ref. [48]. The central result of that theoretical work is the observation that the parton shower may be formally decomposed in terms of *truncated showers*, *hard emissions*, and *vetoed showers*. Reference [48] advocates that the CKKW algorithm may then best model the coherent emission of radiation by including these truncated showers, consisting of only soft emissions, prior to, and between, the hard emissions in the shower history, thereby rendering it angular-ordered. In the following we will develop the full details necessary for our practical implementation of this idea for the process $e^+e^- \to$ hadrons and compare the results of it to LEP data.

The chapter is organised as follows. In Sect. 5.2 we review the original CKKW merging prescription. In Sect. 5.3 we go on to describe the way in which the angular-ordered parton shower may be decomposed into hard emissions, truncated showers, and vetoed showers. Having introduced the relevant conceptual ingredients we then give a more detailed technical description of our modified CKKW algorithm in Sect. 5.4. In Sect. 5.5 we present a validation of our algorithm by comparing to LEP data for $e^+e^- \to$ hadrons, before giving our conclusions in Sect. 5.6.

5.2 CKKW merging

In this section we present an overview and discussion of the original CKKW algorithm for the process $e^+e^- \to$ hadrons. We first describe the algorithm for the case where the parton-shower evolution variable is identical to the merging variable before describing the adaptations which must be made for the Herwig++ angular-ordered parton shower.

5.2.1 Transverse-momentum-ordered CKKW merging

The algorithm is simplest if the merging variable is the same as the ordering variable of the parton shower. We therefore first consider the case where we have a single transverse momentum variable q as both the parton-shower evolution and merging variables.

The basic principle underlying the CKKW approach, is that the distribution of radiation in the region of phase space where all partons are separated by an amount q greater than the *merging scale q_{MS}*, should be given by tree-level matrix elements, while for $q \leq q_{MS}$ it should be given by the parton shower. The algorithm then requires, as input, samples of events of the process with up to N partons in the final state. These input samples are easily obtained using fully automated tree-level event generators such as Madgraph/MadEvent [92, 93][1]. As well as producing the events themselves, for each sample with n partons the generator will provide a finite, tree-level, jet cross section $\sigma_n^{(ME)}(q_{MS})$.

Naïvely, with the input events in hand, one might then consider filling the remaining phase space by selecting events from each sample with n partons, with a probability proportional to $\sigma_n^{(ME)}$, and simply invoking the parton shower on each of the external legs, starting from the scale q_{MS}. However, the merging scale, q_{MS}, is not a physical parameter and so all distributions of partons should be insensitive to its value. This would certainly not be the case for such a naïve procedure, since the distribution of radiation from the parton shower and the fixed-order matrix elements are known to differ, especially in the regions corresponding to high and low q emissions. The great success of the CKKW algorithm is in its ability to correct for the mismatch at the phase-space partition q_{MS} by providing a smooth, physical, interpolation between the matrix-element distribution at high q values and that of the parton shower in the low q region.

To illustrate how this works, consider the simplified case of merging only samples of 2- and 3-parton events, with $q \geq q_{MS}$, for $e^+e^- \rightarrow$ hadrons, with a q-ordered parton shower. In general, the parton-shower cross section analogous to $\sigma_n^{(ME)}(q_{MS})$, with n partons resolved at the merging scale, may be written as the product of the leading-order cross section together with a set of Sudakov form factors and splitting functions. The product of these splitting functions and the leading-order cross section approximate the

---

[1]Currently, computational efficiency limits the total number of final-state particles to around six.

exact tree-level n-jet cross section. For the case of three partons this cross section is

$$\sigma_3^{(PS)}(q_{MS}) = \sigma_2 \times 2\left[\Delta_q(q_I, q_{MS})\right]^2 \int_{q_{MS}}^{q_I} dq\, \alpha_S(q)\, \Gamma_{q \to qg}(q)\, \Delta_g(q, q_{MS}), \qquad (5.1)$$

where q_I is the scale at which the parton shower is initiated and $\alpha_S(q)\Gamma_{\widetilde{ij} \to ij}(q)$ is the probability for a parent parton $\widetilde{ij}$ to branch into two daughter partons i and j, in the interval $[q, q+dq]$ [2]. The overall normalisation factor σ_2 is simply the leading-order cross section. Finally, in Eq. 5.1, $\Delta_{\widetilde{ij}}(q, q_{MS})$ is the Sudakov form factor, which can be interpreted as the probability for the parent parton $\widetilde{ij}$ to evolve from a scale q down to the scale q_{MS} without undergoing a resolvable branching,

$$\Delta_{\widetilde{ij}}(q, q_{MS}) = \exp\left[-\sum_{\widetilde{ij} \to ij} \int_{q_{MS}}^{q} dq'\, \alpha_S(q')\, \Gamma_{\widetilde{ij} \to ij}(q')\right]. \qquad (5.2)$$

In parton-shower (NLL) expansions of the jet cross sections, such as that in Eq. 5.1, the exact tree-level matrix elements are approximated by the product of the leading-order cross section and splitting functions. In order to improve the parton shower with exact tree-level matrix elements, this product should be replaced by the corresponding exact, tree-level jet cross section.

The CKKW merging should not affect the NLL expansion of the jet cross section therefore the NLL expansion of the matrix-element contribution should give the result in Eq. 5.1. Since a NLL expansion of the tree-level matrix elements yields a corresponding product of parton-shower splitting functions, it is clear that in order to retain the NLL form of Eq. 5.1, the matrix-element contribution above q_{MS} should be given by configurations generated according to the tree-level jet cross sections reweighted by appropriate Sudakov and running α_S factors.

In order to determine appropriate reweighting factors for events from the tree-level generator, a pseudo-shower history must be assigned to each event. This shower history interprets the set of external parton momenta as a set of branchings originating from a leading-order configuration. This procedure gives rise to a set of *nodal values*, q_i, for the scales at which each pseudo-branching occurred. These scales provide the arguments for the Sudakov form factors and α_S factors with which the configuration should be reweighted. In the original CKKW publication, this pseudo-shower history is assigned

---

[2]The dependence on auxiliary splitting variables has been suppressed.

by repeatedly clustering the pair of partons[3] with the smallest separation according to the jet resolution variable, until only the particles of the leading-order process remain.

In the case being considered, where the evolution variable has been taken to match the merging scale variable, combining the matrix elements with the parton shower is straightforward. The parton-shower evolution can be split into two parts: first an evolution from the initial scale down to the merging scale, q_{MS}; then an evolution from the merging scale down to the hadronisation scale q_0. This results in a simple procedure for attaching the parton shower to the reweighted matrix elements, where each external parton produces a shower line evolving from the merging scale.

The full CKKW algorithm then proceeds as follows:

1. a jet multiplicity n is generated with probability

$$P_n = \frac{\sigma_n^{(ME)}(q_{MS})}{\sum_N \sigma_i^{(ME)}(q_{MS})}, \tag{5.3}$$

   where all cross sections are evaluated at a fixed strong coupling $\alpha_{S_{ME}}$;

2. a configuration of n parton momenta is generated according to $\mathrm{d}\sigma_n^{(ME)}(q_{MS})$;

3. external partons are clustered, defining a pseudo-shower history with a set of nodal scales q_i;

4. the configuration is reweighted by Sudakov and α_S factors: each internal line between two nodes at q_i and q_{i+1} contributes a factor of $\Delta_f(q_i, q_{MS})/\Delta_f(q_{i+1}, q_{MS})$, each external line emanating from a node with scale q_i contributes $\Delta_f(q_i, q_{MS})$, while each node itself contributes $\frac{\alpha_S(q_i)}{\alpha_{S_{ME}}}$;

5. the parton shower is invoked on each external parton from a starting scale of q_{MS}.

This scheme is independent of the merging scale to NLL order [82]. We have reweighted configurations such that the NLL three-jet cross section resolved at the merging scale is given by Eq. 5.1. This NLL cancellation of merging scale dependence can be seen by considering the cross section for three jets resolved at the hadronisation scale. This cross section is given by the sum of the probability of generating a single emission in the matrix-element region and none in the parton shower, together with the probability of generating no emissions in the matrix-element region and a single emission in

---

[3]Only pairs of partons whose flavours correspond to allowed branchings are considered.

the parton-shower region. The cross section is

$$\sigma_3^{(PS+ME)}(q_0) = \bar{\sigma}_3^{(ME)}(q_{MS}) \left[\Delta_q(q_{MS}, q_0)\right]^2 \Delta_g(q_{MS}, q_0) \tag{5.4}$$
$$+ \sigma_2 \times 2 \left[\Delta_q(q_I, q_0)\right]^2 \int_{q_0}^{q_{MS}} dq\, \alpha_S(q)\, \Gamma_{q \to qg}(q)\, \Delta_g(q, q_0),$$

where $\bar{\sigma}_3^{(ME)}(q_{MS})$ is the reweighted matrix-element contribution for three jets resolved at the merging scale. The first term in Eq. 5.4 corresponds to a single emission above the merging scale followed by parton-shower evolution from the merging scale down to the hadronisation scale with no resolvable emissions. The second term corresponds to no emissions above the merging scale followed by a single parton-shower emission below the merging scale. In the NLL expansion of Eq. 5.4, we replace $\bar{\sigma}_3^{(ME)}(q_{MS})$ by the NLL parton-shower approximation in Eq. 5.1. This results in a simplification of Eq. 5.4

$$\sigma_3(q_0) = \sigma_2 \times 2 \left[\Delta_q(q_I, q_0)\right]^2 \int_{q_0}^{q_I} dq\, \alpha_S(q)\, \Gamma_{q \to qg}(q)\, \Delta_g(q, q_0), \tag{5.5}$$

yielding the expected NLL parton-shower cross section for a single resolved emission which is independent of the merging scale.

5.2.2 Angular-ordered CKKW merging

The merging variable used to define the jet cross sections must regulate both soft and collinear singularities, so it must be a transverse momentum measure. The merging variable in the original CKKW publication is defined in terms of the Durham jet measure [90] for two partons i and j,

$$y_{\mathrm{dur}_{ij}} = \frac{2\min\left(E_i^2, E_j^2\right)}{s}\left(1 - \cos\theta_{ij}\right), \tag{5.6}$$

where $E_{i,j}$ are the energies of the two partons, θ_{ij} is the angle between the two partons and s is the centre-of-mass-energy squared. The merging transverse momentum variable is defined by

$$k_\perp = \sqrt{y_{ij}s}. \tag{5.7}$$

The parton shower with which we wish to merge the matrix elements may not be ordered in transverse momentum, in which case the merging variable cannot be chosen

to be the same as the evolution variable, as was assumed in Sect. 5.2.1. In the Herwig++ parton shower, the evolution variable is the angular variable given in Eq. 2.14.

In order to accommodate the fact that the evolution and merging variables are not identical, the CKKW algorithm must include some additional features to that outlined in Sect. 5.2.1. Changes must be made to the Sudakov form factors with which the matrix elements are reweighted and the initial conditions with which the parton shower is invoked, furthermore, when the shower is invoked, a veto must be applied to prevent it generating emissions with $k_\perp(\tilde{q}, z) > k_{\perp_{MS}}$.

The Sudakov form factor used for the matrix-element reweighting corresponds to the probability of evolving from a scale q down to the hadronisation scale with no emissions resolvable at the merging scale. In the case of Sect. 5.2.1, this was achieved by setting the lower limit on the integral to q_{MS}, however, now this cut, defining what is meant by a resolvable emission, must be implemented as a Θ-function in the Sudakov form factors used in step 4. The Sudakov form factors for the reweighting are then given by

$$\Delta_{\widetilde{ij}}^{R}(\tilde{q}; k_{\perp_{MS}}) = \exp\left[-\sum_{\widetilde{ij}\to ij}\int_{\tilde{q}_0}^{\tilde{q}} \mathrm{d}\mathcal{P}_{\widetilde{ij}\to ij}(\tilde{q}', z)\Theta\left(k_\perp(\tilde{q}', z) - k_{\perp_{MS}}\right)\right].\qquad(5.8)$$

The prescription for constructing the Sudakov weights is then identical to that in Sect. 5.2.1 except for factors of z in the scale from which each child evolves, which are required for the angular-ordered evolution. Each intermediate line, connecting branchings at $(\tilde{q}_1, z_1)$ and $(\tilde{q}_2, z_2)$ in the pseudo-shower history, contributes a factor

$$\Delta_{\widetilde{ij}}^{R}(z_1\tilde{q}_1; k_{\perp_{MS}})/\Delta_{\widetilde{ij}}^{R}(\tilde{q}_2; k_{\perp_{MS}}).\qquad(5.9)$$

Each external line, from a branching at $(\tilde{q}, z)$ in the pseudo-shower history, contributes a factor

$$\Delta_{\widetilde{ij}}^{R}(z\tilde{q}; k_{\perp_{MS}}).\qquad(5.10)$$

5.2.3 Highest-multiplicity treatment

The original CKKW publication did not treat the highest-multiplicity matrix-element contribution any differently to the other multiplicities. In Ref. [85] it was noted that a different treatment of highest multiplicities must be employed in order to fill the phase space in the matrix-element region to all orders in α_S. Since computational limits mean that only matrix elements with up to a maximum of N partons can be calculated, the standard approach leads to a maximum of N partons being generated above the merging scale. The parton shower generates to all orders in α_S and therefore we should also let the matrix-element region generate to all orders. This can be achieved by allowing the highest multiplicity channel parton shower to generate emissions in the region with $k_\perp$ less than that of the lowest transverse momentum of the matrix-element emissions, $k_{\perp_L}$. This is achieved by changing the scale of the parton-shower vetoes and Sudakov form factor cuts from $k_{\perp_{MS}}$ to $k_{\perp_L}$. This procedure is discussed further in Appendix C.1.

5.2.4 Problems with the algorithm

The above procedure is heavily reliant on having an exact mapping between the shower variables and the merging measure $k_{\perp_{MS}}$ so that the parton-shower vetoes and Sudakov cuts can be correctly applied. A mapping from the momentum clustered in step 3 to the corresponding shower variables is also required, so that the correct scales for the Sudakov reweighting and initial shower conditions are obtained. In practice obtaining such mappings may be difficult due to the complexity of the shower kinematics.

The initial scale at which the parton shower is invoked is vital to the algorithm. Initiating the parton shower directly from the merging scale would result in a radiation gap, where emissions with transverse momentum less than the merging scale but evolution scale greater than the merging scale are missed. In the angular-ordered shower, this radiation corresponds to soft, wide-angle emissions. The original CKKW publication attempts to resolve this by invoking the parton shower from each external parton at a scale corresponding to the node at which it was 'created' in the pseudo-shower history. Although adopting this maximal initial scale helps fill the radiation gap, the extra soft, wide-angle radiation that results, is emitted from the external parton in the pseudo-shower history, rather than the intermediates, as implied by colour coherence [48]. The original CKKW publication argued that this should be a sub-leading effect, however, it

will certainly change the colour structure of the configuration, which may cause problems when non-perturbative hadronisation models are applied.

The original CKKW algorithm also assumes that the clustering of momentum in step 3 and subsequent mapping to parton-shower variables results in a set of emission scales that respect the ordering of the parton shower, *i.e.*

$$\tilde{q}_I > \tilde{q}_1 > ... > \tilde{q}_n > \tilde{q}_0. \tag{5.11}$$

The clustering scheme of the original algorithm does not guarantee this.

These issues were studied in Ref. [88] and found to result in problems when the parton shower was not ordered in transverse momentum. It was found that both the CKKW-L and CKKW algorithms provide a reliable merging when implemented in a parton shower in which the evolution variable is given by a transverse momentum variable that is equal to or approximates the merging variable. When the CKKW algorithm was applied to a virtuality-ordered parton shower, it exhibited discontinuities around the merging scale and a resultant dependence on the merging scale. These problems were most prominent in parton-level observables in the merging variable itself. While the application of the hadronisation models results in some smoothing of these features, the problems were seen to persist at hadron level.

In Ref. [87], a study of the algorithm with angular- and virtuality-ordered parton showers was presented. In that work, a number of *ad hoc* adaptations were applied and tuned in order to achieve a reasonably smooth merging at the parton level, nevertheless, some problems remained at the hadron level. In this article we aim to overcome these problems with a set of well motivated modifications based on the POWHEG shower reorganisation.

5.3 Shower reorganisation

The CKKW algorithm generates a set of n emissions above the merging scale, y_{MS}, according to exact tree-level matrix elements up to $\mathcal{O}(\alpha_S^N)$. This defines a set of n hard emissions. In order to reproduce the full shower around this set of hard emissions we employ a generalisation of the POWHEG shower reorganisation. In the following we present an extension of the POWHEG reorganisation, described in Sect. 3.3.1, that is suitable for use in the CKKW case. The notation used relates specifically to that of the
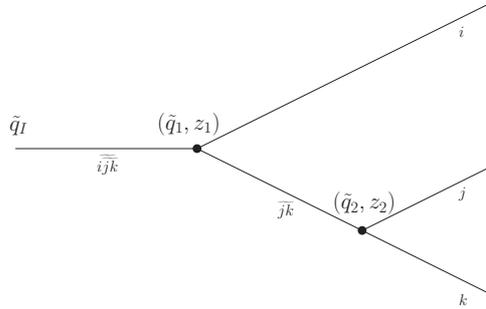
Figure 5.1: An example of a hard shower line configuration where two emissions are generated above $k_{\perp_{MS}}$.

Herwig++ shower, however the treatment is largely independent of the details of the parton shower.

5.3.1 CKKW shower reorganisation

In the POWHEG treatment, reviewed in Sect. 3.3.1, the hardest emission is separated such that it may be corrected with matrix elements. In the CKKW algorithm we aim to improve the parton shower with tree-level matrix elements for all parton multiplicities resolved at the merging scale, $k_{\perp_{MS}}$. We perform a reorganisation of the parton shower, analogous to the POWHEG reorganisation, splitting the shower into two parts: a *hard shower* describing emissions resolved above the merging scale; and another shower producing the rest of the shower emissions around this hard shower. The hard shower can then be generated according to the tree-level matrix elements as required by the CKKW algorithm.

The result of this generalisation of the POWHEG reconstruction is a set of truncated and vetoed showers which fill in the radiation between the hard emissions defined by the hard shower history. In order to see how this works we first consider the next step up from the POWHEG case of a single hard emission, where we have exactly two hard emissions along the hard shower line, generated at scales $\tilde{q}_1$ and $\tilde{q}_2$. One possible configuration of this hard shower line is given in Fig. 5.1. As was done in formulating the POWHEG scheme, the full parton shower can be constructed around this hard shower

line by constructing an equation analogous to Eq. 3.18,

$$
\mathcal{S}^{(2)}_{\widetilde{\widetilde{ijk}}}(\tilde{q}_I) = \int_{\tilde{q}_0}^{\tilde{q}_I} \tilde{\mathcal{S}}^{T}_{\widetilde{\widetilde{ijk}}}(\tilde{q}_I, \tilde{q}_1; k_{\perp_{MS}})\, \mathrm{d}\mathcal{P}_{\widetilde{\widetilde{ijk}} \to \widetilde{ijk}}(\tilde{q}_1, z_1)\tilde{\mathcal{S}}^{V}_i\left((1-z_1)\tilde{q}_1; k_{\perp_{MS}}\right) \tag{5.12}
$$

$$
\times \int_{\tilde{q}_0}^{\tilde{q}_1} \tilde{\mathcal{S}}^{T}_{\widetilde{jk}}(z_1\tilde{q}_1, \tilde{q}_2; k_{\perp_{MS}})\, \mathrm{d}\mathcal{P}_{\widetilde{jk}\to jk}(\tilde{q}_2, z_2)\tilde{\mathcal{S}}^{V}_j\left(z_2\tilde{q}_2; k_{\perp_{MS}}\right)\tilde{\mathcal{S}}^{V}_k\left((1-z_2)\tilde{q}_2; k_{\perp_{MS}}\right).
$$

The superscript (2) on $\mathcal{S}$ denotes that this does not describe a general shower line, but the subset of shower lines with exactly two emissions above the merging scale. Eq. 5.12 contains two truncated showers, one containing parton-shower emissions with $k_\perp < k_{\perp_{MS}}$ before the hard emission $(\tilde{q}_1, z_1)$ and the other containing emissions with $k_\perp < k_{\perp_{MS}}$ between the hard emissions at $(\tilde{q}_1, z_1)$ and $(\tilde{q}_2, z_2)$. The showers $\tilde{\mathcal{S}}^{V}_i\left(z_2\tilde{q}_2; k_{\perp_{MS}}\right)$ and $\tilde{\mathcal{S}}^{T}_i\left(z_2\tilde{q}_2; k_{\perp_{MS}}\right)$ are defined by Eq. 3.20 and Eq. 3.19 respectively, with the replacement

$$
\Theta\left(p_\perp(\tilde{q}, z) - p_{\perp_h}\right) \to \Theta\left(k_\perp(\tilde{q}, z) - k_{\perp_{MS}}\right). \tag{5.13}
$$

The replacement in Eq. 5.13 ensures that subsequent emissions are generated in the phase-space region below the merging scale.

As in the POWHEG case, the splitting functions and Sudakov form factors for the truncated and vetoed showers in Eq. 5.12 do not match each other and are therefore not suitable for a standard Monte Carlo treatment. However, we can use the same manipulations as in the POWHEG formulation to split the Sudakov form factors into a product of a Sudakov form factor that matches the vetoed splitting functions and a remnant Sudakov form factor, as in Eq. 3.21. The statements of Sect. 3.3.1 also hold true in this case, therefore we identify the truncated showers as containing only soft radiation. We therefore set $z_i \to 1$ in the remnant Sudakov form factor of Eq. 3.23 with only subleading differences. The result of this is that the product of remnant Sudakov form factors for a particular truncated or vetoed line combine to give a remnant Sudakov factor. Rather than resulting in a single remnant Sudakov factor as in the POWHEG scheme, we now get a product of remnant Sudakov factors. The weight associated with the product of remnant Sudakov factors for the hard shower configuration of Fig. 5.1 is given by

$$
W_{\mathrm{sud}} = \frac{\Delta^{R}_{\widetilde{\widetilde{ijk}}}(\tilde{q}_I; k_{\perp_{MS}})}{\Delta^{R}_{\widetilde{\widetilde{ijk}}}(\tilde{q}_1; k_{\perp_{MS}})}\Delta^{R}_i((1-z_1)\tilde{q}_1; k_{\perp_{MS}})\frac{\Delta^{R}_{\widetilde{jk}}(z_1\tilde{q}_1; k_{\perp_{MS}})}{\Delta^{R}_{\widetilde{jk}}(\tilde{q}_2; k_{\perp_{MS}})} \tag{5.14}
$$

$$
\times \Delta^{R}_j(z_2\tilde{q}_2; k_{\perp_{MS}})\Delta^{R}_k((1-z_2)\tilde{q}_2; k_{\perp_{MS}}),
$$

where the remnant Sudakov factor is given by

$$\Delta_{\widetilde{ij}}^{R}(\tilde{q}; k_{\perp_{MS}}) = \exp\left[-\int_{\tilde{q}_0}^{\tilde{q}} \sum_{\widetilde{ij}\to ij} \mathrm{d}\mathcal{P}_{\widetilde{ij}\to ij}(\tilde{q}, z)\Theta\left(k_{\perp}(\tilde{q}, z) - k_{\perp_{MS}}\right)\right]. \qquad (5.15)$$

After removing the Sudakov weight Eq. 5.12 may be rewritten in terms of the standard vetoed and truncated showers[4], defined in Eqs. 3.26 and 3.27, as

$$\mathcal{S}_{\widetilde{\widetilde{ijk}}}^{(2)}(\tilde{q}_I) = \int_{\tilde{q}_0}^{\tilde{q}_I} \mathcal{S}_{\widetilde{\widetilde{ijk}}}^{T}(\tilde{q}_I, \tilde{q}_1; k_{\perp_{MS}})\,\mathrm{d}\mathcal{P}_{\widetilde{\widetilde{ijk}}\to\widetilde{ijk}}(\tilde{q}_1, z_1)\mathcal{S}_i^{V}\left((1-z_1)\tilde{q}_1; k_{\perp_{MS}}\right) \qquad (5.16)$$

$$\times \int_{\tilde{q}_0}^{\tilde{q}_1} \mathcal{S}_{\widetilde{jk}}^{T}\left(z_1\tilde{q}_1, \tilde{q}_2; k_{\perp_{MS}}\right)\mathrm{d}\mathcal{P}_{\widetilde{jk}\to jk}(\tilde{q}_2, z_2)$$

$$\times \mathcal{S}_j^{V}\left(z_2\tilde{q}_2; k_{\perp_{MS}}\right)\mathcal{S}_k^{V}\left((1-z_2)\tilde{q}_2; k_{\perp_{MS}}\right)W_{\mathrm{sud}}.$$

In the CKKW algorithm the hard shower is generated by choosing a jet multiplicity n as described in Sect. 5.2.1 and generating n parton momenta according to the appropriate jet cross section. A pseudo-shower history and corresponding shower variables are then assigned by applying a clustering algorithm to the n parton momenta, until they are clustered back to a leading-order configuration. The shower reorganisation presented here results in a product of remnant Sudakov factors, with which these hard shower configurations should be reweighted. These remnant Sudakov factors can generally be found from the pseudo-shower history by applying the following prescription:

- each internal line from a branching at (q_1, z_1) to (q_2, z_2) contributes a factor

$$\frac{\Delta_f^R(z_1\tilde{q}_1; k_{\perp_{MS}})}{\Delta_f^R(\tilde{q}_2; k_{\perp_{MS}})}; \qquad (5.17)$$

- each external line from a branching at (q, z) contributes a factor

$$\Delta_f^R(z\tilde{q}; k_{\perp_{MS}}). \qquad (5.18)$$

These remnant Sudakov factors match the Sudakov factors, in Eq. 5.8, that we argued should be introduced in order to extend the CKKW procedure for transverse momentum showers to the angular-ordered shower.

---

[4]Again, with the replacement in Eq. 5.13.

The parton shower for emissions below the cut is generated by producing truncated and vetoed showers around the hard shower according to the following prescription:

- each internal line from a branching at (q_1, z_1) to (q_2, z_2) results in a truncated shower

$$\mathcal{S}_f^T \left(z_1 \tilde{q}_1, \tilde{q}_2; k_{\perp_{MS}} \right);$$ (5.19)

- each external line from a branching at (q, z) results in a vetoed shower

$$\mathcal{S}_f^V \left(z \tilde{q}; k_{\perp_{MS}} \right).$$ (5.20)

5.4 The algorithm

In order to implement the procedure described in Sect. 5.3.1 we employ the strategy described in Sect.3.4.4, where the hardest emission, or set of hard emissions in this case, are interpreted as parton-shower emissions. This approach leads to a straightforward implementation of the truncated showers, where a truncated shower, evolving between hard emissions at $(\tilde{q}_1, z_1, \phi_1)$ and $(\tilde{q}_2, z_2, \phi_2)$, is generated by initiating a standard parton shower at $z_1 \tilde{q}_1$ with vetoes allowing only non-flavour-changing emissions with $k_\perp < k_{\perp_{MS}}$ and stopping the truncated shower once it has evolved beyond $\tilde{q}_2$, at which point the second hard emission is forced with splitting variables $(\tilde{q}_2, z_2, \phi_2)$. This allows the full shower of truncated showers, hard emissions and vetoed showers to be generated as a single shower evolution from the leading-order configuration. This results in a substantial improvement over earlier CKKW implementations with angular-ordered showers [82,87], since now the *colour structure* in the event is plainly equivalent to that which the shower would have produced by default, *i.e.* it respects colour coherence.

In order to interpret the matrix-element emissions as shower emissions, we require an exact mapping from the set of n external parton momentum and assigned pseudo-shower history to a set of shower splitting variables, $(\tilde{q}, z, \phi)$, describing each emission. Obtaining such a mapping equates to inverting the momentum reconstruction, which is performed at the end of the standard parton shower to translate the set of shower variables into the parton momenta. This procedure may be performed exactly as described in Sect. 3.4.4 with the additional requirement that the decomposition of the unshuffled momenta into the shower variables is iterated so as to find a set of emission variables for each hard emission. Having such a mapping also provides the exact shower variables that are to used for the Sudakov and α_S reweighting.

The full modified CKKW algorithm is described below.

1. The jet multiplicity n is generated with probability

$$P_n = \frac{\sigma_n(k_{\perp_{MS}})}{\sum_N \sigma_i(k_{\perp_{MS}})}, \tag{5.21}$$

   where cross sections are evaluated at a fixed strong coupling $\alpha_{S_{ME}}$.

2. The n external parton momenta are generated according to $\mathrm{d}\sigma(k_{\perp_{MS}})$.

3. Pairs of external parton momenta are clustered[5] down to a leading-order configuration, assigning a pseudo-shower history.

4. The inverse momentum reconstruction is applied to the external momenta and shower history such that a set of shower splitting variables $(\tilde{q}, z, \phi)$ are found, describing $n-2$ hard branchings.

5. The configuration is reweighted to include the Sudakov form factors and running α_S. This corresponds to assigning the configuration a weight W and rejecting the configuration if $W < \mathcal{R}$[6]. The weight is constructed from the pseudo-shower history, according to the following prescription:

   - each hard emission at $(\tilde{q}, z)$ contributes a running α_S factor

   $$\frac{\alpha_S\left(p_\perp(\tilde{q}, z)\right)}{\alpha_{S_{ME}}}; \tag{5.22}$$

   - each internal line between hard emissions at $(\tilde{q}_1, z_1)$ to $(\tilde{q}_2, z_2)$ contributes a Sudakov factor

   $$\frac{\Delta_f^R(z_1 \tilde{q}_1; k_{\perp_{MS}})}{\Delta_f^R(\tilde{q}_2; k_{\perp_{MS}})}; \tag{5.23}$$

   - each external line from a hard emission at $(\tilde{q}, z)$ contributes a Sudakov factor

   $$\Delta_f^R(z \tilde{q}; k_{\perp_{MS}}). \tag{5.24}$$

   If the configuration is rejected[7] return to step 1.

---

[5] The clustering procedure is discussed in Sect. 5.4.2.

[6] $\mathcal{R}$ refers to a random number, generated in the interval $[0, 1]$.

[7] This reweighting procedure relies on the weight generated in this step satisfying $W < 1$. The fixed strong coupling used in the matrix elements α_{ME} can be chosen to be large enough that the α_S weight is always less than one. Individual Sudakov form factors are also guaranteed to be less than one while the ratio of Sudakov form factors contributed by intermediate lines must be less than one due to the angular ordering condition $z_i \tilde{q}_i > \tilde{q}_{i+1}$.

6. Parton-shower lines are initiated from the leading-order configuration which are to be evolved according to the procedure:

   a) If a hard emission exists at a lower scale on the shower line, then the shower is evolved as a truncated shower otherwise proceed with step 6c. The truncated showers evolve as the standard parton shower with vetoes allowing only non-flavour-changing-emissions with $k_\perp < k_{\perp_{MS}}$. Each truncated emission generates a soft gluon which should be evolved according to step 6c.

   b) Once the scale of the next hard emission is reached, the hard emission is forced creating two further shower lines, each of which should be evolved according to step 6a.

   c) Vetoed showers evolve all external shower lines down to the hadronisation scale, with vetoes allowing only emissions with $k_\perp < k_{\perp_{MS}}$.

The above scheme is adapted for the highest-multiplicity channel, where $n = N$, by the replacement $k_{\perp_{MS}} \to k_{\perp_L}$ in the shower vetoes and Sudakov form factors.

The merging algorithm presented is constructed such that the NLL resummation of the parton shower is undisturbed and therefore the dependence on the merging scale cancels at the NLL level. That this is true, follows directly from the shower reorganisation presented in Sect. 5.3 and the fact that the tree-level cross sections, describing emissions in the matrix-element region, may be approximated at NLL accuracy by the product of the leading order cross section and the corresponding set of parton-shower splitting functions. All observable quantities are therefore independent of the merging scale to NLL order. This cancellation of merging scale dependence is illustrated in Appendix C.2 for the three-jet emission rate.

5.4.1 Shower vetoes

The vetoes that are applied to the truncated and vetoed showers and the cuts applied to the remnant Sudakov form factors require a mapping between the shower variables, $(\tilde{q}, z)$ and the merging scale transverse momentum measure $k_\perp$. The merging variable, for an emission $\widetilde{ij} \to ij$, is defined in some jet measure according to, $k_\perp = \sqrt{y_{ij}s}$. We have implemented the merging algorithm with the Durham [90] and LUCLUS [91] jet measures, defined by

$$y_{\mathrm{dur}_{ij}} = \frac{2\min\left(E_i^2, E_j^2\right)}{s} \left(1 - \cos\theta_{ij}\right), \tag{5.25}$$

$$y_{\mathrm{luc}_{ij}} = \frac{2 \left(E_i E_j \right)^2}{s \left(E_i + E_j \right)^2} \left(1 - \cos \theta_{ij} \right).$$ (5.26)

In order to implement these vetoes a mapping between the shower variables $(\tilde{q}, z, \phi)$ and y_{ij}, in the chosen jet measure, must be found. The Herwig++ shower produces off-shell intermediate states and therefore a set of boosts must be applied to each shower line in order to ensure momentum conservation. Since the boosts depend on the full shower history, an exact mapping between the shower variables and the merging variable cannot be found. We use a mapping that is exact for a single shower emission and should give a good approximation for larger numbers of emissions. For clarity in the following, we treat partons as massless while in our implementation parton masses are retained.

In order to relate the jet measure to the parton shower variables, we should write the momenta of partons resulting from a single emission, $q(p_a) \rightarrow q(p_1)g(q_3)$, in the Sudakov basis used in the momentum reconstruction procedure of the parton shower. This was already done in Sect. 1.1.3, yielding the results for the Sudakov parameters in Eq. 1.55.

The vetoes should correspond to vetoes on the reshuffled momenta that have had the boosts, defined in Eq. 2.72, applied to them. We should therefore solve Eq. 2.73 and calculate these boosts before applying Eqs. 5.25 and 5.26. The reconstructed progenitor momenta are given by $q_a = q_1 + q_3$ for the quark jet and $q_b = p_b$ for the anti-quark jet. Inserting these momenta into Eq. 2.73 yields the solution

$$k = 1 - \frac{p_\perp^2}{sz(1 - z)},$$ (5.27)

for the boost parameter. The reshuffling boost for the quark line is then defined by Eq. 2.72. It follows that the three-vector of the shuffled quark progenitor $q_a{}'$ should be given by

$$\mathbf{q}_a{}' = \frac{\sqrt{s}}{2} \left(1 - \frac{p_\perp^2}{sz(1 - z)} \right) (0, 0, 1).$$ (5.28)

The expression in Eq. 5.28 is identical to $\mathbf{q}_a$, as defined by $\alpha_{1,3}$ and $\beta_{1,3}$, and therefore the boost to be applied to the quark jet is the identity matrix. The shuffled momenta for the emitted partons have now been constructed and we can apply Eqs. 5.25 and 5.26

to find expressions for the jet measures used to define the merging scale. These give

$$y_{\text{dur}} = \min\left[z + \frac{p_\perp^2}{sz}, (1-z) + \frac{p_\perp^2}{s(1-z)}\right]^2 \frac{(1-\cos\theta)}{2}, \tag{5.29}$$

$$y_{\text{luc}} = \left[\frac{(p_\perp^2 + (1-z)^2 s)\,(p_\perp^2 + z^2 s)}{p_\perp^2 s + s^2 z(1-z)}\right]^2 \frac{(1-\cos\theta)}{2}, \tag{5.30}$$

where

$$\cos\theta = 1 - \frac{2p_\perp^2 s}{(p_\perp^2 + (1-z)^2 s)\,(p_\perp^2 + z^2 s)}. \tag{5.31}$$

These mappings allow a transverse momentum measure, $k_\perp = \sqrt{ys}$, to be calculated in the merging variable for each parton-shower emission. Parton-shower vetoes and Sudakov cuts can then be applied by comparing this measure to the merging scale.

5.4.2 Clustering scheme

The parton-shower decomposition presented in Sect. 5.3.1 relied on our ability to interpret the series of hard branchings, defined by the matrix-element momenta and assigned pseudo-shower history, as a parton shower. The inverse momentum reconstruction procedure ensures that, given an assigned pseudo-shower history, a set of parton-shower emissions are found that will exactly reproduce the matrix-element momenta.

Section 5.3.1 assumes that the assigned history is angular-ordered; we therefore aim to assign histories that obey the angular-ordering condition

$$\tilde{q}_i z_i > \tilde{q}_{i+1}, \tag{5.32}$$

for all emissions along all shower lines.

The inverse momentum reconstruction allows us to find the shower variables of all branchings in a particular pseudo-shower history. We can therefore determine whether a history is angular-ordered by following all shower lines outwards from the hard process and explicitly checking that all of the branchings satisfy Eq. 5.32.

We employ a clustering procedure that creates all possible pseudo-shower histories and attempts to choose the angular-ordered history that the parton shower was most likely to produce.

It may appear that the best way to choose a history is in a probabilistic way according to the associated shower probability, as formed from the Sudakov form factor and α_S weights[8]. Attempting such a procedure in an angular-ordered shower however would involve applying the shower kinematics to regions in which they are not valid. This can result in finite probabilities being assigned to histories that the shower would never produce. Furthermore, employing a probabilistic choice results in a finite probability of unnatural shower histories being assigned, which can result in technical problems in applying hadronisation models.

We therefore adopt a winner-takes-all strategy, accepting the pseudo-shower history with the smallest scalar sum of the transverse momentum of the emissions. This ensures that the history containing a set of emissions that are closest to the enhanced soft and collinear regions of phase space is chosen. In Appendix C.3, we present some checks of this approach for further justification of this procedure.

Events for which there is no angular-ordered shower interpretation correspond to configurations that occur in a region of phase space that is inaccessible to the parton shower. In the matrix-element region we aim to improve the parton shower description by covering the full phase space of emissions and therefore such configurations should be retained. We therefore choose to force the shower to generate non-angular-ordered emissions in the case that no angular-ordered histories are found. Since such non-angular-ordered emissions are manifestly subleading, the inclusion of such events does not affect the NLL resummation of the parton shower.

In practice the contribution of such events is small (generally $< 1\%$) and all the observable quantities tested were found to be insensitive to their treatment (whether such events were retained or discarded).

The full clustering procedure is:

1. all possible shower histories are created by clustering all pairs of partons whose flavours correspond to allowed branchings;

2. non-angular-ordered histories are discarded;

---

[8]This is the procedure used to assign pseudo-shower-histories in the CKKW-L algorithm in the colour dipole model.

3. the angular-ordered history for which the scalar sum of the transverse momentum of its branchings,

$$\sum_{\text{hard emissions}} |p_\perp(\tilde{q}, z)| \,, \tag{5.33}$$

4. if no angular-ordered histories are found, the unordered history for which Eq. 5.33 is smallest is chosen.

5.5 Results

In this section we present the results of the implementation of the modified CKKW algorithm for the process $e^+e^- \to$ hadrons at a centre-of-mass energy of $91.2\,\text{GeV}$ at both parton and hadron level. The parton-level results provide a test of the algorithm's ability to provide a smooth merging between the matrix element and parton-shower regions of phase space, showing features that may be hidden by the addition of a hadronisation model. The hadron-level results provide the ultimate test of the algorithm's ability to describe data and in particular are sensitive to the parton colour structure assignment which we expect the modified algorithm to improve with respect to traditional CKKW methods.

A key test of the merging algorithm is its insensitivity to changes in the merging scale and merging variable. The algorithm was implemented with two merging variables: the Durham and LUCLUS jet resolution variables. For each merging variable, merging scales of $y_{MS} = 5 \times 10^{-2}$, $y_{MS} = 10^{-2}$ and $y_{MS} = 5 \times 10^{-3}$ were used. Samples of events with all partons separated by $y > y_{MS}$ were generated using MadGraph/MadEvent [92, 93] for the process with up to five partons in the final state[9].

5.5.1 Parton-level results

We present the distributions of the merging variable itself since these should be the most sensitive to problems with the merging procedure. In order to provide a direct comparison to Ref. [88], we first present a systematic look at the algorithm with the

---

[9]The maximum multiplicity for each merging scale was decided according to the phase space available in the matrix-element region.

maximum multiplicity set to three, so that the matrix-element region is responsible for, at most, a single hard emission.

Figure 5.2 shows distributions of the scale at which three jets are resolved in the Durham jet measure for the three chosen merging scales with the Durham jet measure as the merging variable. Jet analyses were performed with the KtJet package [94]. Each of the merging scale choices exhibit a smooth transition between the two phase-space regions, there also appears to be little dependence on the choice of merging scale. The CKKW distributions all closely match the matrix-element correction distributions. This is to be expected since both algorithms aim to improve the parton-shower distributions by applying a correction based on the three-jet matrix elements. The slight differences seen may be attributed to differences in the way the two algorithms apply this correction.

Figure 5.3 shows the same distributions as Fig. 5.2 but with the truncated shower switched off. Switching off the truncated shower results in a radiation gap, meaning that emissions that would be generated at scales greater than that of the hard emission, but with transverse momentum less than that of the hard emission, are never produced. This radiation gap corresponds to a deficit in the amount of soft wide-angle emissions produced from the three-jet samples. Additional parton-shower emissions (on top of the hardest emission) have the effect of smearing the y_{23} distribution, as can be seen in Fig. 5.2, where the two-jet contribution is significantly displaced into the three-jet region. Comparing Figs. 5.2 and 5.3, we see that without the extra soft radiation produced in the truncated shower, the smearing of the two-jet region is not compensated for in the three-jet region and we observe a surplus in the three-jet region close to the merging scale. This effect is more pronounced as the merging scale is lowered and the truncated shower becomes more important. This problem will become more serious as higher multiplicity contributions are included and underlines the importance of the truncated shower in the merging algorithm.

Figure 5.4 shows the same distributions as Fig. 5.2 but with the highest-multiplicity treatment switched off. The result of switching off the highest-multiplicity treatment is that a maximum of three emissions may be generated in the matrix-element region. This violates the all-orders-in-α_S resummation of the parton shower. The effect of this is twofold: first, there is a deficit in the radiation generated in the three-jet channel; second, the three-jet channel receives too great a Sudakov suppression. The main observable effect in Fig. 5.4 is a surplus in the three-jet region of the distribution close to the merging scale. This can again be attributed to the deficit in radiation in the three-jet region, preventing the smearing seen in the two-jet region being compensated by that in
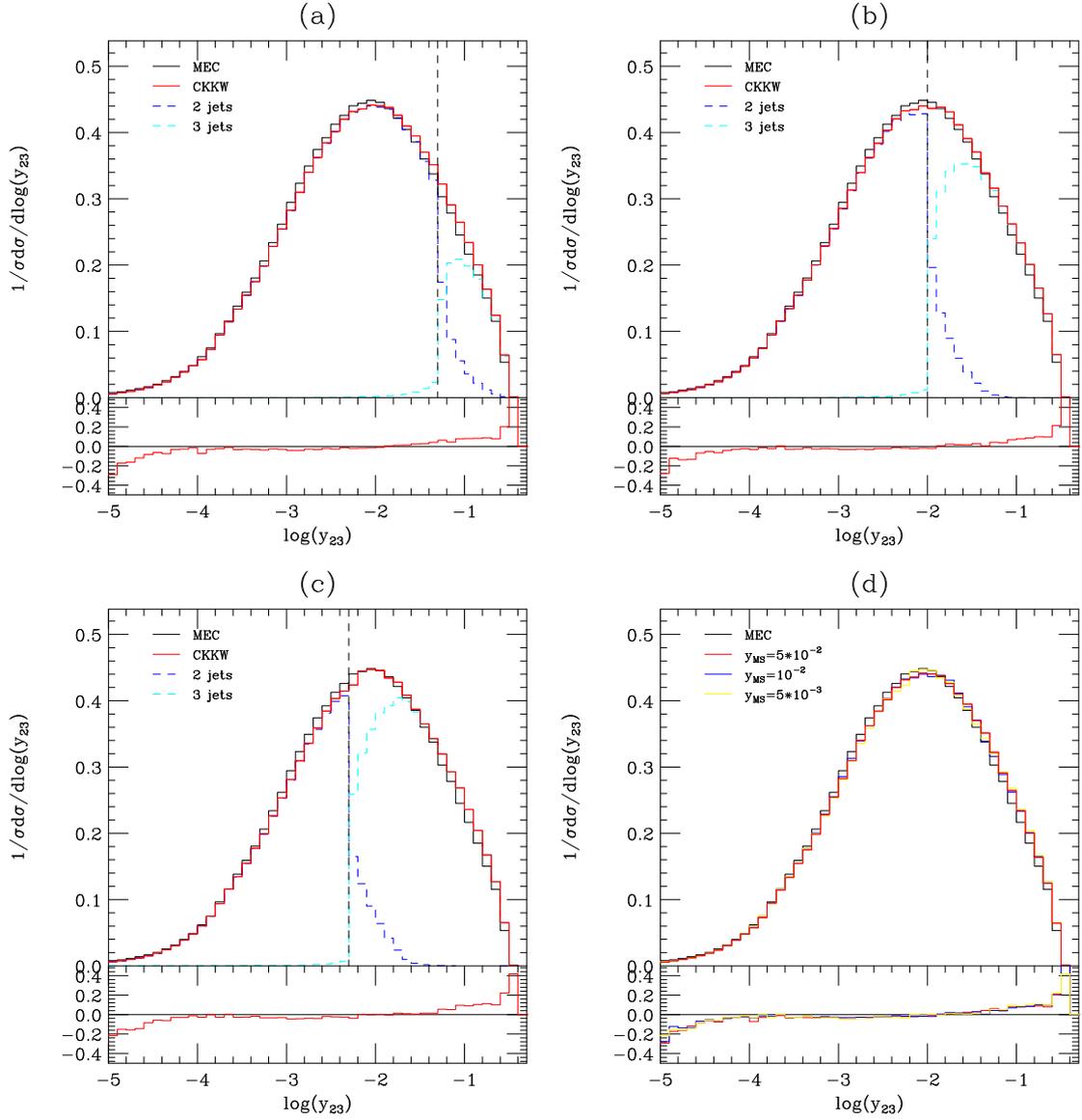
Figure 5.2: Parton level distributions of the scale at which three jets are resolved in the Durham jet measure for $e^+e^- \to$ hadrons at $\sqrt{s} = 91.2\,\text{GeV}$. The red line shows the CKKW distribution with maximum multiplicity set to three and the black line shows the **Herwig++** parton-shower distribution with a matrix-element correction. The blue and cyan lines show the two- and three-jet contributions to the CKKW distribution. Plots (a)-(c) show the CKKW distributions with merging scales set to $y_{MS} = 5 \times 10^{-2}$, $y_{MS} = 10^{-2}$ and $y_{MS} = 5 \times 10^{-3}$ in the Durham jet measure. Plot (d) shows a comparison of the CKKW distributions at the different merging scale choices. The lower panel in all plots shows the difference between the CKKW and matrix element correction lines, $(\text{CKKW} - \text{MEC})/\text{MEC}$.
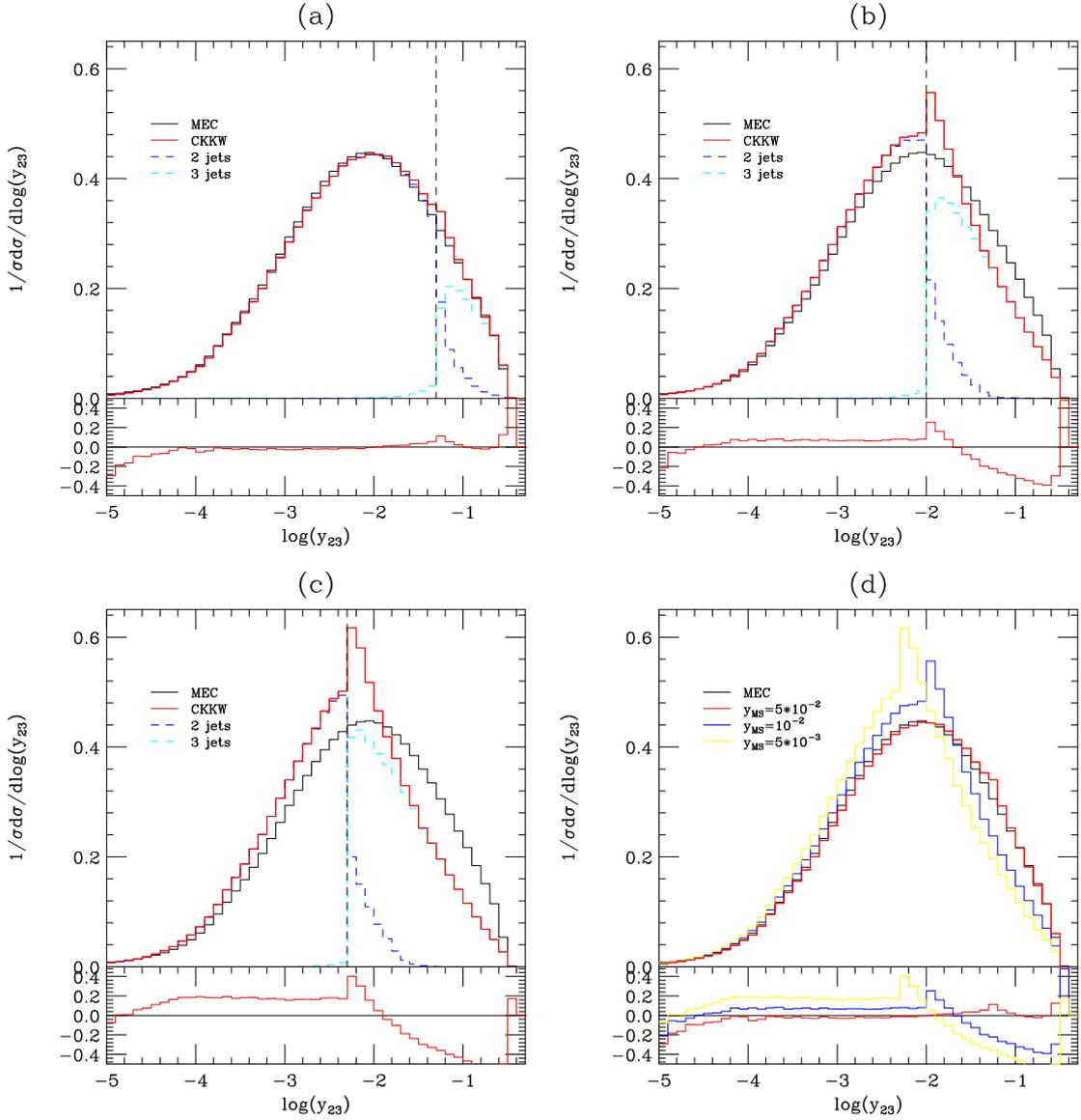
Figure 5.3: The same distributions as in Fig. 5.2 but with the truncated shower switched off in the CKKW treatment.
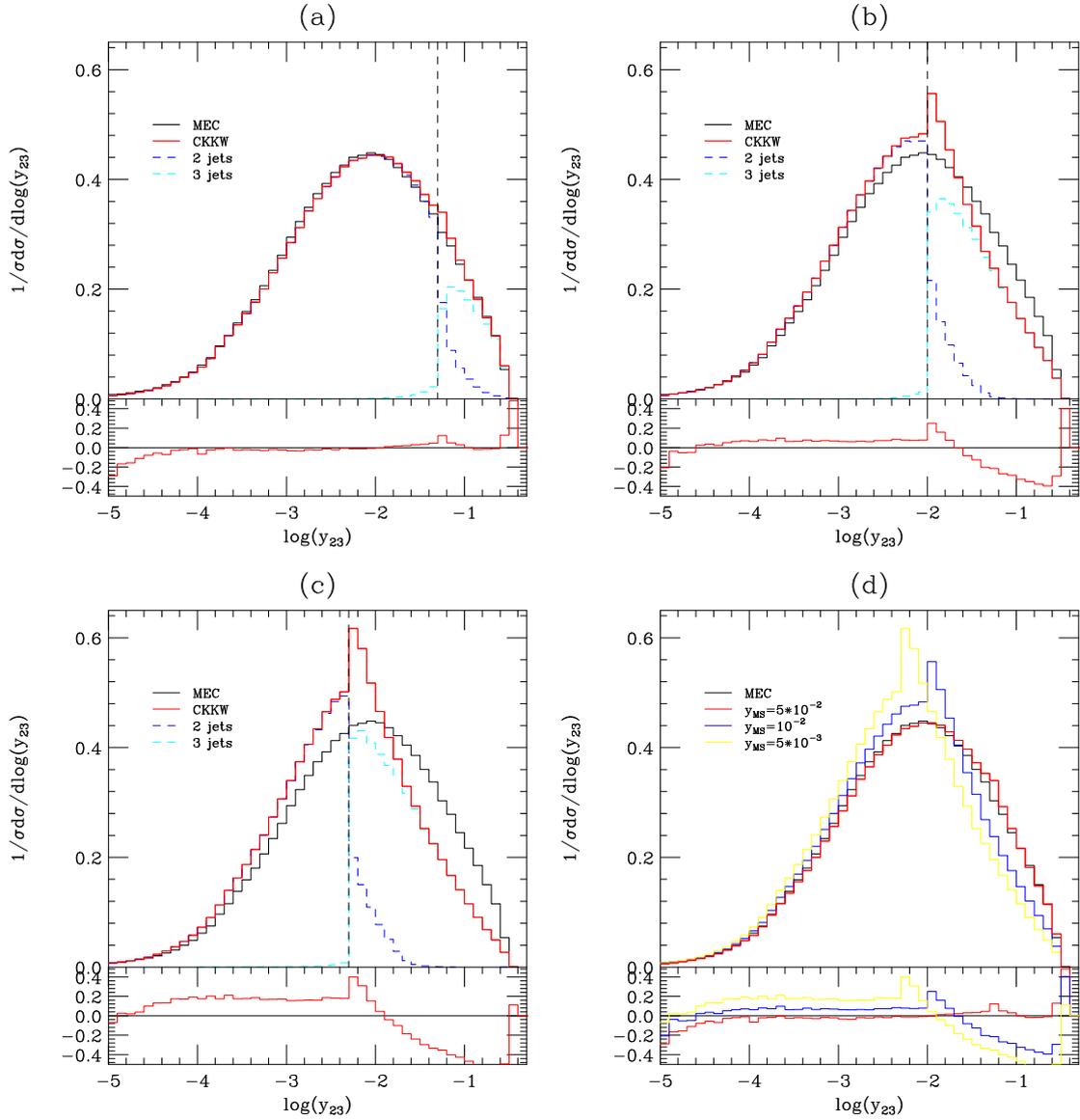
Figure 5.4: The same distributions as in Fig. 5.2 but with the highest multiplicity treatment switched off in the CKKW treatment.

the three-jet region. The suppression of the three-jet region also results in the relative contribution of the two-jet region being too large and we see distributions that are peaked around the merging scale and have a large dependence on the choice of merging scale.

Figures 5.5 and 5.6 show the distributions of the scale at which three jets are resolved, for the algorithm with maximum multiplicity set to up to five jets, with the merging algorithm defined in the Durham and LUCLUS jet measures respectively. As in Fig. 5.2, all distributions appear to be smooth around the merging scale and to be relatively insensitive to the choice of merging scale. The dependency on the merging scale in these
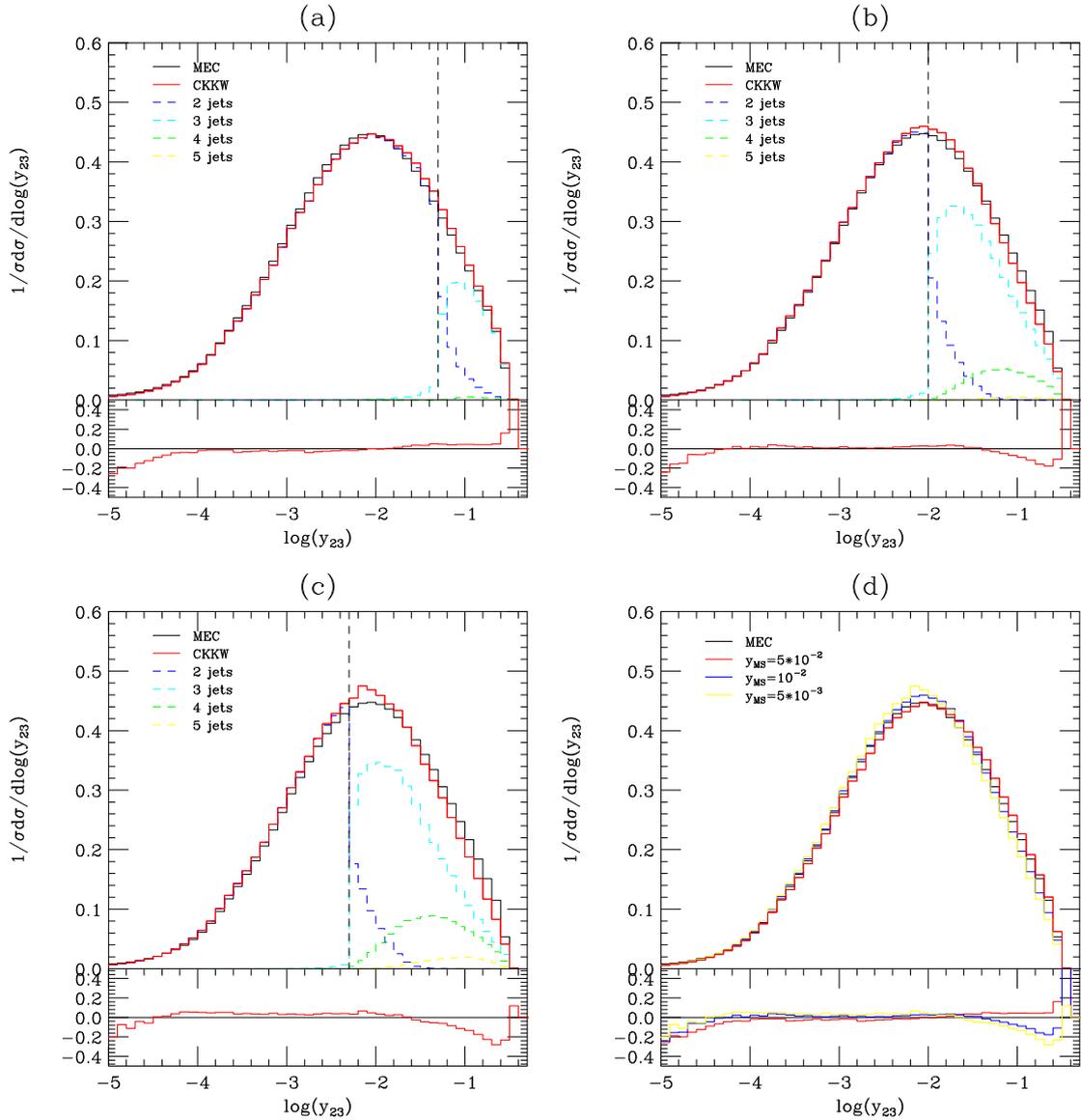
Figure 5.5: Distributions of the scale at which three jets are resolved in the Durham jet measure. The red line in plots (a)-(c) shows the distributions for the CKKW treatment with all multiplicity channels (up to a maximum of five jets) included at a set of merging scale choices in the Durham jet measure. Plot (d) gives a comparison of the different merging scale choices.
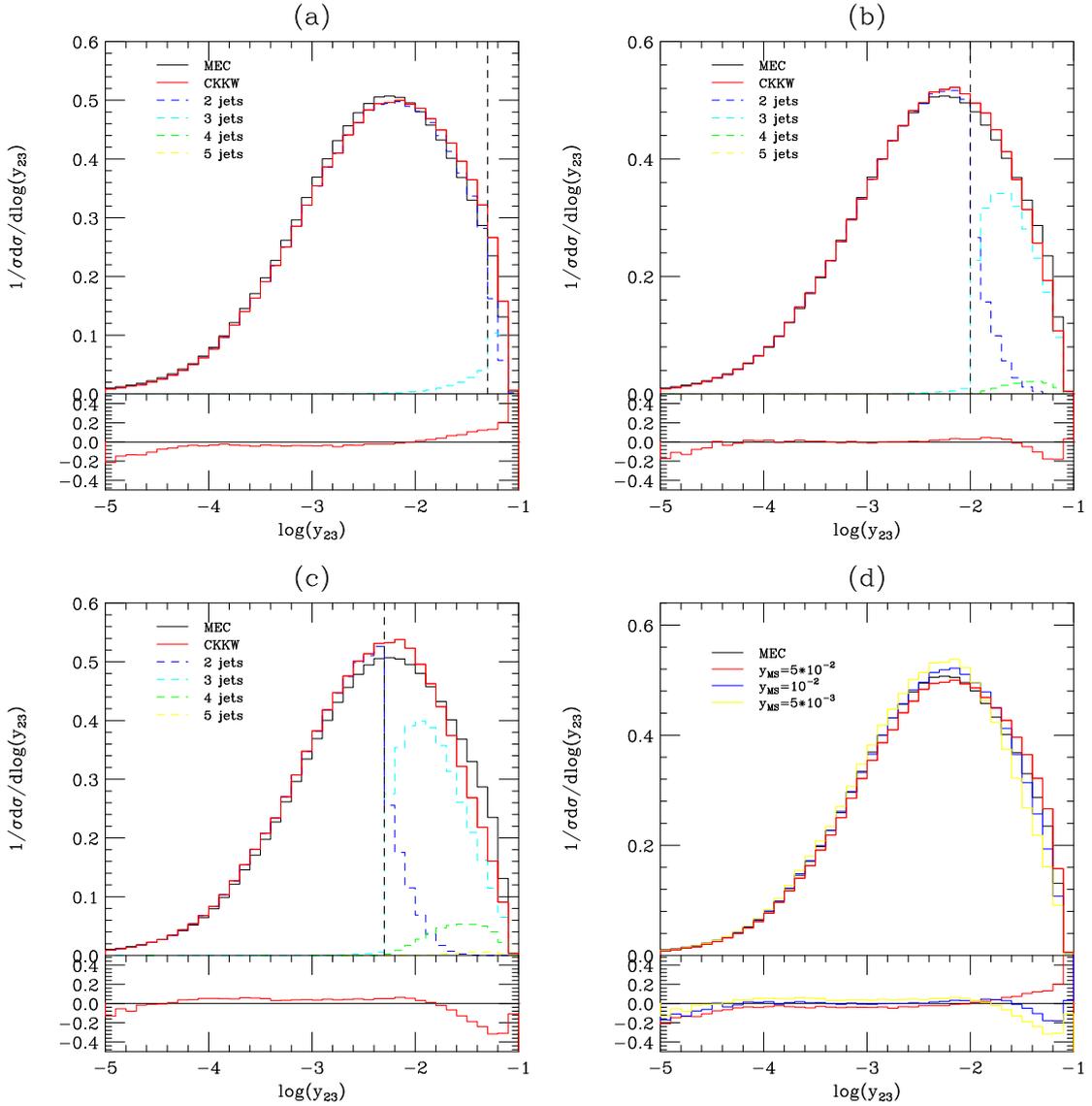
Figure 5.6: Distributions of the scale at which three jets are resolved in the LUCLUS jet measure. The red line in plots (a)-(c) shows the distributions for the CKKW treatment with all multiplicity channels (up to a maximum of five jets) included at a set of merging scale choices in the LUCLUS jet measure. Plot (d) gives a comparison of the different merging scale choices.

y_{MS}	Durham cross section / nb	LUCLUS cross section / nb
5×10^{-2}	38.2	38.6
10^{-2}	36.5	37.1
5×10^{-3}	35.7	35.9

Table 5.1: Table of cross sections of the process $e^+e^- \rightarrow$ hadrons for different choices of the merging scale in the Durham and LUCLUS jet measures.

distributions is greater than that seen in Fig. 5.2 which is to be expected since we are now correcting more emissions and therefore the mismatch between the parton-shower and matrix-element regions of phase space is greater.

Since we are now including higher-multiplicity channels in our merging algorithm we check the distributions of scales at which higher numbers of jets are resolved. This is done in Fig. 5.7 for the resolution of four and five jets in the Durham and LUCLUS jet measures. The merging in these distributions is well behaved.

These distributions demonstrate a degree of insensitivity to the choice of merging scale, which has been varied over an order of magnitude, however there is still some residual dependence on this choice. While the parton shower and merged matrix-element treatments formally have the same large logarithm behavior, there are differences between the two. The degree of these differences will directly influence the amount of residual dependence on the merging scale that is observed. In changing the merging scale we are changing the volume of the matrix-element phase-space region and therefore changing the proportion of parton emissions that are corrected by exact matrix elements. Table 5.1 gives the cross sections for the CKKW treatment at different choices of the merging scale and exhibits variation at the 5% level.

5.5.2 Hadron-level results

We present a comparison of the Herwig++ CKKW implementation with hadronisation switched on to LEP data for a variety of event shapes. It is standard practice to *tune* the free parameters of an event generator to LEP data and this has been done with the default Herwig++ parton shower with matrix-element corrections. Since the CKKW merging algorithm significantly changes the parton-shower component of the event generator and in order to provide a fair comparison with default Herwig++, a new tune was
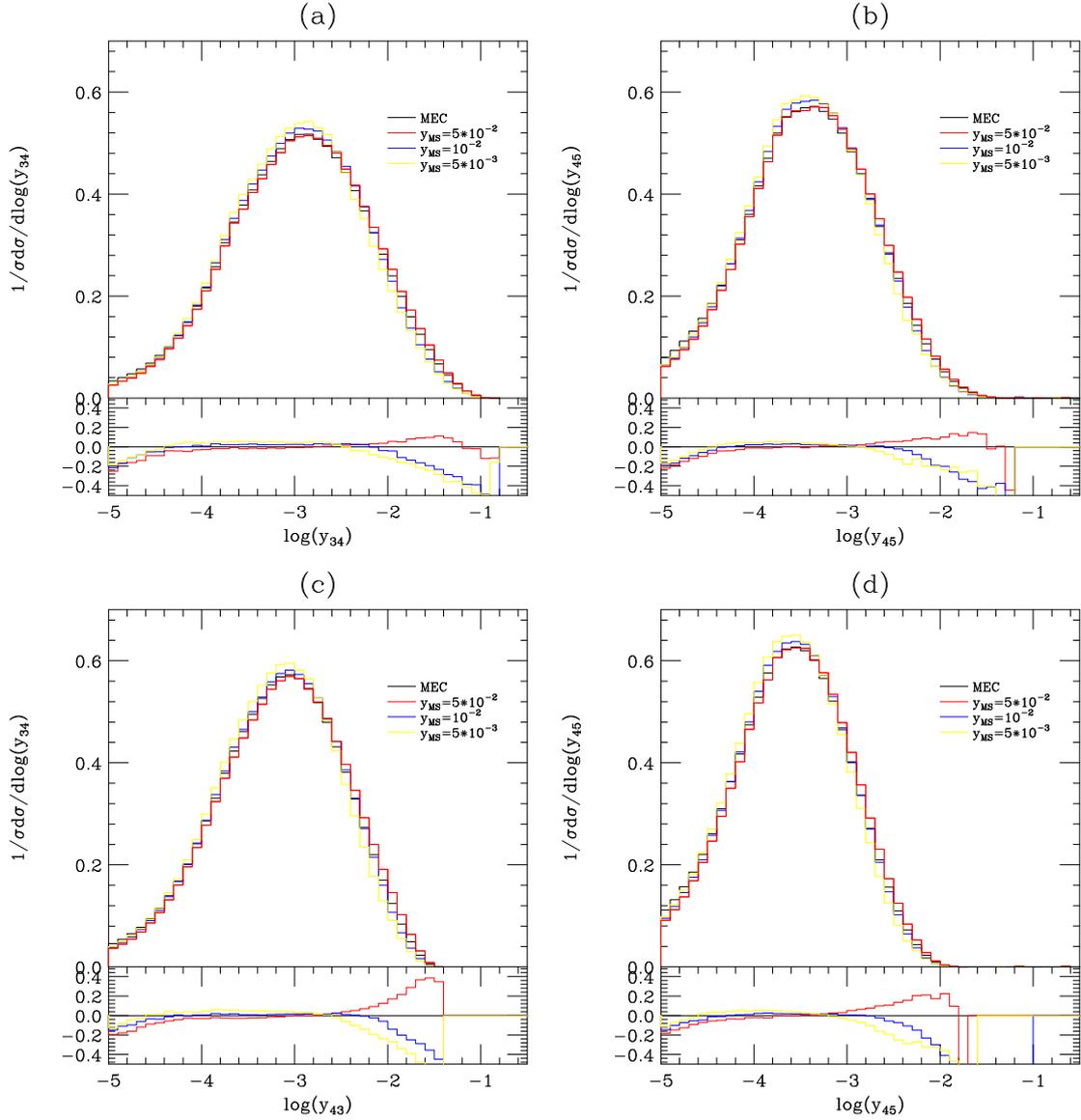
Figure 5.7: Distributions of the scale at which (a) four and (b) five jets are resolved in the Durham jet measure and the resolution scales for (c) four and (d) five jets in the LUCLUS jet measure.

performed on the free parameters for Herwig++ with the CKKW algorithm. This tune was performed with the merging scale set to $y_{MS} = 10^{-2}$ in the Durham jet measure.

Figures 5.8-5.10 show distributions of a range of event shape, jet resolution and four-jet observables in comparison to LEP data. The parton-level analysis shows that the merging scale choice of $y_{MS} = 5 \times 10^{-2}$ leaves only a very small region of phase space that is corrected by the matrix elements. This very high scale choice will therefore not give the improvement expected in introducing the merging algorithm, we therefore omit this merging scale choice from the hadron-level analysis. In each of the figures the red band shows the variation in distributions over the four merging scale choices of $y_{MS} = 10^{-2}$ and $y_{MS} = 5 \times 10^{-3}$ in the Durham and LUCLUS jet measures.

The CKKW distributions (red band) in Figs. 5.8-5.10 all demonstrate improved descriptions of the data in comparison to the default Herwig++ parton shower with matrix-element corrections. In particular the tails of the distributions in Fig. 5.8, corresponding to hard emissions, and the jet resolution distributions of Fig. 5.9 with four and five jets are significantly improved as would be expected given the aims of the merging algorithm. The four-jet angle distributions of Fig. 5.10 are also all improved, with the exception of the α_{34} angle, which was already well described by the default Herwig++ parton shower. The θ_{NR} distribution provides the most notable improvement in its description of the data in comparison to the default Herwig++ parton shower.

The width of the red band on the distributions shows that there is some residual dependence on the merging scale however it does not appear to be too serious and is at a similar level to that observed at parton level. This shows that the problems with colour structure, that appear in the standard CKKW algorithm, are not present here and that the truncated shower is working as intended. It should be noted that a fixed set of Herwig++ shower and hadronisation parameters was used for each of the four merging scale choices; the variation would be reduced further if a tune of the parameters was performed for each merging scale choice.

The χ^2 per degree of freedom values for the distributions in Figs. 5.8-5.10 are given in Table 5.2 for the merging scale choice of $y_{MS} = 10^{-2}$ in the Durham jet measure, which was used in the tune. The CKKW values are lower than those of the default Herwig++ shower in all cases except for the α_{34} angle, where the default implementation already gave a satisfactory description, and in many cases the CKKW values are significantly lower.
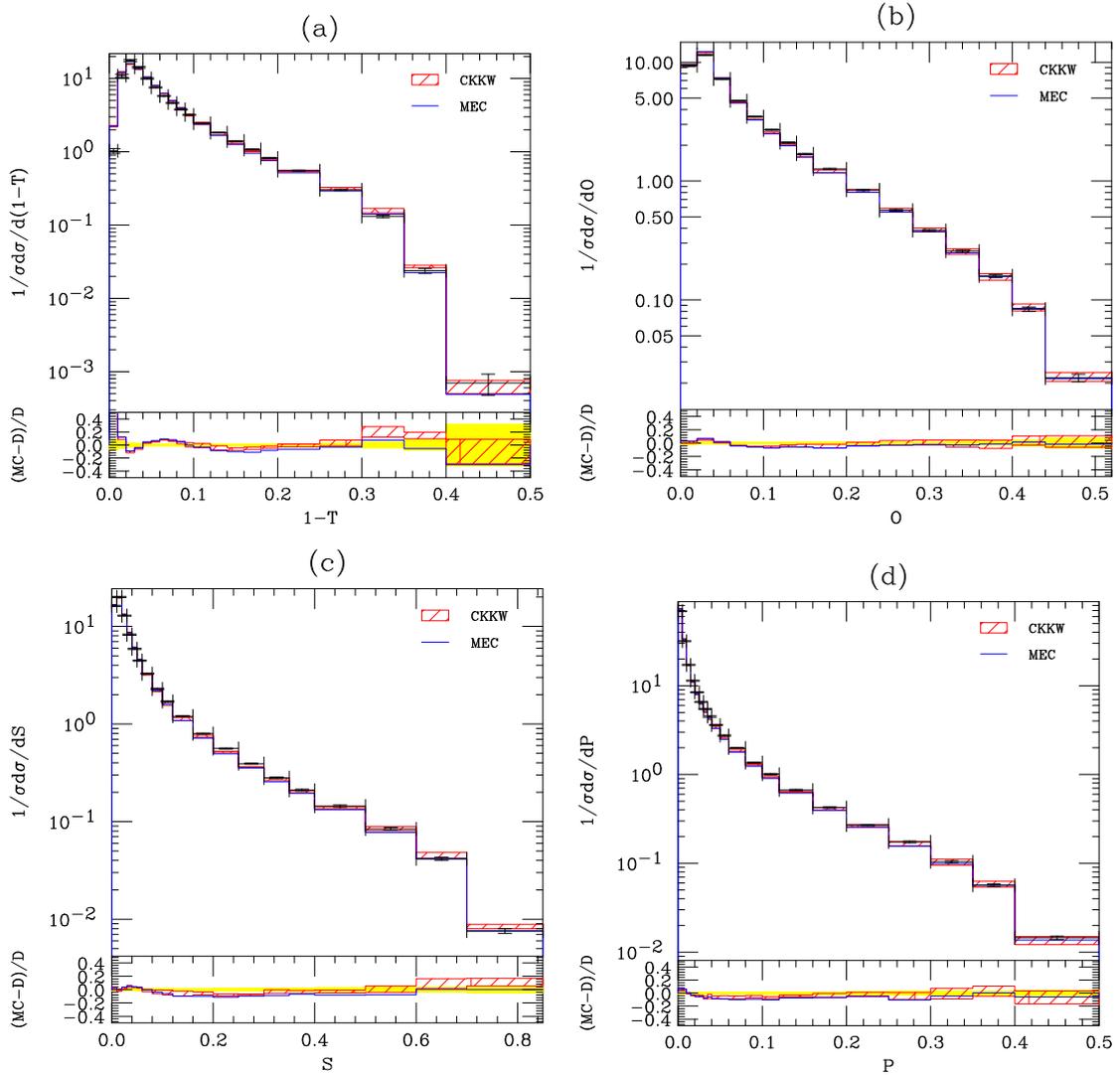
Figure 5.8: Distributions of the event shape variables (a) thrust, (b) oblateness, (c) sphericity and (d) planarity for $e^+e^- \to$ hadrons at a centre-of-mass energy of $\sqrt{s} = 91.2\,\text{GeV}$ in comparison to LEP data (black) [98]. The red band gives the variation of the distributions of the CKKW implementation with merging scales choices of $y_{MS} = 10^{-2}$ and $y_{MS} = 5 \times 10^{-3}$ in the Durham and LUCLUS jet measures. The blue histogram gives the distributions of the default Herwig++ parton shower with matrix-element corrections. The lower panel shows the ratio of the difference between simulation and data to the data in comparison to the error bounds of the data (yellow region).
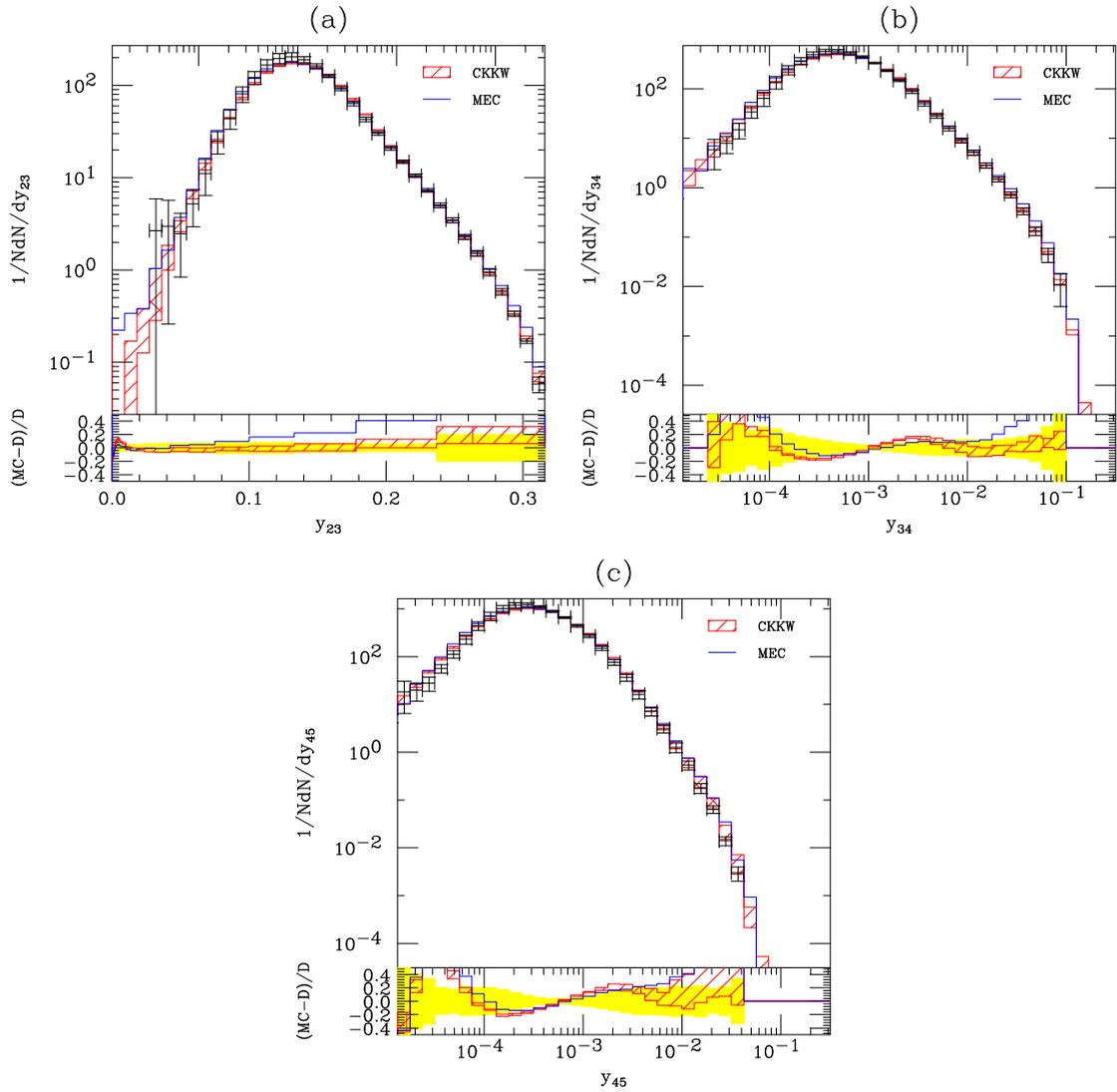
Figure 5.9: Distributions of the scale at which (a) three, (b) four and (c) five jets are resolved in the Durham jet measure for $e^+e^- \rightarrow$ hadrons at a centre-of-mass energy of $\sqrt{s} = 91.2\,\text{GeV}$ in comparison to LEP data [99]. The colours of the lines are the same as those in Fig. 5.8.
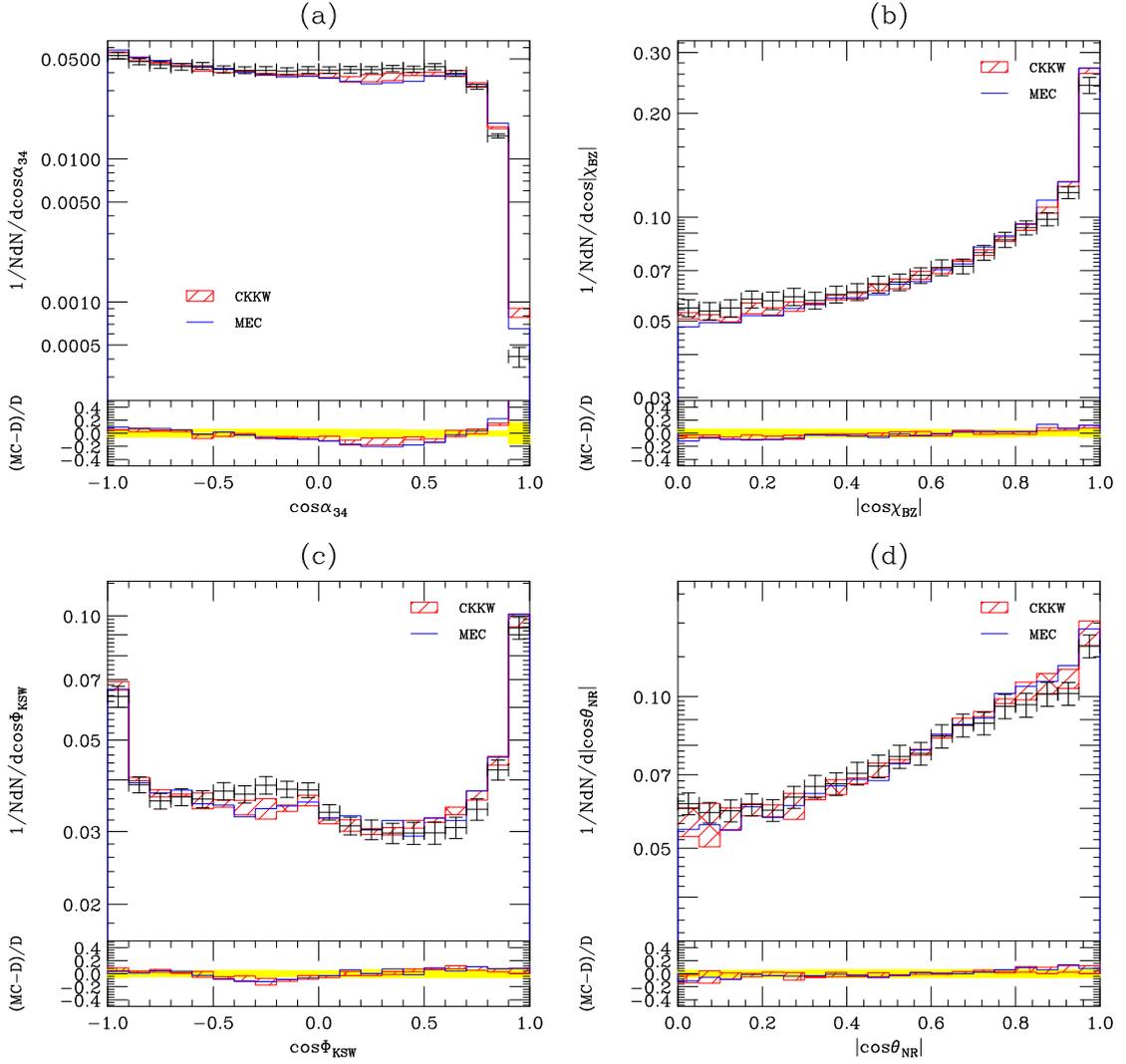
Figure 5.10: Distributions of four-jet angles for $e^+e^- \to$ hadrons at a centre-of-mass energy of $\sqrt{s} = 91.2\,\text{GeV}$ in comparison to LEP data [100]. Figures (a)-(d) give the angle between the lowest energy jets α_{34}, the Bengtsson-Zerwas angle [95] χ_{BZ}, the Korner-Sielshotlz-Willrodt [97] Φ_{KSW} and the Nachtmann-Reiter angle [96] θ_{NR}. The colours of the lines are the same as those in Fig. 5.8.

Observable	Hw+ME χ^2/d.o.f	CKKW χ^2/d.o.f
Thrust	25.78	10.62
Sphericity	9.126	0.580
Oblateness	7.262	0.339
Planarity	3.928	1.211
y_{23}	2.812	0.867
y_{34}	1.912	1.026
y_{45}	4.204	2.018
$\cos\alpha_{34}$	1.043	3.301
$\cos\chi_{BZ}$	0.3138	0.775
$\cos\Phi_{KSW}$	1.645	1.337
$\cos\theta_{NR}$	2.514	0.702

Table 5.2: A comparison of the χ^2 per degree of freedom for event shape observables in $e^+e^- \to$ hadrons with default Herwig++, with matrix-element corrections, and the CKKW implementation, with merging scale set to $y_{MS} = 10^{-2}$ in the Durham jet measure.

5.6 Conclusions

A modified version of the CKKW algorithm has been implemented in Herwig++ for the process $e^+e^- \to$ hadrons. The modified algorithm uses truncated showers in order to provide smooth merging between the Herwig++ angular-ordered parton shower and a set of transverse-momentum-ordered emissions defined by inverting the Herwig++ momentum reconstruction procedure on a samples of parton momenta generated according to exact tree-level matrix elements.

The truncated shower was found to result in a smooth merging between parton-shower and matrix-element regions of phase space with parton-level distributions appearing free of discontinuities around the merging scale and relatively insensitive to changes in the merging scale.

A full tune of the Herwig++ free parameters was performed for the CKKW implementation with a merging scale of $y_{MS} = 10^{-2}$ in the Durham jet measure. This was found to give a good description of LEP data, demonstrating a significant improvement over the results from the default Herwig++ parton shower with matrix-element corrections applied.

The results show a comparable level of merging scale dependence and agreement with LEP data to that found in Ref. [101], in which a similar CKKW merging approach was performed with a transverse-momentum-ordered dipole shower.

Chapter 6

Merging matrix elements with initial-state parton showers

6.1 Introduction

In order to provide a matrix-element merging algorithm which is useful for the simulation of hadron-hadron collisions, it is necessary to extend the algorithm to include the treatment of space-like emissions. This introduces significant complications since it involves the merging of a backwards parton shower and the inclusion of PDFs. The extension of the original CKKW algorithm to include initial-state corrections was proposed in Ref. [84] and implemented within the Pythia and HERWIG event generators in Ref. [87], and the SHERPA event generator in Refs. [102] and [83]. The CKKW-L algorithm was also extended to include initial-state corrections in Ref. [103].

In this chapter we describe an extension of the modified CKKW algorithm described in Chapter 5 to include initial-state corrections. A general procedure for initial-state corrections is described, following the same POWHEG-style shower reorganisation that was used in the final-state case. As in the final-state case, the modified algorithm provides a theoretical improvement over the standard CKKW algorithm by consistently taking differences in the ordering and merging variables into account via truncated showers.

An implementation of the algorithm is presented for the case of Drell-Yan vector production. This represents the simplest hadron-hadron process and provides the cleanest test bed for the initial-state algorithm. In order to verify the algorithm, a detailed comparison of the simulation to Tevatron data is performed.
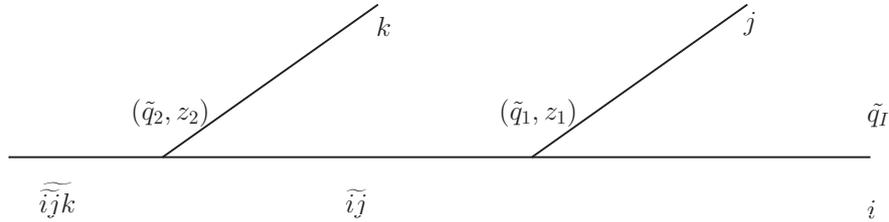
Figure 6.1: An example of an initial-state hard shower line configuration where two emissions
are generated above $k_{\perp_{MS}}$.

The production of jets together with a vector boson is also an important background
to many processes at the LHC. As such, an accurate simulation of the Drell-Yan process,
particularly with jets, is crucial for potential discoveries at the LHC. Since parton show-
ers alone are deficient in their description of high-jet-multiplicity states, the development
and verification of merging algorithms is an important area of current event generator
development.

The chapter is organised as follows. In Sect. 6.2 the formal reorganisation of the
initial-state shower, in terms of a set of hard emissions with truncated and vetoed show-
ers, is presented. In Sect. 6.3 further details of the algorithm are described, detailing
the vetoing, reweighting and clustering procedures. In Sect. 6.4 the results of the imple-
mentation are presented in comparison to Tevatron data for Z/γ- and W-production.

6.2 Initial-state CKKW reorganisation

The initial-state parton shower can be decomposed into a set of hard emissions which
are dressed with POWHEG truncated and vetoed showers in order to reproduce the full
shower. In order to illustrate this reorganisation we consider, analogously to Sect. 5.3.1,
the case of exactly two emissions along an initial-state shower line which we will then
extrapolate to a general procedure. This case is shown in Fig. 6.1. Applying the same
decomposition as that leading to Eq. 5.16 to the initial-state case, the evolution equation

of Eq. 3.35, for configurations of this type may be written

$$
\begin{aligned}
\bar{\mathcal{S}}_i^{(2)}(\tilde{q}_I, x) \;=\; & \int_{\tilde{q}_0}^{\tilde{q}_I} \bar{\mathcal{S}}_i^T(\tilde{q}_I, \tilde{q}_1; x, k_{\perp_{MS}}) \frac{\mathrm{d}\mathcal{P}_{\widetilde{ij}\to ij}(\tilde{q}_1, z_1)}{z_1} \mathcal{S}_j^V((1-z_1)\tilde{q}_1; x, k_{\perp_{MS}}) \\
\times \; & \int_{\tilde{q}_0}^{\tilde{q}_1} \bar{\mathcal{S}}_{\widetilde{ij}}^T(\tilde{q}_1, \tilde{q}_2; x/z_1, k_{\perp_{MS}}) \frac{\mathrm{d}\mathcal{P}_{\widetilde{ijk}\to\widetilde{ij}k}(\tilde{q}_2, z_2)}{z_2} \\
\times \; & \mathcal{S}_k^V((1-z_2)\tilde{q}_2; k_{\perp_{MS}}) \bar{\mathcal{S}}_{\widetilde{ijk}}^V(\tilde{q}_2; x/(z_1 z_2), k_{\perp_{MS}}) W_{\mathrm{Sudakov}} W_{\mathrm{PDF}}.
\end{aligned}
\tag{6.1}
$$

where the the introduced Sudakov weight is given by

$$
\begin{aligned}
W_{\mathrm{Sudakov}} \;=\; & \frac{\Pi_i^R(\tilde{q}_I; x, k_{\perp_{MS}})}{\Pi_i^R(\tilde{q}_1; x, k_{\perp_{MS}})} \frac{\Pi_{\widetilde{ij}}^R(\tilde{q}_1; x/z_1, k_{\perp_{MS}})}{\Pi_{\widetilde{ij}}^R(\tilde{q}_2; x/z_1, k_{\perp_{MS}})} \\
\times \; & \Pi_{\widetilde{ijk}}^R(\tilde{q}_2; x/(z_1 z_2), k_{\perp_{MS}}) \Delta_j^R((1-z_1)\tilde{q}_1; k_{\perp_{MS}}) \Delta_k^R((1-z_2)\tilde{q}_2; k_{\perp_{MS}}),
\end{aligned}
\tag{6.2}
$$

and the PDF weight is

$$
W_{\mathrm{PDF}} = \frac{f_{\widetilde{ij}}(x/z_1, \tilde{q}_1)}{f_i(x, \tilde{q}_1)} \frac{f_{\widetilde{ijk}}(x/(z_1 z_2), \tilde{q}_2)}{f_{\widetilde{ij}}(x/z_1, \tilde{q}_2)}.
\tag{6.3}
$$

The initial-state remnant Sudakov form factor, $\Pi_i^R(\tilde{q}; x, k_{\perp_{MS}})$, space-like truncated shower, $\bar{\mathcal{S}}_i^T(\tilde{q}_1, \tilde{q}_2; x, k_{\perp_{MS}})$ and vetoed shower, $\bar{\mathcal{S}}_i^V(\tilde{q}; x, k_{\perp_{MS}})$ are given by Eqs. 3.32, 3.36 and 3.37, respectively, with the replacement

$$
\Theta\left(p_\perp(\tilde{q}, z) - p_{\perp_h}\right) \to \Theta\left(k_\perp(\tilde{q}, z) - k_{\perp_{MS}}\right).
\tag{6.4}
$$

In the CKKW procedure of generating a hard configuration according to the exact cross section, the set of splitting functions and a PDF factor are replaced by the corresponding differential cross section weight. In the case of the configuration in Fig. 6.1 the weight coming from the cross section can be approximated in terms of the parton-shower splitting functions as

$$
W_{\mathrm{cross-section}} = \frac{\mathrm{d}\mathcal{P}_{\widetilde{ij}\to ij}(\tilde{q}_1, z_1)}{z_1} \frac{\mathrm{d}\mathcal{P}_{\widetilde{ijk}\to\widetilde{ij}k}(\tilde{q}_2, z_2)}{z_2} \frac{f_{\widetilde{ijk}}(x, \mu)}{f_i(x, \tilde{q}_I)} \frac{1}{W_{\alpha_S}}.
\tag{6.5}
$$

in Eq. 6.1. The factor W_{α_S} is a strong coupling weight, identical to that constructed in the final-state scheme, consisting of the product of the ratios of the parton shower and matrix element couplings for each emission vertex. The scale μ is the fixed factorisation scale used to evaluate the PDFs in generating the hard configurations. The factors

of z in Eq. 6.5 are Jacobian factor due to the convolution over PDFs being over the variable x/z_1z_2 in the cross section but x in the parton shower. The ratio of PDFs in Eq. 6.5 accounts for the fact that the PDF factor introduced by the cross section and its parton-shower approximation do not match.

The initial-state shower decomposition of Eq. 6.1 implies a CKKW merging procedure where hard configurations from exact cross sections are reweighted by a set of PDF and Sudakov factors, while truncated and vetoed showers from the hard configurations generate emissions below the merging scale. The initial-state truncated and vetoed showers are completely analogous to those introduced in Sect. 5.3 for the final-state case. From Eqs. 6.1 and 6.5, it is seen that the reweighting factors for the case shown in Fig. 6.1, is given by

$$W_{\alpha_S} W_{\text{Sudakov}} W_{\text{PDF}} \frac{f_i(x/(z_1 z_2), \tilde{q}_I)}{f_{\widetilde{ijk}}(x, \mu)}. \tag{6.6}$$

This decomposition may be generalised to any configuration yielding a general merging procedure for initial-state showers. The procedure is identical to that for the final-state case, described in Sect. 5.4, with the exception that configurations are reweighted by a different set of Sudakov factors and additional PDF factors. The Sudakov weights are constructed according to the following prescription:

- each internal space-like line for a parton of flavour i and momentum fraction x, between the scales $\tilde{q}_1$ and $\tilde{q}_2$, contributes the factor

$$\frac{\Pi_i^R(\tilde{q}_1; x, k_{\perp_{MS}})}{\Pi_i^R(\tilde{q}_2; x, k_{\perp_{MS}})}; \tag{6.7}$$

- each external space-like line for a parton of flavour i and momentum fraction x, starting from a scale $\tilde{q}$ contributes the factor

$$\Pi_i^R(\tilde{q}; x, k_{\perp_{MS}}). \tag{6.8}$$

The PDF weights are constructed according to the following procedure:

- each space-like emission $\widetilde{ij} \to ij$, from a parton of flavour i and momentum fraction x, at $(\tilde{q}, z)$, contributes the factor

$$\frac{f_{\widetilde{ij}}(x/z, \tilde{q})}{f_i(x, \tilde{q})};$$ (6.9)

- each space-like parton with flavour i and momentum fraction x, entering the underlying leading-order subprocess contributes the factor

$$f_i(x, \tilde{q}_I);$$ (6.10)

- each external space-like parton with flavour i and momentum fraction x contributes the factor

$$\frac{1}{f_i(x, \mu)}.$$ (6.11)

The contributions to the PDF weight coming from external partons corresponds to dividing out the PDF factors that were present in the cross sections used to generate the hard configurations.

6.3 The algorithm

6.3.1 Vetoes

As described in Sect. 2.2.6, the momenta of the initial-state partons are reconstructed in the partonic centre-of-mass frame, which is related to the hadronic centre-of-mass frame by a longitudinal boost along the beam direction. It is therefore convenient to use a merging variable that is invariant under longitudinal boosts. A convenient choice of this variable, which was also used in the original initial-state CKKW algorithm [84], is given by the hadronic jet measure introduced in ref. [105]. For a pair of final-state partons i, j the hadronic jet measure is defined by

$$y_{ij} = \frac{\min\left(p_{\perp_i}^2, p_{\perp_j}^2\right) R_{ij}}{\hat{s}},$$ (6.12)

where $p_{\perp_i}$ is the transverse momentum of parton i relative to the beam axis and the jet separation R_{ij} is defined by

$$R_{ij} = (\eta_i - \eta_j)^2 + (\phi_i - \phi_j)^2 \,, \tag{6.13}$$

where η_i and ϕ_i are the pseudo-rapidity and azimuth of parton i respectively. For a final-state parton i and an initial-state parton i the hadronic jet measure is

$$y_{ij} = \frac{p_{\perp_i}^2}{\hat{s}}. \tag{6.14}$$

In order to apply vetoes to emissions generated in the parton shower, it is necessary to relate the hadronic jet measure, defined in Eqs. 6.12 and 6.14, to the shower variables. As in the final-state case, we approximate this mapping to that of a single emission.

For an emission from an initial-state parton, the jet measure is given by Eq. 6.14 and we identify $p_{\perp_i}$ as the transverse momentum of the initial-state emission defined in Eq. 2.29.

The jet measure of a final-state emission is given by Eq. 6.12 where, for a single emission, we identify $p_{\perp_{i,j}}$ as the transverse momentum of the final-state emission defined in Eq. 2.14. In the massless approximation used in treating initial-state radiation, the pseudo-rapidity of the partons coincides with the rapidity of the partons and is given by

$$\eta = \frac{1}{2} \log \left[\frac{E + p_z}{E - p_z} \right], \tag{6.15}$$

where E is the parton's energy and p_z is the component of the parton's momentum in the beam direction. For a single final-state emission, $\widetilde{ij} \to ij$, the on-shell reconstructed parton momenta are parameterised in the normal Sudakov decomposition according to Eq. 1.49. In terms of these Sudakov variables, the pseudo-rapidity is

$$\eta_i = \frac{1}{2} \log \left[\frac{\alpha_i}{\beta_i} \right], \tag{6.16}$$

where, analogously to Eq. 1.55, the Sudakov variables are

$$\alpha_i = z, \qquad \beta_i = \frac{p_\perp^2}{zs},$$

$$\alpha_j = 1 - z, \qquad \beta_j = \frac{p_\perp^2}{(1-z)s}.$$

Transverse momentum conservation dictates also that for a single emission,

$$\phi_i - \phi_j = \pi, \tag{6.17}$$

completing the definition of the hadronic jet measure in terms of the shower variables.

6.3.2 Dynamic Sudakov weights

In the final-state implementation, described in Chapter 5, the Sudakov form factors, $\Delta_i^R(\tilde{q}; k_{\perp_{MS}})$, could be implemented by tabulating the integral in Eq. 5.8 and providing two-dimensional interpolation between the tabulated values. Since, in the initial-state case the corresponding Sudakov factor, $\Pi_i^R(\tilde{q}; x, k_{\perp_{MS}})$, also depends on the momentum fraction, x, the integration and interpolation procedures are not feasible. Instead we use a trick, first introduced in Ref. [85], to generate the appropriate Sudakov weights dynamically from the parton shower. This results in a particularly simple implementation where the desired reweighting is achieved by a vetoing of events.

The Sudakov weights that are introduced in the reweighting procedure, described in Sects. 5.4 and 6.2, correspond to the probability of generating no emissions with $k_\perp > k_{\perp_{MS}}$ in the parton shower that is produced around the set of hard emissions. Given this correspondence the Sudakov reweighting may be achieved by, rather than just vetoing the emission, throwing the whole event away if an emission with $k_\perp > k_{\perp_{MS}}$ is generated in the truncated or vetoed showers. We refer to this process as *dynamic Sudakov reweighting*.

To see that the dynamic Sudakov reweighting produces the correct reweighting, we consider the case of two hard emissions at $(\tilde{q}_a, z_a)$ and $(\tilde{q}_b, z_a)$. The probability, P_{retain}, of retaining the event in the truncated showering of this line is given by the probability of generating no emissions with $k_\perp > k_{\perp_{MS}}$. This is equal to the probability of generating

any number of emissions with $k_\perp < k_{\perp_{MS}}$ and is given by[1]

$$
\begin{aligned}
P_{\text{retain}} &= \Delta(z_a \tilde{q}_a, \tilde{q}_b) + \int_{\tilde{q}_b}^{z_a \tilde{q}_a} \Delta(z_a \tilde{q}_a, \tilde{q}_b) \mathrm{d}\mathcal{P}(\tilde{q}_1, z_1) \Theta\left(k_{\perp_{MS}} - k_\perp(\tilde{q}_1, z_1)\right) \\
&+ \int_{\tilde{q}_b}^{z_a \tilde{q}_a} \Delta(z_a \tilde{q}_a, \tilde{q}_1) \mathrm{d}\mathcal{P}(\tilde{q}_1, z_1) \Theta\left(k_{\perp_{MS}} - k_\perp(\tilde{q}_1, z_1)\right) \\
&\times \int_{\tilde{q}_b}^{z_a \tilde{q}_1} \Delta(z_1 \tilde{q}_1, \tilde{q}_b) \mathrm{d}\mathcal{P}(\tilde{q}_2, z_2) \Theta\left(k_{\perp_{MS}} - k_\perp(\tilde{q}_2, z_2)\right) + \ldots .
\end{aligned}
\tag{6.18}
$$

In the usual POWHEG approximation we identify the emissions as soft-gluon radiation, allowing the replacement $z \to 1$ in Eq. 6.18[2]. The Sudakov form factors can therefore be combined yielding

$$
P_{\text{retain}} = \Delta(z_a \tilde{q}_a, \tilde{q}_b) \left\{ 1 + \sum_{n=1}^{\infty} \prod_{i=1}^{n} \int_{\tilde{q}_b}^{\tilde{q}_{i-1}} \mathrm{d}\mathcal{P}(\tilde{q}_i, z_i) \Theta\left(k_{\perp_{MS}} - k_\perp(\tilde{q}_i, z_i)\right) \right\},
\tag{6.19}
$$

where $q_0 = z_a \tilde{q}_a$. The nested integrals can then be exponentiated in the usual way giving

$$
\begin{aligned}
P_{\text{retain}} &= \Delta(z_a \tilde{q}_a, \tilde{q}_b) \exp\left[\int_{\tilde{q}_b}^{z_a \tilde{q}_a} \mathrm{d}\mathcal{P}(\tilde{q}_i, z_i) \Theta\left(k_{\perp_{MS}} - k_\perp(\tilde{q}_i, z_i)\right) \right] \\
&= \Delta^R(z_a \tilde{q}_a, \tilde{q}_b; k_{\perp_{MS}}),
\end{aligned}
\tag{6.20}
$$

which is the same reweighting factor that was used previously.

6.3.3 Clustering procedure

The clustering procedure used is a direct extension of that described in Sect. 5.4.2 for final-state radiation. All possible pseudo-shower histories are first created, one of which is selected according to some criteria that ensures that the history that the parton shower is most likely to produce is chosen. In the final-state case, the selection procedure minimised the scalar sum of the transverse momentum of the branchings.

Since in the case of initial-state radiation, transverse momenta are relative to the beam direction, employing the same clustering scheme would not ensure the most sensible choice of history. In particular, for the case of a single emission this scheme would select a history where the final-state parton was clustered to both incoming partons with

---

[1]For clarity of notation we ignore the flavour of the emissions.
[2]This also justifies our omission of flavour indices since all flavour changing emissions are subleading.

equal probabilities. However, the parton shower would favour a history where the final-state parton was more collinear to the emitted parton. In order to take this into account the clustering procedure is augmented to favour collinear emission. This is achieved by using the total transverse momentum measure

$$\sum_{\text{hard emissions}} a \left| p_\perp(\tilde{q}, z) \right|, \tag{6.21}$$

where an extra factor, a, has been introduced which is set to a constant less than one, a_{collin}, for initial-state emissions where the longitudinal momentum of the emitted time-like parton is of the same sign as that of the space-like parent and one for all other emissions. The default value used for this parameter is $a_{\text{collin}} = 0.9$ however results were found to be insensitive to the value provided it remains close to one. This ensures that for histories with equal, or very similar, total transverse momentum, the more collinear history is selected.

There are a set of diagrams which lead to configurations that have no parton-shower interpretation. These correspond to electro-weak corrections to an underlying QCD process. Such configurations correspond to genuine corrections but have no analogy in the parton shower. We therefore choose to retain such configurations, showering them directly. In practice, we find that neglecting such contributions has no visible effect, justifying the decision to not provide a more sophisticated treatment.

6.3.4 Corrections to the dead zone

The merging scale should be chosen in the region where the validity of the parton shower and matrix elements overlap. This must be low enough that the correction is applied fully to the region in which it is most required and also high enough to avoid the cut-offs that are applied in the parton shower.

The CKKW scheme ensures that the dead zone is filled above the merging scale but remains empty below the merging scale. The phase space accessible to the parton shower was discussed in Sect. 2.2.4 and we require that the parton shower and matrix elements provide a full coverage of the phase space.

The phase space for a single initial-state emission in the Drell Yan process is shown in Fig. 6.2 for a range of merging scale choices. It is clear that if the merging scale is chosen to be sufficiently small then the overlap between the dead zone and the region that is not
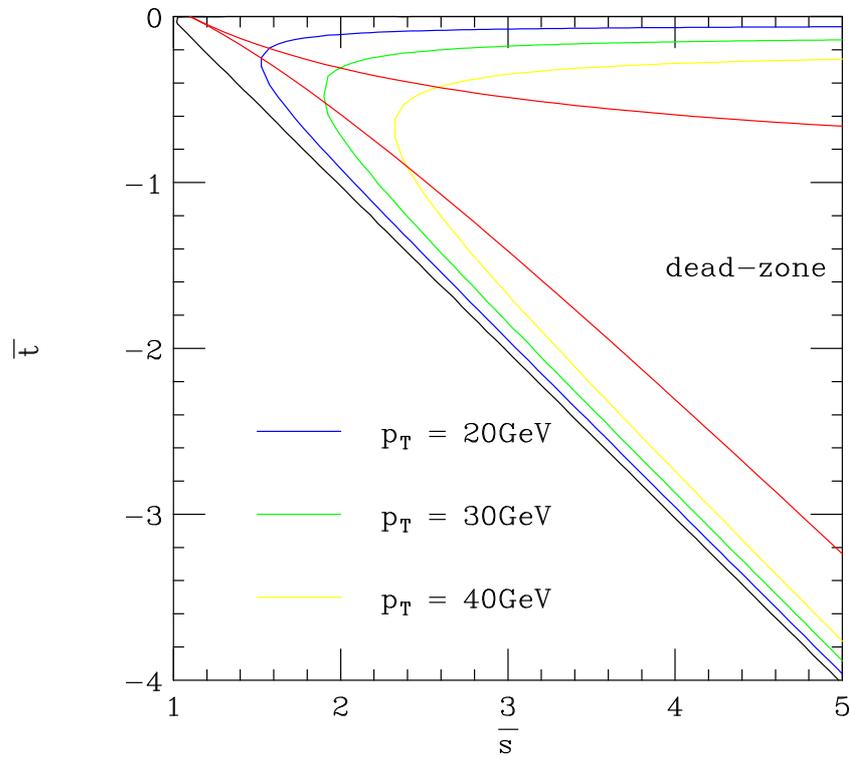
Figure 6.2: The phase-space regions accessible to initial-state parton-shower and matrix-element emissions in Drell-Yan vector boson production at $\sqrt{s} = 2\,\mathrm{TeV}$. The red line shows the limits on the phase space into which the shower can emit, with the dead zone inside. The blue, green and yellow lines show the merging-scale contours with $p_\perp = 20\,\mathrm{GeV}$, $30\,\mathrm{GeV}$, and $40\,\mathrm{GeV}$ respectively. The matrix-element region lies to the right of each of these contours and the parton-shower region lies to the left.

filled by matrix elements is negligible. However, for a merging scale of $k_{\perp_{MS}} = 40\,\text{GeV}$ there is a significant region that will be filled by neither the parton shower or matrix elements.

In order to ensure that the dead zone is filled, a modified treatment of events with no matrix-element emissions is employed. The POWHEG implementation presented in Chapter 4 generates a single emission, according to exact matrix elements, allowing a full coverage of the dead zone. The first emission of events with no matrix-element emissions may therefore be generated with the POWHEG hard generator. Subsequent emissions are then generated around this emission using the standard truncated and vetoed showers. In order to retain the correct vetoes and Sudakov reweighting, events are vetoed if an emission with jet measure above the merging scale is generated in the POWHEG hard emission or subsequent emissions.

6.4 Results

In this section we present results of the implementation for Drell-Yan vector boson production at the Tevatron, with the vector boson decaying into first generation leptons, at a centre-of-mass energy of $1.96\,\text{TeV}$.

Matrix-element samples were generated using MadGraph/MadEvent [92, 93] for the process with up to four extra jets. Merging scales of $k_{\perp_{MS}} = 20\,\text{GeV}$, $30\,\text{GeV}$ and $40\,\text{GeV}$ were used.

The CTEQ6L1 PDF set [106] was used, with the LHAPDF interface [75], in both the generation of matrix-element samples and the Herwig++ parton shower.

The set of hadronisation parameters, generated in the tune to LEP data, were also used for this process.

The intrinsic transverse momentum was tuned to a value of $1\,\text{GeV}$.

The CKKW algorithm should show the biggest improvement over the standard parton shower for observables that are sensitive to configurations with multiple well separated jets. We therefore compare the simulation to a set of distributions of $V + \text{jets}$ production. The analyses were performed using Rivet [107].
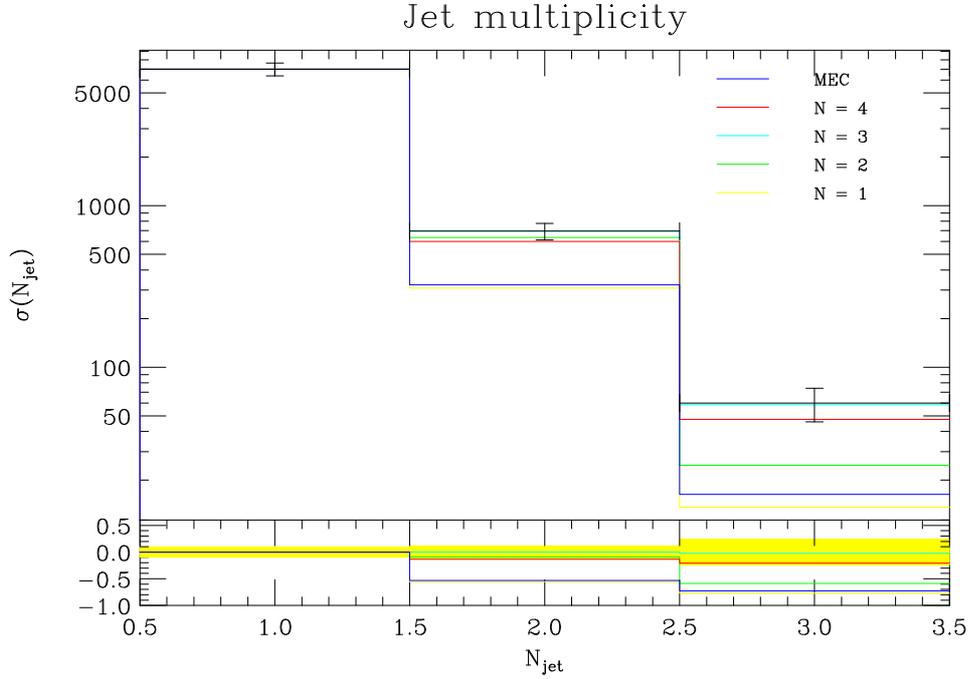
Figure 6.3: Jet multiplicity distributions in Z/γ-productions at the Tevatron with $\sqrt{s} = 1.96\,\text{TeV}$ in comparison to CDF data [108]. The red, cyan and green lines show the CKKW distribution with a maximum of 4, 3, 2 and 1 jets described by matrix elements. The blue line shows the distribution for default Herwig++ with a matrix-element correction. The lower panel shows $(\text{MC} - \text{data})/\text{data}$ for each distribution.

6.4.1 $Z/\gamma + \text{jets}$

Figure 6.3 shows the inclusive jet cross sections for different choices of N, where N is the maximum number of jets that are described by the matrix elements. Final-state hadrons are clustered into jets with a cone algorithm, requiring a minimum separation between jets of $R_{ij} = 0.7$. The merging scale is set to $k_{\perp_{MS}} = 20\,\text{GeV}$ for each of the CKKW distributions shown.

The distributions are compared to CDF data [108]. Since the normalisation in the CKKW method corresponds to a leading-order cross section, it is necessary to introduce a K-factor. This was calculated by normalising the distributions to the $n_{\text{jet}} = 1$ bin. The same K-factor was then used for all subsequent distributions.

As expected, the distribution for CKKW with $N = 1$ matches closely that of default Herwig++, with a matrix-element correction. As a higher number of emissions are included in the matrix-element region, a significant improvement is observed with a

	cross section / nb		
N	$k_{\perp_{MS}} = 20\,\mathrm{GeV}$	$k_{\perp_{MS}} = 30\,\mathrm{GeV}$	$k_{\perp_{MS}} = 40\,\mathrm{GeV}$
4	0.269	0.269	0.268
3	0.270	0.269	0.268
2	0.272	0.269	0.268
1	0.270	0.267	0.266

Table 6.1: Table of the total cross sections obtained for the process $p\bar{p} \to Z/\gamma$ at the Tevatron run II ($p\bar{p}$ at $\sqrt{s} = 1.96\,\mathrm{TeV}$), for different choices of $k_{\perp_{MS}}$ and N.

good description of the data being obtained for $N \geq 3$. In all subsequent plots we set $N = 4$.

The total cross-sections obtained for the different choices of $k_{\perp_{MS}}$ and N are presented in Table 6.1. The cross-section is extremely stable, in both the merging scale and maximum multiplicity, exhibiting variation at the percent level.

Figure 6.4 shows the distribution of jet transverse momentum in events with $n_{\mathrm{jet}} \geq 1$ and $n_{\mathrm{jet}} \geq 2$ resolved jets. The variation in the CKKW distribution for the three choices of merging scale is represented by the red band. This is compared to CDF data [108] and the default Herwig++ distribution. For $n_{\mathrm{jet}} \geq 1$ the default Herwig++ implementation provides an adequate description and the CKKW distribution is comparable to this, however for $n_{\mathrm{jet}} \geq 2$ there is a clear improvement in the CKKW distribution, indicating that providing a correction to more than just one emission is important in describing the data. The merging-scale dependence for the inclusive jet cross sections is shown in Fig. 6.5. The merging-scale dependences are seen to be at an acceptable level with only small variation.

Figure 6.5 shows the CKKW distribution and merging-scale dependence for the transverse momentum of the Z/γ-boson in comparison to D0 data [78]. The CKKW distribution demonstrates a similar level of agreement with data as the default Herwig++ distribution and the POWHEG implementation shown in Fig. 4.7. There is a slight improvement visible in the mid-region which showed a deficiency in the POWHEG and matrix-element correction distributions, where only a single emission is corrected. This may be attributed to an improved description of higher multiplicity contributions.
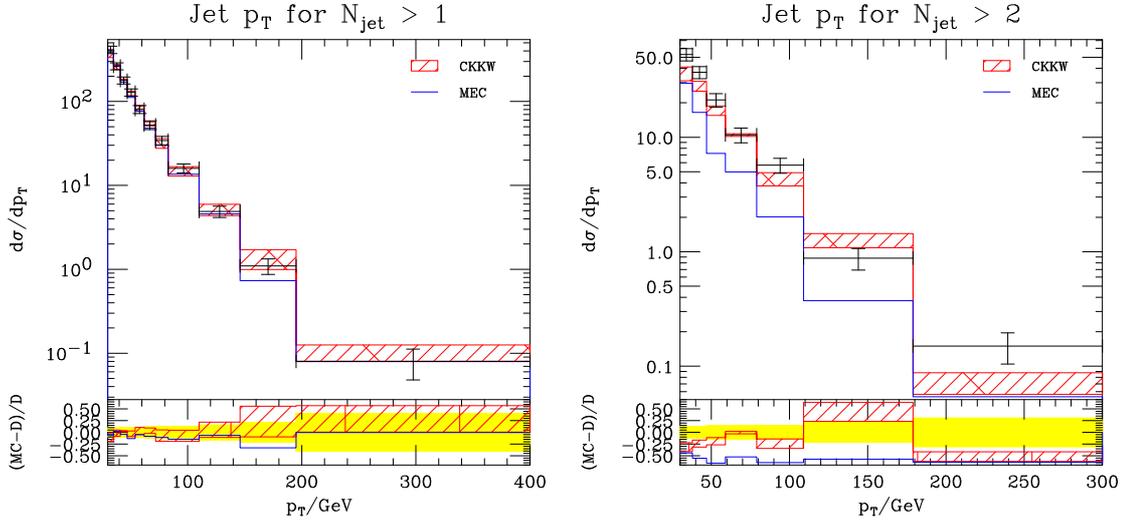
Figure 6.4: Distributions of jet transverse momentum in Z/γ + jet (Tevatron run II) production events, with $n_{\text{jet}} \geq 1$ and $n_{\text{jet}} \geq 2$ in comparison to CDF data [108]. The red band shows the variation in the CKKW result for merging scale choices of $k_{\perp MS} = 20\,\text{GeV}$, $30\,\text{GeV}$, and $40\,\text{GeV}$ and the blue line shows the default Herwig++ distribution. The lower panel shows $(\text{MC} - \text{data})/\text{data}$ for each distribution.
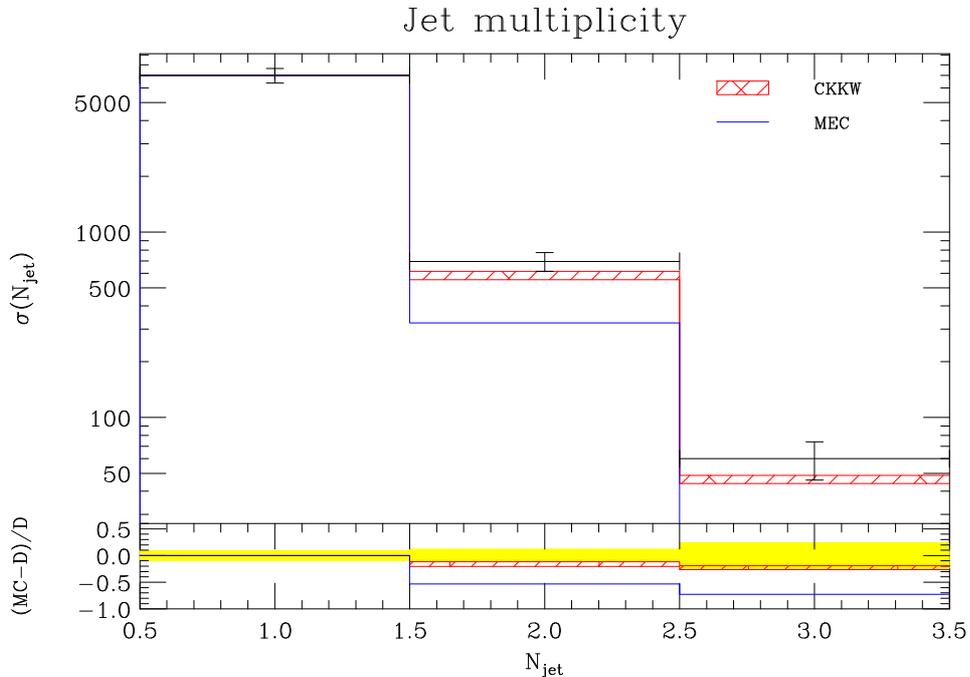
Figure 6.5: Jet multiplicity distributions in Z/γ-productions at the Tevatron run II, showing the merging-scale dependence, in comparison to CDF data [108]. Line colours are the same as those in Fig. 6.4.
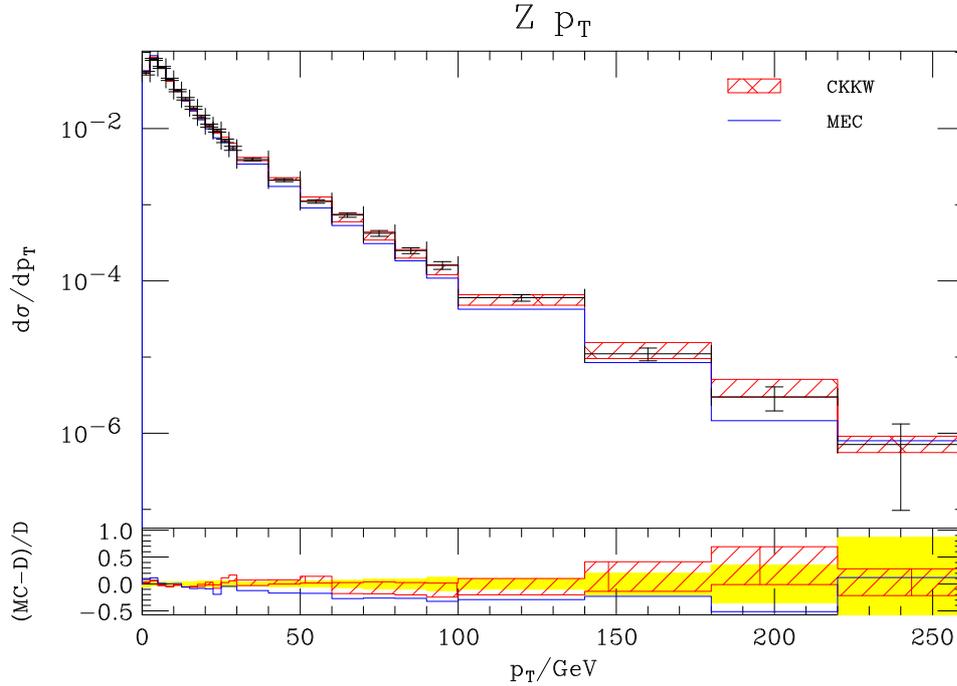
Figure 6.6: Distributions of the vector boson transverse momentum in Z/γ production at the Tevatron run II in comparison to D0 data [78]. Line colours are the same as those in Fig. 6.4.

6.4.2 W + jets

Figure 6.7 shows the inclusive jet cross sections for W-production for different choices of N in comparison to CDF data [109]. Again, clear improvement in the description of the data is seen as N is increased and good agreement is observed for $N \geq 2$, for all jet cross sections up to $n_{jet} = 4$.   The total cross sections for W-production at run II of the Tevatron are shown in Table 6.2. As in the case of Z-production, good stability of the cross section, with variation at the percent level, is observed for changes in N and $k_{\perp_{MS}}$.

Figure 6.8 shows the distributions of the transverse energy of the 1st, 2nd and 3rd highest-$p_\perp$ jets and the inclusive jet cross sections in comparison to CDF data [109]. The transverse energy of the jets is defined by

$$E_\perp = E \sin \theta, \tag{6.22}$$

where E and θ are the energy and angle, with respect to the beam axis, of the clustered jet momentum. When jet-multiplicity channels up to $N \geq 3$ are included, a good
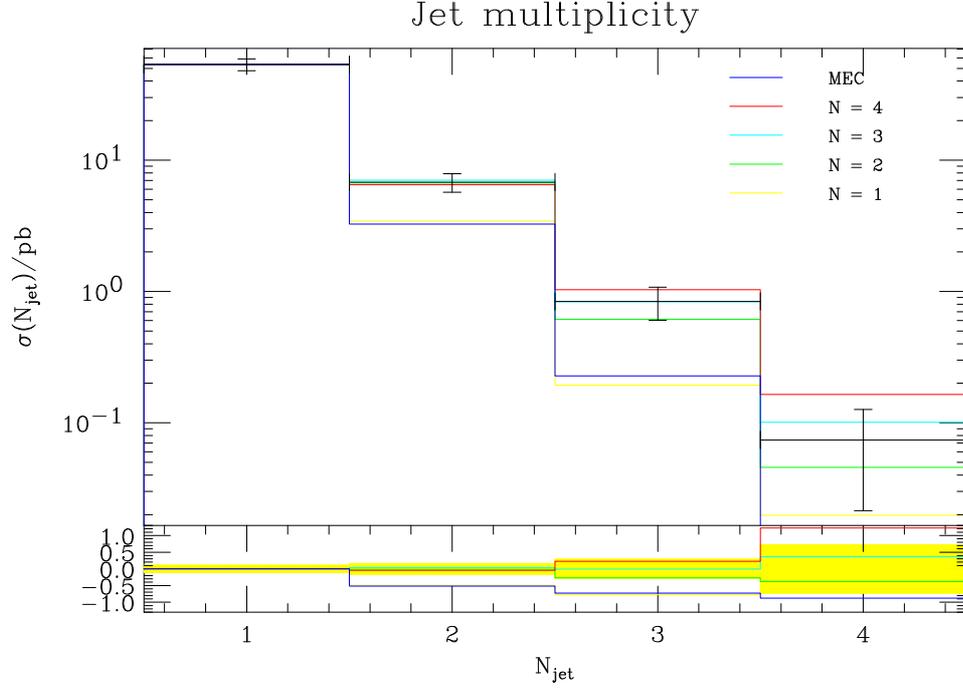
Figure 6.7: Jet multiplicity distributions in W-productions at the Tevatron run II with in comparison to CDF data [109]. Line colours are the same as those in Fig. 6.4.

	cross section / nb		
N	$k_{\perp_{MS}} = 20\,\text{GeV}$	$k_{\perp_{MS}} = 30\,\text{GeV}$	$k_{\perp_{MS}} = 40\,\text{GeV}$
4	1.97	1.96	1.95
3	1.98	1.96	1.95
2	1.99	1.96	1.95
1	1.98	1.94	1.93

Table 6.2: Table of the total cross sections obtained for the process $p\bar{p} \to W$ at the Tevatron run II, for different choices of $k_{\perp_{MS}}$ and N.
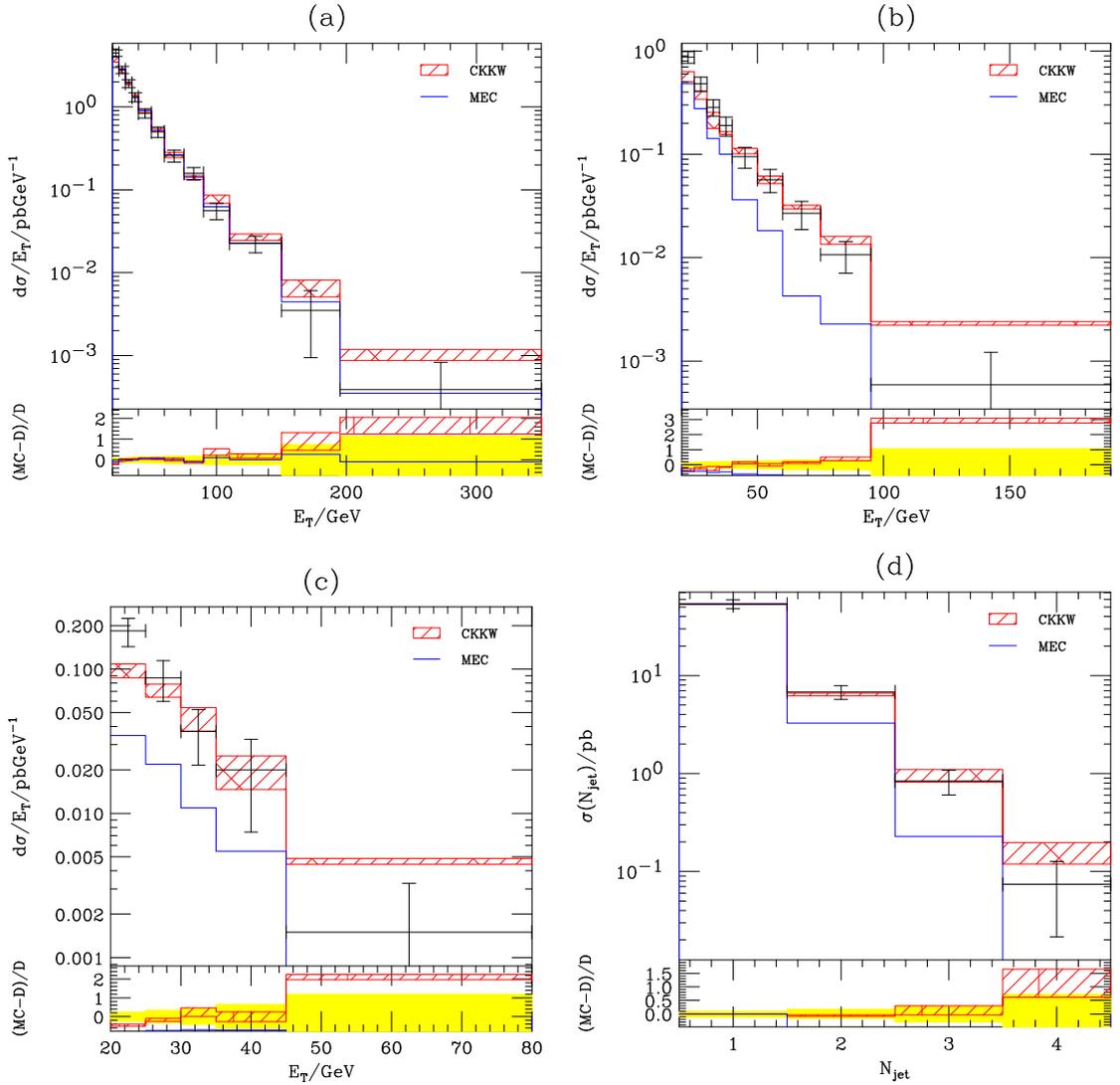
Figure 6.8: Plot (a)-(d) show the distribution of the transverse energy of the 1st, 2nd and 3rd highest-$p_\perp$ jets and the inclusive jet cross sections, respectively, in $W +$ jet production at run II of the Tevatron. The distributions are compared to CDF data [109]. Line colours are the same as those in Fig. 6.4.

description of the data is observed. Merging-scale variation is represented by the red-bands in Fig. 6.8 demonstrating a low level of merge scale dependence.

6.5 Conclusions

In this chapter we have presented an extension to the modified CKKW algorithm, described in Chapter 5, to include corrections to initial-state radiation. This has been

implemented in Herwig++ for Drell-Yan W- and Z/γ-production. A comparison to data from run II of the Tevatron was performed and a good agreement was seen for all observables provided that a high enough jet-multiplicity is included in the matrix elements.

An improvement was observed in the description of the CKKW distributions over that of default Herwig++ which applies a correction to only one emission. The improvement is particularly large for observables that are sensitive to high jet-multiplicity configurations. The dependence on the merging scale was investigated and found to be acceptable, with small variation seen in the distributions and good stability in the total cross sections.

Chapter 7

Conclusions

Monte Carlo event generators are important tools that are widely used in the planning and analysis of collider experiments. As we enter the era of the LHC, the potential for making new discoveries is dependent on the accuracy of event generators in describing both signal and background processes. Much effort has been put into developing a new generation of event generators for the LHC and these represent sophisticated simulations capable of describing a wide range of phenomena. One particular area that has seen much attention is the improvement of parton showers using exact matrix elements.

Parton showers provide a resummation of the large-logarithmic terms that are associated with soft and collinear parton emissions. This approach has been shown to be remarkably successful, however there are limits to its applicability. In particular, in the region of emissions with large transverse momentum, the parton-shower approximation becomes unreliable and there exists a region of phase space, referred to as the dead zone, into which the parton shower cannot radiate. Fixed-order calculations present a complimentary set of virtues, giving a good description of large-transverse-momentum emissions and featuring a full treatment of interferences. Matrix-element merging algorithms aim to combine both approaches such that the resummation of the parton shower is retained while improving the description with exact matrix elements.

In this thesis, two matrix-element merging algorithms have been studied within the Herwig++ event generator. The first is the POWHEG NLO matching scheme, which combines the parton shower with NLO matrix elements. The second is the CKKW matrix-element merging algorithm, which combines the parton shower with tree-level matrix elements that describe the process with any number of parton emissions up to some maximum multiplicity.

NLO matching schemes aim to retain the resummation of the parton shower while providing predictions for infra-red safe observables that agree with the exact NLO cross section. The most well-developed of these methods is the MC@NLO scheme, however the POWHEG method is a novel scheme which has the advantage of producing only positive-weight events and having a decreased dependence on the parton shower in which it is implemented. The main features of the method are: a reorganisation of the parton shower in terms of truncated showers, vetoed showers and a hardest emission; and a reformulation of the NLO cross section.

The POWHEG method was first implemented within Herwig++, for the process $e^+e^- \to$ hadrons. This is the simplest possible process and represents an important test bed for the implementation of the method. The implementation presented is the first to provide a full treatment of the truncated shower. The POWHEG implementation was found to give a reasonable description of LEP data. No significant differences between the matrix-element correction and POWHEG methods are observed for this process. This is to be expected since both methods correspond to a correction of the hardest emission that is equivalent in the NLL approximation.

The POWHEG method was then implemented for Drell-Yan vector boson production. This process involves a correction to an initial-state emission and a more complicated cross section. The accurate simulation of this process is important for the LHC, where it is an important background to many potential discovery signals. The implementation demonstrates a good description of Tevatron data for a range of observables exhibiting a slight improvement on the description provided by MC@NLO. It was found in all cases that the NLO schemes resulted in distributions that were lower in the large-transverse-momentum tail than matrix-element correction methods. This can be attributed to the fact that the NLO schemes provide the correct NLO normalisation while matrix-element correction methods require the application of a K-factor.

The principle of the POWHEG shower reorganisation may be extended to any number of emissions, enabling a set of hard emissions to be generated separately, and then have the angular-ordered (or otherwise) parton shower generated around them. This idea has been used to develop a modified version of the CKKW matrix-element merging algorithm which has been implemented in Herwig++. The modified algorithm uses truncated showers in order to provide smooth merging between the Herwig++ angular-ordered parton shower and a set of transverse-momentum-ordered emissions defined by inverting the Herwig++ momentum reconstruction procedure on a samples of parton momenta generated according to exact tree-level matrix elements.

The algorithm was first implemented for the process $e^+e^- \rightarrow$ hadrons. A smooth merging between the parton-shower and matrix-element regions of phase space was observed, with parton-level distributions appearing free of the discontinuities that have been seen in implementations of the standard CKKW algorithm. Distributions also demonstrated a small dependence on the merging scale. The algorithm was found to give a good description of LEP data, demonstrating a significant improvement over the results from the default Herwig++ parton shower with matrix-element corrections applied.

The algorithm was extended to include corrections to initial-state radiation and implemented for Drell-Yan vector boson production. This required the inclusion of PDF reweighting factors and the use of dynamic Sudakov reweighting. A modification was also made to the algorithm to ensure that the dead zone was filled below the merging scale. A comparison to data from run II of the Tevatron was performed and a good agreement was seen for all observables provided that a high enough jet-multiplicity is included in the matrix elements. An improvement was observed in the description of the CKKW distributions over that of default Herwig++ which applies a correction to only one emission. The improvement is particularly large for observables that are sensitive to high jet-multiplicity configurations. The dependence on the merging scale was investigated and found to be acceptable, with small variation seen in the distributions and good stability in the total cross sections.

The subject of combining matrix elements and parton showers is an area of continued development. The implementation of the POWHEG NLO matching algorithm is ongoing for a number of processes. Merging algorithms also continue to be developed and improved, with work being done on including one-loop matrix elements in the CKKW merging scheme as well as the treatment of electro-weak corrections.

In summary, we have presented research in the implementation and development of matrix-element merging algorithms within Herwig++ aiming to improve the simulation of hard QCD radiation. The results have shown these implementations to be successful, with many significant improvements seen in comparison to the standard Herwig++ description. Improvements to the simulation, such as these, are extremely important. This is an exciting time; the LHC promises to shed light on new physics and Monte Carlo event generators will play a major role in the discoveries it makes.

Bibliography

[1] K. Hamilton, P. Richardson and J. Tully, *A Positive-Weight Next-to-Leading Order Monte Carlo Simulation of Drell-Yan Vector Boson Production*, JHEP **0810** (2008) 015 [arXiv:0806.0290 [hep-ph]].

[2] K. Hamilton, P. Richardson and J. Tully, *A modified CKKW matrix element merging approach to angular-ordered parton showers*, JHEP **0911** (2009) 038 [arXiv:0905.3072 [hep-ph]].

[3] S. Gieseke, P. Stephens and B. Webber, *New formalism for QCD parton showers*, JHEP **0312**, 045 (2003) [arXiv:hep-ph/0310083].

[4] S. Gieseke, A. Ribon, M. H. Seymour, P. Stephens and B. Webber, *Herwig++ 1.0: An event generator for e+ e- annihilation*, JHEP **0402**, 005 (2004) [arXiv:hep-ph/0311208].

[5] M. Bahr *et al.*, *Herwig++ 2.3 Release Note* arXiv:0812.0529 [hep-ph].

[6] M. Bahr *et al.*, *Herwig++ Physics and Manual*, Eur. Phys. J. C **58**, 639 (2008) [arXiv:0803.0883 [hep-ph]].

[7] G. Corcella *et. al.*, *HERWIG 6: An Event Generator for Hadron Emission Reactions With Interfering Gluons (including supersymmetric processes)*, JHEP **01** (2001) 010, [arXiv:0011.363 [hep-ph]].

[8] S. Catani, S. Dittmaier and Z. Trocsanyi, *One-loop singular behaviour of QCD and SUSY QCD amplitudes with massive partons*, Phys. Lett. B **500**, 149 (2001) [arXiv:hep-ph/0011222].

[9] G. Dissertori, I. G. Knowles and M. Schmelling, *Quantum Chromodynamics: High Energy Experiments and Theory*, Oxford University Press (2003).

[10] M. E. Peskin and D. V. Schroeder, *An Introduction to Quantum Field Theory*, Westview Press (1995).

[11] R. K. Ellis, W. J. Stirling and B. R. Webber, *QCD and Collider Physics*, Cambridge University Press (1996).

[12] C. Amsler et al. (Particle Data Group), Physics Letters B667, 1 (2008)

[13] G. Marchesini and B. R. Webber, *Monte Carlo Simulation of General Hard Processes with Coherent QCD Radiation*, Nucl. Phys. B **310**, 461 (1988).

[14] H. D. Politzer, *Reliable Perturbative Results For Strong Interactions?*, Phys. Rev. Lett. **30** (1973) 1346.

[15] D. J. Gross and F. Wilczek, *Ultraviolet Behaviour Of Non-Abelian Gauge Theories*, Phys. Rev. Lett. **30**, 1343 (1973).

[16] L. D. Faddeev and V. N. Popov, *Feynman diagrams for the Yang-Mills field*, Phys. Lett. B **25** (1967) 29.

[17] W. E. Caswell, *Asymptotic Behavior Of Nonabelian Gauge Theories To Two Loop Order*, Phys. Rev. Lett. **33** (1974) 244.

[18] F. Bloch and A. Nordsieck, *Note on the Radiation Field of the electron*, Phys. Rev. **52** (1937) 54.

[19] T. Kinoshita, *Mass Singularities Of Feynman Amplitudes* J. Math. Phys. **3** (1962) 650.

[20] T. D. Lee and M. Nauenberg, *Degenerate Systems and Mass Singularities*, Phys. Rev. **133** (1964) B1549.

[21] G. Altarelli and G. Parisi, *Asymptotic Freedom In Parton Language*, Nucl. Phys. B **126** (1977) 298.

[22] V. N. Gribov and L. N. Lipatov, *Deep Inelastic e P Scattering In Perturbation Theory*, Sov. J. Nucl. Phys. **15**, 438 (1972) [Yad. Fiz. **15**, 781 (1972)].

[23] A. Bassetto, M. Ciafaloni, G. Marchesini and A. H. Mueller, *Jet Multiplicity And Soft Gluon Factorization*, Nucl. Phys. B **207**, 189 (1982).

[24] A. Bassetto, M. Ciafaloni and G. Marchesini, *Jet Structure And Infrared Sensitive Quantities In Perturbative QCD*, Phys. Rept. **100**, 201 (1983).

[25] S. Catani and M. Ciafaloni, *Many Gluon Correlations And The Quark Form-Factor In QCD*, Nucl. Phys. B **236**, 61 (1984).

[26] M. Ciafaloni, *Exponentiating Soft Emission In QCD* Phys. Lett. B **95**, 113 (1980).

[27] Y. L. Dokshitzer, V. A. Khoze and S. I. Troian, *Coherence And Physics of QCD Jets*, Adv. Ser. Direct. High Energy Phys. **5**, 241 (1988).

[28] A. H. Mueller, *On The Multiplicity Of Hadrons In QCD Jets*, Phys. Lett. B **104**, 161 (1981).

[29] B. I. Ermolaev and V. S. Fadin, *Log - Log Asymptotic Form Of Exclusive Cross-Sections In Quantum Chromodynamics*, JETP Lett. **33**, 269 (1981) [Pisma Zh. Eksp. Teor. Fiz. **33**, 285 (1981)].

[30] Y. L. Dokshitzer, V. S. Fadin and V. A. Khoze, *Coherent Effects In The Perturbative QCD Parton Jets*, Phys. Lett. B **115**, 242 (1982).

[31] A. Giovannini, *QCD Jets As Markov Branching Processes*, Nucl. Phys. B **161** (1979) 429.

[32] P. Cvitanovic, P. Hoyer and K. Zalewski, *Parton Evolution As A Branching Process*, Nucl. Phys. B **176**, 429 (1980).

[33] P. Cvitanovic, P. Hoyer and K. Konishi, *Partons And Branching*, Phys. Lett. B **85** (1979) 413.

[34] G. C. Fox and S. Wolfram, *A Model For Parton Showers In QCD*, Nucl. Phys. B **168**, 285 (1980).

[35] T. Sjostrand, *A Model For Initial State Parton Showers* Phys. Lett. B **157** (1985) 321.

[36] G. Marchesini and B. R. Webber, *Simulation Of QCD Jets Including Soft Gluon Interference*, Nucl. Phys. B **238**, 1 (1984).

[37] G. Marchesini and B. R. Webber, *Simulation of QCD coherence in heavy quark production and decay*, Nucl. Phys. B **330** (1990) 261.

[38] D. Amati, A. Bassetto, M. Ciafaloni, G. Marchesini and G. Veneziano, *A Treatment Of Hard Processes Sensitive To The Infrared Structure Of QCD*, Nucl. Phys. B **173** (1980) 429.

[39] T. Sjostrand, S. Mrenna and P. Skands, *PYTHIA 6.4 Physics and Manual*, JHEP **0605**, 026 (2006) [arXiv:hep-ph/0603175].

[40] T. Sjostrand, S. Mrenna and P. Skands, *A Brief Introduction to PYTHIA 8.1*, Comput. Phys. Commun. **178**, 852 (2008) [arXiv:0710.3820 [hep-ph]].

[41] T. Gleisberg, S. Hoche, F. Krauss, M. Schonherr, S. Schumann, F. Siegert and J. Winter, *Event generation with SHERPA 1.1*, JHEP **0902** (2009) 007 [arXiv:0811.4622 [hep-ph]].

[42] F. James, *Monte Carlo Theory And Practice*, Rept. Prog. Phys. **43**, 1145 (1980).

[43] M. Bengtsson and T. Sjostrand, *A Comparative Study of Coherent and Noncoherent Parton Shower Evolution*, Nucl. Phys. B **289** (1987) 810.

[44] M. H. Seymour, *Matrix Element Corrections To Parton Shower Algorithms*, Comput. Phys. Commun. **90**, 95 (1995) [arXiv:hep-ph/9410414].

[45] E. Norrbin and T. Sjostrand, *Production and hadronization of heavy quarks*, Eur. Phys. J. C **17**, 137 (2000) [arXiv:hep-ph/0005110].

[46] G. Corcella and M. H. Seymour, *Matrix element corrections to parton shower simulations of heavy quark decay*, Phys. Lett. B **442**, 417 (1998) [arXiv:hep-ph/9809451].

[47] S. Catani and M. H. Seymour, *A general algorithm for calculating jet cross sections in NLO QCD*, Nucl. Phys. B **485** (1997) 291 [Erratum-ibid. B **510** (1998) 503] [arXiv:hep-ph/9605323].

[48] P. Nason, *A New Method for Combining NLO QCD with Shower Monte Carlo Algorithms*, *JHEP* **11** (2004) 040.

[49] P. Nason and G. Ridolfi, *A Positive-Weight Next-to-leading-Order Monte Carlo for Z pair Hadroproduction*, *JHEP* **08** (2006) 077.

[50] S. Frixione and B. R. Webber, *Matching NLO QCD computations and parton shower simulations*, JHEP **0206**, 029 (2002) [arXiv:hep-ph/0204244].

[51] S. Frixione, P. Nason and B. R. Webber, *Matching NLO QCD and parton showers in heavy flavour production*, JHEP **0308**, 007 (2003) [arXiv:hep-ph/0305252].

[52] S. Frixione, E. Laenen, P. Motylinski and B. R. Webber, *Single-top production in MC@NLO*, JHEP **0603**, 092 (2006) [arXiv:hep-ph/0512250].

[53] S. Frixione and B. R. Webber, *The MC@NLO 3.3 event generator*, [arXiv:hep-ph/0612272].

[54] S. Frixione, E. Laenen, P. Motylinski and B. R. Webber, *Angular correlations of lepton pairs from vector boson and top quark decays in Monte Carlo simulations*, JHEP **0704**, 081 (2007) [arXiv:hep-ph/0702198].

[55] S. Frixione, E. Laenen, P. Motylinski, B. R. Webber and C. D. White, *Single-top hadroproduction in association with a W boson*, JHEP **0807**, 029 (2008) [arXiv:0805.3067 [hep-ph]].

[56] S. Frixione, P. Nason, and G. Ridolfi, *The POWHEG-hvq Manual Version 1.0*, [arXiv:0707.3081 [hep-ph]].

[57] S. Frixione, P. Nason, and C. Oleari, *Matching NLO QCD Computations with Parton Shower Simulations: the POWHEG Method*, *JHEP* **11** (2007) 070, [arXiv:0709.2092 [hep-ph]].

[58] S. Frixione, P. Nason, and G. Ridolfi, *A Positive-Weight Next-to-Leading-Order Monte Carlo for Heavy Flavour Hadroproduction*, *JHEP* **09** (2007) 126, [arXiv:0707.3088 [hep-ph]].

[59] O. Latunde-Dada, S. Gieseke, and B. Webber, *A Positive-Weight Next-to-Leading-Order Monte Carlo for e^+e^- Annihilation to Hadrons*, *JHEP* **02** (2007) 051, [arXiv:0612.281 [hep-ph]].

[60] S. Alioli, P. Nason, C. Oleari and E. Re, *NLO vector-boson production matched with shower in POWHEG*, JHEP **0807** (2008) 060 [arXiv:0805.4802 [hep-ph]].

[61] S. Alioli, P. Nason, C. Oleari and E. Re, *NLO Higgs boson production via gluon fusion matched with shower in POWHEG*, JHEP **0904** (2009) 002 [arXiv:0812.0578 [hep-ph]].

[62] K. Hamilton, P. Richardson and J. Tully, *A Positive-Weight Next-to-Leading Order Monte Carlo Simulation for Higgs Boson Production*, JHEP **0904** (2009) 116 [arXiv:0903.4345 [hep-ph]].

[63] S. Alioli, P. Nason, C. Oleari and E. Re, *NLO single-top production matched with shower in POWHEG: s- and t-channel contributions* arXiv:0907.4076 [hep-ph].

[64] L. Lonnblad, *Ariadne Version 4: A Program For Simulation Of QCD Cascades Implementing The Color Dipole Model,* Comput. Phys. Commun. **71** (1992) 15.

[65] P. Nason and B. R. Webber, *Non-perturbative corrections to heavy quark fragmentation in e+ e- annihilation*, Phys. Lett. B **395** (1997) 355 [arXiv:hep-ph/9612353].

[66] R. Kleiss, *From two to three jets in heavy boson decays: an algorithmic approach*, Phys. Lett. B **180**, 400 (1986).

[67] P. De Causmaecker, R. Gastmans, W. Troost and T. T. Wu, *Multiple bremsstrahlung in gauge theories at high-energies. 1. general formalism for quantum electrodynamics*, Nucl. Phys. B **206**, 53 (1982).

[68] G. Altarelli, R. K. Ellis and G. Martinelli, *Leptoproduction And Drell-Yan Processes Beyond The Leading Approximation In Chromodynamics*, Nucl. Phys. B **143**, 521 (1978) [Erratum-ibid. B **146**, 544 (1978)].

[69] J. Kubar-Andre and F. E. Paige, *Gluon Corrections To The Drell-Yan Model*, Phys. Rev. D **19**, 221 (1979).

[70] M. H. Seymour, *A Simple Prescription For First Order Corrections To Quark Scattering And Annihilation Processes*, Nucl. Phys. B **436**, 443 (1995) [arXiv:hep-ph/9410244].

[71] L. Lonnblad, *ThePEG, Pythia7, Herwig++ and Ariadne*, Nucl. Instrum. Meth. A **559**, 246 (2006).

[72] G. P. Lepage, *VEGAS: An Adaptive Multidimensional integration program*, CLNS-80/447.

[73] J. M. Campbell and R. K. Ellis, *Radiative corrections to Z b-$\bar{b}$ production*, Phys. Rev. D **62**, 114012 (2000) [arXiv:hep-ph/0006304].

[74] A. D. Martin, R. G. Roberts, W. J. Stirling and R. S. Thorne, *NNLO global parton analysis*, Phys. Lett. B **531**, 216 (2002) [arXiv:hep-ph/0201127].

[75] M. R. Whalley, D. Bourilkov and R. C. Group, *The Les Houches Accord PDFs (LHAPDF) and Lhaglue*, arXiv:hep-ph/0508110.

[76] V. M. Abazov *et al.* [D0 Collaboration], *Measurement of the shape of the boson rapidity distribution for $p\bar{p} \to Z/\gamma \to e^+e^-$ + X events produced at $\sqrt{s}$ of 1.96-TeV*, Phys. Rev. D **76**, 012003 (2007) [arXiv:hep-ex/0702025].

[77] A. A. Affolder *et al.* [CDF Collaboration], *The transverse momentum and total cross section of e^+e^- pairs in the Z boson region from $p\bar{p}$ collisions at $\sqrt{s} = 1.8$ TeV*, Phys. Rev. Lett. **84**, 845 (2000) [arXiv:hep-ex/0001021].

[78] V. M. Abazov *et al.* [D0 Collaboration], *Measurement of the shape of the boson transverse momentum distribution in $p\bar{p} \to Z/\gamma^* \to e^+e^-$ + X events produced at $\sqrt{s} = 1.96 - TeV$*, Phys. Rev. Lett. **100**, 102002 (2008) [arXiv:0712.0803 [hep-ex]].

[79] B. Abbott *et al.* [D0 Collaboration], *Measurement of the shape of the transverse momentum distribution of W bosons produced in $p\bar{p}$ collisions at $\sqrt{s} = 1.8$ TeV*, Phys. Rev. Lett. **80**, 5498 (1998) [arXiv:hep-ex/9803003].

[80] E. L. Nurse, *A Measurement of the Inclusive $Z/\gamma^* \to \mu^+\mu^-$ Cross-Section and Study of W and Z Events in $p\bar{p}$ Collisions at D0*, FERMILAB-THESIS-2005-05.

[81] A. D. Martin, R. G. Roberts, W. J. Stirling and R. S. Thorne, *Uncertainties of predictions from parton distributions. 1: Experimental errors*, Eur. Phys. J. C **28**, 455 (2003) [arXiv:hep-ph/0211080].

[82] S. Catani, F. Krauss, R. Kuhn, and B. R. Webber, *QCD Matrix Elements + Parton Showers*, JHEP **11** (2001) 063,

[83] A. Schälicke and F. Krauss, *Implementing the ME+PS Merging Algorithm*, JHEP **07** (2005) 018,

[84] F. Krauss, *Matrix Elements and Parton Showers in Hadronic Interactions*, JHEP **08** (2002) 015,

[85] L. Lönnblad, *Correcting the Colour-Dipole Cascade Model with Fixed Order Matrix Elements*, JHEP **05** (2002) 046,

[86] M. L. Mangano, M. Moretti, and R. Pittau, *Multijet Matrix Elements and Shower Evolution in Hadronic Collisions: $Wb\bar{b} + (n)$ jets as a Case Study*, Nucl. Phys. **B632** (2002) 343–362,

[87] S. Mrenna and P. Richardson, *Matching Matrix Elements and Parton Showers with HERWIG and PYTHIA*, JHEP **05** (2004) 040,

[88] N. Lavesson and L. Lonnblad, *Merging parton showers and matrix elements – back to basics*, JHEP **0804**, 085 (2008)

[89] J. Alwall *et. al.*, *Comparative Study of Various Algorithms for the Merging of Parton Showers and Matrix Elements in Hadronic Collisions*, Eur. Phys. J. **C53** (2008) 473–500,

[90] S. Catani, Y. L. Dokshitzer, M. Olsson, G. Turnock and B. R. Webber, *New clustering algorithm for multi - jet cross-sections in e+ e- annihilation*, Phys. Lett. B **269**, 432 (1991).

[91] T. Sjostrand, *The Lund Monte Carlo for e^+e^- jet physics*, Comput. Phys. Comm. B **28**, 229 (1983).

[92] F. Maltoni and T. Stelzer, *MadEvent: Automatic event generation with MadGraph*, JHEP **0302** (2003) 027

[93] J. Alwall *et al.*, *MadGraph/MadEvent v4: The New Web Generation*, JHEP **0709** (2007) 028

[94] J. M. Butterworth, J. P. Couchman, B. E. Cox and B. M. Waugh, *KtJet: A C++ implementation of the K_T clustering algorithm*, Comput. Phys. Commun. **153** (2003) 85

[95] M. Bengtsson and P. M. Zerwas, *Four jet events in e^+e^- annihilation: testing the three gluon vertex*, Phys. Lett. B **208**, 306 (1988).

[96] O. Nachtmann and A. Reiter, *A test for the gluon self coupling in the reactions $e^+e^- \rightarrow$ four jets and $Z^0 \rightarrow$ four jets*, Z. Phys. C **16**, 45 (1982).

[97] J. G. Korner, G. Schierholz and J. Willrodt, *QCD predictions for four jet final states in e^+e^- annihilation. 2. angular correlations as a test of the triple gluon coupling*, Nucl. Phys. B **185**, 365 (1981).

[98] P. Abreu *et al.* [DELPHI Collaboration], *Tuning and test of fragmentation models based on identified particles and precision event shape data*, Z. Phys. C **73**, 11 (1996).

[99] P. Pfeifenschneider *et al.* [JADE collaboration and OPAL Collaboration], *QCD analyses and determinations of α_S in e+ e- annihilation at energies between 35-GeV and 189-GeV*, Eur. Phys. J. C **17**, 19 (2000) [arXiv:hep-ex/0001055].

[100] A. Heister *et al.* [ALEPH Collaboration], *Measurements of the strong coupling constant and the QCD colour factors using four-jet observables from hadronic Z decays*, Eur. Phys. J. C **27**, 1 (2003).

[101] S. Hoeche, F. Krauss, S. Schumann and F. Siegert, *QCD matrix elements and truncated showers*, JHEP **0905** (2009) 053 [arXiv:0903.1219 [hep-ph]].

[102] F. Krauss, A. Schalicke, S. Schumann and G. Soff, *Simulating W/Z+ jets production at the Tevatron*, Phys. Rev. D **70** (2004) 114009 [arXiv:hep-ph/0409106].

[103] N. Lavesson and L. Lonnblad, *W + jets matrix elements and the dipole cascade,* JHEP **0507** (2005) 054 [arXiv:hep-ph/0503293].

[104] S. Hoche, F. Krauss, N. Lavesson, L. Lonnblad, M. Mangano, A. Schalicke and S. Schumann, *Matching parton showers and matrix elements,* arXiv:hep-ph/0602031.

[105] S. Catani, Y. L. Dokshitzer, M. H. Seymour and B. R. Webber, *Longitudinally invariant k_T clustering algorithms for hadron hadron collisions,* Nucl. Phys. B **406** (1993) 187.

[106] J. Pumplin, D. R. Stump, J. Huston, H. L. Lai, P. M. Nadolsky and W. K. Tung, *New generation of parton distributions with uncertainties from global QCD analysis,* JHEP **0207** (2002) 012 [arXiv:hep-ph/0201195].

[107] B. M. Waugh, H. Jung, A. Buckley, L. Lonnblad, J. M. Butterworth and E. Nurse, *HZTool and Rivet: Toolkit and framework for the comparison of simulated final states and data at colliders,* arXiv:hep-ph/0605034.

[108] T. Aaltonen *et al.* [CDF - Run II Collaboration], *Measurement of inclusive jet cross-sections in $Z/\gamma (\to e^+e^-)$ + jets production in $p\bar{p}$ collisions at $\sqrt{s}$ = 1.96-TeV,* Phys. Rev. Lett. **100** (2008) 102001 [arXiv:0711.3717 [hep-ex]].

[109] T. Aaltonen *et al.* [CDF Collaboration], *Measurement of the cross section for W^- boson production in association with jets in $p\bar{p}$ collisions at $\sqrt{s}$ = 1.96-TeV,* Phys. Rev. D **77** (2008) 011108 [arXiv:0711.4044 [hep-ex]].

Appendix A

Monte Carlo algorithms

In this appendix we review the Monte Carlo algorithms that are used throughout this thesis.

A.1 Generating according to a probability distribution

The problem central to a Monte Carlo event generator is to generate 'events', $\mathbf{x}$, according to a probability distribution $f(\mathbf{x})$. This corresponds to *unweighting* of the samples in Eq. 1.109 such that each point has a unit weight and can be considered to be an event.

In order to illustrate the method, we limit ourselves to a one-dimensional problem. The probability for having a value between x_{min} and x is given by

$$P(x_{\text{min}} < x' < x) = \frac{\int_{x_{\text{min}}}^{x} \mathrm{d}x' f(x')}{\int_{x_{\text{min}}}^{x_{\text{max}}} \mathrm{d}x' f(x')}. \tag{A.1}$$

Since this yields a probability in the interval $[0, 1]$, we can replace the left-hand-side by the random number operator, $\mathcal{R}$, and x can be found from

$$x = F^{-1} \left[\mathcal{R} \left(F(x_{\text{max}}) - F(x_{\text{min}}) \right) + F(x_{\text{min}}) \right], \tag{A.2}$$

where $F(x)$ is the primitive integral of $f(x)$.

The function $f(x)$ may be sufficiently complicated that the inverse of the primitive integral, $F^{-1}(x)$, is not be known. In this case we can instead use a simpler function

$g(x)$, for which the inverse of the primitive integral, $G^{-1}(x)$ is known. If we choose the function $g(x)$ to be an enveloping function of $f(x)$ such that

$$g(x) > f(x) \quad \forall x \in [x_{\min}, x_{\max}], \tag{A.3}$$

then x may be distributed according to $f(x)$ by first generating the event according to $g(x)$, using Eq. A.2, and then accepting the configuration only if

$$\mathcal{R} < \frac{f(x)}{g(x)}. \tag{A.4}$$

The probability of accepting an event x is then given by the product of $g(x)$ and the acceptance probability $f(x)/g(x)$, yielding the desired distribution $f(x)$. Evidently the efficiency of this procedure is related to the proportion of events that are rejected and therefore the closer $g(x)$ is to $f(x)$, the better the efficiency.

This can easily be extended to a distribution of n variables, $f(\mathbf{x}) = f(x_1, .., x_n)$, by choosing a bounding function $g(\mathbf{x})$ that can be written in the factorized form $g_1(x_1)...g_n(x_n)$. An event is then generated by generating each variable x_i independently according to Eq. A.2 with $g_i(x_i)$. The event is then accepted, as before, if

$$\mathcal{R} < \frac{f(\mathbf{x})}{g(\mathbf{x})}. \tag{A.5}$$

A.2 The veto algorithm

In the parton shower we evolve down in an ordering variable, t, from an initial scale t_I and generate the scale at which the next branching occurs. The scale of the next branching should be selected according to a probability distribution of the form

$$P(t) = f(t)\Delta(t_I, t). \tag{A.6}$$

This represents a correctly normalised probability distribution, where the term $f(t)$ corresponds to the branching probability, while $\Delta(t_I, t)$ is the Sudakov form factor giving the probability that a branching has not already occurred in evolving from t_I down to

t. This is given by

$$\Delta(t_I, t) = \exp\left[-\int_t^{t_I} dt' f(t')\right]. \tag{A.7}$$

If we assume that we can define a primitive integral of $f(t)$, $F(t)$, with a known inverse, then we can write the inclusive probability for an emission between t_I and t as

$$P(t_I > t' > t) = 1 - \exp\left[F(t) - F(t_I)\right]. \tag{A.8}$$

As before we can replace the inclusive probability, or equivalently one minus the probability, by the the random number operator $\mathcal{R}$ and solve for t yielding[1]

$$t = F^{-1}\left[\log \mathcal{R} + F(t_I)\right]. \tag{A.9}$$

In general, $f(t)$ is not sufficiently simple for us to use Eq. A.9 directly, however we can again employ a method that uses a simpler function $g(x)$, defined such that it satisfies Eq. A.18. The correct prescription for using the bounding function $g(x)$ in this case is given by the *veto algorithm* [39]. The veto algorithm dictates that t should be selected according to the following procedure:

1. start at $i = 0$ with $t_0 = t_I$;
2. the next scale is found according to

$$t_i = G^{-1}\left[\log \mathcal{R} + G(t_{i-1})\right]; \tag{A.10}$$

3. the scale t_i is accepted according to

$$\mathcal{R} < \frac{f(t_i)}{g(t_i)}; \tag{A.11}$$

4. if t_i is rejected then return to step 2.

That this algorithm does indeed generate values of t according Eq. A.6 can be seen by considering the probability of generating the scale t after different numbers of veto algorithm iterations. Each veto algorithm iteration i that is not accepted, introduces a probability given by the product of generating the scale t_i and it then being rejected,

---

[1]Note that this is equivalent to solving $\mathcal{R} = \Delta(t_I, t)$ as in Eq. 1.113.

given by

$$(g(t_i) - f(t_i)) \exp \left[- \int_{t_i}^{t_{i-1}} dt' g(t') \right]. \tag{A.12}$$

The final iteration, at which the scale t is accepted after n rejections, introduces a probability

$$f(t) \exp \left[- \int_t^{t_n} dt' g(t') \right]. \tag{A.13}$$

It is clear that, regardless of how many rejection steps occur before a scale is accepted, the exponential factors in Eqs. A.12 and A.13 combine. The intermediate rejected scales t_i should be integrated over such that they are ordered. The probability of generating the scale t after n rejections is therefore given by

$$P_n = f(t) \exp \left[- \int_t^{t_I} dt' g(t') \right] \prod_{i=1}^n \int_t^{t_{i-1}} dt_i \, (g(t_i) - f(t_i)). \tag{A.14}$$

The n nested integrals can be ordered in $n!$ ways where the sum of these orderings complete the integral over the n-dimensional hypercube. We can therefore decouple the integrals in Eq. A.14, giving

$$P_n = f(t) \exp \left[- \int_t^{t_I} dt' g(t') \right] \frac{1}{n!} \left[\int_t^{t_{i-1}} dt_i \, (g(t_i) - f(t_i)) \right]^n. \tag{A.15}$$

The full probability of selecting a scale t is then given by the sum of all P_n, yielding

$$
\begin{aligned}
P &= f(t) \exp \left[- \int_t^{t_I} dt' g(t') \right] \sum_{n=0}^\infty \frac{1}{n!} \left[\int_t^{t_{i-1}} dt_i \, (g(t_i) - f(t_i)) \right]^n \\
&= f(t) \exp \left[- \int_t^{t_I} dt' f(t') \right],
\end{aligned}
\tag{A.16}
$$

as required.

A.3 The bivariant veto algorithm

In general the branching probability depends also on an auxiliary splitting variable z. In this section we describe an extension of the veto algorithm referred to as the

bivariant veto algorithm which allows the generation of the variables (t, z) according to the distribution

$$P(t) = f(t, z)\Delta(t_I, t),$$ (A.17)

where the Sudakov form factor now also includes the integral over the variable z.

The auxiliary variable may be generated simultaneously by introducing a bounding function $g(t, z)$ defined such that,

$$g(t, z) = g_1(t)g_2(z) > f(t, z) \quad \forall(t, z) \in R,$$ (A.18)

where R is the allowed phase space region. The correct prescription is then to:

1. start at $i = 0$ with $t_0 = t_I$;
2. generate the scale t_i according to Eq. A.10 but with $g(t) = g_1(t)\int \mathrm{d}z g_2(z)$;
3. generate z according to

$$z = G_2^{-1}\left[\mathcal{R}\left(G_2(z_{\max}) - G_2(z_{\min})\right) + G_2(z_{\min})\right],$$ (A.19)

where $G_2(z)$ is the primitive integral of $g_2(z)$;
4. the event is accepted if

$$\mathcal{R} < \frac{f(t, z)}{g(t, z)};$$ (A.20)

5. if t_i is rejected then return to step 3.

A.4 The veto algorithm for competing processes

Often, the branching probability, $f(t)$, will be of the form

$$f(t) = \sum_i f_i(t),$$ (A.21)

where i corresponds to a channel with a different subprocess. We may need to select a value of t and the subprocess (for example in a situation where each i corresponds to a different flavour configuration) it came from where values of t coming from the

subprocess i should be distributed according to

$$P_i(t) = f_i(t) \exp\left[-\int_t^{t_I} dt' f(t')\right].$$

(A.22)

This is achieved by generating by *competition* as described in Ref. [44]. This requires that a value of t is generated for each channel, according to the standard veto algorithm with $f(t) \to f_i(t)$ with the largest of the values being selected. The channel from which this value was generated is the subprocess in which the branching occurred. The probability of a value t being generated in the channel i is then given by the probability of generating the value t from the veto algorithm with $f(t) \to f_i(t)$, multiplied by the probability that no values in the interval $[t_I, t]$ were generated in the other channels this is given by

$$f_i(t) \exp\left[-\int_t^{t_I} dt' f_i(t')\right] \times \prod_{i' \neq i} \exp\left[-\int_t^{t_I} dt' f_{i'}(t')\right],$$

(A.23)

which we identify as the required probability in Eq. A.22.

Appendix B

Plus distributions

In this appendix we present further details of the plus distributions used in Chapter 4.

In order to subtract the divergences from the radiative corrections as poles in ϵ, we write Eq. 4.12 in terms of the plus distributions defined by

$$\int_0^1 \mathrm{d}x F_+(x) G(x) = \int_0^1 \mathrm{d}x \left(F(x) G(x) - F(x) G(1) \right). \tag{B.1}$$

The plus distributions are only defined when considered in the convolution with another arbitrary finite function, $G(x)$.

B.1 Plus distributions for the two-body phase space

We first consider the divergent integral

$$I = \int_0^1 \mathrm{d}x (1-x)^{-1-\epsilon} G(x). \tag{B.2}$$

This integral is divergent in the limit $\epsilon \to 0$. Adding and subtracting $(1-x)^{-1-\epsilon} G(1)$ and using the definition of the plus distribution, we can write this as

$$I = \int_0^1 \mathrm{d}x \left\{ \left(\frac{(1-x)^{-\epsilon}}{(1-x)} \right)_+ + \delta(1-x) \int_0^1 \mathrm{d}x' x'^{(1-\epsilon)} \right\} G(x). \tag{B.3}$$

The integral in the second term can be evaluated yielding a pole in ϵ and the first term is finite and can be expanded in ϵ giving

$$
\begin{aligned}
I \;=\;& \int_0^1 \mathrm{d}x \left\{ \frac{1}{(1-x)_+} - \epsilon \left(\frac{\log(1-x)}{(1-x)} \right)_+ \right. \\
& \left. + \frac{\epsilon^2}{2} \left(\frac{\log^2(1-x)}{(1-x)} \right)_+ - \frac{1}{\epsilon}\delta(1-x) \right\} G(x) + \mathcal{O}(\epsilon^3).
\end{aligned}
\tag{B.4}
$$

from which we identify

$$
\begin{aligned}
(1-x)^{-1-\epsilon} \;=\;& -\frac{1}{\epsilon}\delta(1-x) + \frac{1}{(1-x)_+} - \epsilon \left(\frac{\log(1-x)}{(1-x)} \right)_+ \\
& + \frac{\epsilon^2}{2} \left(\frac{\log^2(1-x)}{(1-x)} \right)_+ + \mathcal{O}(\epsilon^3).
\end{aligned}
\tag{B.5}
$$

In order to arrive at the result in Eq. 4.18 we are required to write the function

$$
\mathcal{J}(x,v) = x^\epsilon (1-x)^{-1-2\epsilon} v^{-1-\epsilon}(1-v)^{-1-\epsilon},
\tag{B.6}
$$

in terms of plus distributions. This is achieved by a set of manipulations of the result in Eq. B.5. The x dependent factor in Eq. B.6 is found by applying the substitution $\epsilon \to 2\epsilon$, multiplying by x^ϵ and expanding in ϵ. The result of this is

$$
\begin{aligned}
x^\epsilon (1-x)^{-1-2\epsilon} \;=\;& -\frac{1}{2\epsilon}\delta(1-x) + \frac{1}{(1-x)_+} \\
& + \; \epsilon \frac{\log x}{(1-x)} - 2\epsilon \left(\frac{\log(1-x)}{(1-x)} \right)_+ + \mathcal{O}(\epsilon^2).
\end{aligned}
\tag{B.7}
$$

The v dependent factors are given by Eq. B.5 with the substitutions $(1-x) \to v$ and $x \to v$ yielding[1]

$$
\begin{aligned}
v^{-1-\epsilon}(1-v)^{-1-\epsilon} \;=\;& \left(-\frac{1}{\epsilon}\delta(v) + \frac{1}{v_+} - \epsilon \left(\frac{\log(v)}{v} \right)_+ + \frac{\epsilon^2}{2} \left(\frac{\log^2(v)}{v} \right)_+ \right) \\
& \times \left(-\frac{1}{\epsilon}\delta(1-v) + \frac{1}{(1-v)_+} - \epsilon \left(\frac{\log(1-v)}{(1-v)} \right)_+ + \frac{\epsilon^2}{2} \left(\frac{(\log(1-v))^2}{(1-v)} \right)_+ \right).
\end{aligned}
\tag{B.8}
$$

---

[1]The plus distributions of functions that are divergent in the limit $v \to 0$ are defined with the subtraction at $v = 0$ rather than $v = 1$.

This may be simplified by applying the following identities for products of plus distributions

$$\frac{1}{v_+}\frac{1}{(1-v)_+} = \frac{1}{v_+} + \frac{1}{(1-v)_+}, \tag{B.9}$$

$$\frac{1}{v_+}\left(\frac{\log(1-v)}{(1-v)}\right)_+ = \frac{\log(1-v)}{v} + \left(\frac{\log(1-v)}{(1-v)}\right)_+, \tag{B.10}$$

$$\left(\frac{\log(v)}{v}\right)_+\left(\frac{\log(1-v)}{(1-v)}\right)_+ = \left(\frac{\log(v)}{v}\right)\left(\frac{\log(1-v)}{(1-v)}\right). \tag{B.11}$$

Equation B.8 then gives

$$v^{-1-\epsilon}(1-v)^{-1-\epsilon} = -\frac{1}{\epsilon}\delta(v) - \frac{1}{\epsilon}\delta(1-v) + \frac{1}{v_+} + \frac{1}{(1-v)_+} \tag{B.12}$$
$$-\epsilon\left[\frac{\log(1-v)}{v} + \frac{\log(v)}{(1-v)} + \left(\frac{\log(v)}{v}\right)_+ + \left(\frac{\log(1-v)}{(1-v)}\right)_+\right].$$

The result in Eq. 4.18 is then found by calculating the product of Eqs. B.7 and B.12 up to $\mathcal{O}(\epsilon)$. The resulting terms may be split into terms proportional to the three δ-functions as defined by Eq. 4.18. Since all ϵ-poles are accompanied by a δ-function, the terms containing no δ-functions are found from the product of the finite $\mathcal{O}(1)$ terms in Eqs. B.7 and B.12, giving

$$\mathcal{H}(x,v) = \frac{1}{(1-x)_+}\left(\frac{1}{v_+} + \frac{1}{(1-v)_+}\right), \tag{B.13}$$

as in Eq. B.13. The terms proportional to $\delta(1-x)$ are given by

$$\mathcal{S} = \frac{1}{2\epsilon^2}[\delta(v) + \delta(1-v)] - \frac{1}{\epsilon}\left[\frac{1}{v_+} + \frac{1}{(1-v)_+}\right] \tag{B.14}$$
$$+\frac{\log(1-v)}{v} + \frac{\log(v)}{(1-v)} + \left(\frac{\log(v)}{v}\right)_+ + \left(\frac{\log(1-v)}{(1-v)}\right)_+.$$

The product of matrix element, Jacobean and flux factors with which $\mathcal{J}(x,v)$ is convoluted depends only on the combinations x, $\hat{s}$, $\hat{t}$, $\hat{u}$ and $x_{\oplus}$, all of which are independent of v in the limit $x \to 1$. This allows us to replace all the plus distributions in Eq. B.14 by zero and all other functions of v by their integrated value. This gives

$$\mathcal{S} = \frac{1}{\epsilon^2} - \frac{\pi^2}{6}, \tag{B.15}$$

as in Eq. 4.19a. Finally, the remaining $\mathcal{O}(1)$ terms are proportional to $(\delta(v) + \delta(1 - v))$ and give the result in Eq. 4.19b,

$$\mathcal{C}(x) = -\frac{1}{\epsilon}\frac{1}{(1-x)_+} - \frac{\log x}{(1-x)} + 2\left(\frac{\log(1-x)}{1-x}\right)_+ . \tag{B.16}$$

B.2 Plus distribution identities for the implementation of $\bar{B}$

In order to implement the collinear $(\mathcal{C}_{ab})$ terms in the real-emission contributions to $\bar{B}(\boldsymbol{\Phi_n})$, the following relations are required

$$\int_{\bar{x}(v)}^1 \mathrm{d}x \ \frac{f(x)}{(1-x)_+} = \int_0^1 \mathrm{d}\tilde{x} \ (1 - \bar{x}(v)) \left[\frac{f(x(\tilde{x},v)) - f(x(1,v))}{1 - x(\tilde{x},v)} \right. \tag{B.17}$$
$$\left. + \frac{f(x(1,v))}{1 - \bar{x}(v)}\log(1 - \bar{x}(v))\right],$$

and

$$\int_{\bar{x}(v)}^1 \mathrm{d}x \ f(x) \left(\frac{\log(1-x)}{1-x}\right)_+ = \int_0^1 \mathrm{d}\tilde{x} \ (1 - \bar{x}(v)) \times \tag{B.18}$$
$$\left[(f(x(\tilde{x},v)) - f(x(1,v)))\left(\frac{\log(1 - x(\tilde{x},v))}{1 - x(\tilde{x},v)}\right) + \right.$$
$$\left. \frac{f(x(1,v))}{2(1 - \bar{x}(v))}\log^2(1 - \bar{x}(v))\right],$$

with $\tilde{x}$ defined in Eq. 4.56 and $v \in [0,1]$. For the hard $(\mathcal{H}_{ab})$ contribution to the real radiation components in $\bar{B}(\Phi_B)$

$$\int_0^1 \mathrm{d}v \int_{\bar{x}(v)}^1 \mathrm{d}x \ f(x,v) \ \frac{1}{(1-x)_+}\left(\frac{1}{(1-v)_+} + \frac{1}{v_+}\right) = \tag{B.19}$$
$$\int_0^1 \mathrm{d}v \int_0^1 \mathrm{d}\tilde{x}\frac{1}{1-\tilde{x}}\left(\frac{f(x(\tilde{x},v),v) - f(1,v) - f(x(\tilde{x},1),1) + f(1,1)}{(1-v)} + \right.$$
$$\left. \frac{f(x(\tilde{x},v),v) - f(1,v) - f(x(\tilde{x},0),0) + f(1,0)}{v}\right) + $$
$$\int_0^1 \mathrm{d}v \int_0^1 \mathrm{d}\tilde{x} \ \left(\frac{f(1,v)\log(1 - \bar{x}(v)) - f(1,1)\log(1 - \bar{x}(1))}{(1-v)} + \right.$$
$$\left. \frac{f(1,v)\log(1 - \bar{x}(v)) - f(1,0)\log(1 - \bar{x}(0))}{v}\right),$$

where in the last line of Eq. B.20 we have introduced the identity as $\int_0^1 \mathrm{d}\tilde{x}$. Similar relations are derived, in different variables, in Ref. [57].

Appendix C

Further matrix-element merging details

C.1 Highest-multiplicity treatment

In order to show the necessity of the highest-multiplicity treatment, we consider the case where we merge matrix elements with a maximum multiplicity of $N = 3$, *i.e.* the matrix elements describe at most one emission. For clarity we proceed as in Sect. 5.2.1, considering the algorithm in the simplest case where the parton-shower evolution variable and merging variable are a transverse momentum measure q. In this case the merged NLL cross section $\sigma_n^{ME+PS}(q_0)$ for n up to three jets resolved at the hadronization scale q_0 is unchanged by the highest multiplicity. However, for jet multiplicities $n > N$, the correct NLL cross section is only achieved with the highest-multiplicity treatment. To illustrate this we consider the four-jet cross section. The NLL parton-shower approximation to the four-jet cross section with partons resolved at the scale q_{MS} is given by

$$\sigma_4^{(PS)}\left(q_I, q_{MS}\right) = \sigma_2 \times 2\left[\Delta_q\left(q_I, q_{MS}\right)\right]^2 \int_{q_{MS}}^{q_I} \mathrm{d}q\, \alpha_S\left(q\right)\Gamma_{q \to qg}\left(q\right)\Delta_g(q, q_{MS}) \times \qquad \text{(C.1)}$$

$$\int_{q_{MS}}^{q} \mathrm{d}q'\, F_{q\bar{q}g}^{PS}\left(q', q_{MS}\right),$$

where $F_{q\bar{q}g}^{PS}\left(q', q_{MS}\right)$ is a function describing the probability of a single emission, from a $q\bar{q}g$ parton configuration, in the region $[q', q' + \mathrm{d}q']$ and subsequent evolution down to a

scale q_{MS}. It is given by

$$F_{q\bar{q}g}^{PS}(q', q_{MS}) = 2\alpha_S(q')\,\Gamma_{q\to qg}(q')\,\Delta_g(q', q_{MS}) \tag{C.2}$$
$$+ \alpha_S(q')\,\Gamma_{g\to gg}(q')\,\Delta_g(q', q_{MS})$$
$$+ \alpha_S(q')\,\Gamma_{g\to qq}(q')\,\frac{[\Delta_q(q', q_{MS})]^2}{\Delta_g(q', q_{MS})}.$$

The four-jet NLL merged cross section is given by the sum of a term where exactly one emission is generated by the matrix elements and one by the parton shower and a term where the parton shower produces exactly two emissions. Without the highest-multiplicity treatment this is given by

$$\sigma_4^{(PS+ME)}(q_0) = \sigma_4^{(PS)}(q_{MS}, q_0) \tag{C.3}$$
$$+ \bar{\sigma}_3^{(ME)}(q_{MS})\,[\Delta_q(q_{MS}, q_0)]^2\,\Delta_g(q_{MS}, q_0)\int_{q_0}^{q_{MS}} dq'\, F_{q\bar{q}g}^{PS}(q', q_0),$$

where $\bar{\sigma}_3^{(ME)}(q_{MS})$ is the reweighted matrix-element contribution for three jets resolved at the merging scale. By design, at NLL, the reweighted three-jet matrix-element cross section $\bar{\sigma}_3^{(ME)}(q_{MS})$ is given by the corresponding NLL parton-shower cross section

$$\bar{\sigma}_3^{(ME)}(q_{MS}) = \sigma_2 \times 2\,[\Delta_q(q_I, q_{MS})]^2 \int_{q_{MS}}^{q_I} dq\,\alpha_S(q)\,\Gamma_{q\to qg}(q)\,\Delta_g(q, q_{MS}) + \mathcal{O}(\text{NNLL}). \tag{C.4}$$

The NLL expansion of Eq.(C.3) is therefore given by,

$$\sigma_4^{(PS+ME)}(q_0) = \sigma_2 \times 2\,[\Delta_q(q_I, q_0)]^2 \int_{q_{MS}}^{q_I} dq\,\alpha_S(q)\,\Gamma_{q\to qg}(q)\,\Delta_g(q, q_0)\times \tag{C.5}$$
$$\int_{q_0}^{q_{MS}} dq'\, F_{q\bar{q}g}^{PS}(q', q_0) + \sigma_4^{(PS)}(q_{MS}, q_0) + \mathcal{O}(\text{NNLL}).$$

This cannot be simplified any further, is not independent of the merging scale and does not produce the NLL parton-shower cross section as desired. The reason for this is that the procedure presented only allows a single emission to be generated in the region $q > q_{MS}$; the highest-multiplicity treatment corrects this.

The highest-multiplicity treatment dictates that in the highest-multiplicity channel the cuts applied to the Sudakov form factors used in the reweighting of the matrix elements and the vetoes applied to the parton shower should be changed from the merging

scale to the transverse momentum of the matrix-element emission with smallest transverse momentum. In the case considered, this transverse momentum is q and the result of the highest-multiplicity treatment is the following changes to the first term the three-jet channel) in Eq. (C.3):

$$\sigma_4^{(PS+ME)}(q_0) \rightarrow \hat{\sigma}_3^{(ME)}(q_{MS}) \Delta_g(q, q_0) \int_{q_0}^{q} dq' \, F_{q\bar{q}g}^{PS}(q', q_0) + \sigma_4^{(PS)}(q_{MS}, q_0). \qquad (C.6)$$

where $\hat{\sigma}_3^{(ME)}(q_{MS})$ is the matrix-element three-jet cross section reweighted according to the highest-multiplicity treatment. Its NLL expansion is again, by design, given by the parton-shower cross section but now with Sudakov cuts set to q rather than q_{MS}.

$$\hat{\sigma}_3^{(ME)}(q) = \sigma_2 \times 2 \int_{q_{MS}}^{q_I} dq \, [\Delta_q(q_I, q)]^2 \, \alpha_S(q) \, \Gamma_{q \rightarrow qg}(q) + \mathcal{O}(\text{NNLL}). \qquad (C.7)$$

Inserting this NLL expansion into Eq. (C.6), we observe that the integrands of the two terms in Eq. (C.6) are identical, differing only in the integration regions of q. The two terms may then be combined, completing the integration region $[q_I, q_0]$ and yielding the result

$$\sigma_4^{(PS+ME)}(q_0) = \sigma_4^{(PS)}(q_I, q_0) + \mathcal{O}(\text{NNLL}), \qquad (C.8)$$

which, to NLL, matches the parton-shower four-jet cross section and is independent of the merging scale.

C.2 Merging scale independence of the three-jet emission rate

In the following, we extend our pedagogical example concerning the merging of the two- and three-parton matrix-element configurations to illustrate the cancellation of the merging scale dependence at NLL level.

For clarity of notation we define the remnant and vetoed Sudakov form factors

$$\Delta_i^{R,V}(\tilde{q}_1, \tilde{q}_2) = \frac{\Delta_i^{R,V}(\tilde{q}_1; k_{\perp MS})}{\Delta_i^{R,V}(\tilde{q}_2; k_{\perp MS})}, \qquad (C.9)$$

where the dependence on the merging scale $k_{\perp MS}$ is implicit.

The parton-shower rate for the production of three-parton configurations via emission from the quark line (and none from the anti-quark) is given by

$$
\begin{aligned}
\mathcal{P}^{q\bar{q}g} &= \frac{1}{\sigma_{\text{tot}}} \, \mathrm{d}\sigma^{q\bar{q}} \, \mathrm{d}\mathcal{P}_{q\to qg}\left(\tilde{q}, z\right) \\
&\times \ \Delta_q\left(\tilde{q}_I, \tilde{q}\right) \Delta_q\left(z\tilde{q}, \tilde{q}_0\right) \Delta_g\left((1-z)\tilde{q}, \tilde{q}_0\right) \Delta_{\bar{q}}\left(\tilde{q}_I, \tilde{q}_0\right).
\end{aligned}
\tag{C.10}
$$

In the modified CKKW algorithm, emissions above the merging scale are generated according to the hard matrix element, initially with probability

$$
\mathcal{P}^{q\bar{q}g}\left(y_{ij} > y_{MS}\right) = \frac{1}{\sigma_{\text{tot}}} \, \mathrm{d}\sigma^{q\bar{q}g}.
\tag{C.11}
$$

Depending on whether the p_T of the gluon is smaller with respect to the quark or anti-quark a shower history is assigned to the configuration in which the former or latter is deemed to have emitted the gluon. Let us assume that the gluon p_T with respect to the quark was the smaller of the two, the event is then assigned the relevant Sudakov and coupling-constant weights

$$
\begin{aligned}
\mathcal{P}^{q\bar{q}g}\left(y_{ij} > y_{MS}\right) &\to \ \frac{1}{\sigma_{\text{tot}}} \, \mathrm{d}\sigma^{q\bar{q}g} \, \frac{\alpha_S\left(p_\perp\left(\tilde{q}, z\right)\right)}{\alpha_{S_{ME}}} \\
&\times \ \Delta_q^R\left(\tilde{q}_I, \tilde{q}\right) \Delta_q^R\left(z\tilde{q}, \tilde{q}_0\right) \Delta_g^R\left((1-z)\tilde{q}, \tilde{q}_0\right) \Delta_{\bar{q}}^R\left(\tilde{q}_I, \tilde{q}_0\right).
\end{aligned}
\tag{C.12}
$$

For this configuration to remain a three-parton configuration, no further radiation should be generated in the truncated and vetoed shower. The probability of generating no emissions in the vetoed and truncated showers is found from Eqs. 3.26 and 3.27 respectively. The result is that the emission probability receives further vetoed and remnant Sudakov form factors, resulting in the aggregate emission probability

$$
\begin{aligned}
\mathcal{P}^{q\bar{q}g}\left(y_{ij} > y_{MS}\right) &= \ \frac{1}{\sigma_{\text{tot}}} \, \mathrm{d}\sigma^{q\bar{q}g} \, \frac{\alpha_S\left(p_\perp\left(\tilde{q}, z\right)\right)}{\alpha_{S_{ME}}} \\
&\times \ \Delta_q^R\left(\tilde{q}_I, \tilde{q}\right) \Delta_q^R\left(z\tilde{q}, \tilde{q}_0\right) \Delta_g^R\left((1-z)\tilde{q}, \tilde{q}_0\right) \Delta_{\bar{q}}^R\left(\tilde{q}_I, \tilde{q}_0\right) \\
&\times \ \Delta_q^V\left(\tilde{q}_I, \tilde{q}\right) \Delta_q^V\left(z\tilde{q}, \tilde{q}_0\right) \Delta_g^V\left((1-z)\tilde{q}, \tilde{q}_0\right) \Delta_{\bar{q}}^V\left(\tilde{q}_I, \tilde{q}_0\right).
\end{aligned}
\tag{C.13}
$$

Recalling the definitions of the vetoed and remnant Sudakov form factors (Eqs. 3.22 and 3.23), it is clear from the fact that each remnant Sudakov form factor is accompanied by an analogous vetoed Sudakov form factor, that the emission rate does not depend on the merging scale y_{MS}.

Furthermore, if we take the NLL approximation of this we may replace $d\sigma^{q\bar{q}g}$ with the factorized form it approaches in the soft and collinear limits[1],

$$d\sigma^{q\bar{q}g} \rightarrow \frac{\alpha_{S_{ME}}}{\alpha_S\left(p_\perp\left(\tilde{q}, z\right)\right)} d\sigma^{q\bar{q}} d\mathcal{P}_{q \rightarrow qg}\left(\tilde{q}, z\right) . \tag{C.14}$$

In this approximation we see that the emission rate is identical to that of the parton shower in Eq. C.10,

$$\mathcal{P}^{q\bar{q}g}\left(y_{ij} > y_{MS}\right) \approx \mathcal{P}^{q\bar{q}g}. \tag{C.15}$$

Beneath the merging scale three-parton configurations arise through the emission of a single parton from a configuration generated according to the two-parton matrix element. These hard two-parton configurations are initially generated with probability

$$\mathcal{P}^{q\bar{q}} = \frac{1}{\sigma_{\text{tot}}} d\sigma^{q\bar{q}} \tag{C.16}$$

and then reweighted according to the prescription in Sect 5.4, such that

$$\mathcal{P}^{q\bar{q}} \rightarrow \frac{1}{\sigma_{\text{tot}}} d\sigma^{q\bar{q}} \Delta_q^R\left(\tilde{q}_I, \tilde{q}_0\right) \Delta_{\bar{q}}^R\left(\tilde{q}_I, \tilde{q}_0\right) . \tag{C.17}$$

It follows from the vetoed shower equation (Eq. 3.26) that the aggregate probability for an emission to be subsequently generated from the quark line (and none from the external anti-quark line) is

$$\begin{aligned} \mathcal{P}^{q\bar{q}g}\left(y_{ij} < y_{MS}\right) &= \frac{1}{\sigma_{\text{tot}}} d\sigma^{q\bar{q}} d\mathcal{P}_{q \rightarrow qg}\left(\tilde{q}, z\right) \\ &\times \Delta_q^R\left(\tilde{q}_I, \tilde{q}\right) \Delta_q^R\left(\tilde{q}, \tilde{q}_0\right) \Delta_{\bar{q}}^R\left(\tilde{q}_I, \tilde{q}_0\right) \\ &\times \Delta_q^V\left(\tilde{q}_I, \tilde{q}\right) \Delta_q^V\left(z\tilde{q}, \tilde{q}_0\right) \Delta_g^V\left(\left(1-z\right)\tilde{q}, \tilde{q}_0\right) \Delta_{\bar{q}}^V\left(\tilde{q}_I, \tilde{q}_0\right) . \end{aligned} \tag{C.18}$$

where, for comparison with Eq. C.14 we have rewritten the first remnant Sudakov form factor in Eq. C.18 as $\Delta_q^R\left(\tilde{q}_I, \tilde{q}\right) \Delta_q^R\left(\tilde{q}, \tilde{q}_0\right)$. It appears that the remnant and vetoed Sudakov factors in Eq. C.14 do not match, spoiling the cancellation of the merging scale, however we note that we rectify this by writing one of the remnant Sudakovs as

$$\Delta_q^R\left(\tilde{q}, \tilde{q}_0\right) \approx \Delta_q^R\left(z\tilde{q}, \tilde{q}_0\right) \Delta_g^R\left(\left(1-z\right)\tilde{q}, \tilde{q}_0\right) . \tag{C.19}$$

---

[1]The ratio of coupling constants enters here due to the fact that $d\sigma^{q\bar{q}g}$ while the shower branching probability contains the running coupling evaluated at $p_\perp$.

This replacement results in only subleading differences; we can see this by considering the soft and non-soft emission regions separately[2]. The region of soft emissions corresponds to the limit $z \to 1$ where $\Delta_g^R((1-z)\tilde{q}, \tilde{q}_0) \to 1$ and $\Delta_q^R(z\tilde{q}, \tilde{q}_0) \to \Delta_q^R(\tilde{q}, \tilde{q}_0)$, satisfying Eq. C.19. Away from the soft region we have $\tilde{q} \approx p_\perp$ and since $p_\perp < p_{\perp_{MS}}$, the Θ-function results in all remnant Sudakov factors approaching one, so Eq. C.19 is trivially satisfied. Making this approximation we find that, to NLL accuracy, the emission rate is independent of the merging scale and is given by the parton shower emission rate of Eq. C.10,

$$\mathcal{P}^{q\bar{q}g}\left(y_{ij} > y_{MS}\right) \approx \mathcal{P}^{q\bar{q}g}. \tag{C.20}$$

We see that to NLL the proposed algorithm yields emission rates that are independent of the merging scale and are identical to the emission rates of the parton shower. We note that all three components: truncated showers; vetoed showers; and Sudakov reweighting, are essential in achieving this smooth merging and independence from the merging scale.

C.3 Parton-shower merging test

As a check of the validity of the pseudo-shower history assignment procedure (as outlined in Sect. 5.4.2) and the approximations made in applying the vetoes (as outlined in Sect. 5.4.1), we present a test of reproducing the shower by merging two showers describing emissions above and below the merging scale y_{MS}.

The test was performed by generating the parton shower with a veto applied such that only events with $k_\perp > k_{\perp_{MS}}$ are produced. The partons produced by this shower represent the shower approximation to a set of hard emissions. This set of hard emissions are then read back into the parton shower and showered with the CKKW truncated and vetoed showers, generating emissions with $k_\perp < k_{\perp_{MS}}$.

Ideally the resultant distributions would exactly match those of the default shower. In practice, we have used approximations in the vetoes and an inexact history assignment and so we expect some differences. There are also some subleading differences inherent in the shower reorganisation as discussed in Sect. 5.3.

Figure C.1 shows parton level three-jet resolution distributions in the Durham jet measure which was also used to define the merging scale. We expect these plots to

---

[2]The arguments here are exactly those used in the POWHEG shower reorganisation.
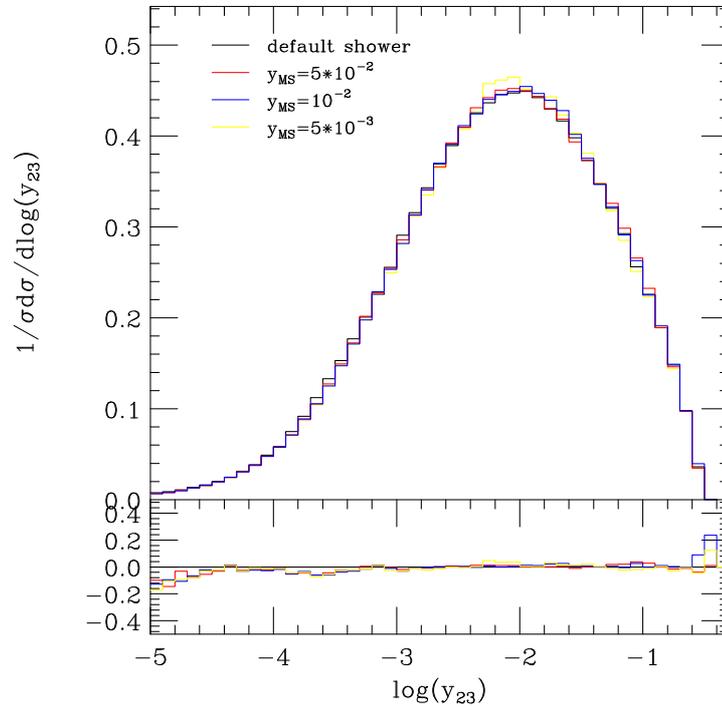
Figure C.1: Parton level distributions of the scale at which three jets are resolved in the Durham jet measure for $e^+e^- \to$ hadrons at $\sqrt{s} = 91.2\,\mathrm{GeV}$ comparing the default parton shower with no matrix-element correction (black line) to a parton shower merged around y_{MS} with with merging scales set to $y_{MS} = 5 \times 10^{-2}$, $y_{MS} = 10^{-2}$ and $y_{MS} = 5 \times 10^{-3}$ in the Durham jet measure. The lower panel in each of the plots shows $(m - d)/d$ where m is the merged distribution and d is the default distribution.

be sensitive to any problems that may arise. Figure C.1 shows that the merged shower matches the default shower result closely for all three merging scale choices. As expected, the distributions exhibit some slight differences however these are at an acceptable level, indicating that the approximations made in the vetoes and pseudo-shower history are valid.

List of figures

List of tables